AGH UNIVERSITY OF SCIENCE AND TECHNOLOGY

FACULTY OF ENERGY AND FUELS

PhD THESIS

ADVANCED CARBON CAPTURE AND STORAGE TECHNOLOGIES

ZAAWANSOWANE TECHNOLOGIE WYCHWYTU I SKŁADOWANIA DITLENKU WĘGLA

Agnieszka Ćwik

Supervisors:

Prof. Ignasi Casanova

Dr hab. Katarzyna Zarębska, Prof. AGH

AGH University of Science and Technology, Krakow,
Faculty of Energy and Fuels
Department of Coal Chemistry and Environmental Sciences,
Barcelona, 2019

Acknowledgements

I would like to express my special appreciation and thanks to my research supervisors, Professor Ignasi Casanova, Professor Katarzyna Zarębska and Dr Paweł Baran, for their patient guidance, enthusiastic encouragement and useful critiques of this research work.

I am particularly grateful for the assistance given by Kwon Rausis, who helped me with the experimental parts of my thesis as well as the interpretation of results.

I am grateful for all the support I received from my family and friends throughout my PhD studies.

Very special thanks go to the SELECT+ Erasmus Mundus Joint Degree PhD Programme for providing the funding for the work.

Finally, I would like to give special thanks to InnoEnergy PhD School for giving me the chance to obtain extra-curricular education.

Uprzedzony o odpowiedzialności karnej na podstawie art. 115 ust. 1 i 2 ustawy z dnia 4 lutego 1994 r. o prawie autorskim i prawach pokrewnych (t.j. Dz.U. z 2006 r. Nr 90, poz. 631 z późn. zm.): „ Kto przywłaszcza sobie autorstwo albo wprowadza w błąd co do autorstwa całości lub części cudzego utworu albo artystycznego wykonania, podlega grzywnie, karze ograniczenia wolności albo pozbawienia wolności do lat 3. Tej samej karze podlega, kto rozpowszechnia bez podania nazwiska lub pseudonimu twórcy cudzy utwór w wersji oryginalnej albo w postaci opracowania, artystyczne wykonanie albo publicznie zniekształca taki utwór, artystyczne wykonanie, fonogram, wideogram lub nadanie.", a także uprzedzony o odpowiedzialności dyscyplinarnej na podstawie art. 211 ust. 1 ustawy z dnia 27 lipca 2005 r. Prawo o szkolnictwie wyższym (t.j. Dz. U. z 2012 r. poz. 572, z późn. zm.) „Za naruszenie przepisów obowiązujących w uczelni oraz za czyny uchybiające godności studenta student ponosi odpowiedzialność dyscyplinarną przed komisją dyscyplinarną albo przed sądem koleżeńskim samorządu studenckiego, zwanym dalej "sądem koleżeńskim"", oświadczam, że niniejszą pracę dyplomową wykonałem(-am) osobiście i samodzielnie i że nie korzystałem(-am) ze źródeł innych niż wymienione w pracy.

....

podpis autora pracy

Table of Contents

Introduction

CO_2, which is the main component of greenhouse gases, is the reason for global warming and a direct cause of climate change. In the last century, human action has added to the increasing carbon dioxide emissions via constantly increasing industrialization and the burning of large quantities of fossil fuels. Without taking any action to reduce the current levels of CO_2 emissions, global temperatures will continue to rise, and this scenario will have disastrous consequences. Earth's fauna and flora, together with the human race, may be endangered.

In order to decrease global carbon dioxide emissions, three main actions have been taken: improving energy efficiency, increasing the use of non-polluting sources of energy and the introduction of carbon capture, sequestration and utilization techniques (CCSU). These approaches must be taken in order to meet the objective of the Paris Agreement made by the United Nations, which aims to keep the global temperature rise this century under 2°C above pre-industrial levels.

Current CCSU research focuses mainly on CO_2 storage technologies, with a special emphasis on the assessment of geological reservoirs as traps for injected CO_2. Reactive technologies such as mineral carbonation have not yet been fully explored, probably due to the scarcity of relevant experimental data and the complexity of the mineral systems involved.

In this work, the research is focused on the study of sorption of carbon dioxide and methane on coal samples, and the implications for swelling when maintaining the processes under different conditions. Modelling of methane and carbon dioxide sorption and sorption-induced coal expansion has also been performed, in order to achieve a better understanding of the process.

The second part of the work is concerned with carbon dioxide utilization processes in waste materials. It was identified that high-calcium fly ashes are potential substrates for mineral carbonation. In this process, CO_2 is transformed into stable chemical forms called carbonates. Due to the very low utilization rate of high-calcium fly ashes, a feasibility study was undertaken for this type of fly ash carbonation.

Preliminary results on fly ash carbonation gave a reason to extend the research to different types of fly ashes produced in Europe. A selection of different types of waste material was made and a comparative study was undertaken regarding their potential for carbonation. As a complement to this, the carbonation process was optimized, in order to discover the influence of temperature, pressure, time, addition of water vapour and different types of pressure system on the reaction. To find the best conditions for the process, sequestration capacities and process efficiencies were calculated.

Along with CO_2 utilization through fly ash carbonation, an additional aim of this research was to determine the free lime decrease in the fly ash after carbonation. Reducing the free lime content in high-calcium fly ash could potentially increase the use of this type of waste in construction materials.

Aims of the PhD Thesis

The aims of this PhD thesis are as follows.

- Study of methane and carbon dioxide sorption under different temperature conditions.
- Optimization of the carbonation process conditions in order to achieve the best carbonation efficiency.
- Comparative study of the potential of different fly ashes for carbonation.
- Comparison of the carbonation of fly ash with simulated flue gas and a pure CO_2 stream.
- Reducing the free lime content in high-calcium fly ash via carbonation reactions.

Objectives of this thesis are as follows.

- Identification of high-calcium fly ash as a good substrate for carbonation and for CO_2 utilization.
- Acceleration of carbonation by increasing temperature or pressure, or by the addition of water vapour.
- Carbonation of high-calcium fly ashes leading to reduced free lime content.

Chapter 1. Carbon Capture Technologies

The Earth's climate has changed many times throughout its history. There have been seven cycles of glacial advance and retreat, with the end of the last ice age occurring 7,000 years ago. After that, the modern climate era started, along with human civilization. The observed current warming trend has almost 100% probability of being caused by human activity, starting in the 20^{th} century and proceeding at a high rate. Data collected from earth-orbiting satellites and other technological appliances provide strong evidence of a changing climate [1]. The heat-trapping property of carbon dioxide and other gases was already understood in the mid-19^{th} century. Greenhouse gases have the ability to transfer infrared energy through the atmosphere, in effect, warming the earth. There will be many effects of climate change: temperature rise, changes in growing seasons and precipitation patterns, increased probability of droughts, heat waves and hurricanes and a rise in sea levels. Global warming is the biggest environmental issue for the current human generation [2]. To address this phenomenon, UNFCCC (United Nations Framework Convention on Climate Change) signed the Paris Agreement in 2015, agreeing to take action to keep the global temperature rise below 2°C. In order to achieve this, worldwide carbon dioxide emissions must be reduced. Many different actions are being implemented. The three main approaches introduced are using non-polluting sources of energy, increasing energy efficiency and the expansion of carbon capture, sequestration and utilization techniques.

Carbon capture, sequestration and utilization (CCSU) encompasses all the techniques for capturing, storing and/or utilizing carbon dioxide which would otherwise be emitted or remain in the atmosphere [3]. These techniques are usually applied at places with significant carbon emissions: fossil fuel power stations, cement manufacturing plants, ammonia production plants, iron and non-ferrous metal production plants, industrial boilers and refineries. The general idea behind applying CCSU is to allow continued use of fossil fuels while still reducing CO_2 emissions into the atmosphere. World Energy Outlook [4] has shown that energy from fossil fuels will still be present in the world energy consumption mix in 2040, as shown in Figure 1. Global demand for energy is expected to increase by 25% by 2040. It is led by a constantly growing human population, increasing electrification and the expansion of economies, especially in the Asia-Pacific region [5]. In the future, there will be a need to use all energy sources to satisfy the growing demand. Oil and natural gas are expected to provide 60% of the global supply, while nuclear and renewables will grow by about 50%, providing 35% of the energy mix.

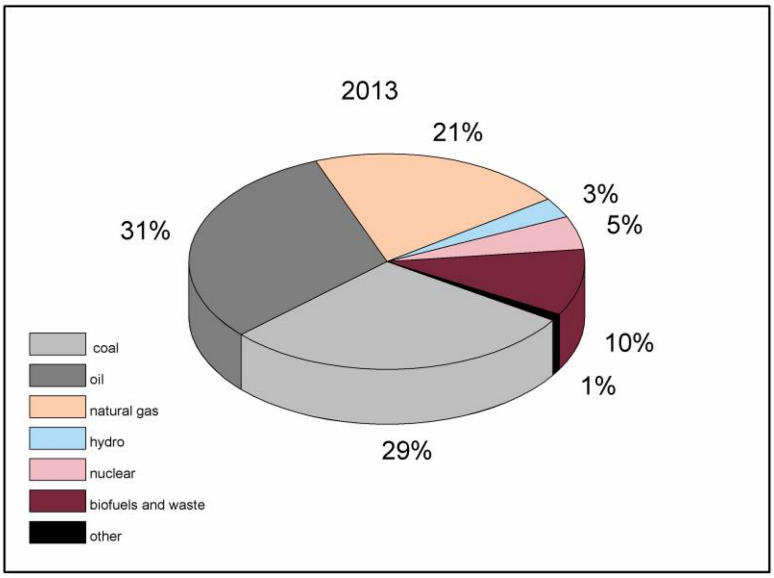

a)

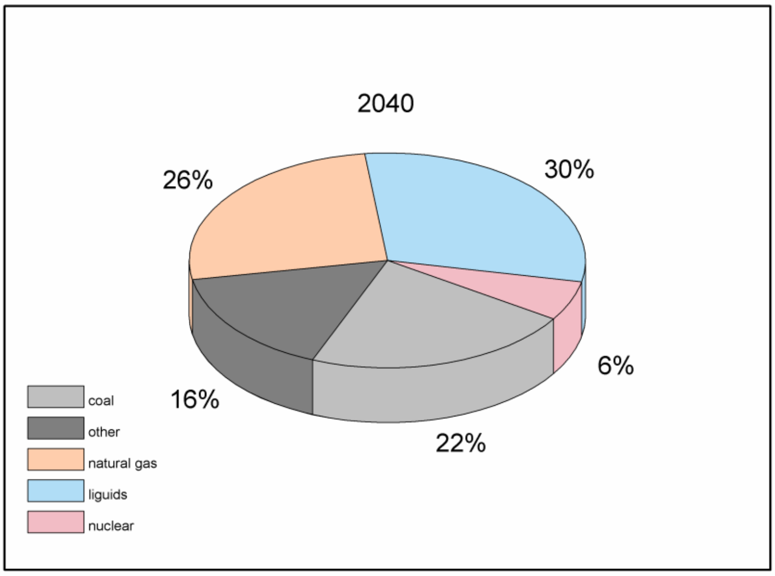

b)

Figure 1. World energy consumption in 2013 (a) and that predicted for 2040 (b) by fuel source (International Energy Outlook, 2017).

According to International Energy Outlook, energy-related emissions will increase from 33.9 billion metric tons (tonnes) in 2015 to 36.4 billion tonnes in 2030 and to 39.3 billion tonnes in 2040. This growth will be caused by economic development in non-OECD countries, as emissions in OECD countries will remain stable. The main sources of carbon dioxide emissions are: industrial processes, power generation, energy transformation, transport, residential and services [6]. Considering that polluting energy sources are expected to be in continued use, CCSU is the only option for achieving the aims of the 2015 Paris Agreement. Carbon capture and sequestration technologies can be generally divided into the processes of capturing and compressing CO_2, transporting it and either storing it in underground deposits or utilizing it for other purposes.

1.1 CO_2 Capture Technologies

Three main CO_2 capture technologies have been developed: pre-combustion, post-combustion and oxy-fuel combustion [7]. These technologies can be installed at power plants where energy from fossil fuels is generated.

1.2 Pre-Combustion CO_2 Capture Process

A pre-combustion system is applicable to integrated gasification combined cycle power plants (IGCC). In the pre-combustion method, a special air separation system is installed which produces a stream of a pure oxygen. This gas is injected into the gasifier, where it reacts with pulverized coal, and synthetic gas or 'syngas' ($CO + H_2$) is created. Next, steam is added to it in a water gas shift reactor, converting carbon monoxide into carbon dioxide. CO_2 is captured from this stream by physical washing and, after compression, is ready for either storage or utilization. The hydrogen is used as a fuel for turbine power and electricity. Recovered heat is used for producing steam that also drives a turbine generator for electricity. The carbon dioxide is captured from the syngas before it is combusted in the gas turbine [8]. The scheme of this technology is presented in Figure 2 [9].

This process is in principle the same for coal, oil or natural gas. However, when using coal or oil, more gas purification stages are needed to remove ash, sulphur or other impurities. Installing a pre-combustion CO_2 capture system in a gas-fired combined power plant causes a 16-percentage-point efficiency loss, as recent studies have shown [9]. The major efficiency losses are caused by syngas production (six percentage points), the WGS section (three percentage points), the H_2/CO_2 separation section (five percentage points) and the CO_2 compression and drying section (two percentage points). Research and development concerning pre-combustion technology involves efficiency improvements in all its stages: syngas and oxygen production, the water gas shift reaction, H_2/CO_2 separation, CO_2 compression and power production using hydrogen as fuel [10].

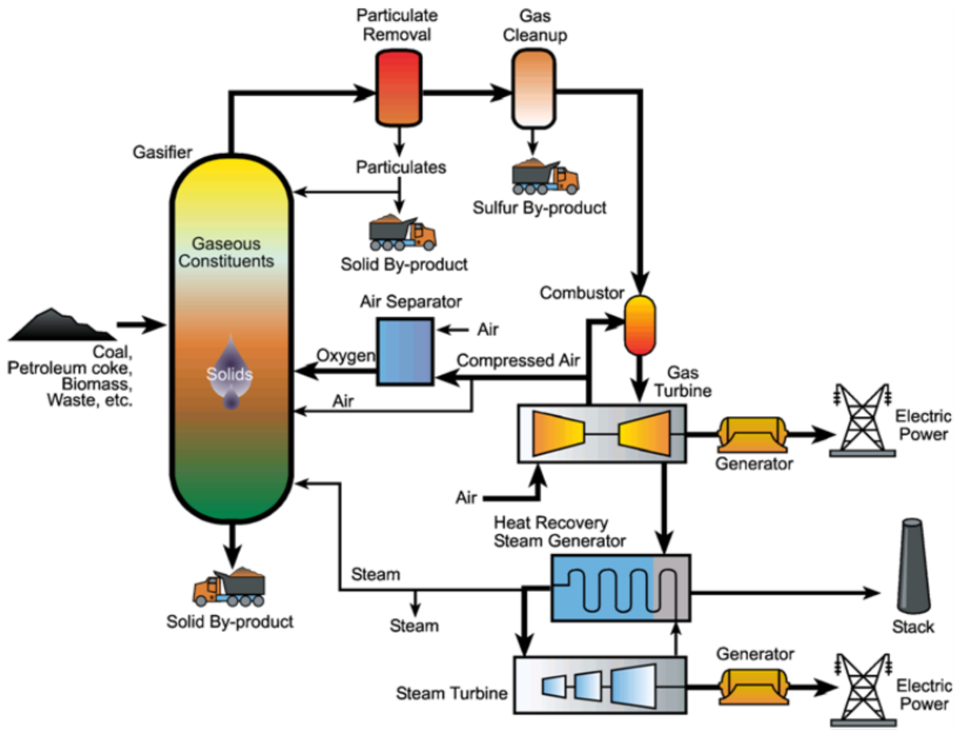

Figure 2. Integrated gasification combined cycle power plant diagram (US Department of Energy).

This technology has the advantage of producing carbon-free fuel (H_2) and carbon dioxide at elevated pressure (CO_2/H_2 concentration at the inlet is between 2 and 7 MPa), thus reducing the power consumption needed for the gas compression required for transportation and storage of CO_2.

One of the challenges in this capture technique is the adsorption process, during which syngas is scrubbed with a liquid solvent in order to selectively remove acid components, (i.e., CO_2 or H_2S). The absorption process is carried out in a column fitted with trays or structured packing. The acid components are discharged upon regeneration, after which the solvent is recirculated to the absorber. Gas components can be either attached physically or bound chemically to the solvent; thus, absorption processes are characterized as either physical or chemical. Sometimes mixing of physical and chemical solvents is used, exploiting the beneficial characteristics of both solvents. The capacity of the chemical solvents is determined by the amount of amine in the solution. Regeneration in chemical absorption is achieved by the addition of heat at low pressure through the reboiler of the stripping column. Chemical solvents are generally used for CO_2 removal from the gas stream at low CO_2 partial pressure, because they have a high affinity for carbon dioxide. The energy requirements are rather high for this type of solvent regeneration. In the case of physical solvents, their loading capacity depends on Henry's law, resulting in a linear dependency between the partial pressure of the removed component and the solvent loading [11].

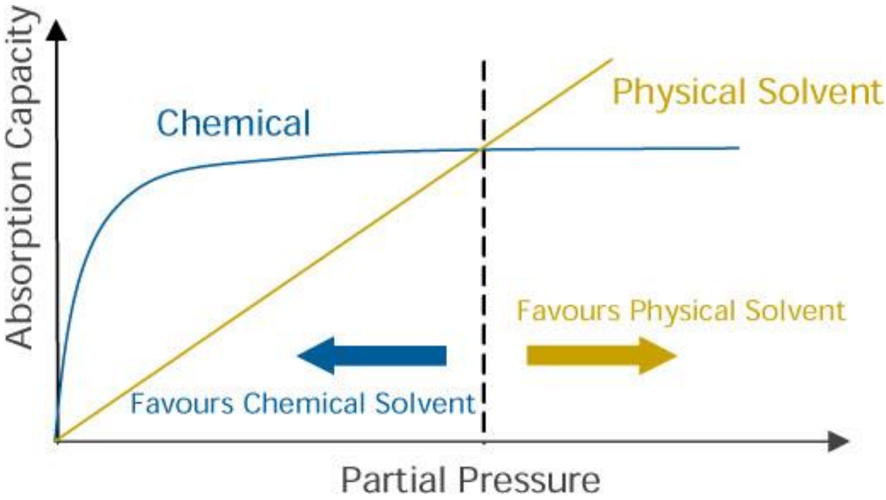

Figure 3. Comparison between chemical and physical solvents for pre-combustion processes (Global CCS Institute).

As there is a dependency between partial pressure and solvent regeneration, pressure reduction can be used for solvent recovery. Physical solvents are typically used to remove CO_2 and H_2S from raw gases made from oil and coal gasification. Physical solvents for pre-combustion capture are dependent on temperature and pressure, i.e., high partial pressures of CO_2 and low temperatures accelerate the absorption. High CO_2 partial pressures at the absorber mean that physical absorption is suitable for CO_2 capture in an IGCC system.

After gas separation, the CO_2 is compressed. In spite of being separated at moderately high pressures, at the end of the process the CO_2 is available as pure gas at about ambient pressure. The CO_2 stream is primarily compressed near the critical pressure; the compression energy consumption is optimized by using multiple intercooled stages. Next, the carbon dioxide is cooled to achieve the liquid phase. Lastly, liquefied CO_2 is pumped to the delivery pressure (110-150 bar, according to transport specifications). Depending on the separation technology used, the CO_2 stream could contain traces of N_2, H_2 and CH_4. Therefore, to achieve a higher purity level for storage or utilization, an additional purification process should be employed [12-14]. The cost of 1 tonne of CO_2 capture using pre-combustion technology is 24-41 US dollars for IGCC power plants and 42-87 US dollars for IGCC power plants based on supercritical pulverized coal [15].

1.3 Post-Combustion CO_2 Capture Processes

Units installed after fuel combustion to capture CO_2 are called post-combustion capture systems. Usually, they are installed after traditional purification structures for reducing contaminants such as

NO_x, SO_x and other small particles. Many different post-combustion capture technologies have been developed over many years: chemical absorption [16], adsorption [17], membrane separation [12,18], Ca looping technology [19–21] and cryogenic fractionation [22]. These methods are presented in Figure 4 [23]. Some of them are not yet commercially used for CO_2 capture in industrial processes [24]. One of the reasons limiting implementation of these types of technologies at coal power plants is low CO_2 partial pressure in the flue gas. Usually, the flue gas is at atmospheric pressure with only 12-15% concentration of carbon dioxide, and therefore it is problematic to separate it from the flue gas. In 2015, Rubin et al. [15] calculated the cost of capturing of 1 tonne of CO_2 at 36-53 US dollars for traditional power plants with pulverized coal-fired boilers and 48-111 US dollars for natural gas combined cycle (NGCC) power plants.

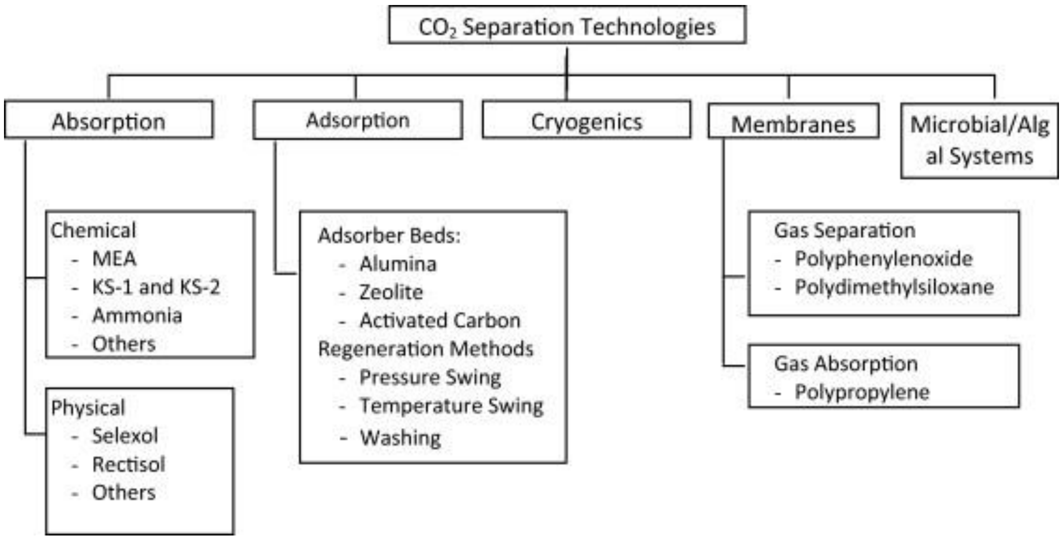

Figure 4. Post-combustion capture technologies (Wang, 2011).

Chemical Absorption

Among the technologies listed, chemical absorption is so far the most economical and feasible for implementation in industry. Monoethanoamine (MEA) is typically used as a solvent.

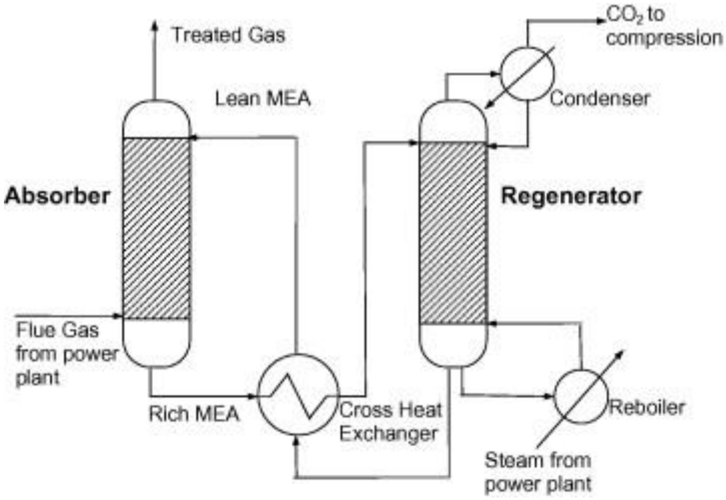

Figure 5. Chemical absorption technology for CO_2 capture (Lawal, 2010).

The chemical absorption technology scheme is presented in Figure 5 [25]. The flue gas passes through the absorber from the bottom upwards as the solvent solution flows downwards, creating a counterflow. During the contact of these two streams, some of the CO_2 from the flue gas is absorbed into the amine solution. After that, the solution rich in CO_2 is pumped up to the head of the stripper. In the stripper, there is also a counterflow, appearing when the CO_2 solution flows down the column and strips steam generated in the reboiler. Heat from stripping the steam breaks the chemical bonds between CO_2 and the solvent, and CO_2 is carried up by the ascending steam to the overhead condenser. When the condensed steam is directed back to the stripper as a reflux, the product stream with high CO_2 purity (around 99%) is collected. Subsequently, the clean amine solution is circulated back to the absorber. The CO_2 can be compressed for storage afterwards [26]. In this technology, the solvent regeneration in the reboiler has the highest energy consumption. For a 600 MW coal-fired power plant, the regeneration of MEA in the chemical absorption process requires 3.8-4.0 GJ/tonne CO_2. Three aspects of this process require optimization in order to reduce the energy consumption: operational parameters, process modifications and solvent development.

Adsorption

Adsorption on solid sorbents has several advantages compared to liquid-based absorption. From an engineering perspective, using solid sorbents eliminates the creation of liquid waste streams. Disposal routes for benign solid wastes are simpler and there is broad range of compatible operating temperatures [27]. Moreover, solid adsorbents are not volatile, and therefore the large energy penalties associated with the regeneration of liquid absorbents due to water evaporation in the stripper, are avoided. In a materials context, solid sorbents have higher cyclic CO_2 capacities per unit weight than liquid absorbents and can be more easily regenerated. Figure 6 presents a simplified scheme for solid sorbent CO_2 capture [28]. There are two types of adsorption technologies: fixed or moving. In fixed-bed adsorption, pelletized or structured sorbents are usually used in the form of packed beds. Packed beds can be configured as single vessels or moving/rotating vessel arrangements. Fluidized beds are one example of a moving adsorption system. The adsorber size is chosen depending on the cycle time (CO_2 uptake per cycle or per unit volume of material) and the CO_2 uptake required. Cyclic capacity depends on the sorbent material and the adsorber design. The main challenges for selecting solid sorbents for this process are sintering, attrition and chemical deactivation [29]. Costs related to adsorption are associated with the regeneration process and energy penalties caused by modifications to the system by the addition of the capture system. Thus, an adsorber system should not require significant modification of the sorbent material and its application to the existing apparatus should be easy.

Temperature swing adsorption (TSA) is another interesting approach in sorption technologies, as it can use the waste heat from the process itself. For example, waste heat sources can be found in cement and iron/steel processes [27]. Usually pressure swing adsorption (PSA) is preferred, as it is much faster than TSA. TSA must be combined with vacuum swing adsorption (VSA) in order not to pressurize the flue gas prior to adsorption. An alternative method to TSA is rapid temperature swing adsorption (RTSA). In this technology, hollow fibre adsorbents containing an impermeable core incorporating cooling or heating media are used, for efficient adsorption and faster regeneration.

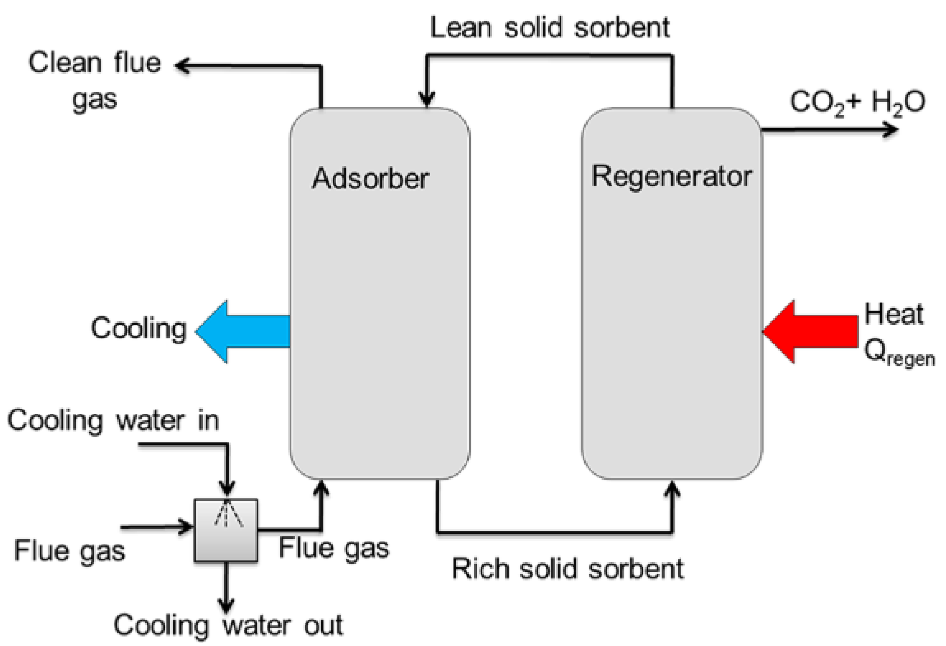

Figure 6. Scheme of solid sorbent CO_2 capture (Dijkstra, 2017).

Membrane Separation

Figure 7 illustrates the process for flue gas membrane separation technology [30]. The process starts with cooling the flue gas in a wet scrubber to achieve a suitable temperature for entering the membrane system. Next, a portion of the carbon dioxide passes through the membrane and a stream (permeate gas) with a higher CO_2 concentration is obtained on the other side. The residue part of the flue gas is called the retentate gas. As mentioned before, the partial pressure of CO_2 is very low, and a compressor plus vacuum pump arrangement is used to increase the partial pressure difference between the two different sides of the membrane.

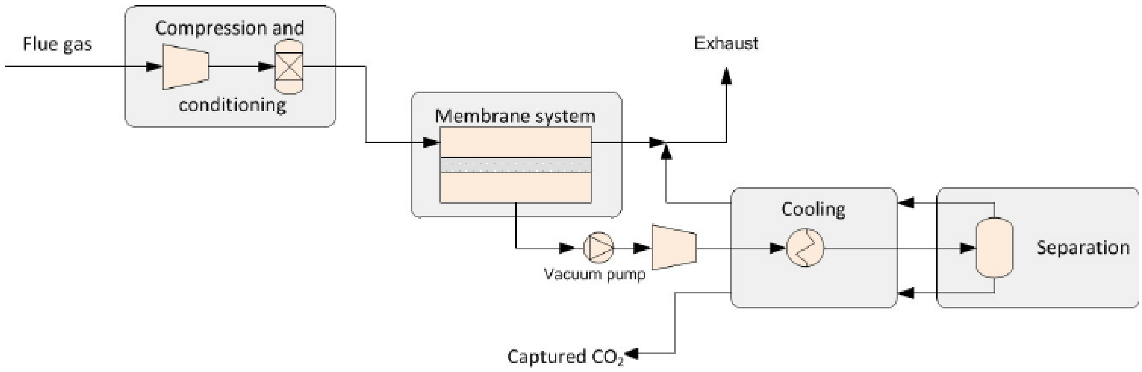

Figure 7. Membrane separation technology (Anantharaman, 2014).

Compared to the chemical absorption process, the membrane separation process seems to be simpler, since it has fewer components. Most of the energy consumption is generated by the compressor and vacuum pump [31]. There are two properties of the membrane material that affect the selectivity degree and CO_2 concentration in the permeate gas: permeability and selectivity. Materials used for the membrane are either inorganic (ceramic), organic (polymeric) or hybrid. Although this separation method has a high potential to be a low-energy and low-cost solution for CO_2 capture, its application is still limited by some practical problems: energy consumption of the compressor and pump, large membrane volume and cost.

Calcium Looping Technology

Calcium looping technology is a low-cost second-generation capture technology developed in recent years [32]. In this process, CaO is used as a recoverable sorbent for carbonation/calcination cycles, as presented in Figure 8 [33]. Therefore, CO_2 present in the flue gas stream (15% concentration) is captured by partial carbonation of the calcium oxide particles in a fluidized bed reactor (carbonator) at 650°C under atmospheric pressure. This temperature secures a low value of the equilibrium CO_2

concentration (~1% by volume) and fast enough reaction kinetics for carbonation to take place with a short reaction time, achieving reduction of the CO_2 concentration in the gas exiting the carbonator [34]. Calcium carbonate particles flow into a second reactor (calciner), where calcination takes place to regenerate the sorbent at temperatures above 930°C in a CO_2 environment with 70% and 90% concentration. The CO_2 gas exiting the calciner is thus ready for the next stage of processing or transport. Calcium looping technology has already been validated in pilot-scale coal-fired plants of capacity 1-2 MWth [33,35].

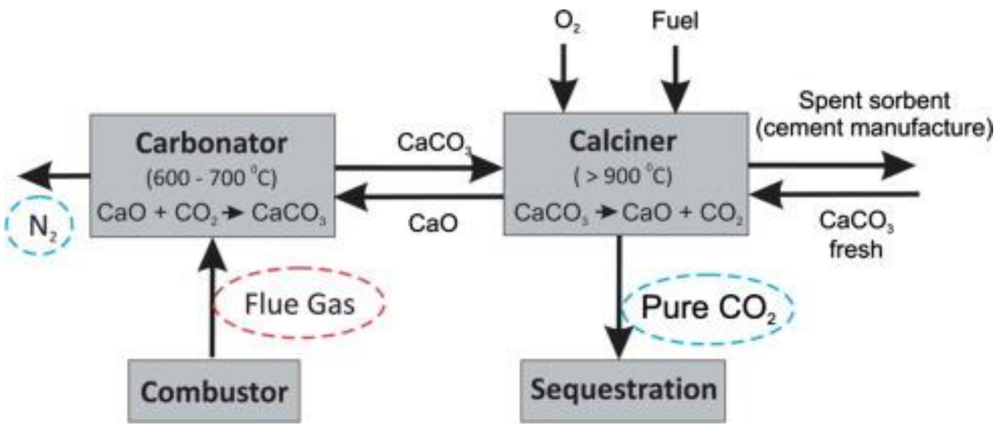

Figure 8. Calcium looping technology (A. Perejon, 2016).

Limestone ($CaCO_3$) is used to produce CaO by precalcination (prior to capture). During this process, some carbon dioxide is produced. The high fuel and oxygen consumption in this method creates an energy penalty. It is calculated that the heat consumption for this process imposes a net efficiency penalty of five to eight percentage points, which is lower than the penalties imposed by other capture methods [36]. It has been discovered that improving the multicyclic activity of the sorbent would considerably improve the energetic efficiency of this process [37].

1.4 Oxy-Fuel Combustion Technology

The concept underlying oxy-fuel capture technology is to extract nitrogen from the combustion air prior to combustion by the air separation unit. A simplified model of this technology is presented in Figure 9 [38].

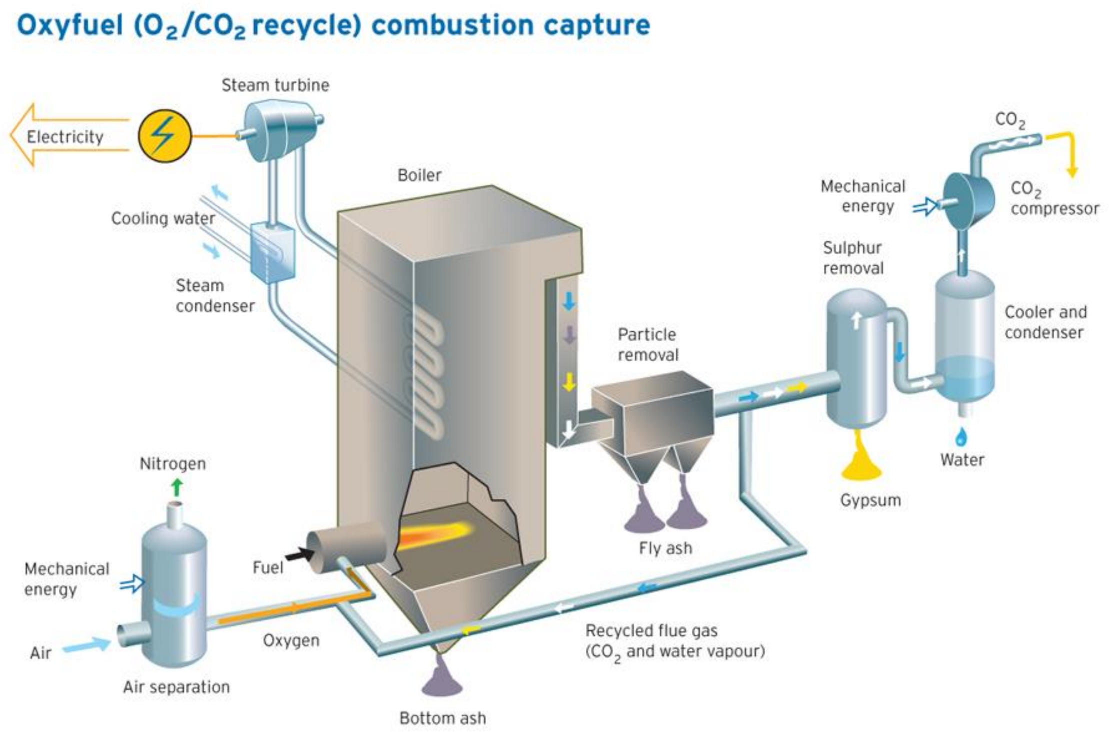

Figure 9. Simplified model of oxy-fuel capture unit (White, 2013).

To capture carbon dioxide, exhaust gas with a high concentration of CO_2 and water vapour is generated, followed by separation of CO_2 from the flue gas through dehydration and low-temperature purification processes.

Oxy-fuel combustion for power generation mainly consists of the following consecutive units.

• Air separation unit (ASU) – for oxygen production

• Boiler/gas turbine – for combustion of fuel and heat generation

• Flue gas processing unit – for flue gas cleaning or as a control system for gas quality (GQCS)

• CO_2 processing unit (CPU) – for final purification of the CO_2 in order to prepare it for transport and storage [39].

Removing nitrogen from the oxidant leads to the creation of a stream of highly concentrated CO_2 after the combustion process. Usually, recycled flue gases are used to substitute nitrogen and regulate the combustion temperature. The idea of applying oxy-fuel technology with flue gas recycling in fossil-fuelled plants to control emissions and produce high-concentration CO_2 streams for enhanced oil recovery (EOR), was first proposed in 1982 [40]. The main goal of this technology, as applied in coal-fired plants, is not to achieve high temperatures but to recover carbon dioxide in an air-like combustion environment. In existing power plants equipped with a conventional air combustion system, the combustion temperature and heat transfer rate are deliberately maintained, in order to use the existing equipment. In oxy-fuel technology, the operating conditions are similar to an air combustion environment and therefore do not create any economic or safety concerns. For these reasons, this system is seen not only as an adequate technology for new plants but also as a retrofit strategy for existing units [41]. The cost of capturing of 1 tonne of CO_2 using oxy-fuel combustion technology is 36-67 US dollars [15].

Chapter 2. CO_2 Storage in Underground Reservoirs

Geological carbon storage (GCS) is a promising technology for mitigation of increasing CO_2 concentrations in the atmosphere. Injection of the carbon dioxide into permeable subsurface formations is the only storage technology that has already been deployed and demonstrated on a commercial scale [42]. Ongoing projects on carbon dioxide storage are presented in Figure 10 and Table 1 [43].

Figure 10. CO_2 storage projects worldwide (Helmholtz Zentrum Potsdam, 2017).

To be suitable for carbon dioxide storage, geological formations must have the following characteristics.

- A depth of more than 800 m to keep the gas in a supercritical state
- A large storage volume
- Covered by a seal rock to prevent vertical flow of the gas
- Leak-free
- Permeable, in order to allow CO_2 injection at reasonable rates [44].

The injection of supercritical CO_2 into geological formations disrupts the physical and chemical state of the subsurface. The reservoir rock and overlying cap rock can be exposed to changes in the following: pore fluid pressure, thermal state, chemical reactivity and stress distribution. These changes can lead to mechanical deformation of the rock mass, affecting existing fractures or initiating new ones, which finally can affect the integrity of the overall geological carbon storage system (crucial for successful carbon dioxide storage) over a period of years [45]. GCS sites are practically unified systems. However, they can be divided by the physical and spatial scales of scientific investigations. For most applications, decoupling the physics by regarding the surrounding system as a boundary condition, works well. The coupling processes merge different combinations of thermal, hydrological, chemical, mechanical and biological effects. Coupled processes are dependent upon timescale and length scale. There is an indisputable necessity for understanding the coupling processes during GCS.

Table 1. Large CCS projects worldwide (Olajire, 2013).

Project	Location	Capture process	Storage	Year
Rangely Weber Sand Unit CO_2 injection project	USA	Gas processing	EOR with MMV (measurements, monitoring and verification)	1986
Sleipner CO_2 injection	Norway	Gas processing	Deep saline formation	1996
Weyburn-Midale	Canada/USA	Pre-combustion	EOR with MMV	2000
Enid Fertilizer	USA	Pre-combustion	EOR	2003
Salt Creek EOR	USA	Gas processing	EOR	2004
In Salah CO_2 injection	Algeria	Gas processing	Deep saline formation	2005
Snøhvit CO_2 injection	Norway	Gas processing	Deep saline formation	2006
Appalachian Basin R.E. Burger Plant	USA	Gas processing	Deep saline formation	2008
Michigan Basin, State-Charlton	USA	Gas processing	Deep saline formation	2008
Schwarze Pumpe	Germany	Oxy-fuel	Depleted gas	2008
ECO_2 Burger	USA	Post-combustion	Vented	2008
Pleasant Prairie	USA	Post-combustion	Vented	2008
Cincinnati Arch East Bend Station	USA	Gas processing	Deep saline formation	2009
AEP Mountaineer	USA	Post-combustion	Saline	2009
Shidongkou	China	Post-combustion	Commercial uses	2009
Lacq	France	Oxy-fuel	Depleted gas	2010
Puertollano	Spain	Pre-combustion	Recycled	2010
Brindisi	Italy	Post-combustion	EOR	2011
Buggenum	Netherlands	Pre-combustion	Vented	2011
Callide-A Oxyfuel	Australia	Oxy-fuel	Saline	2011
Plant Barry Project	USA	Post-combustion	Deep saline formation	2011

Ordos project	China	Post-combustion	Deep saline formation	2011
Mongstad	Norway	Post-combustion	Saline	2012
Ferrybridge	UK	Post-combustion	Depleted oil	2012
Carson (DF2)	USA	Post-combustion	EOR	2012
Big Bend Station	USA	Post-combustion	Vented	2013
Polk	USA	Post-combustion	Saline	2013
TCEP	USA	Pre-combustion	EOR	2014
Trailblazer	USA	Post-combustion	EOR	2014
Kemper County	USA	Pre-combustion	EOR	2014
HECA	USA	Pre-combustion	EOR	2014
Belchatow	Poland	Post-combustion	Saline	2014
Karlshamn	Sweden	Post-combustion	Vented	2014
FutureGen	USA	Oxy-fuel	Saline	2015
Daqing	China	Oxy-fuel	EOR	2015
ROAD	Netherlands	Post-combustion	Saline	2015
Compostilla	Spain	Oxy-fuel	Saline	2015
Gorgon CO_2 injection	Australia	Gas processing	Deep saline formation	2015
BP Peterhead (DF1)	UK	Post-combustion	Depleted gas	2015
Don Valley Power Project	UK	Post-combustion	EOR	2015
Teeside Low Carbon	UK	Pre-combustion	Depleted oil	2016
Killingholme	UK	Pre-combustion	Saline	2016
White Rose	UK	Oxy-fuel	Saline	2016
WA Parish	USA	Post-combustion	EOR	2017
Bow City	Canada	Post-combustion	EOR	2017

During injection, CO_2 is transferred to the geological reservoir at depths between 800 m and 5,000 m, where the pressure is higher than 74 bar. Thus, the CO_2 is in a supercritical state. At a depth of 800m, 1 tonne of carbon dioxide occupies 1-2 m^3, allowing significant amounts of the gas to be stored in a relatively small space [44].

Geological reservoirs are composed of porous rocks: sandstones and carbonates, with pores that can be filled with CO_2. A thick and impermeable fine-grained or rock salt cap rock is placed on top of the reservoir, preventing any CO_2 from escaping to the surface. This cap rock is important for maintaining a closed reservoir and for preserving the injected CO_2 at a proper depth.

Different sources lead to different cost estimates for CO_2 storage in geological formations. A typical range for onshore storage costs on a common basis is between 1 and 18 US dollars/tonne of CO_2 [15]. There are different types of geological reservoirs for carbon dioxide storage, as shown in Figure 11.

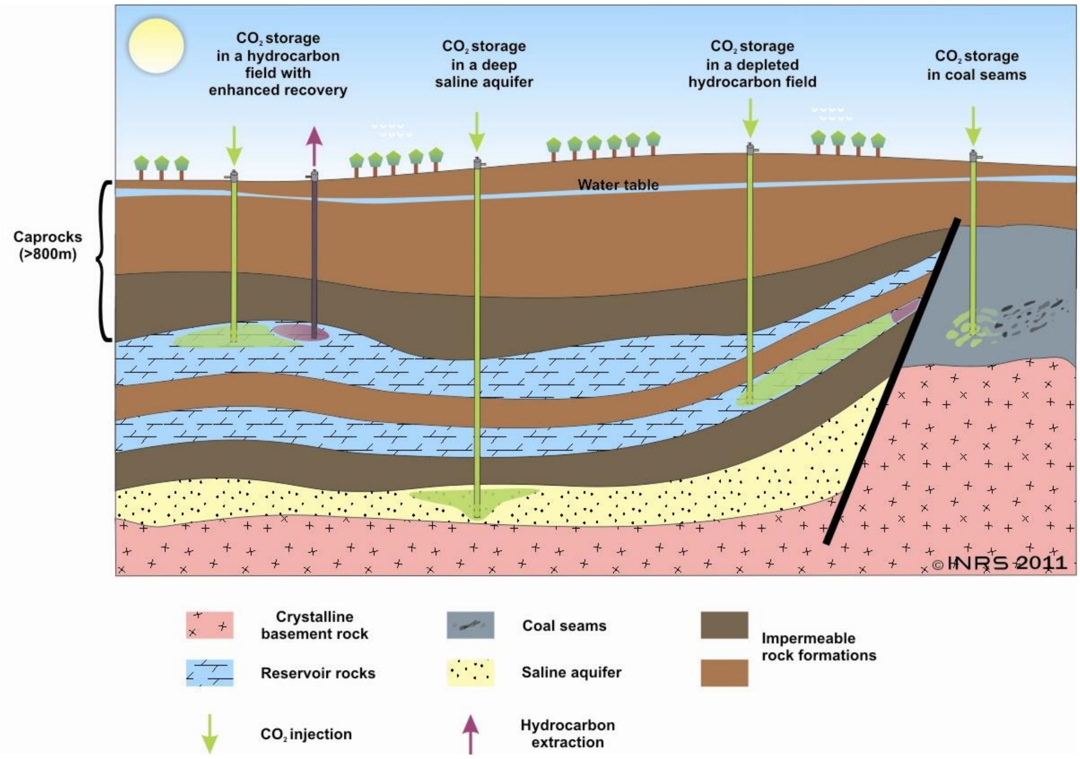

Figure 11. Different types of reservoirs for the geological storage of CO_2 (GRREBS, 2018).

2.1 Geological Storage of CO_2 in Depleted Oilfields and Natural Gas Fields or Fields Undergoing Depletion

One of the options for storing captured CO_2 is to inject the gas into oilfields, at the same time enhancing the production of oil from the fields. This option, called CO_2 enhanced oil recovery (CO_2-EOR), is an economical approach to achieving a low-carbon future. Revenues from CO_2 sales to the EOR industry can partially offset the costs of CO_2 capture. This technology has been commercially deployed in the US and Canada for many years. Some of the projects were not developed with CO_2 storage as one of the objectives. CO_2-EOR is not a new invention – commercial and profitable systems have existed for 30 years where suitable oilfields are combined with easy access to carbon dioxide [45]. In 2018, more than 100 CO_2-EOR projects in the US resulted in 250,000 barrels per day of incremental oil. An extensive pipeline system has been developed to transport the carbon dioxide needed for oil recovery.

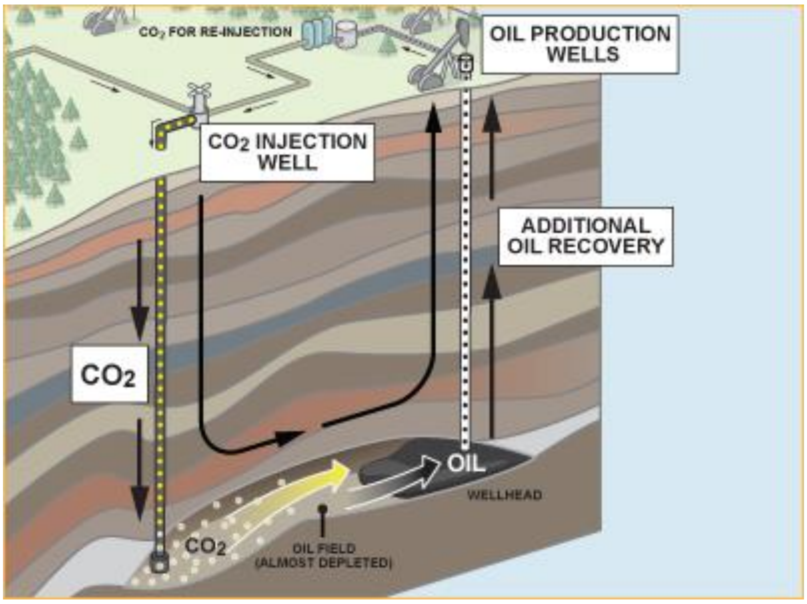

Figure 12. Enhanced oil recovery technology (Clean Air Task Force, 2018)

Suitable oilfields where this technology could be deployed need to meet the technical criteria for achieving miscibility and must have sufficient amounts of unrecovered oil. CO_2-EOR technology has the potential to store significant amounts of carbon dioxide: 54 of the largest oil basins in the world could produce 470 to 1,070 barrels of oil and store 140-320 billion tonnes of CO_2 [46].

The mechanism of CO_2-EOR is as follows [47].

- Oil viscosity reduction
- Oil swelling due to CO_2 dissolution in crude oil
- Removal of near-well damage
- Solution gas driving via gravity drainage
- Improved drainage of reduced viscosity oil by encroaching water
- Vaporization of lighter oil components by CO_2
- Reduction of water permeability
- Reduction of interfacial tensions.

In the US, roughly half of the potential CO_2 demand for ongoing CO_2-EOR projects can be satisfied by large, anthropogenic CO_2 sources within distances comparable to existing and planned CO_2 pipelines serving EOR projects (800 km).

Many techno-economic models have been developed in order to estimate the cost of CO_2-EOR systems. Estimating the storage capacity in hydrocarbon reservoirs is simple, since the reservoir intervals are well described and capacity estimation is done using the replacement principle, in which the equivalent volume of oil and/or gas can be used for CO_2 storage. Torleif et al. studied the economic potential of this technology in the North Sea [48]. Eighteen Norwegian and 30 UK oilfields were considered, with 40 years of project lifetime and CO_2 deposition at a constant rate of 178 million tonnes/year. The potential for additional oil production was estimated at between 658 and 696 million m^3. The price of CO_2 was calculated as between 23-94 US dollars/tonne and that of the oil as 20-150 US dollars/bbl. When oil prices reach 90-100 US dollars/bbl, then the CO_2 price is close to the cost of CO_2 capture, i.e., 50 US dollars/tonne [48].

2.2 Geological Storage of CO_2 in Deep Saline Aquifers

In contrast to the estimation of CO_2 storage capacity in oil and gas reservoirs, calculations for storage in saline aquifers are much more problematic. The concepts are either based on considering the whole aquifer or considering structural and stratigraphic traps. In addition, carbon dioxide can be considered either as a free phase or in solution. CO_2 can be physically trapped (in structural and stratigraphic traps, at irreducible saturation in the pore space) or chemically trapped (in solution form or by transforming it into a mineral), or both simultaneously [49]. Another difficulty in estimating the storage potential in saline aquifers is that different CO_2 bonding processes occur over different periods of time [50]. For the purpose of evaluation, the time of CO_2 injection is important, as well as the time of CO_2 free-phase immobilization, when this phase no longer migrates, and the final extent of the CO_2 plume can be determined (Figure 13). When CO_2 is injected into a structural or stratigraphic trap or a closed aquifer, then the times of immobilization and cessation of injection are the same. If carbon dioxide injection occurs in an open aquifer, then the immobilization occurs after the cessation of injection. Therefore, a closed aquifer is defined as an aquifer where CO_2 reaches the aquifer's boundaries before injection ends, while in an open aquifer, gas migrates due to its buoyancy and reaching the aquifer's boundaries takes a longer time.

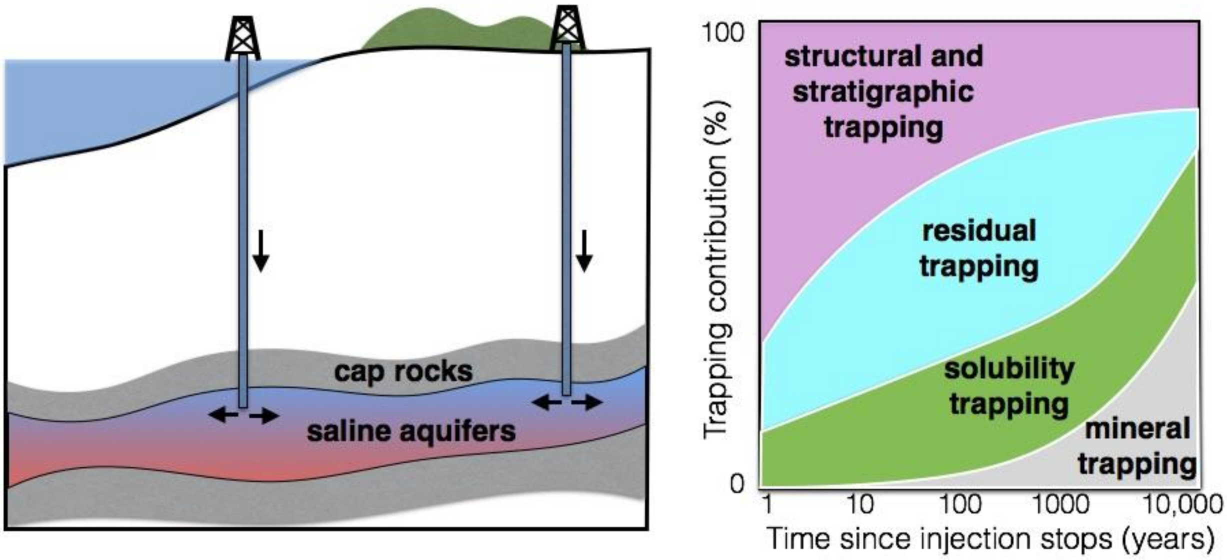

Figure 13. The scheme of CO_2 storage in saline aquifers (Gan, 2017).

As can be seen in Figure 13, mineral trapping occurs over times longer than 10 years, and for this reason it does not contribute to the storage capacity during the gas injection and is not considered in the capacity estimation. Carbon dioxide which dissolves in the aquifer water has its density reduced by 1% and sinks to the bottom of aquifer due to gravitation and consecutive missing [51].

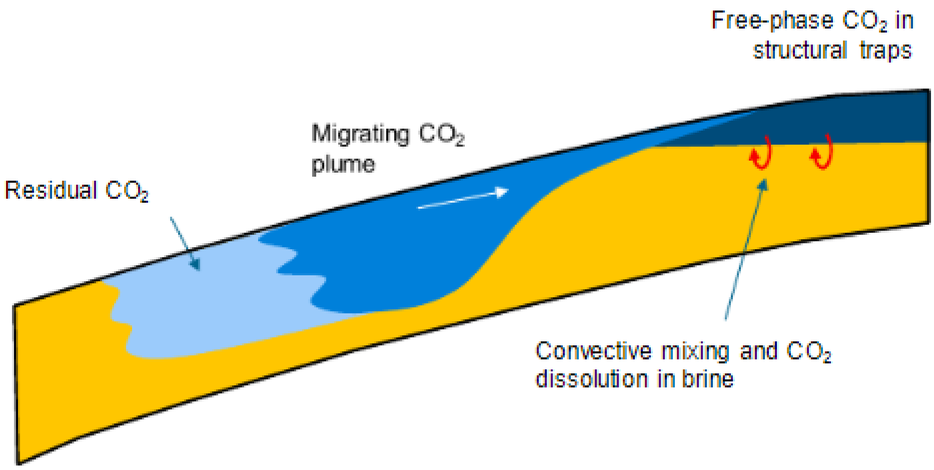

Figure 14. Main trapping mechanisms for saline aquifer storage of CO_2 (Ringrose, 2018).

In situ factors influencing the CO_2 solubility are pressure, temperature and salinity. Usually, both mineral trapping and solubility in water are omitted when estimating the storage capacity. The effective storage capacity is based on a storage efficiency approach, where not all the pore space is available and saturated with CO_2. Recently, the storage efficiency and efficiency coefficients have been calculated for gas storage in the free phase in deep saline aquifers. These are the basics of the techno-economic resource-reserve pyramid presented by Bachu et al. [52].

The characteristics of the storage aquifer are as follows.

- In situ conditions: pressure, temperature and salinity. These parameters directly affect the density and viscosity of the fluids inside the reservoir
- Displacement characteristics of the CO_2/brine system, among other irreducible saturations and the relative permeability of CO_2 and water
- Internal characteristics: lithology, environment of deposition, porosity and permeability distributions, heterogeneity and compressibility
- External characteristics: area extent, thickness, slope and topography of the aquifer top, local structural traps and boundaries.

Two commercial ongoing projects where CO_2 is stored in saline aquifers, are Sleipner, started in 1996 and Snøhvit, started in 2008, both located in the offshore territory of Norway [53]. A total of 22 Mt of CO_2 has been stored in these two projects combined. In Sleipner, CO_2 is injected and stored in the Utsira formation at a depth of 800-1,000 m below sea level. One shallow long-reach well is used for the gas injection, 2.4 km from the production platform. The CO_2 plume-monitoring observations at Sleipner reveal an overall storage efficiency of 5% (after 14 years of injection). Nearly one tenth of this volume is dissolved in the brine phase. The second project is part of the Snøhvit gas field development in the Barents Sea. Carbon dioxide is extracted from the gas at the onshore gas processing plant (Melkøya) and transported through a 150-km pipeline to a subsea injection location.

2.3 Storage in Unmineable Coal Seams

Carbon dioxide can be effectively stored in unmineable coal seams, i.e., seams which cannot be mined for energy purposes. Since any action with respect to the coal, such as mining, combustion or gasification, would release the gas stored in the seam, only unmineable coal seams are seen as suitable for CO_2 storage [54]. There are many factors affecting coal mineability. The reservoir cannot be mined if it is too deep, thin or small, or of poor quality. In addition, there may be land restrictions or mining may have low economic feasibility. Coal is defined as unmineable if its placed deeper than 350 m of overburden, according to the Department of Energy (DOE). The Midwest Geological Sequestration Consortium defines all coals shallower than 152 m as mineable and those at depths of 152-305 m as unmineable. As mining technologies are constantly being improved, the definition of mineable coals constantly changes, and it is problematic to quantify the possible CO_2 storage capacity in coal. Practical thinking leads to the estimation of the potential CO_2 storage in coal at the current time, keeping in mind that part of the coal could eventually be mined, and the potential may be smaller. The Department of

Energy Regional Carbon Sequestration Partnership calculated that between 60 and 117 billion tonnes of CO_2 could be stored in coal, but other sources estimate the storage capacity at up to 200 billion tonnes of CO_2.

The processes responsible for CO_2 storage in coal are adsorption and diffusion [54]. Diffusion takes place when the CO_2 molecules move through large (greater than 30 nm) pores, fractures and cleats. Sorption of the gas occurs via different adsorption processes: onto internal surfaces, into the molecular structure and as free gas in fractures, cleats and voids. An additional process is the dissolution of CO_2 in groundwater. The adsorption process leads to CO_2 bonding with the coal, causing the gas to be physically trapped on the coal when sufficient pressure is maintained. According to Ceglarska and Zarebska [55], adsorption is considered to be the most important process for CO_2 retention in coal. Another important insight is that when the gas is absorbed into the coal, processes of adsorption and gas penetration of the solid matrix often lead to swelling of the coal [56]. Successful storage of CO_2 in coal seams requires sufficient permeability along pores and fractures.

Storage of carbon dioxide can be connected with recovery of methane (CH_4), which is sometimes trapped within the coal seams. This process is called CO_2-enhanced coal bed methane recovery (CO_2-ECR) and is similar to the CO_2-EOR [57] process presented in Figure 15. Coal seam methane, or coal bed methane is an inherent part of coal and forms during coalification.

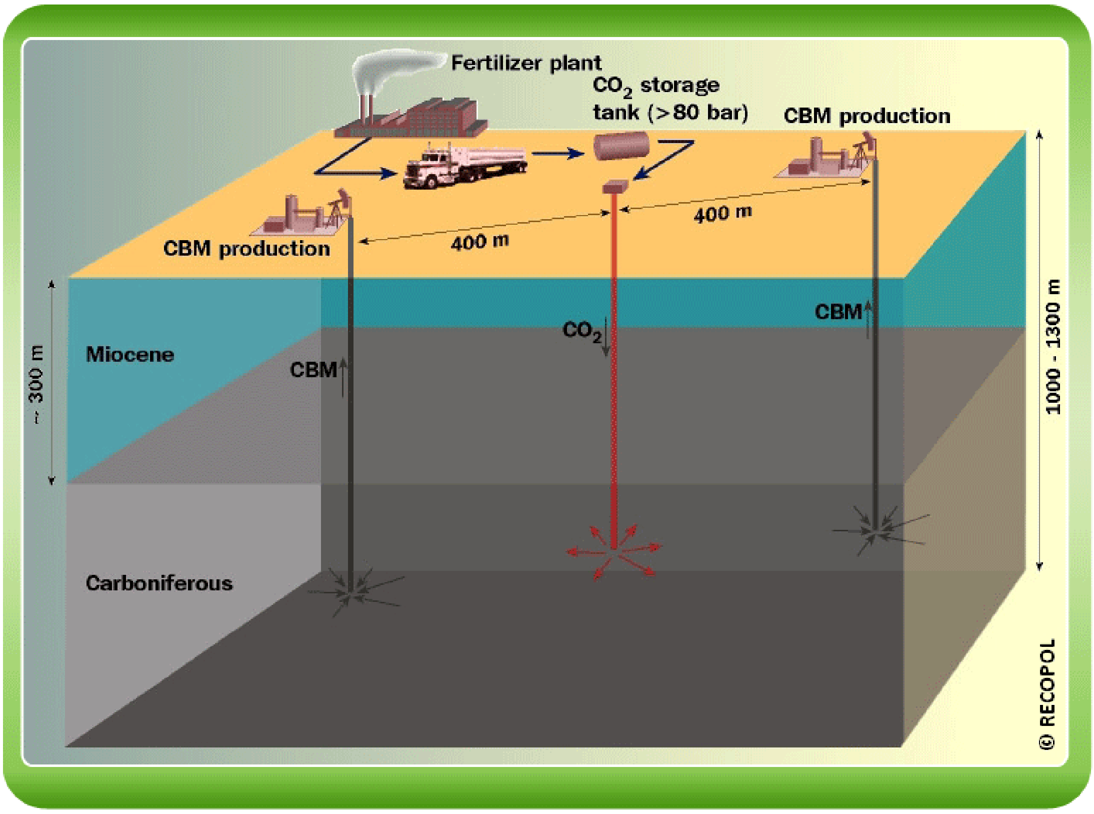

Figure 15. Concept of enhanced coal bed methane (ECBM) recovery, enabling exploitation of the natural gas (methane) found in coal combined with CO_2 storage (CCUS, 2011).

There are two methods for recovering methane from coal deposits. The first method uses a pressure gradient between the underground seam and atmospheric pressure. The second method is called enhanced coal bed methane recovery. In this technology, the pressure gradient is achieved by various induced or artificial processes: dewatering, hydraulic fracturing or injecting another gas to decrease the partial pressure of natural gases present in the reservoir. The gases injected are commonly N_2, CO_2 or a mixture of these, and this process is called displacement desorption. When CO_2 is injected into coal, its molecules are entirely adsorbed in the coal micropores, and if methane is present, they replace the methane molecules, which diffuse through the pore spaces in the matrix and flow through the fractures or cleats. This phenomenon occurs because coal displays a higher sorption affinity towards CO_2 than CH_4, due to the higher adsorption energy and smaller molecular diameter of CO_2. The CH_4 is collected and used as source of energy. The replacement of CH_4 by CO_2 in coal reduces anthropogenic CO_2 and contributes to the reduction of climate change, while providing methane recovery, creating additional energy for sustainable development. Nevertheless, it is important to point out that the recovered CH_4, when combusted, will emit CO_2 to the atmosphere.

In 1995, the first CO_2-EMR project was tested in San Juan Basin, New Mexico, US. It helped to identify problems which may be faced during the process, causing decreasing formation permeability and slow rates of CO_2 injection. The following tests were done in Fenn and Big Valley (Canada), the Isikari coal fields (Japan), the Upper Silesian Basin (Poland), Quinshui Basin (China), Appalachian Basin (US), Illinois Basin (US) and Black Warrior Basin (US).

The field experiment RECOPOL in the Upper Silesian Basin in Poland (Figure 16) started in August 2004, with CO_2 injection into three seams of Carboniferous age, at depths between 900 and 1,200 m [58].

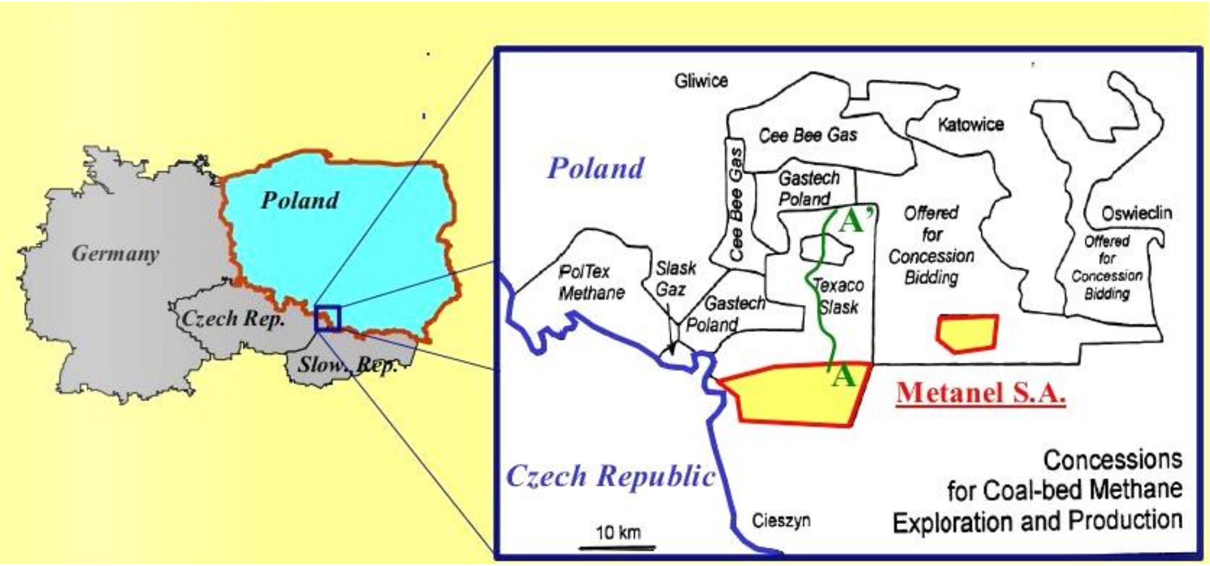

Figure 16. RECOPOL project location (Wageningen, 2009).

This pilot project was located next to the existing well for methane recovery, to establish a baseline production. Injections of 14-15 tonnes of CO_2/day were made up to April 2005. The medium used was liquid CO_2 from an industrial source. During the tests, the seam was fractured because of the reduction in the permeability of the coal, possibly due to its swelling. In addition, the injection pressure needed to be twice as high as the reservoir pressure. A total of 760 tonnes of CO_2 were injected during the whole testing period. Methane production increased significantly during the CO_2 injections, compared to the baseline production. It is predicted that in the Upper Silesian Basin district, other coal seams with high permeability, thicker seams and seams with high gas content exist, where the next projects could take place [59].

Chapter 3. Mineral Carbonation

Mineral carbonation (MC) is a process of CO_2 fixation in the form of stable carbonate minerals, i.e., calcite ($CaCO_3$), magnesite ($MgCO_3$) or siderite ($FeCO_3$), which was first described by Lackner et al. in 1995 [60]. In nature, this process is called silicate weathering and occurs over geological timescales with very slow kinetics. Silicates act as a source of alkaline and alkaline earth metals, which react with carbon dioxide. The process of carbonation usually refers to a simple two-step chemical reaction producing stable magnesium carbonates or calcium carbonates [61]. Firstly, hydration of the calcium/ magnesium oxide occurs, followed by carbonation of the calcium/magnesium hydroxide.

1. $$CaO + H_2O \rightarrow Ca(OH)_2 \tag{1}$$

   $$Ca(OH)_2 + CO_2 \rightarrow CaCO_3 + H_2O \tag{2}$$

2. $$MgO + H_2O \rightarrow Mg(OH)_2 \tag{3}$$

   $$Mg(OH)_2 + CO_2 \rightarrow MgCO_3 + H_2O \tag{4}$$

The potential for CO_2 storage in the earth's crust in the form of carbonates is substantial. The current total mass of CO_2 in the atmosphere is 800 Gt, while 39 million Gt of carbon exists in rocks, in the form of marble, limestone and chalk [62]. Next to silicates, another resource that can be used for mineral carbonation is industrial wastes that are rich in alkaline metals, such as Ca, Mg or Fe [63], as shown in Figure 17 [64]. Nevertheless, from the storage perspective, magnesium-based silicates are favoured, since significant amounts are available worldwide and, in theory, they could bind all fossil fuel-produced carbon.

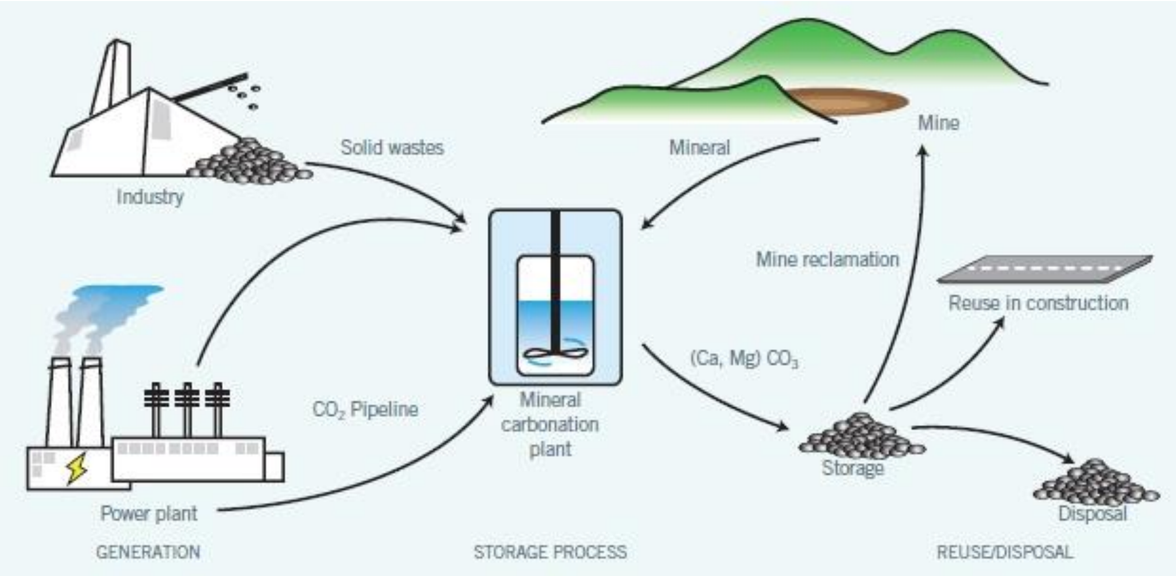

Figure 17. CO_2 as feedstock for mineral carbonation (Global CCS Institute, 2014).

Magnesium silicates can be divided into olivine [$(Mg,Fe)SiO_4$], forsterite ($MgSiO_4$), serpentine [$Mg_2Si_2O_5(OH)_4$] and some other smaller groups in lower quantities. The full list of all the natural minerals studied for carbonation includes basalt, brucite, chrysolite, dunite, forsterite, harzburgite, olivine, orthopyroxene, peridotite, pyroxenite, serpentine and wollastonite. Oxides and hydroxides of Ca and Mg are good materials for carbonation, and they can be found in mafic and ultramafic silicate minerals which can be carbonated as carbonic acid (H_2CO_3, pKa = 6.3), which is more acidic than silicic acid [$Si(OH)_4$, pKa = 9.5]. Rocks containing magnesium silicate display a higher MgO concentration (up to 50% by weight) than rocks with calcium silicates, (i.e., basalts), which have a CaO content of around 10%, implying a smaller theoretical CO_2 storage capacity. High metal oxide content is an important characteristic as it implies a lower R_{CO2} factor (ratio of the mass of mineral needed to the mass of CO_2 fixed, with complete conversion assumed). Specific data are presented in Table 2 [60].

Table 2. Compositions of minerals and their CO_2-specific storage characteristics (Lackner et al., 1995).

Rock	MgO (wt%)	CaO (wt%)	R_{CO2} (tonne rock/tonne CO_2)
Olivine	49.5	0.3	1.8
Serpentine	40	-	2.3
Wollastonite	-	35	3.6
Talc	44	-	2.1
Basalt	6.2	9.4	7.1

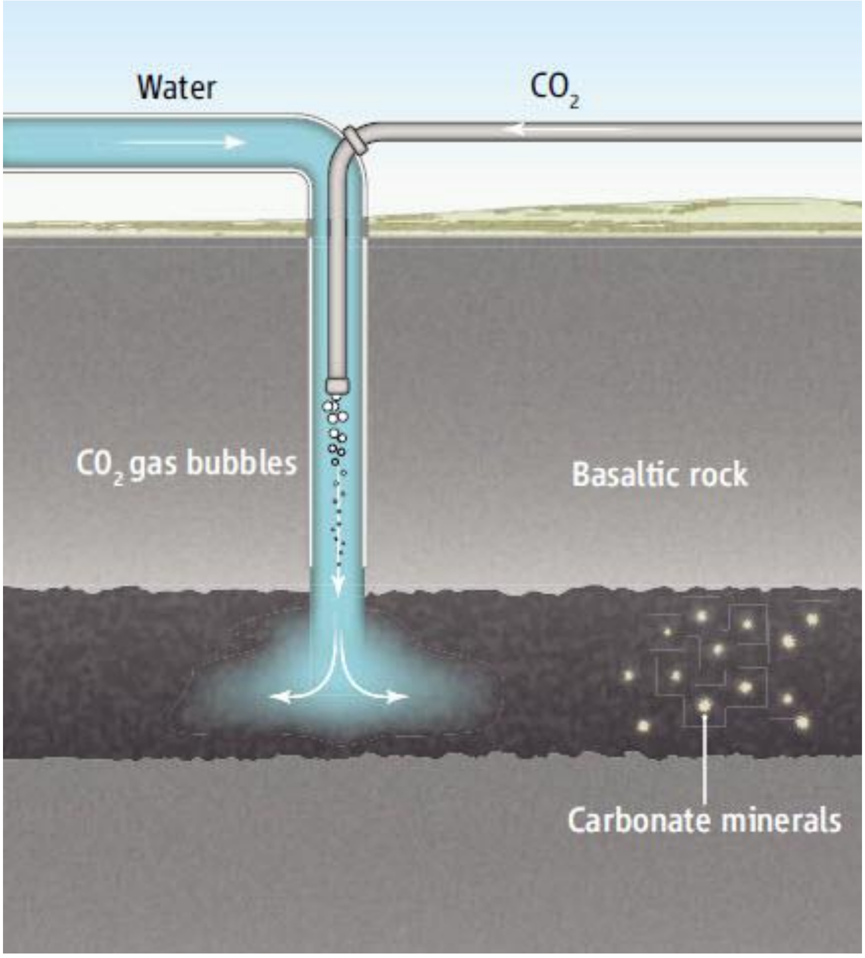

Figure 18. In situ carbonation - the CarbFix project (CarbFix, 2014).

There are two types of carbonation processes: ex situ (Figure 17), where the reaction is held in a chemical plant and silicates are mined before the reaction and undergo pretreatment and in situ (Figure 18) [65], where CO_2 is injected into silicate-rich geological formations. In the ex situ process, carbon dioxide is transported from the source location to the carbonation reactor and combined with crushed Ca/Mg-bearing minerals, and if appropriate conditions are met, the reaction will take place. Afterwards, the process products are separated, collected and used as a raw material or transported back to the mining site.

The carbonation reaction is exothermic [66]. Depending on the substrate, more or less heat can be released during this process. The exothermic effect of silicates carbonation is smaller than for the reaction with $Mg(OH)_2$ or $Ca(OH)_2$.

Olivine: $Mg_2SiO_4 + 2CO_2 \rightarrow 2MgCO_3 + SiO_2 + 90$ kJ/mol (5)

Wollastonite: $CaSiO_3 + CO_2 \rightarrow CaCO_3 + SiO_2 + 90$ kJ/mol (6)

Serpentine:

$Mg_2Si_2O_5(OH)_4 + 3CO_2 \rightarrow 3MgCO_3 + 2SiO_2 + 2H_2O + 64$ kJ/mol (7)

Formation of carbonate phases is thermodynamically favourable during the reaction between CO_2 and silicates [61]. As this reaction releases heat, low temperatures are suitable for the reaction to occur. At temperatures above 900°C (for calcite) and 300°C (for magnesite) and a CO_2 partial pressure of 1 bar, the reverse reaction, called calcination, occurs. One problematic aspect that can arise in the reaction is the formation of a silica or carbonate layer over the substrate surface, which tends to hinder further reaction and limits the conversion rate [67]. Research into carbonation is attempting to solve this issue by accelerating the process and increasing the kinetics.

As previously stated, as well as natural minerals, industrial alkaline wastes can be used for the carbonation process. Most of these are easily accessible at low cost, have high reactivity and can be found in close proximity to CO_2 sources, and the reaction itself can change their properties and increase utilization. Studies show that a successful process does not need such extreme conditions as those for ultramafic rocks, and a high conversion rate is achieved [68]. Nevertheless, industrial waste production is not enough to cover all CO_2 emissions, as can be achieved in the case of natural minerals. The list of all studies on alkaline waste for MC includes studies on: argon oxygen decarburization slag, air-pollution control fly ash, biomass ash, blast furnace slag, bottom ash, industrial brines, cement wastes, chrysolite mining tailings, coal-combustion fly ash, ladle slag, lignite-combustion fly ash, mine tailings, municipality ash, Nirex Reference Vault Backfill, oil shale ash, paper mill waste, paper waste water incineration ash, pressed lime waste composites and steelmaking slag [69–71]. Mine tailings are generated during mining activities, and although they are classified as wastes, most of them contain minerals.

3.1 Ex Situ Mineral Carbonation

Different process routes have been developed in order to optimize carbonation, namely, ex situ routes, in situ routes and other MC routes (Figure 19) [72,73]. The ex situ process is an above-ground carbonation of alkaline-bearing materials through chemical processes. This route usually has two steps, involving pretreatment of the material and subsequent sequestration. In the case of rocks, pretreatment involves mining, crushing and milling prior to carbonation, in order to increase the reactive surface of the substrate. Two different concepts for this method have been identified: direct and indirect methods. In direct technologies, carbonation is performed in a single step and can be achieved via either a gas-solid dry reaction or in aqueous solution. In the indirect method, reactive metals are first extracted from the waste or rock, and then carbonated as a separate step.

There are three main challenges for the implementation of ex situ MC on an industrial scale. With current technology development, there are large energy costs and a need to accelerate the process in order to make it efficient. Furthermore, large amounts of silicates are needed to sequester significant amounts of carbon dioxide. A 4-MW power plant emits 1.1 Mt of CO_2. To capture this, 6.4 Mt of forsterite (the most efficient silicate for fixing CO_2) would be needed. This process would result in the creation of 2.6 million m^3 of magnesite. In addition, forsterite is only one among a number of different minerals in rock, so the total mass of rock required to utilize CO_2 is much bigger.

Ex situ carbonation operations are characterized by high costs, as a result of transporting minerals to the carbonation reactor, grinding the material, heating the system and storing/disposing of the final product. The extent of these operations influence the final cost of carbonation. It was found that the final cost of carbonation alone would be around 54 dollars/tonne of CO_2 [74]. Additional costs, for example those associated with mining and moving the rocks and final product storage, significantly increase the final price. Placing the carbonation reactor in a close proximity to the CO_2 emission source would result in no additional cost related to the gas transport. Another possibility is using CO_2 captured directly from the air.

Direct Carbonation Methods

Gas-Solid Dry Carbonation

In this route, an alkaline solid reacts with gaseous CO_2, usually at increased pressure and temperature. Only a few research groups are still investigating gas-solid carbonation of reactive waste, as the conditions of this process are not appropriate for silicates. Most of the studies of dry carbonation of natural minerals gave insignificant or negligible results, even at high pressures. Montes-Hernandez et al. [75] achieved a high degree of carbonation (greater than 0.9) using CaO in isothermal conditions at 600°C and 800°C, and a much lower carbonation conversion rate for $Ca(OH)_2$ at 400°C. Until very recently, studies involving dry carbonation had been practically abandoned, as this reaction has a very slow reaction rate, and only examples of successful dry carbonation on industrial waste were presented [76-79]. Exergy analysis of direct dry carbonation shows that this process has a positive net exothermic effect [66]. It has also been proved that the addition of a small amount of water vapour to the reaction mixture accelerates the reaction [80]. Some researchers are trying to activate the substrates using heat treatments, but this strongly affects the economic feasibility of carbonation [81]. The topic of gas-solid dry carbonation will be resumed in the experimental part of this thesis, as a substantial part of this research is based on this method.

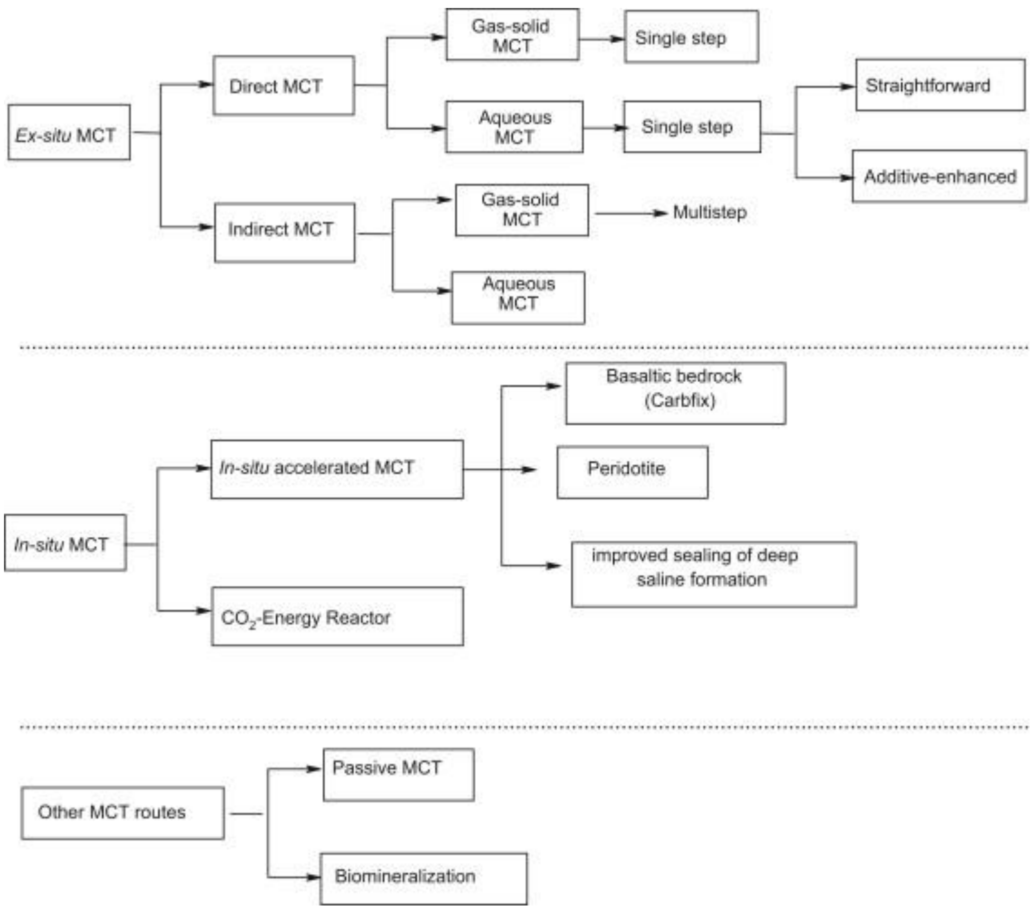

Figure 19. Mineral carbonation process routes (Olajire, 2013).

Aqueous Carbonation

Direct wet carbonation in a single reactor is divided into three phases. In the first phase, CO_2 dissolves in water and transforms into carbonate ions, changing the environment into an acidic one.

$CO_{2(g)} + H_2O_{(l)} \rightarrow H_2CO_{3(aq)} \rightarrow H^+ + HCO_3^-{}_{(aq)}$ (8)

The second phase involves metals leaching from the mineral matrix.

$(Ca/Mg)\text{-silicates}_{(s)} + 2H^+_{(aq)} \rightarrow (Ca/Mg)^{2+}_{(aq)} + SiO_{2(s)} + H2O_{(l)}$ (9)

The final stage is carbonates precipitation.

$(Ca/Mg)^{2+}_{(aq)} + HCO_3^-{}_{(aq)} \rightarrow (Ca/Mg)CO_{3(s)} + H^+_{(aq)}$ (10)

For this route, it is known that silicate dissolution is the rate-limiting step in the whole process. Most of the scientific effort is directed towards improving the kinetics of the second step by varying the process conditions (temperature, pressure, CO_2 flow rate and solid-to-liquid ratio) or by decreasing the particle size, changing the pH or adding catalysts [82]. The silicate dissolution step can differ for different minerals. For example, serpentine dissolution is divided into two steps: rapid dissolution followed by a comparatively slower phase. Studies performed on the mechanism of wet carbonation indicate that the dissolution step could be improved by increasing the particles' specific area or by removing the SiO_2 layer.

Indirect Carbonation Methods

The difference between direct and indirect routes is that the second group is divided into two or more steps, probably taking place in separate reactors. The benefit of such a division is that they can be optimized separately, independently of each other.

Multi-Step Gas-Solid Route

This process involves conversion of Ca/Mg-based silicates to $(Ca/Mg)(OH)_2$ hydroxides. This route was developed by Zevenhoven et al. [83]. Two alternative methods for serpentine carbonation via MgO and $Mg(OH)_2$ are presented in Figure 20.

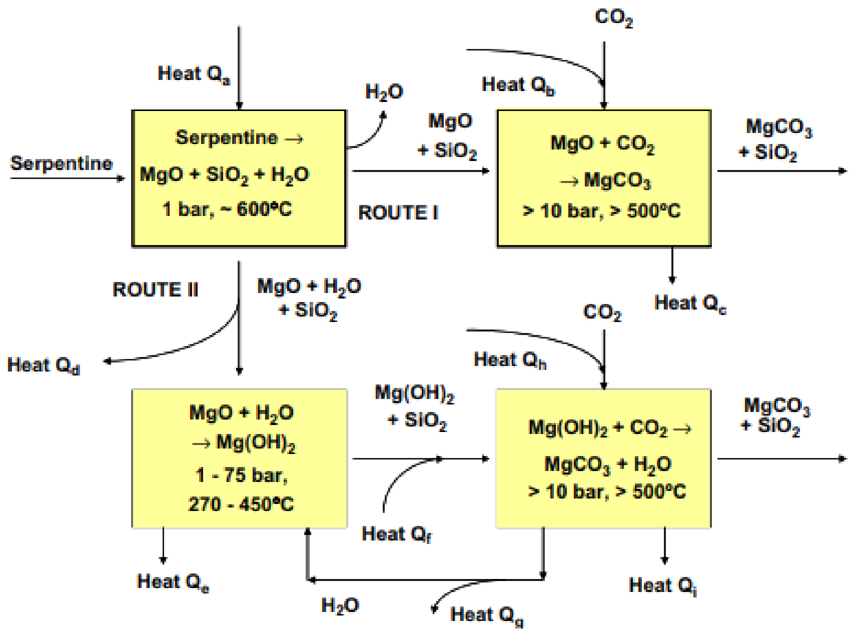

Figure 20. Two alternative routes for serpentine carbonation via MgO or $Mg(OH)_2$ (Zevenhoven et al., 2008).

First, either MgO or $Mg(OH)_2$ is produced from serpentine, since direct carbonation from magnesium silicate cannot be achieved at a sufficient rate. Production of magnesium hydroxide occurs upon addition of water vapour, as follows.

$$Mg_3Si_2O_5(OH)_{4(s)} \rightarrow 3MgO_{(s)} + 2SiO_{2(s)} + 2H_2O \quad (11)$$

$$MgO_{(s)} + H_2O \rightarrow Mg(OH)_{2(s)} \quad (12)$$

$$Mg(OH)_{2(s)} + CO_2 \rightarrow MgCO_{3(s)} + H_2O_{(l)} \quad (13)$$

Route I – two-step serpentine carbonation via MgO (Figure 20).
MgO is produced at atmospheric pressure at around 600°C. Next, the carbonation process is held at the supercritical pressure of CO_2 (~73 bar) and temperatures of up to 600°C.

Route II – three-step serpentine carbonation via $Mg(OH)_2$ (Figure 20).
The first step is the same as for route I. Following this, hydration of MgO occurs at elevated pressure and temperature, in order to improve the kinetics. The third step is again the same as for route I. According to the author of this process, this route has better energy efficiency and exhibits faster kinetics.

Currently, these processes are being optimized at Åbo Akademi University (AA). The production of $Mg(OH)_2$ needs more heat than is generated by the subsequent process of carbonation. However, it has better energy economics than straightforward carbonation (0.9-1.2 vs 1.0-2.3 kWh/kg CO_2 sequestered).

Indirect Aqueous Carbonation
Like indirect gaseous carbonation, this process is characterized by separation into two steps: extraction of the Mg/Ca and carbonation. The usually independent steps are performed using different additives. To achieve high-purity carbonation products, the additives must be recovered, and in general this is a problematic step.
HCl extraction route.
Extraction of metals via hydrochloric acid is an easy process to perform as this additive has a very low pH. This route was first proposed by Lackner et al. (1995). The process using serpentine as a raw material is described below.

$$Mg_3Si_2O_5(OH)_{4(s)} + 6HCl_{(l)} + H_2O_{(l)} \rightarrow 3MgCl_2 \cdot 6H_2O_{(aq)} + 2SiO_{2(s)} \quad (14)$$

$$2MgCl(OH)_{(l)} \rightarrow Mg(OH)_{2(s)} + MgCl_{2(l/s)} \quad (15)$$

$$Mg(OH)_{2(s)} + CO_{2(g)} \rightarrow MgCO_{3(s)} + H_2O_{(l/g)} \quad (16)$$

The main challenge associated with this method is the cost imposed by the use of HCl, for example, its production or the need to use anti-corrosion materials. The energy consumption of the whole process significantly exceeds the energy produced at a power station. The cost of 1 tonne of CO_2 sequestered was calculated as 150 US dollars [84].

HCl/HNO_3 extraction route.
Another acid used for the first step in the aqueous route is HNO_3. Studies on the extraction of magnesium from serpentine using nitric acid were described by Teir et al. (2007) [85].

$$Mg_3Si_2O_5(OH)_{4(s)} + 6(HNO_3/HCl)_{(aq)} \rightarrow 3Mg^{2+}_{(aq)} + 6(NO_3^-/Cl^-)_{(aq)} \quad (17)$$

$$5Mg((NO_3)_2/Cl_2)_{(aq)} + 10NaOH_{(aq)} + 4CO_{2(g)} \rightarrow 10Na(NO_3/Cl)_{(aq)} + Mg_5(OH)_2(CO_3)_4 \cdot 4H_2O_{(s)} \qquad (18)$$

Firstly, serpentine is dissolved in 4M HNO_3 or HCl at 70°C. Next, the excess solvent is evaporated, and magnesium salt is produced. In the subsequent carbonation step, NaOH is added, in order to increase the pH, due to the acidity of the salt solution [$Mg((NO_3)_2/Cl)(aq)$]. Serpentine conversion to hydromagnesite in the experiment was found to be 83% using nitric acid and 70% using hydrochloric acid. The consumption of the materials in order to produce 1 tonne of CO_2 was 2.4 tonnes NaOH and 3.6 tonnes HNO_3 or 2.1 tonnes HCl.

Acetic Acid Route

This process was reported to be sufficient for wollastonite and industrial waste processing [86]. The reactions involving carbonation of wollastonite are presented below.

$$CaSiO_{3(s)} + 2CH_3COOH_{(l)} \rightarrow Ca^{2+}{}_{(aq)} + 2CH_3COO^-{}_{(aq)} + H_2O_{(l)} + SiO_{2(s)} \qquad (19)$$

$$Ca^{2+}{}_{(aq)} + 2CH_3COO^-{}_{(aq)} + CO_{2(g)} + H_2O_{(l)} \rightarrow CaCO_{3(aq)} + 2CH_3COOH_{(l)} \qquad (20)$$

An energy consumption rate of 20 MW has been calculated for a power plant with 100 MW of power production. A cost of 21€/tonne of CO_2 fixed has been estimated. The process is presented in Figure 21 [87]. The main advantage of this process is reducing the cost of additives, as HCl is not needed and the costs associated with using it are eliminated.

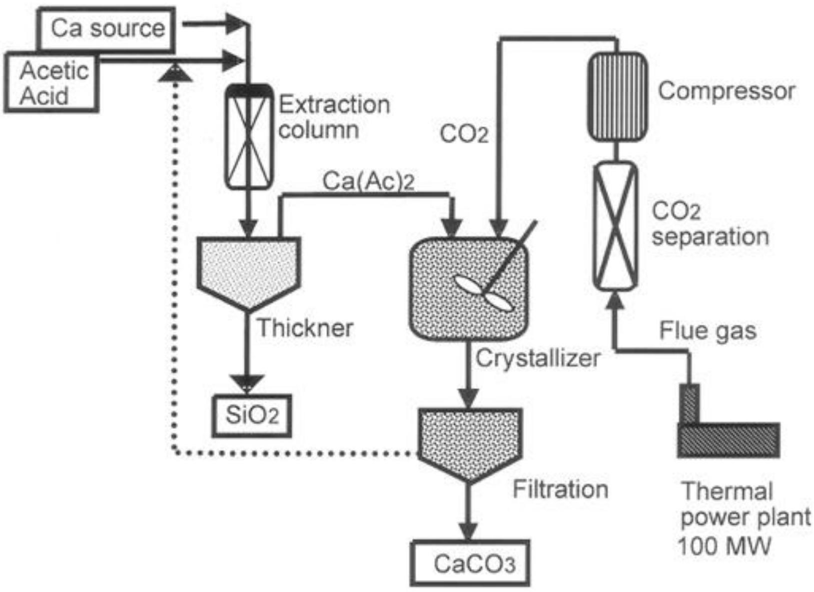

Figure 21. Process scheme for acetic acid route (Kakizawa et al., 2001).

Recyclable Ammonium Salts Extraction

Wang and Maroto-Valer (2011) [88] created a pH-swing CO_2 carbonation process using recyclable ammonium salts (Figure 22).

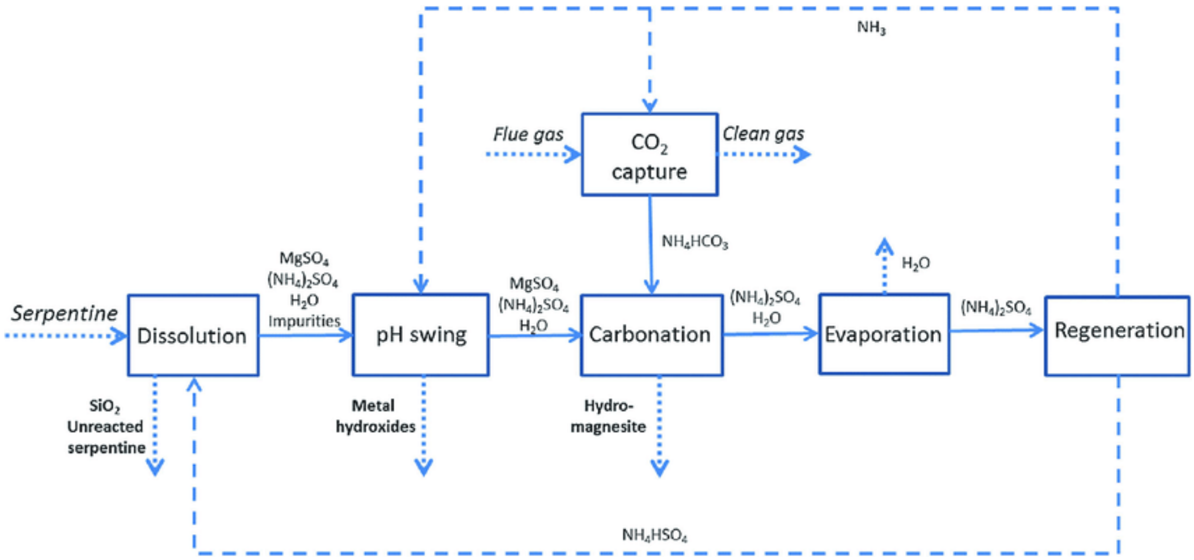

Figure 22. Process route for pH-swing CO_2 sequestration with recyclable ammonium salts (Wang and Maroto-Valer, 2011).

In this route, NH_4HSO_4 is used as an additive to extract Mg from serpentine. The pH of the process is increased by adding ammonia. This leads to extraction of iron (if present) and silica from the mix.

$$Mg_3Si_2O_5(OH)_{4(s)} + 6NH_4HSO_{4(aq)} \rightarrow 3MgSO_{4(aq)} + 2SiO_{2(s)} + 5H_2O_{(l)} + 3(NH_4)_2SO_{4(aq)} \quad (20)$$

$$NH_4HSO_{4(aq)} + NH_3 \cdot H_2O_{(aq)} \rightarrow (NH_4)_2SO_{4(aq)} + H_2O_{(l)} \quad (21)$$

A 40% excess of NH_4HSO_4 is used to intensify Mg extraction. To obtain pure magnesium carbonate, impurities such as Fe, Al, Cr, Zn, Cu and Mn are discarded from the mix by further increasing the pH. Hydromagnesite is obtained by reaction with NH_3 and NH_4HCO_3 as follows.

$$MgSO_{4(aq)} + NH_4HCO_3 + NH_3 \cdot H_2O_{(aq)} + 2H_2O_{(l)} \rightarrow MgCO_3 \cdot 3H_2O_{(s)} + NH_4HSO_{4(aq)} \quad (22)$$

The last stage of the process is the regeneration of $NH_4HSO_{4(aq)}$ and NH_3 by thermal decomposition of $(NH_4)_2SO_4$.

Indirect Molten Salt Process

This process uses other metal extraction agents instead of HCl. This is in order to avoid the energy consumption related to the H_2O evaporation step which is present in carbonation using hydrochloric acid. An example is the process of serpentine carbonation using $MgCl_2$ (T = 150°C):

$Mg_3Si_2O_5(OH)_{4(s)} + 3MgCl_2{\cdot}3.5\ H_2O_{(l)} \rightarrow 6Mg(OH)Cl_{(l)} + 2SiO_{2(aq)} + 2.5\ H_2O_{(l)}$ (23)

After silica precipitation, water is added, obtaining $Mg(OH)_2$.

$2Mg(OH)Cl_{(l)} + nH_2O_{(l)} \rightarrow MgCl_2{\cdot}\ nH_2O_{(l)} + Mg(OH)_{2(s)}$ (24)

In the temperature range of 110-250°C, magnesium hydroxide is partially dehydrated in order to recover $MgCl_2$.

$MgCl_2{\cdot}n\ H_2O_{(l)} \rightarrow MgCl_2{\cdot}3.5\ H_2O_{(l)} + (n\text{-}3.5)H_2O_{(l)}$ (25)

The final stage is the carbonation of $Mg(OH)_2$.

$Mg(OH)_{2(s)} + CO_{2(g)} \rightarrow MgCO_{3(s)} + H_2O_{(g)}$ (26)

Chemically Enhanced Wet Carbonation

Acceleration of the extraction of Mg/Ca metals from silicates by adding various different chemicals, has been explored. Park et al. (2004) studied a wide range of solvents affecting the dissolution process of magnesium. In principle, these agents are responsible for weakening the chemical bonds of magnesium within the serpentine structure, as well as increasing its solubility [89]. One of the outcomes of this work was to show that a mix of orthophosphoric acid, oxalic acid and ethylenediaminetetraacetic acid (EDTA), had a lesser effect on dissolution compared to HCl. Single agents, such as phosphoric and sulphuric acid or sodium hydroxide, were also used to extract magnesium from the silicate matrix and to increase the surface area [90]. The use of sulphuric acid resulted in increasing the surface area from 8 m^2/g to 330 m^2/g. The process was undertaken according to the following reactions.

$Mg_3Si_2O_5(OH)_{4(s)} + 3H_2SO4_{(aq)} \rightarrow 3MgSO_4 + 2SiO_2 + 5H_2O$ (27)

$3MgSO_4 + 2NaOH \rightarrow Mg(OH)_2 + Na_2SO_4$ (28)

$Mg(OH)_2 + CO_{2(g)} + H_2O \rightarrow MgCO_{3(s)} + 2H_2O$ (29)

$MgSO_4 + Ca(NO_3)_2 + 2H2O \rightarrow CaSO_4{\cdot}2H_2O + Mg(NO_3)_2$ (30)

$Mg(NO_3)_2 + Ca(OH)_2 \rightarrow Mg(OH)_2 + Ca(NO_3)_2$ (31)

$Mg(OH)_2 + CaSO_4{\cdot}2H_2O + 2CO_{2(g)} \rightarrow MgCO_{3(s)} + CaCO_{3(s)} + H_2SO_4 + H_2O_{(l)}$ (32)

After the dissolution step (27), the solution was titrated with Na(OH), resulting in $Mg(OH)_2$ production (28). Next, the carbonation step was performed (29) at increased temperature and pressure. Different routes (30-32) use $Ca(NO_3)_2$ and $Ca(OH)_2$.

As well as acids, salt solvents have been investigated for increasing the ionic strength of the solution and also for forming new compounds with Ca or Mg. This results in a decrease in the activity of metal ions in solution and an enhanced release of Mg or Ca from silicates. It was found that using these solvents allows the same carbonation rates to be obtained, but in much shorter times. For example, NaCl, $(Na/K)NO_3$ and $NaHCO_3$ have been studied for use in aqueous carbonation. The latter increases the concentration of HCO_3^- ions while buffering the pH from 7.7 to 8.0.

Regeneration of the solvent is very important from the cost and environmental perspectives. Only salts where the anion will not precipitate with Ca/Mg can be selected.

Indirect wet carbonation seems to be technologically and energetically feasible, but its cost is still too high for industrial implementation. Further cost reductions must be made, for example through the development of reactors and improvement of solvents and solvent mixtures, to achieve better carbonation efficiencies.

3.2 In Situ Mineral Carbonation

The in situ carbonation approach corresponds to CO_2 injection into porous rocks in the earth's subsurface, where it can directly react with the rock. The general advantage of in situ over ex situ carbonation is that there is no need for mineral transport and storage, which could result in lower cost. The choice of rock is very important, as it must be rich in either magnesium or calcium and must be permeable and porous in order to store the carbonate mineral products. Calculations have been made regarding in situ mineralization rates in sandstone and sandstone shales rich in iron, for example chlorite. It has been estimated that with the typical reaction rate (occurring in nature), it would take 100,000 years to produce 90 kg of carbonate mineral per m^3 of sandstone [91]. In contrast, injections of CO_2 into ultramafic or basaltic rocks seem to be much more effective, with faster carbonation kinetics [82, 92].

Typical basalt rock contains ~10% Ca, ~7% Mg and ~10% Fe (Table 2). Substantial amounts of Mg, Ca and Fe-bearing minerals makes them suitable for storing CO_2 in the form of carbonates. Even though less than 10% of the earth's surface is covered by basalt, it consumes around one third of all carbon dioxide during natural weathering. Enormous amounts of mafic and ultramafic rocks are present globally. Their capacity exceeds that necessary to capture all the anthropogenic CO_2 production. For example, Columbia River basalts could sequester more than 100 Gt of CO_2.

Many simulations have been done in order to understand the reactive transport of CO_2 within different host rocks and to estimate their capacities. Carbonation of basaltic rock by carbonated water results in the production of silica, goethite (FeOOH) and clay kaolinite. After about one year, siderite, dolomite and magnesite precipitates are observed, and substantial carbonation is achieved after 10-100 years [93]. As the total mass of the cap rock increases, available pore spaces become clogged, leading to a loss of permeability over the years, limiting the carbonation rate.

The CarbFix project (Figure 18) demonstrated the feasibility of in situ carbonation in basaltic rocks [92]. Gislason et al. (2018) successfully injected more than 200 tonnes of CO_2 into subsurface basalt formations during the years 2012-2013. Carbon dioxide, injected in the form of carbonated water, was obtained from a geothermal power plant near Hellisheiði. Monitoring of the injection wells proved that more than 95% of the carbon dioxide was mineralized within a year. The principle of this operation is to achieve preferential carbonates precipitation over other secondary products such as oxides, clays or zeolites. This can be done by improving mineral-fluid interactions using highly porous rocks and hydrofracturing during gas injection. Temperature and/or fluid composition can also affect the process. Another rock which has been studied for in situ carbonation is peridotite. Although it is less abundant than basalts, it is richer in magnesium (40-45%). Peridotite consumes CO_2 naturally. A method of implementing this natural process was proposed by Kelemen and Matter (2008) (Figure 23). The process starts with the drilling of peridotite through the impermeable cap rock followed by hydrofracturing of the rock. CO_2 in the form of hot fluid is injected at a temperature of 185°C in the pressure range 100-300 bar. The use of surface CO_2-saturated water at atmospheric pressure is also proposed. This results in slower carbonation but lower cost. The authors propose maintaining the 185°C temperature via the exothermic effect of the reaction, if it is fast enough to produce heat while overcoming heat loss caused by cold surroundings and the rising cold CO_2 fluid. The energy penalty compared to non-enhanced injection into the subsurface is 9-23%.

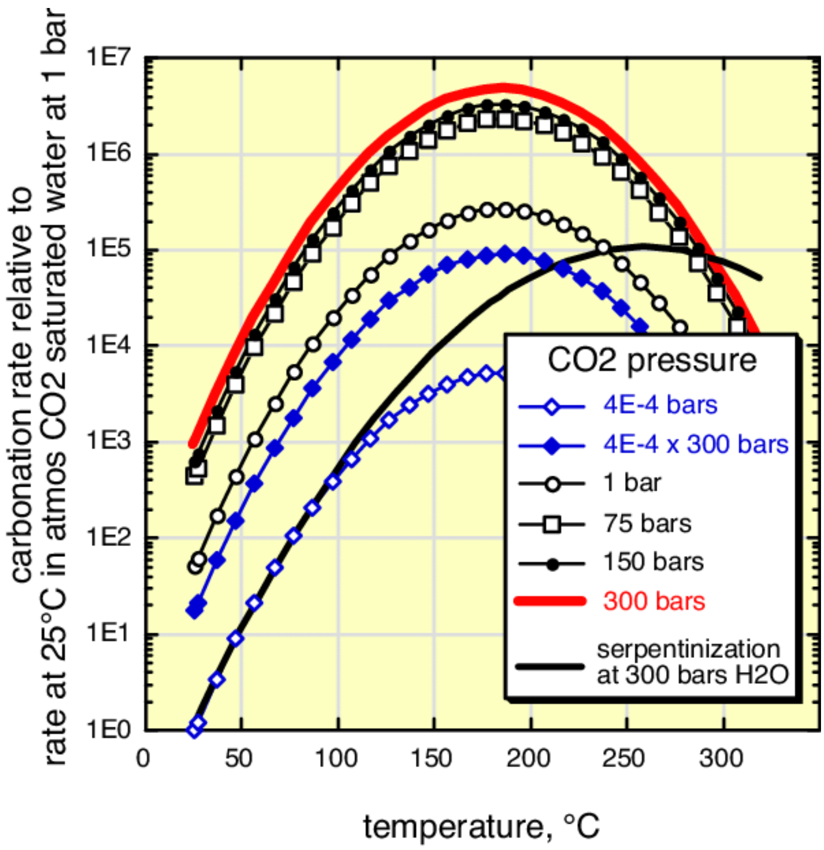

Figure 23. Rates of olivine carbonation (Kelemen and Matter, 2008).

The main challenges faced when considering in situ carbonation are the need for water for dissolving CO_2, the need for fracturing the impermeable cap rock above the silicates for carbonation and the possible tracing of toxic metals released during the reactions.

There are two ways to dissolve CO_2 in water for carbonation purposes: before injection into the rock or in the form of a gas which will finally dissolve in existing groundwater. Significant amounts of water are needed for dissolving the gas prior to injection: 1 tonne of CO_2 at 25 bar and 25°C needs ~27 tonnes of water. This amount increases to 341 tonnes if the partial pressure of CO_2 is 2 bar. Large quantities of carbonated water require significant permeability in the drilled injection hole. The cost of this process depends on the energy penalty associated with pumping carbonated water down the hole. In situ carbonation in oceanic basalts has the advantage of the huge amounts of available water. Injection of the gaseous form of CO_2 does not require the availability of water. However, gas diffusion into groundwater might be a slow process, relying on the hydrological system and the chemical composition of water.

As explained previously, carbonation reactions usually have very slow kinetics, and it is necessary to keep dissolved CO_2 in contact with the host rock for long enough to achieve mineralization. Impermeable cap rocks will prevent ions from exiting. These cap rocks are usually found in oilfield reservoirs; they are less common in basalt or ultramafic rocks. Any fractures of cap rocks lead to an alteration in permeability.

Accompanying the carbonation reaction where carbonic ions react with metals from minerals in the rock, other reactions take place which may lead to the release of trace and toxic metals. These compounds can migrate, depending on the hydrology and chemistry of the system. It has been shown that reactions between basalt and CO_2-rich water have led to the release of trace and toxic metals. Further reactions of those substances caused an increase in the pH of groundwater [94].

3.3 Carbonation of Industrial Residues

As well as minerals, industrial wastes rich in calcium, magnesium or iron are suitable feedstocks for CO_2 mineralization [70, 95]. These materials are available at low cost and usually close to the industrial source of carbon dioxide. Compared to natural minerals, they have a higher reactivity, due to their chemical instability [68]. Various alkaline solid wastes have been investigated as sources of calcium or magnesium for the carbonation process: coal and municipal waste combustion fly ash, bottom ash, brine alkaline solutions, waste concrete and cement, steel slag and mining and air-pollution control residues (Table 3) [96–98]. Typical chemical compositions of alkaline wastes are similar to those of igneous rocks but enriched in trace elements. Studies of wastes carbonation have been undertaken both from the perspective of process potential and the perspective of the leaching properties of heavy and trace elements [63].

Table 3. List of industrial residues studied for mineral carbonation (Torrontequi, 2010).

Industrial waste	Industrial sector
Argon oxygen decarburization (AOD) slag	Steel manufacture
Air-pollution control fly ash (APC)	-
Biomass ash	Energy production
Blast furnace slag	Steel manufacture
Bottom ash	Energy production
Industrial brines	Energy production
Cement wastes, (e.g., kiln dust)	Cement
Chrysolite mining tailings	Asbestos mining
Coal combustion fly ash	Energy production
Ladle slag	Steel manufacture
Lignite combustion fly ash	Energy production
Mine tailings (platinum, asbestos)	Mining
MSWI fly ash	Municipalities
Nirex Reference Vault Backfill	Radioactive waste management
Oil shale ashes	Oil extraction
Paper mill waste	Paper manufacture
Paper waste water incineration ash	Paper manufacture
Pressed lime-waste composites	-
Steelmaking slag	Steel manufacture

The carbonation of Ca-bearing minerals is the main reaction for CO_2-fixing in residues, for example portlandite and lime.

$$Ca(OH)_2 + CO_{2(g)} \rightarrow CaCO_{3(s)} + H_2O_{(l)} \quad (33)$$

$$CaO + CO_{2(g)} \rightarrow CaCO_{3(s)} \quad (34)$$

It has been reported that this reaction takes place during, e.g., municipal solid waste incineration (MSWI) and the production of bottom ash [99] and cement [100].

Other compounds present in some of the wastes are Ca silicates.

$$CaSiO_3 + CO_{2(g)} \rightarrow CaCO_{3(s)} + SiO_{2(s)} \quad (35)$$

Such reactions are found in cement and steel slag carbonation [78].

Another main component found in many wastes, e.g., cement wastes, is ettringite, and the reaction for this is as follows.

$3CaO·Al_2O_3·3CaSO_4·3H2O + 3CO_2 \rightarrow 3CaCO_3 + 3CaSO_4·2H_2O + Al_2O_3·xH_2O + (26\text{-}x)H_2O$ (36)

Dissolution of ettringite and precipitation of calcium carbonate is the main reaction for oil shale residue, and this process lowers the pH to 9.0 after carbonation. Some studies address the fact that the presence of other ions can influence the carbonation. For example, sulphate ions (SO_4^{2-}) have an effect on calcite formation, due to gypsum precipitation. It was reported that the rate at which Ca^{2+} in fly ash reacts with carbon dioxide is directly proportional to the sulphur concentration. The presence of magnesium ions in the solution inhibits the precipitation of calcium carbonate and directs the reaction towards formation of aragonite instead of calcite [101].

In some wastes, as well as calcium, magnesium is also present in small amounts, e.g., in oil shale residue.

$Mg_2SiO_3 + 2CO_{2(g)} \rightarrow 2MgCO_{3(s)} + SiO_{2(s)}$ (37)

Carbonation of wastes is usually easier than carbonation of ores. Wastes are rich in calcium, which is known to be carbonated faster than magnesium [68], whereas the predominant alkaline component in ores is usually olivine. Residues usually have an open structure and a significant surface area. Additionally, as wastes are produced at high temperatures and subsequently cooled, they are usually geochemically unstable and therefore reactive.

Chapter 4. CO_2 Storage in Coal

4.1 Sorption of Methane and Carbon Dioxide in Isothermal and Non-Isothermal Conditions

Geological storage of CO_2 in unmined coal beds was described in section 2.3. Coal beds are particularly interesting from a CO_2 storage perspective as they store natural methane, which is easily displaced by injecting CO_2. The process of CO_2 storage in coal can be followed by the production of clean hydrocarbons, whose economic value can balance the sequestration expenses. Additionally, tests have shown that double the amount of CO_2 can be absorbed by coal compared to methane, giving this sequestration method substantial sequestration potential [102,103]. Sorption of coal bed gases (methane and carbon dioxide) in the coal matrix may eventually change the mechanical properties of the coal. One of the effects of sorption is coal swelling, evidenced by stress and strain variations in a coal bed under overburden pressure. Previous studies suggest that hard coal shows an anisotropic swelling behaviour [104,105]. This behaviour, as well as the anisotropic framework of coal, is attributed to the stress conditions under which the coal was generated. Anisotropic swelling of coal samples subjected to adsorption/desorption cycles using CO_2 can be measured with the aid of strain gauges and transducers. The swelling process plays a significant role in defining the strength of coal, the speed at which coal can absorb gases and the impact of permeability changes on the gas-flow mechanics in the reservoir [106].

The aim of this experimental chapter is to show the mechanical behaviour of hard coal in a changing temperature environment, when subjected to sorption of carbon dioxide and methane. In order not to change the porous structure of the coal, the investigation was performed on cuboid-shaped coal samples, not crushed before the experiment. Temperature variations affect the sorption equilibrium, resulting in volumetric strains in the coal mass. From a geological point of view, it is highly important to investigate possible temperature fluctuations, given that strains in the coal mass can lead to stress in rock layers, followed by uncontrolled gas leaks [107].

The research presented in this chapter has been published in [108].

4.1.1 Test Material

Experiments were performed on two different hard coal samples from a Polish colliery – KWK Pniówek. They belong to the sedimentary cyclothem of coal in the Upper Silesian Coal Basin. This cyclothem forms a series of mudstones consisting of sedimentary rocks (both clastic and clay rocks).

Clastic rocks are mudstones and sandstones made of grains that vary in size, whereas clay consists of siltstones and coal shales. Selected results regarding the physico-chemical properties of coal samples from coal seams 360/1 and 404/1 are summarized in Table 4. The elemental analysis was performed in the Central Mining Institute in Katowice. The moisture content was determined in accordance with the procedure described in the standard PN-80/G-04511 and ash content was established in accordance with PN-80/G-04512. The oxygen content was computed as the remainder of 100%, taking into account the moisture and ash content.

Table 4. Characteristics of the coal material (Baran, 2018).

Colliery /coal seam	C^{daf}	S^{daf}	H^{daf}	N^{daf}	O^{daf}	W^{a}	A^{a}	V^{daf}
Pniówek 1 (360/1)	84.24	0.39	4.58	1.52	4.58	1.75	3.01	27.12
Pniówek 2 (404/1)	84.96	0.58	4.60	1.70	3.76	0.68	3.78	25.50

The petrographic analysis of the tested coal samples is summarized in Table 5. This testing was carried out using Axioskop and POLMI optical and polarizing microscopes from Opton.

Table 5. Maceral composition (%) of selected coals (Baran, 2018).

Coal	Vitrinite	Liptinite	Inertinite
Pniówek 1	73	7	20
Pniówek 2	53	8	39

4.1.2 Experimental

For the experiment, specially designed equipment was used, enabling parallel measurements of sorption and dilatometric characteristics of coal samples (Figure 24). The apparatus can be used for measuring two samples of coal simultaneously. Sorption capacity was measured by the manometric method. The device is placed in a water thermostat in order to maintain a constant temperature with an accuracy of 0.1°C. Carbon dioxide of known volume and pressure is decompressed and flows from the reference cell to sample cell 1, which contains coal sample 1. As the dead volume of the apparatus and the volume of the dosing gas unit are known, the amount of absorbed gas can be calculated on the basis of the gas laws. The deviations from ideal gas behaviour must be taken into account in the calculations.

In the pressure and temperature range, the difference between an ideal and a real gas can be determined using the equation of state for CO_2 and CH_4. The volume of the dosing gas unit was computed by measuring the nitrogen outflow, with an EL-FLOW F-111B (Bronkhorst) flowmeter. The dead volume of the reference cell was determined using glass balls, and the value was derived with the use of helium. Cuboid-shaped coal strains were measured with a strain gauge engineered at the Strata Mechanics Research Institute of the Polish Academy of Sciences. Linear deformations were controlled by an electric resistant wire strain meter, combined with a resistance transducer. Results are shown as an alphanumeric display stored in internal memory or forwarded via a serial port. The strain measuring system can be programmed by introducing the parameters of linked strain gauges and transducers, setting the current time and creating measurement data recording criteria. The operating rule of the strain gauge uses the physical changes in the resistance of the conductor under strain. Minor resistance changes (several percent) are measured using a Wheatstone bridge. A more detailed description of the test facilities and apparatus is given in [109].

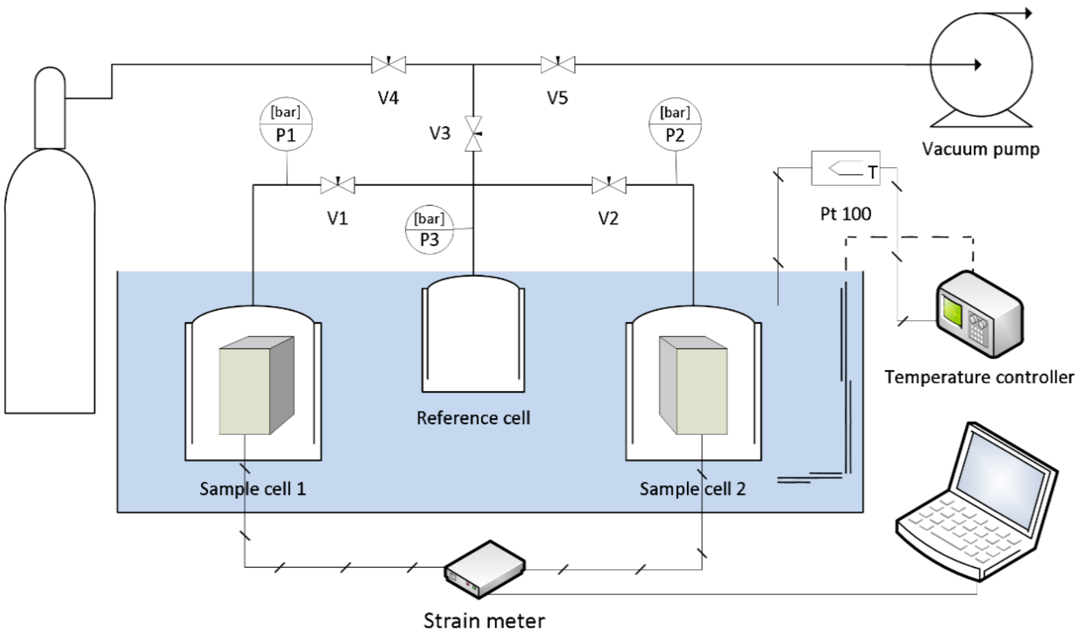

Figure 24. Configuration of the measuring apparatus (Baran, 2015).

4.1.3 Test Procedure

The samples were cut from the primary coal fragments. Samples were cuboid-shaped pieces of hard coal with a weight of about 20g and dimensions of 18 x 18 x 40 mm. On the faces of each cuboid, resistance strain gauges were attached, arranged lengthwise and transverse to the bedding plane. Following this, the samples were placed inside the test ampoule and connected to the strain gauge.

Before the experiment, each sample was degassed, the sample cell volume was determined using helium and following that, the whole system was degassed in order to reach a static vacuum of 10^{-2} Pa. At the beginning of the procedure, all valves were locked, and the strain gauge was set at zero. Firstly, methane was admitted to the reference cell, and when the pressure was constant, gas was introduced to the sample cell. At the same moment, recording of the kinetics of the pressure drop began in the measurement system. The data for the kinetics of linear strains in the cuboid coal sample were stored in the memory of the strain gauge. The kinetics of volumetric changes and the sorption at a temperature of 25°C, were observed for 50 hours. At the end of the isothermal part of the experiment, the second phase started, including the registering of the gas pressure and linear strains in the system with a change in temperature of the system from 25 to 50°C. The rate at which the temperature was increased was 1°C every five minutes. The highest temperature of 50°C was reached after three hours and the samples were monitored for the following 10 hours in isothermal conditions. After the part of the investigation using methane as the sorption gas, the system was degassed and measurements with carbon dioxide were performed, according to the procedure described above.
The kinetics of volumetric strains (ε_V) were determined according to the equation:

$$\varepsilon_V = \varepsilon_\perp + \varepsilon_\parallel \qquad (38)$$

where $\varepsilon\perp$ represents coal-induced strains in a perpendicular direction and $\varepsilon\parallel$ indicates strains in a parallel direction.

4.1.4 Results and Discussion

As in previous research, the results for both coal samples show higher sorption capacity for the CO_2 experiments, compared to the CH_4 sorption investigation (Figure 25). A gas with adequate adsorption affinity and kinetic diameter of its molecules, is favoured in the adsorption process. The properties of carbon dioxide, i.e., smaller kinetic diameter size and higher adsorption energy compared to methane, allow the gas particles to diffuse more easily into the coal matrix pores. Thus, the microporous matrix can adsorb larger amounts of carbon dioxide than of methane. CO_2 has a kinetic diameter of 0.33 nm. For CH_4 molecules, whose kinetic diameter has value of 0.38 nm, it is much harder to penetrate the hard coal network of pores, which are of ultra-micropore size (less than 0.8 nm diameter) [110]. Preferential adsorption of CO_2 is not only connected to its physico-chemical properties but also to the presence of functional groups in coal and its electrical properties (quadrupole moment). The presence of reactive oxygen groups in the coal polymer structure can restrict the access of the tetrahedral molecules of CH_4 to the pores, while the reaction between CO_2 molecules and the oxygen groups can take a different course [111,112]. Another reason for the preferential sorption of carbon dioxide is the difference between the boiling temperatures of CO_2 and CH_4. The boiling temperature of carbon dioxide is higher (-78.5°C) than that of methane (-161.6°C). Thus, the sorption affinity for CO_2 is higher than for CH_4. Some of the pores are inaccessible to the methane molecules because this gas needs to expend substantial energy to expand the pore walls in order to penetrate them. When the coal sample-methane interaction is prolonged, and at the same time the sorption space becomes saturated, vibrations of the coal copolymer network and the presence of an elastic phase permit the spherical CH_4 molecule to penetrate those areas that did not have a significant role in the coal-gas interactions required to expand the pore walls. It is possible that methane molecules prompt stress relaxation and creep, within the framework molecular elements.

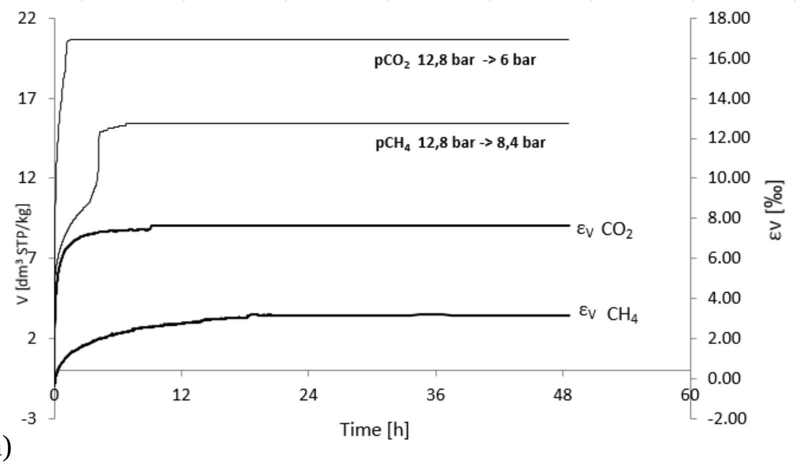

a)

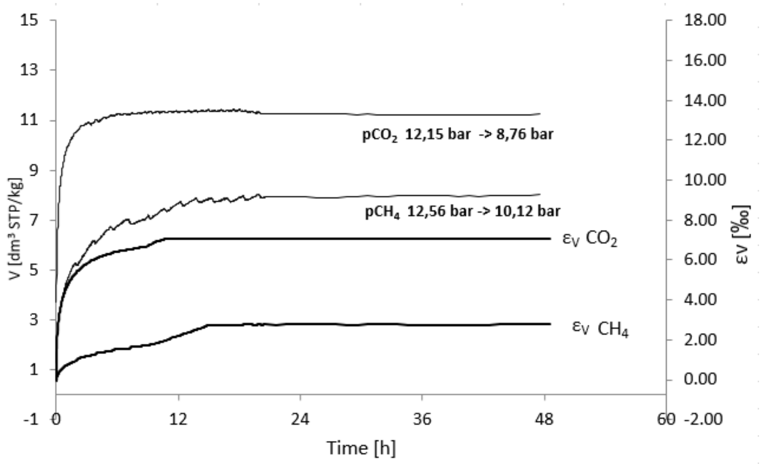

b)

Figure 25. Kinetics of CO_2 and CH_4 sorption and volume strains at 25°C for a) Pniówek 1 and b) Pniówek 2 (Baran, 2018).

When the sorption processes on the hard coal are analysed, it is important to take into consideration the specification of the coal behaviour in that process. In the first stage, gas molecules are being adsorbed onto the coal surface relatively fast. In second stage the adsorbed molecules diffuse into the coal's internal structure, destroying the distinction between pure adsorption and absorption. The co-occurrence of these two processes can be described as sorption. After a considerable period of time, the coal structure is rearranged. The process is typically slow because this transformation involves the large-scale motion of molecules. During exposure to the vapour of dissolved substances, coal tends to behave like a deformed glassy polymer [113,114]. Carbon dioxide dissolves in coal, giving rise to coal swelling. For this reason, coal should not be treated as a straightforward solid, as this can lead to incorrect interpretation of measurement data.

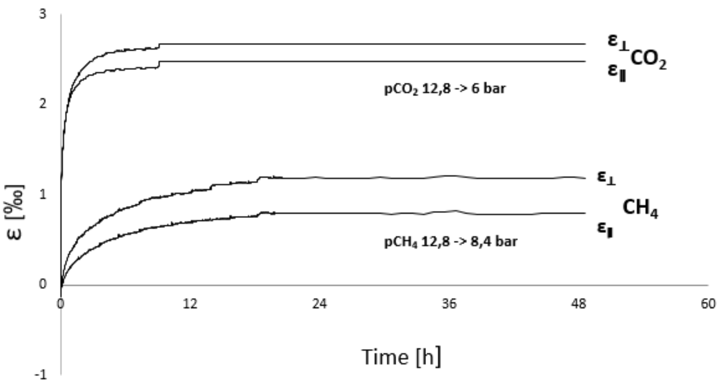

a)

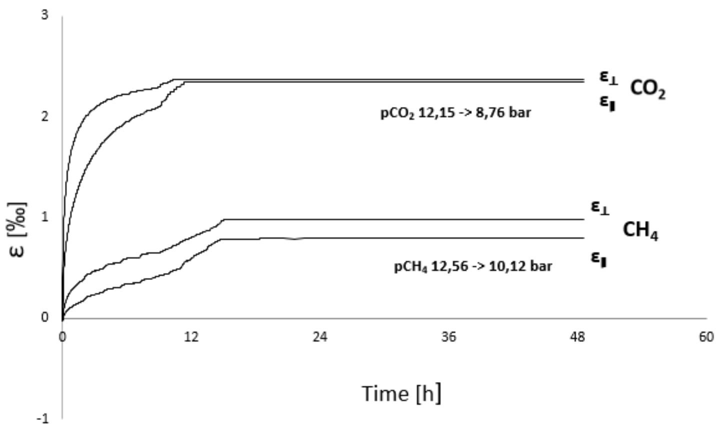

b)

Figure 26. Kinetics of linear strains (in directions parallel and perpendicular to the bedding plane) of the coal sample when exposed to methane and carbon dioxide at 25°C: a) results for Pniówek 1 and b) results for Pniówek 2 (Baran, 2018).

Regarding the linear expansion, Figure 26 shows that results for both hard coal samples, Pniówek 1 and Pniówek 2, are quite similar for the sorption processes undertaken at 25°C. Linear expansion of the coal samples tends to increase when both gases are admitted. In addition, for both samples, the coal tends to expand more in the direction perpendicular to the bedding plane. This is consistent with results reported by other authors [115,116]. Even though the initial pressure of the gas being dosed had comparable values (12.15 and 12.56 bar), the samples expand at a faster rate and by more than twice as much when exposed to carbon dioxide, rather than methane. Additionally, for both samples, the shapes of the kinetic

plots in Figure 26 for sorption-dilatometric (volumetric) phenomena are very similar, which confirms the hypothesis that deformations of the coal sample are attributable to gas deposition.
Mining operations in the coal bed can cause temperature changes of 10°C or more, which can easily disturb the equilibrium of the coal-gas system. The temperature change can initiate a gas pressure change, and thus the amount of gas absorbed by the coal will also change. These phenomena should be taken into account when designing the system. Measurement at 25°C became the starting point for further investigation of the gas sorption, which involved the recording of pressure and volumetric strain variations occurring on the temperature increase of the coal-gas system. Results are presented in Figure 27, showing the pressure increases with increased temperatures (by about 2 bar for CO_2 and 1.5 bar for CH_4 for Pniówek 1 and 2.2 bar for CO_2 and 1.4 bar for CH_4 for Pniówek 2).

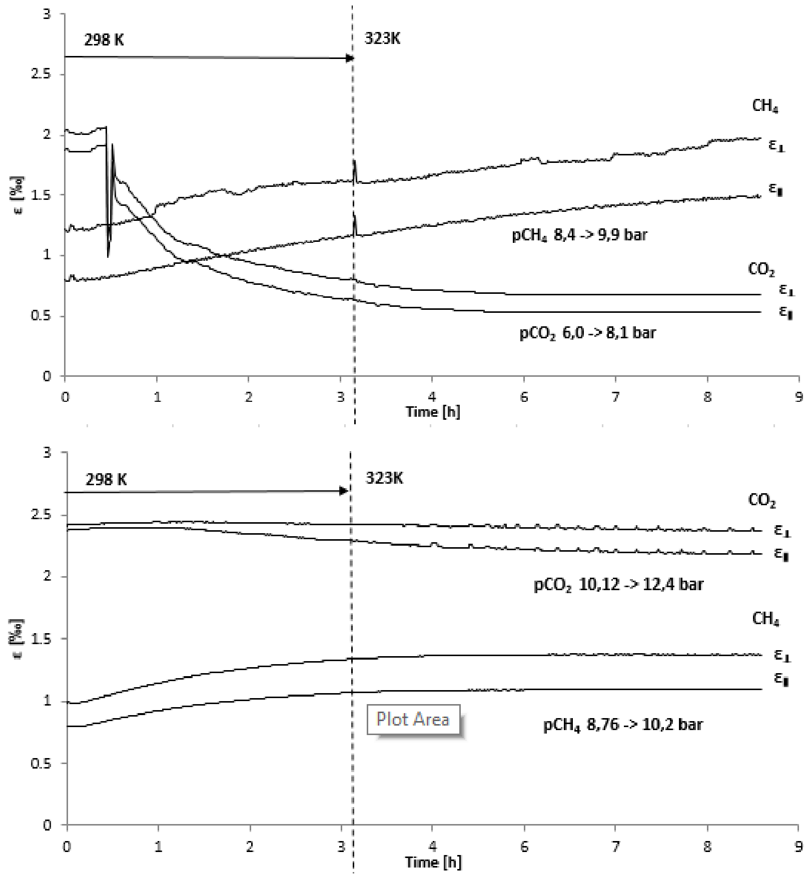

a)

b)

Figure 27. Kinetics of the development of linear strains during the temperature increase step for the samples (Baran, 2018).

In case of non-isothermal sorption, tested samples show slightly different results. For Pniówek 1, CO_2 sorption started with minor swelling of the sample, followed by rapid shrinkage after 25 minutes from the start of the experiment (lateral and longitudinal dimensions changed by approximately 1‰), with continued gradual contraction and shrinking. The shrinkage of the coal matrix can give rise to expansion of the existing cracks in the coal bed or can cause new cracks. Due to this phenomenon, the lateral stresses which maintain the coal in the compact form tend to disappear. Relatively fast shrinking is registered near the critical temperature of CO_2 (31°C). The surface tension, density of liquid and vapour under equilibrium conditions, pressure of saturated vapour and variations of these parameters with temperature and pressure, are very interesting in the near-critical region. Sorption in the near-critical region exhibits the characteristics of mechanism transition [117].

The observed changes can be explained by a different mechanism of CO_2 molecule deposition. CO_2 accumulated in pores undergoes a rapid phase transition, leading to rapid desorption and shrinking of the coal sample. For Pniówek 2, slight shrinkage of the sample can be observed – from 2.5‰ to 2‰ change in volumetric strain, for coal-induced strains in both perpendicular and parallel directions. Significant differences in the course of sample dimension changes can be caused by the petrographic composition of the coal rock. Both samples are from the same mine, but from two different decks: 360/1 for Pniówek 1 and 404/1 for Pniówek 2. While the chemical composition of the samples is very similar (Table 4), the petrographic composition is significantly different. There is considerable variation in the content of each maceral group (Table 5). The impact of the petrographic composition on the coal sorption capacity has previously been discussed in the literature [118,119]. In his study, Karacan (2007) formulated a relationship between the amount of CO_2 sorption and the porosity. The study proved that microlitotypes rich in macerals of inertinite show a much higher porosity than microlitotypes rich in macerals of vitrinite and liptinite. This phenomenon is probably related to the presence of mesopores in inertinite and also the lower coal sorption capacity of the vitrinite maceral groups, due to the presence of micropores which hinder the internal transport of carbon dioxide [106]. Moreover, Karacan demonstrated that in areas of coal with a higher porosity, the absorption of CO_2 occurs more rapidly than in other areas, due to better permeability. This allows the hypothesis to be formulated that coals which contain more macerals from the inertinite group may be more useful in the process of sequestration. In the case of macerals from the vitrinite group, the CO_2 sorption reaction led to an increase in volume. This has a negative impact, due to the possibility of bumps and shocks occurring and consequently, the possibility of the rock mass unsealing and the rapid desorption of CO_2 into the atmosphere from the coal seam. This may explain the different course of coal deformation during the non-isothermal measurement. The Pniówek 2 sample contains much lower levels of macerals of the vitrinite group, suggesting that the absorption is much lower. Thus, a temperature increase in the system causes CO_2 desorption located in the pores to be dominant over CO_2 secretion from inside the carbon matrix. Hence, the volumetric changes of the sample due to gas desorption will be much smaller than for the Pniówek 1 sample, for which the CO_2 absorption is much higher.

In the case of non-isothermal methane sorption, for both samples Pniówek 1 and Pniówek 2, temperature changes give rise to sample swelling. The behaviour of the entire system is rather unexpected. Previous investigations showed that the desorption processes give rise to coal rock shrinkage [115,116], so the increase in temperature of the system leads to methane desorption. At the same time, the pressure increase causes the equilibrium point to be shifted towards the adsorption range (2.1 bar for Pniówek 1 and 1.44 bar for Pniówek 2). This results in a lower amount of methane absorbed/adsorbed at the final temperature of 50°C compared to the amount at 25°C, even though the dimensions of the coal sample increased. Therefore, it can be concluded that the temperature increase in the case of methane sorption is a major determinant of volumetric strains in the sample.

As previously indicated, considering the copolymer model of the coal, studies on the behaviour of sorption systems should also reflect the coal porosity, since the gas deposition mechanism depends on the pore size. The investigated coal samples belong to the middle rank coals, whose structural elements differ in size. In the copolymer coal model, the sorption process involves the interactions of gas molecules with the absorbing phase, the elastic phase and also the molecular phase. Sorbate molecules are attached between surface groups and molecular bonds in coal, causing them to straighten or expand, and as a result increasing the distance between molecular structures. It is essential that the distance between the groups must be equal to, or smaller than, the diameter of the gas molecules. Sorbate molecules accumulate on the coal surface, retaining contact with the aliphatic structure. Therefore, volumetric strain is involved, and the deformation of the coal is a deformation of the elastic macromolecular network, where the sorbate is the 'lubricant' within the structural elements. Methane, with its kinetic diameter of 0.38 nm and lower adsorption energy than carbon dioxide, penetrates those coal pores in which its physically adsorbed. Some of the pores continue to be inaccessible, since the sorbate molecules require considerable energy to expand the pore walls. When the coal sample-methane interaction is prolonged and at the same time the adsorption space is saturated, vibrations of the coal polymer network and the existence of an elastic phase allow the spherical methane to penetrate the regions which did not take part in the coal-gas interactions needed to expand the pore walls. This leads to the conclusion that the CH_4 adsorbed in sub-micropores desorbs, due to the temperature increase, leading to the expansion of transport pores and an increase in the sample's dimensions. These properties, known as rheological properties, correspond to the coal expansion and gas desorption during the temperature increase.

The temperature rise causes additional stresses between macromolecular elements. Fluctuations in the state of stress in coal rock strata and in neighbouring rocks ahead of the front, cause them to break, which results in a non-elastic increase in the rock volume. These strains give rise to a gas pressure increase and lead to coal bed permeability, which in consequence leads to the release of gas. This is a main cause of rock-gas outbursts, as these factors can trigger the methane phase transition from the adsorbed to the gaseous phase.

4.2 Modelling of Reactions

The aim of this section is to investigate the ability of kinetic equations to describe the sorption kinetics and expansion rate of a solid coal sample. In order to address this issue, the sorption kinetics of methane and carbon dioxide on bituminous coal were studied (Figure 25). At the same time, the changes occurring in the sample's overall dimensions, which accompanied the sorption processes, were monitored (Figure 26). The experiments are described in chapter 4.1. The stretched exponential equation (SE) modelling approach and equations are proposed to fit the kinetic curves of gas deposition, as well as to adequately describe the kinetics of coal swelling. Compared to other models described in the literature, the stretched exponential equation seems to give the best fit to the experimental data [120,121].

Sorption kinetics usually describe the relationship between the amount of absorbed substance and time, in terms of mathematical dependence. Single-pore sorption/diffusion and gas transport models are often used to interpret and quantify the observed gas uptake rates in coal, using various equations [122].

The stretched exponential (SE) equation was developed as a global kinetic equation by Kolmogorov, Erofeev, Kozeeva, Avrami and Mampel, and is therefore called the KEKAM equation [123]. Staib et al. (2015) [124] adapted the two-parameter SE model for gas sorption kinetics in the following form.

$$\frac{Mt}{M\infty} = 1 - [exp - (kt)^b] \tag{39}$$

This model is described by stretching parameter b and rate coefficient k. The idea behind using this model for coal sorption processes can be easily explained. The physical changes that coal undergoes when exposed to solvents are similar to those of glassy polymers, and their structures are often compared, as both materials exhibit viscoelasticity and swelling behaviour [108]. Staib et al. (2015) [124] used the above model for describing the sorption kinetics for medium-volatility, bituminous coals with a wide range of maceral composition. The experimental data they obtained fit the SE model much better than the often-used two-stage model treating sorption as a process having a single fast and a single slow component.

Staib et al. (2015) [124] also discussed the variation of the two parameters k and b of the model, as a function of pressure, coal and gas type. They found that the b coefficients were similar for CO_2 and CH_4 in the same coal at the same pressures, indicating that b is an intrinsic coal property. The variation of b with pressure was different for different tested coals. A higher characteristic rate parameter k was found for CO_2 compared with CH_4, which is in agreement with the relative sorption rates in the literature, but the ratios of diffusion rates for CO_2 and CH_4 varied between tested coals.

As the majority of studies assume that the swelling of coal is proportional to the amount of absorbed gas, in this investigation it is assumed that the SE model could be used to described not only the kinetics of the gas sorption but also the sorption-induced strains of the coal.

For purposes of this analysis, the following form of the SE equation were used.

$$V_{(t)} = V_{eq}\{1 - \exp[-(kt)^A]\} \quad (40)$$

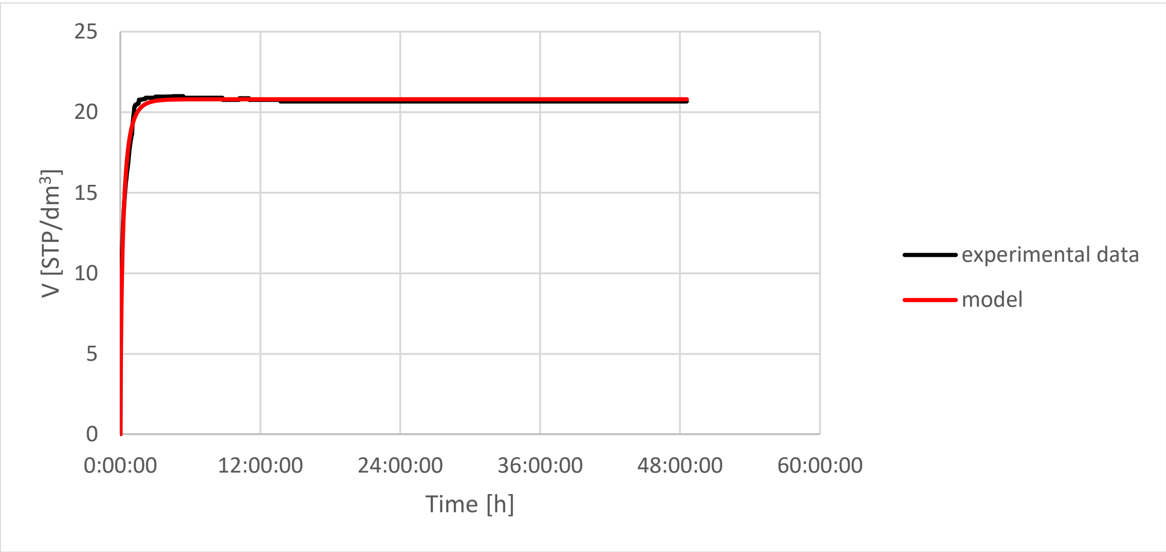

a)

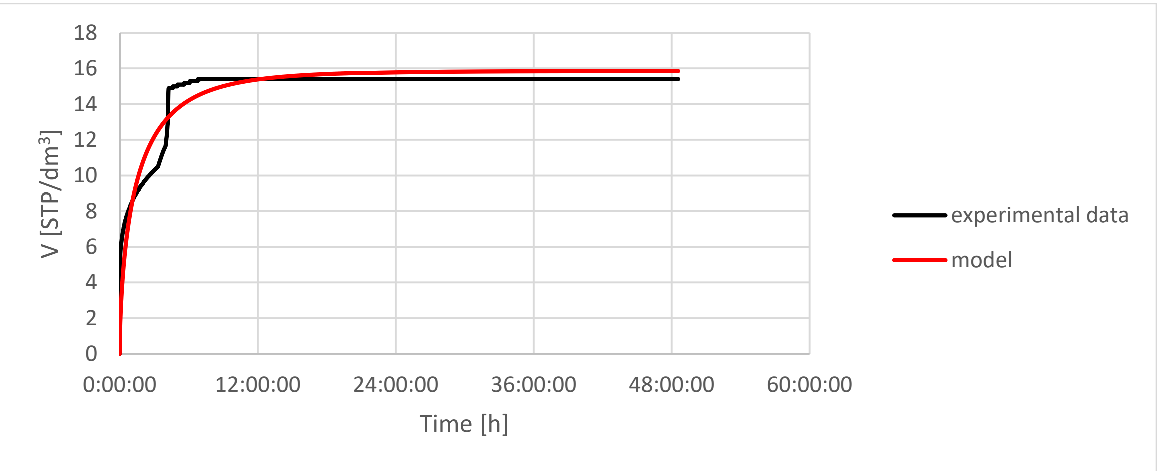

b)

Figure 28. Application of the SE equation to the kinetics for (a) CO_2 and (b) CH_4 sorption, for Pniówek 2.

a)

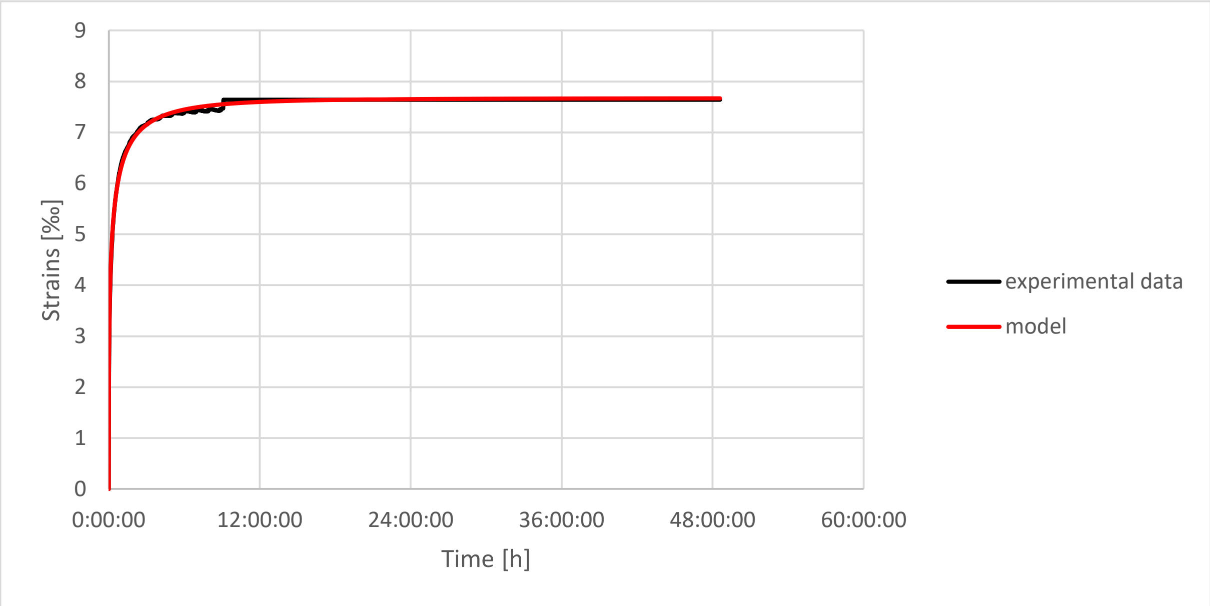

b)

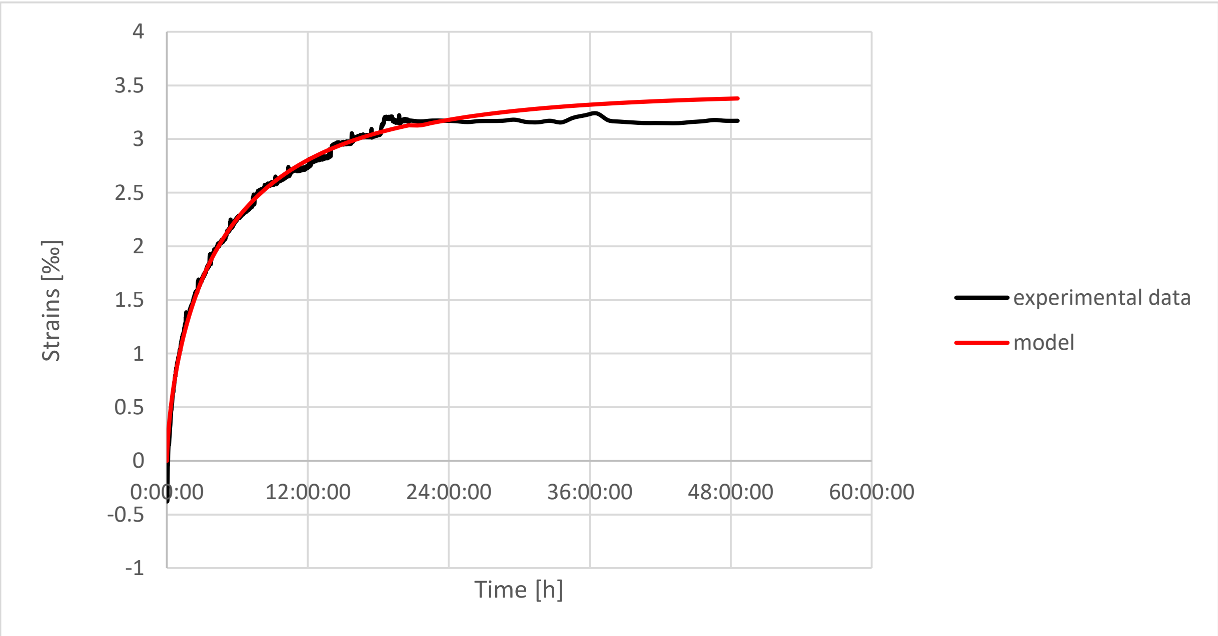

Figure 29. Application of the SE equation to the kinetics for (a) CO_2 and (b) CH_4 sorption-induced swelling of coal, for Pniówek 2.

In Figure 28, the application of the SE equation to the sorption kinetics of CO_2 and CH_4 for the Pniówek 2 sample is shown. The SE model shows a very good agreement with the experimental data obtained for Pniówek 2 coal for both gases' sorption kinetics (Figure 28) and for sorption-induced swelling of coal (Figure 29). This equation is able to accurately describe the sorption kinetics of CH_4 and CO_2. However, it can be seen that the models fit the experimental data for sorption and swelling better for CO_2 than for CH_4. It has been suggested by other authors [116] that this may be attributed to various factors, including

(1) the measured strain being a net effect of swelling and of any shrinkage caused by sample mechanical compression and (2) the influence of the petrographic composition and the appearance of a network of fractures [106]. The swelling of coal during sorption of CO_2 can be a heterogeneous process, depending on the maceral composition of the coal.
The values of the characteristic rate parameter k and the stretching parameter b are different for the two gases (Tables 6 and 7).

Table 6. Stretching parameters b and characteristic parameters k calculated for sorption kinetics, for sample Pniówek 2.

	b	k
CO_2	0.67	0.011
CH_4	0.63	0.00017

Table 7. Stretching parameters b and characteristic parameters k calculated for sorption-induced swelling kinetics, for sample Pniówek 2.

	b	k
CO_2	0.4	0.0011
CH_4	0.66	0.00005

As can be seen from Table 6, the rate parameter k is higher for CO_2 sorption than for CH_4 sorption, by approximately a factor of 10, as stated in [124]. The parameter b is also higher in the case of CO_2 sorption compared to the parameter b obtained by simulation of CH_4 sorption. Values of parameter b are between 0.55 and 0.75, which reflects a relatively narrow distribution of characteristic relaxation times. Staib et al. (2015) [124] state that stretching parameter b is connected with the intrinsic properties of the coal, (e.g., pore structure and composition) rather than influenced by the coal-gas interaction. In their experiments, the parameter b for CO_2 is similar to that for CH_4 for the same coal at the same pressure. This is similar to the findings presented in this chapter.
Regarding the parameters b and k obtained by applying the SE equation to swelling-induced kinetics, parameter b is lower for CO_2 than for CH_4 (Table 7) and not comparable with the value for sorption processes. In contrast, parameter k is higher for CO_2 than for CH_4 in similar way to the parameters obtained by modelling the sorption kinetics.

4.3 Conclusions

In this chapter, measurements of hard coal swelling induced by the sorption of carbon dioxide and methane under isothermal and non-isothermal conditions were made. The research shows that the coal strains attributed to CO_2 sorption are about twice the size of strains caused by CH_4. The expansion is greater in the direction perpendicular to the bedding plane than in the parallel direction. Regarding the non-isothermal research data, an observation was made that in the coal-CH_4 and coal-CO_2 systems, sorption-induced volumetric changes for the samples under the research conditions took a different course. This variation can be explained by differences in their petrographic composition.

Regarding the section on reaction modelling, finding the parameters b and k, as well as modelling sorption and swelling kinetics, helps to determine the process of the coal response to the gases introduced into the system, and calculations can be made predicting the changes in the coal transport-sorption and storage properties.

Chapter 5. CO_2 Utilization in Fly Ash

5.1 Fly Ash and its Use in the Construction Industry

The combustion of coal at a power station results in the production of a number of residues classified as a coal combustion products (CCPs). In 2010, the worldwide production of coal combustion products was approximately 0.75-1 billion tonnes, and 70% of this was in the form of fly ashes [125]. Fly ash is the residue remaining after coal combustion. Typically, it is a complex variety of organic (1-9%) and inorganic (90-99%) constituents, of which 30-84% are amorphous and 17-63% are crystalline [126]. The physical and chemical characteristics of this material differ greatly, according to the types of fuel and equipment used at the power plant. Fly ash is generally divided into two groups: siliceous type F, produced mainly by burning of bituminous or anthracite coals with a composition of more than 70 wt% of SiO_2+Al_2O_3+Fe_2O_3 and high-calcium type C (HCFA; calcareous) which is a residue from burning lignite or sub-bituminous coals with content of SiO_2+Al_2O3+Fe_2O_3 between 50% and 70% [127]. Many different types of oxides are reported in different types of fly ashes: CaO, SiO_2, Al_2O_3, Fe_2O_3, MgO, K_2O, Na_2O, SO_3, P_2O_5, TiO_2 and MnO [128]. The chemical composition is used to assess fly ashes for use as a cement replacement material. Siliceous (low-calcium) fly ashes are mainly composed of round particles – cenospheres, composed mainly of aluminosilicate glass and quartz, but sometimes also containing mullite, calcite, iron oxides, calcium silicates and sulphates [129, 130]. The microstructural composition of a fly ash is presented in Figure 30. The sizes of cenospheres vary between 8 and 1,000 µm.

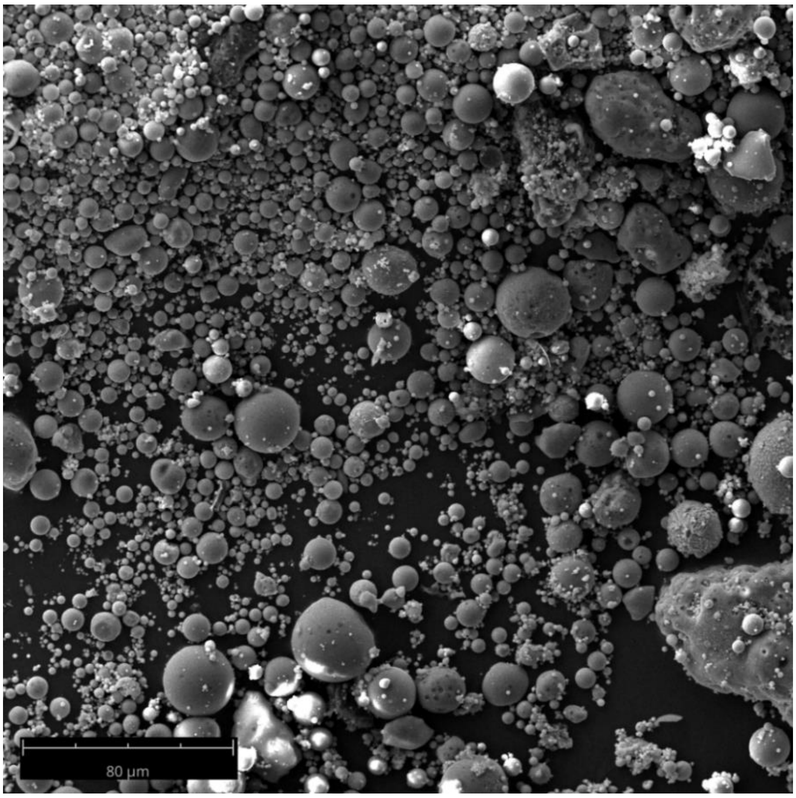

Figure 30. SEM picture of calcareous fly ash, Andorra.

Fly ash type C also contains cenospheres, but they are less abundant and other particles are also present, which have been identified as lime (Figure 31).

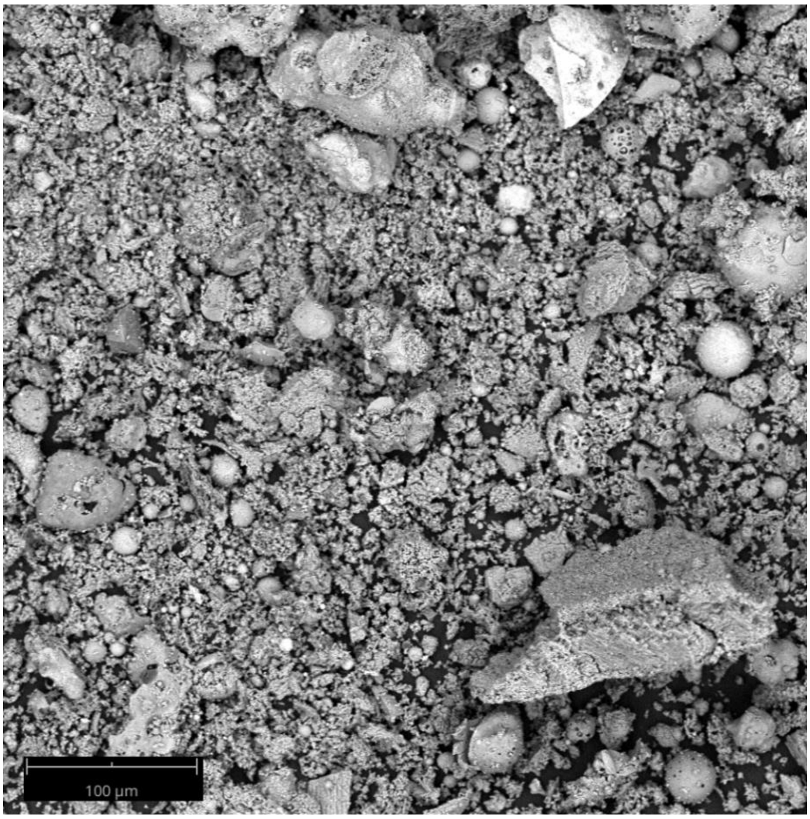

Figure 31. SEM picture of HCFA fly ash, La Pereda.

In Europe, more than 50% of the total production of fly ash is HCFA [131, 132].

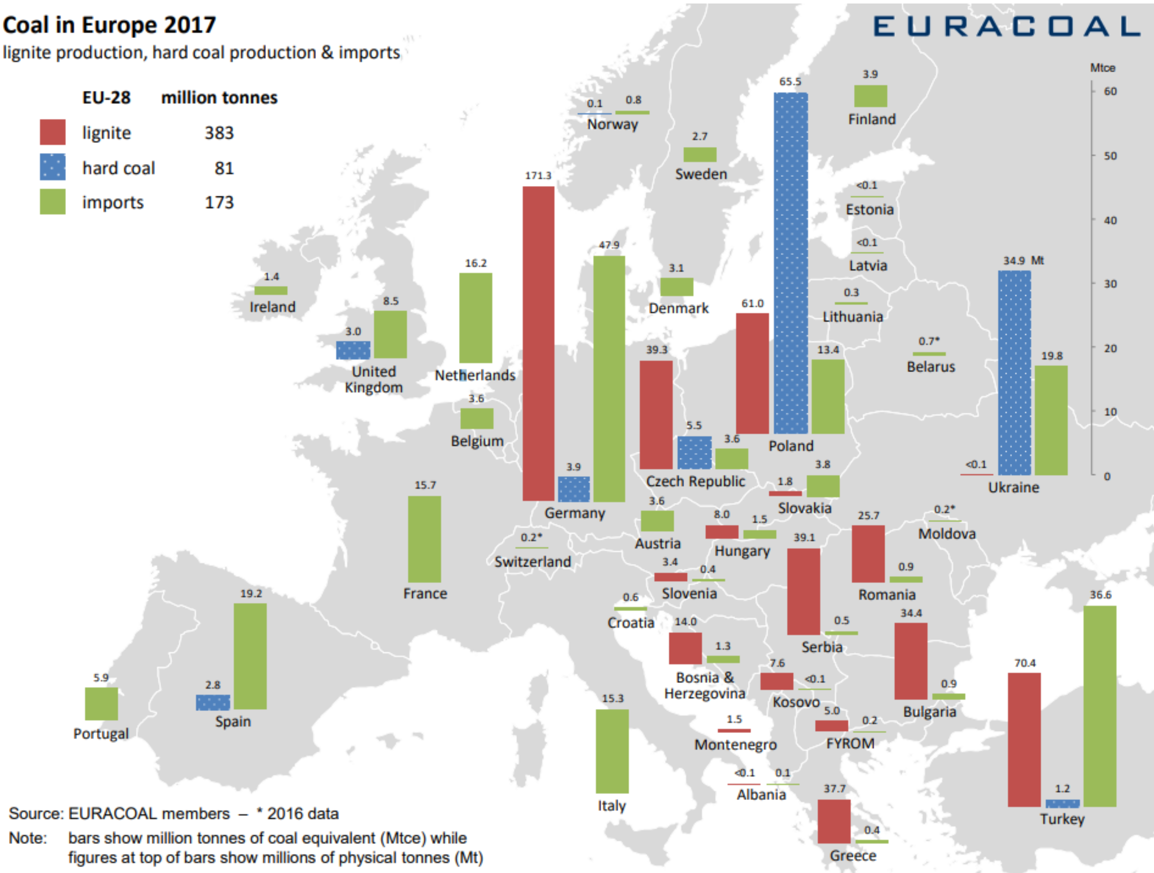

Figure 32. Coal produced and imported in Europe in 2017 (Eurocoal, 2017).

The utilization rate in the EU is 80% for the siliceous type and 20% for HCFA [133]. The production of coal ash is constantly growing and disposal of a large amount of ash waste is a considerable environmental problem.

The current fly ash utilization factor is from 3% to 97%, varying for different countries, with a world average of 16% [125]. A broad description of fly ash utilization technologies is given in [96]. To date, there have been investigations into fly ash utilization for: road sub-base material, construction industry applications, mine backfill, soil enrichment, use as an adsorbent for flue gas cleaning, removal of toxic metals and other components from waste water and synthesis of zeolites [96].

The European Union has a regulatory framework called EN 450-1 [134] on the ‘Use of Siliceous Fly Ashes in Concrete’. Its definition, specifications and conformity criteria and main requirements are shown in Table 8 [125, 134]. According to Table 8, the maximum value of free calcium oxide content in fly ash should be less than or equal to 1.5%. If this value is higher, additional tests for soundness must be performed.

Table 8. Selected requirements for fly ash, according to EN 450-1:2012.

Property of fly ash	Unit	Requirement according to EN 450-1:2012
LOI	% by mass	5-9 (depending on class)
water requirement	%	≤ 95
total phosphate (P_2O_5)	mg/kg	≤ 5
sum SiO_2 + Al_2O_3 + Fe_2O_3	% by mass	≥ 70
total content of alkalis	%	≤ 5
reactive CaO	%	≤ 10
sulphate (SO_3)	%	≤ 3
free CaO	%	if ≥ 1.5%, fly ash is checked for soundness
soundness	mm	≤ 10
magnesium oxide MgO	% by mass	≤ 4
chloride (Cl^-)	% by mass	≤ 0.10

Regarding HCFA, there are no general regulations at the European level for the utilization of this waste in concrete. EN 197 standards allow the use of HCFA in blended-type cements [135]. Type C fly ash is predominantly produced in many European countries and the lack of standards for its utilization has a negative impact on the economy and the environment [136]. Some countries have developed their own standards regarding the use of HCFA. Spain has approved the regulation 'UNE83420 – Concrete Additions - Fly Ashes Specifications for Fly Ashes with CaO Content in Excess of 10%' [137], Greece has sanctioned the regulation 'Hellenic Specification for the Use of High-Calcium Fly Ashes in Unreinforced Concrete or Cement Products' and in Poland, some certifications are recognized regarding the use of HCFA in concrete for road construction [133]. The problem associated with the use of HCFA in cement is the presence of lime in this ash type. During concrete curing, lime can additionally trigger cementitious properties in the presence of water. Moreover, the calcium oxides and the alkali sulphates can engage in cementitious and pozzolanic reactions in concrete in moist conditions. The considerable variability in the amount of lime and sulphates in HCFA is a matter of great concern when considering the admixture of this type of fly ash in cement [138].

5.2 Use of Fly Ash for Mineral Carbonation Processes

High-calcium fly ash seems to be a suitable substrate for the CO_2 carbonation process, since it has a significant content of calcium oxide (> 10%). It is also one of the most complex materials, because of its high content of silica, alumina, lime, iron oxide and unburned coal. The capacity of fly ash to sequester CO_2 depends directly on the proportion of binary oxides (CaO and MgO) and hydroxides ($Ca(OH)_2$, $Mg(OH)_2$) contained in the ash matrix. The mechanisms of various carbonation methodologies for fly ash and other waste materials have been described in chapter 3. Due to the high lime content, HCFA cannot be used to any great extent for building purposes and is currently collected in storage ponds [139]. Thus, fly ash carbonation could not only add to the mitigation of carbon dioxide emissions, but by binding the free calcium content into carbonates it may allow carbonated fly ashes to be used in more industrial applications.

In coal-fired power plants, both carbon dioxide and fly ash are produced on site. Therefore, if the carbonation reactor is placed near the power plant, the cost of carbon storage could be reduced, since there is no need for CO_2 or fly ash transportation [140, 141]. Selected available data regarding fly ash carbonation have been adapted from [139] and are presented in Table 9.

Table 9. Selected sequestration capacities and experimental conditions for fly ash carbonation experiments (Dindi, 2019).

Direct/indirect	% CaO	Method	Sequestration potential (kg/tonne)	T(ºC); p(bar); t(h)
aqueous	27.3	autoclave	296	20; 13.6
dry	2.31	fluidized bed reactor	207	45-44; 0.88-1.44; 0.03
aqueous	4.1	autoclave	26	25-60; 20; 2
aqueous	9.2	autoclave	65	90; 40; 1
aqueous	9.2	natural weathering	68	-
aqueous	29.1	autoclave	55	35; 0.15; 24
dry	32	gas adsorption cell	182	45; 1-15
indirect	29.7	autoclave	264	60; 10
indirect	11.5	autoclave	230	75; 0.1; 2-4.5
direct (semi-dry)	28	autoclave	211	25-80; 0.2-0.3; 2

aqueous	7.2	Erlenmeyer flask	8	30; 0.15; 18
direct (semi-dry)	39.8	autoclave	7.6	40; 30; 10
direct	6.74	batch reactor	26.3	40; 10; 1
aqueous	6.74	with $NaHCO_3$	50.3	30; 4; 2
aqueous	4.2	autoclave	31.1	25; 0.33kPa; 2
indirect	4.2	autoclave	28.8	25; 0.33kPa; 2

In the case of HCFA, besides utilizing CO_2, mineral carbonation may decrease the amount of free lime in fly ash through transformation to calcium carbonate. Eventually, carbonated fly ash could be used as a cement admixture [142, 143]. The literature shows that there is great interest in HCFA carbonation [140, 144, 145] and the use of carbonated fly ash in cement production [146]. It has been shown that the addition of approximately 5% of carbonated fly ash as a cement admixture could save 1.96 US dollars per tonne of cement produced [143].

5.3 Selection of Different Types of Fly Ash Materials

For the carbonation studies, different fly ashes with various CaO contents were selected. Samples were kindly provided by AGH University of Science and Technology (Belchatow and biomass fly ash), CERTH Centre for Research and Technology, Hellas (Ptolemais and Megalopoli), UPC Universitat Politècnica de Catalunya (Andorra) and Térmica La Pereda (La Pereda). Preliminary studies were performed on fly ashes from Poland, i.e., fly ash from Belchatow and fly ash derived from biomass.

5.3.1 Belchatow

Belchatow fly ash comes from a Polish coal-fired power plant with 5,298 MWe of installed electric power and 375.5 MWt of available thermal power. The batch fuel in the power plant is brown coal. The power plant is equipped with 13 electric blocks and flow pulse boilers. An XRF analysis of the chemical composition was carried out for the Belchatow fly ash sample (Table 10). The tested fly ash is characterized by more than 15% calcium oxide. In addition to the high calcium content, the examined material contains relatively large amounts of unburned carbon, the particles of which are visible in Figure 33.

Table 10. X-ray fluorescence analysis of Belchatow fly ash.

Content [%]	Belchatow
Na_2O	0.927
MgO	0.853
Al_2O_3	13.145
SiO_2	37.217
P_2O_5	0.451
SO_3	2.929
K_2O	0.205
CaO	15.336
TiO_2	1.586
V_2O_5	0.039
Cr_2O_3	0.023
MnO	0.024
Fe_2O_3	4.989
Co_3O_4	0.018
NiO	0.009
CuO	0.006
ZnO	0.013
BaO	0.021

Calculated from XRD results, the maximum theoretical CO_2 capacity of this fly ash is 120.5 gCO_2/kg fly ash.

The technical analysis of Belchatow fly ash is shown in Table 11.

Table 11. Technical analysis of Belchatow fly ash.

Content	Fly ash Belchatow
Water content [%]	0.30
Volatile matter [%]	2.54
Ash [%]	98.10
H [%]	0.02
C [%]	1.91
S [%]	0.56
Helium/real density [g/cm^3]	2.43

Figure 33. Photograph of the Belchatow fly ash.

Powder X-ray diffraction (XRD) was used to determine the mineralogical composition of the sample (Figure 34). The fly ash is rich in quartz (SiO_2) and mullite ($Al_6Si_2O_{13}$).

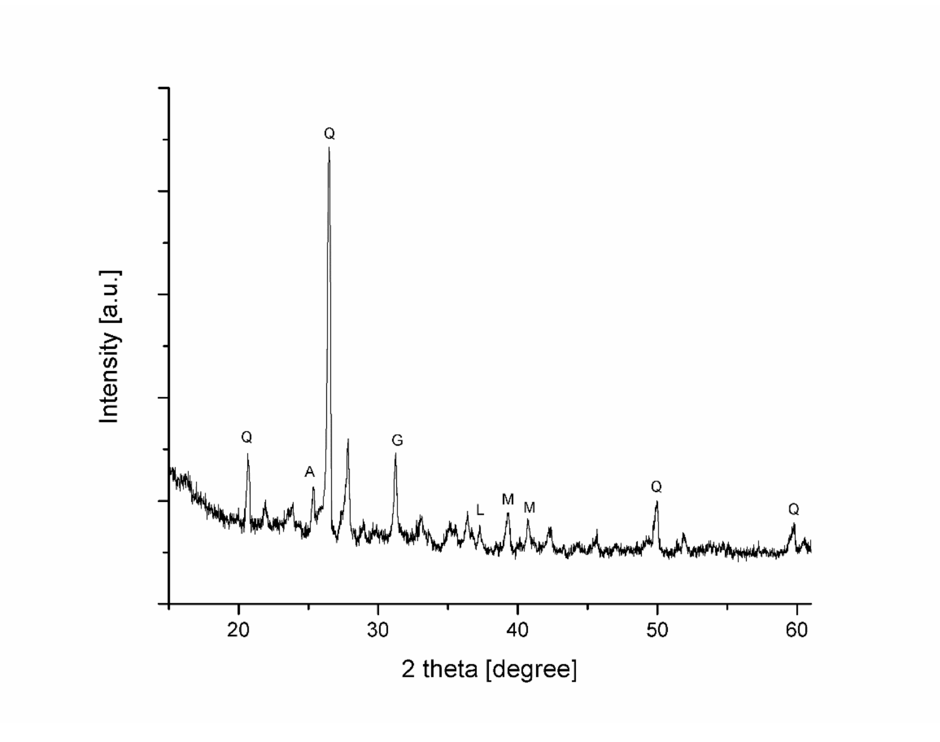

Figure 34. XRD analysis of the Belchatow fly ash sample. Q – quartz, A – anhydrite, G – gehlenite, L – lime, M – mullite.

Thermogravimetric analysis (TGA) of the untreated Belchatow fly ash is shown in Figure 35.

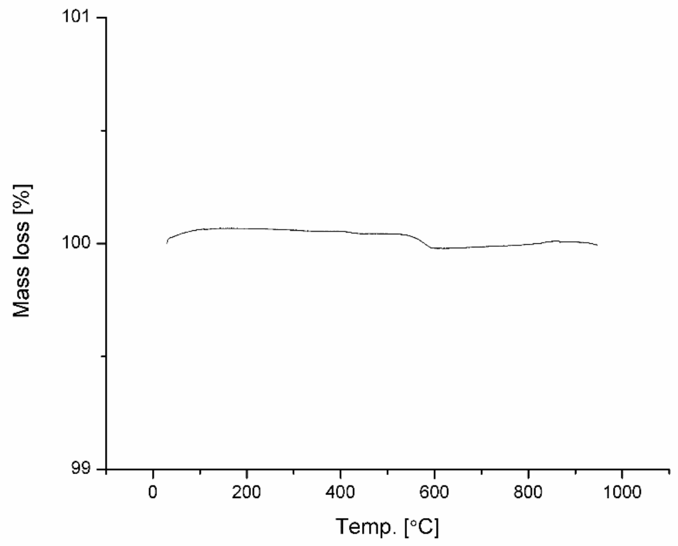

Figure 35. TGA analysis of the Belchatow fly ash.

A scanning electron microscopy study of the fly ash is shown in Figure 36. It is rich in cenospheres, i.e., spherical structures made of aluminosilicate glass and quartz with diameters of about 30-40 μm.

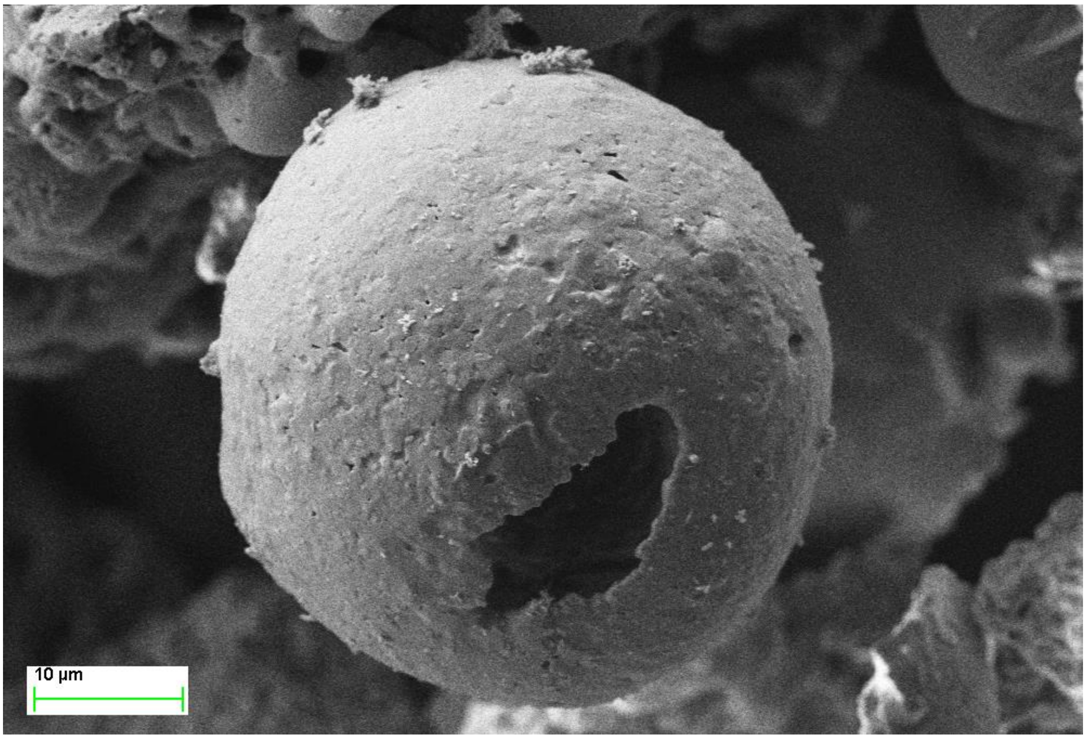

Figure 36. SEM picture of the Belchatow fly ash.

5.3.2 Biomass Fly Ash

The biomass fly ash is a waste produced during the burning of sunflower biomass. It was generated at a Polish power plant consisting of seven electric blocks with 1,882 MWe of electric capacity, where one 225-MWe block is 100% biomass-fired. The chemical composition is presented in Table 12. This fly ash is characterized by 12.01% total CaO content.

Table 12. X-ray fluorescence analysis of biomass fly ash.

Content [%]	Biomass fly ash
SiO_2	51.33
CaO	12.014
Al_2O_3	10.419
MgO	3.183
Na_2O	0.371
P_2O_5	2.178
SO_3	5.658
K_2O	8.090
TiO_2	0.265
Cr_2O_3	0.011
MnO	0.293
Fe_2O_3	1.303
NiO	0.055
ZnO	0.056
BaO	0.057
Cl	1.641
SrO	0.049
ZrO_2	0.024
CuO	0.016
Rb_2O	0.014
PbO	0.014

The technical analysis of biomass fly ash is shown in Table 13.

Table 13. Technical analysis of biomass fly ash.

Content	Biomass fly ash
Water content [%]	0.30
Volatile matter [%]	2.46
Ash [%]	97.60
H [%]	0.01
C [%]	0.90
S [%]	1.04
Helium/real density [g/cm^3]	2.20

The powder X-ray diffraction results are presented in Figure 37.

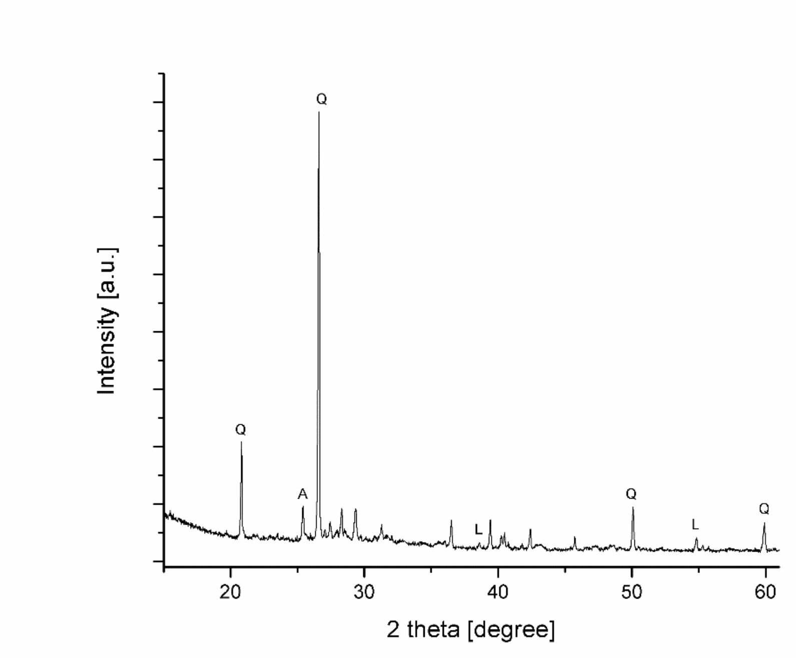

Figure 37. XRD analysis of the biomass fly ash. Q – quartz, A – anhydrite, L – lime.

The TGA analysis is shown in Figure 38. Biomass fly ash is characterized by a significant initial carbonation, visible as a mass loss between 550 and 900°C. A scanning electron micrograph of the biomass fly ash sample can be seen in Figure 39.

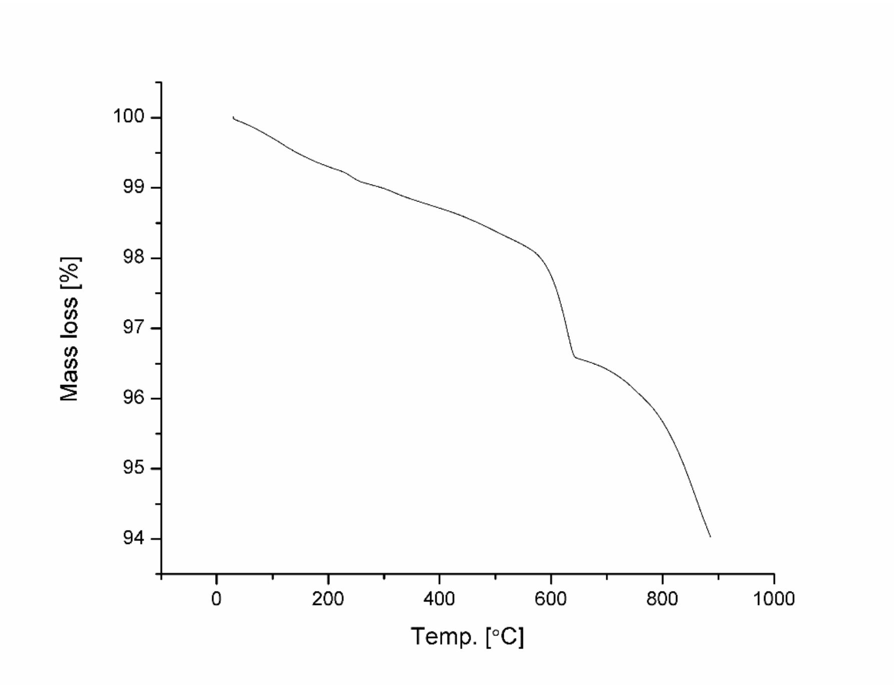

Figure 38. TGA analysis of the biomass fly ash.

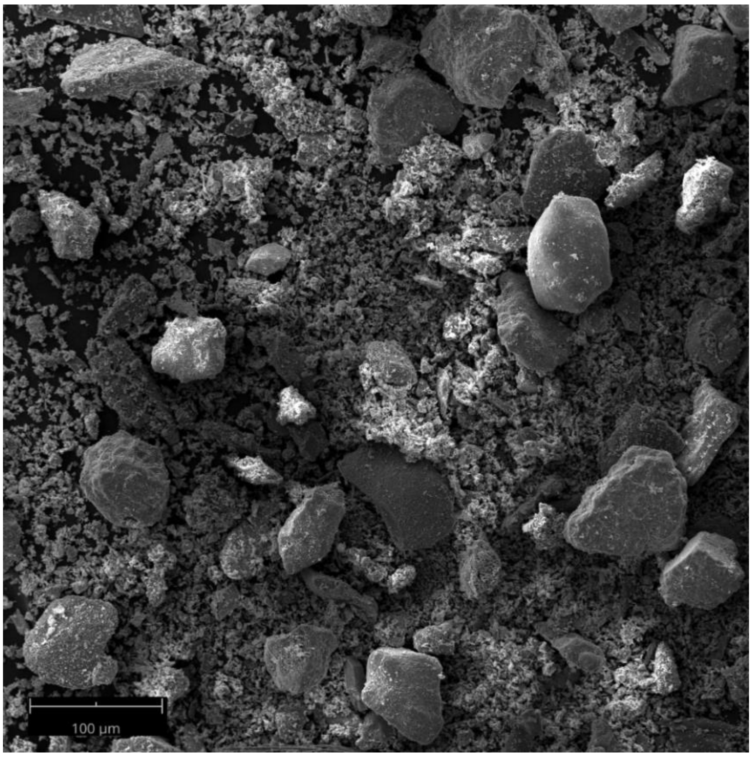

Figure 39. SEM picture of biomass fly ash.

5.3.3 Andorra

Andorra fly ash is a residue remaining after burning lignite coal at the Andorra Power Plant in Aragón, Teruel. This power plant has a 1,050-MW power capacity. This fly ash is classified as silico-aluminous with some content of calcium oxide (8.3%), as can be seen from the XRF analysis (Table 14).

Table 14. Chemical composition of Andorra fly ash.

Content [%]	Andorra
Al_2O_3	24.7
SiO_2	40.6
MgO	1.5
Fe_2O_3	20.0
CaO	8.30
P_2O_5	0.4
SO_3	0.6
K_2O	1.2
TiO_2	0.8
SrO	0.1
Na_2O	0.3
LOI	1.7

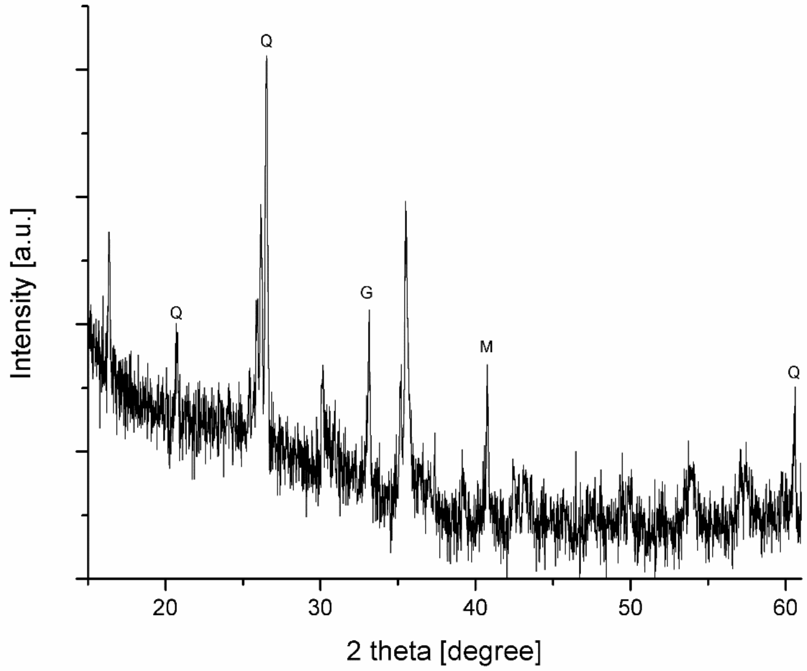

Figure 40. XRD analysis of the Andorra fly ash sample. Q – quartz, G – gehlenite, M – mullite.

As can be seen in Figure 40, the mineral composition of Andorra fly ash is dominated by the presence of quartz, gehlenite and mullite. An SEM micrograph of Andorra fly ash is shown in Figure 30. The majority of the visible particles are identified as cenospheres.

5.3.4 La Pereda

Fly ash from La Pereda (Spain) comes from the La Pereda Thermal Power Plant located in Asturias, Spain. This is a co-fired power plant with a power capacity of 50 MW, where coal fuel, cob gas and biomass are used. The increased content of CaO in the fly ash (Table 15) is due to the post-combustion capture technology used on site, where lime acts as an adsorber for the CO_2 and some of the residues are mixed with the fly ash [147].

Table 15. X-ray fluorescence analysis of the La Pereda fly ash.

Content [%]	La Pereda
SiO_2	46.68
CaO	10.33
Al_2O_3	22.72
MgO	1.33

Na_2O	0.72
SO_3	4.69
K_2O	3.33
Fe_2O_3	6.51
TiO_2	0.97
P_2O_5	0.09

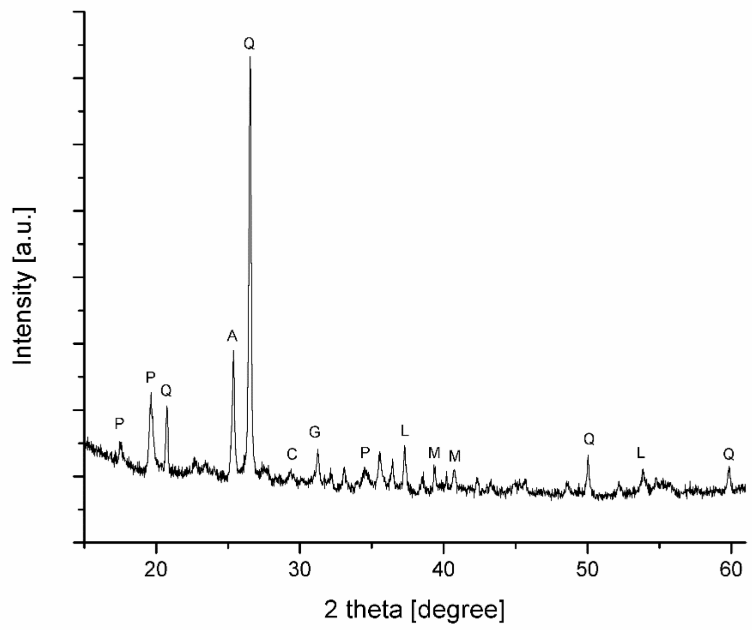

Figure 41. XRD analysis of the La Pereda fly ash. Q – quartz, C – calcite, P – portlandite, A – anhydrite, G – gehlenite, L – lime, M – mullite.

As can be seen in Figure 41, there are many crystal phases detected in the La Pereda sample: quartz, anhydrite, lime, gehlenite, mullite and some portlandite and calcite.

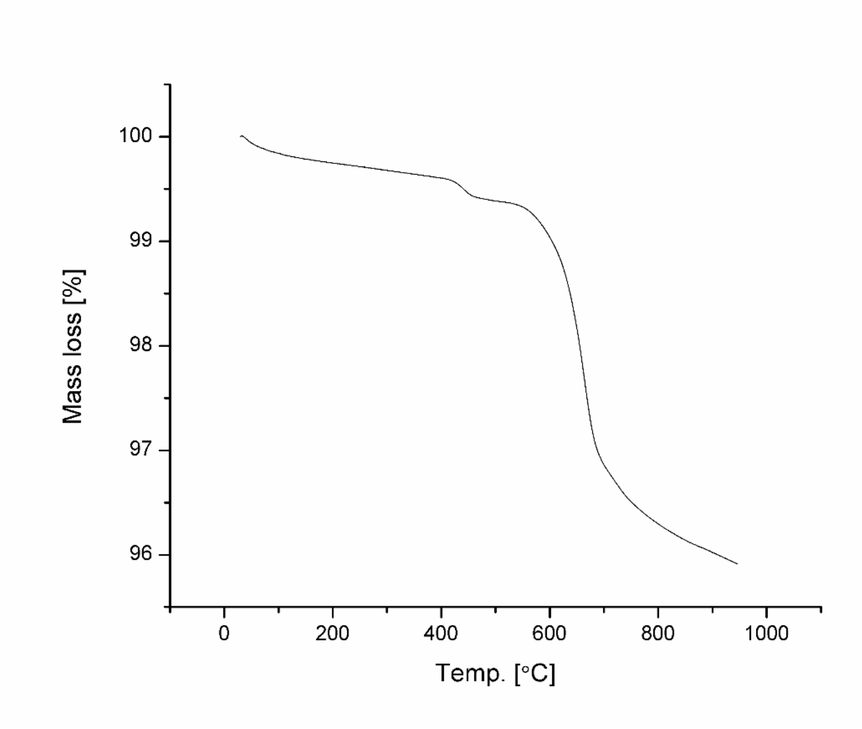

Figure 42. TGA analysis of La Pereda fly ash.

The TGA analysis of La Pereda fly ash confirms the presence of portlandite, as evidenced by a decomposition peak between 400 and 600°C. This fly ash has a significant amount of initial natural carbonation, equal to 29.5% of its capacity to store CO_2. SEM analysis of the untreated fly ash sample identified a lack of cenospheres in the material.

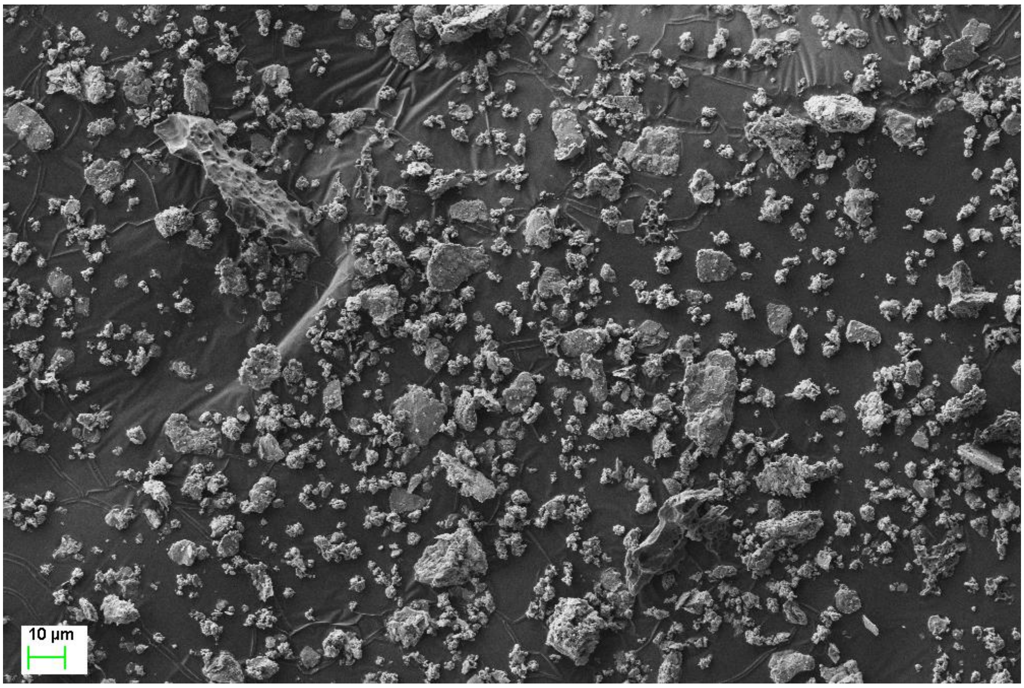

Figure 43. SEM picture of the La Pereda fly ash.

5.3.5 Ptolemais

Ptolemais is a high-calcium fly ash originating from burning lignite coal from the main and northern lignite fields in Ptolemais, Greece. It was produced at the Ptolemais power station, which has 660 MWe of installed electrical power. This power plant has five electric blocks equipped with electrostatic precipitators as filters. Fly ash production reaches 7.6 Mt/year, with only 300 kt being recycled. The rest is being disposed of in exhausted mine workings. A limited amount is used by cement companies for the manufacture of blended cements and specialized Portland cements. Since 2002, Ptolemais fly ash has been accepted under European Standard EN 197-1 [148]. Chemical analysis was performed for this sample (Table 16).

Table 16. X-ray fluorescence analysis of the Ptolemais fly ash.

Content [%]	Ptolemais
SiO_2	33.11
CaO	35.27
Al_2O_3	13.76
MgO	3.21
Na_2O	1.33
SO_3	4.98
K_2O	0.95
Fe_2O_3	5.72
TiO_2	0.67
P_2O_5	0.35

The major components of the fly ash are: SiO_2 (33%), CaO (35%) and Al_2O_3 (13%). Compared to other HCFA samples, the Ptolemais fly ash has one of the highest values of CaO in the world [128]. The crystalline phases detected by the XRD analysis in the fresh sample (Figure 44) are lime, quartz, gehlenite, anhydrite and calcite. The presence of calcite in the pre-reaction sample may be related to the reaction of fresh ash with carbon dioxide in the air, prior to the experiments.

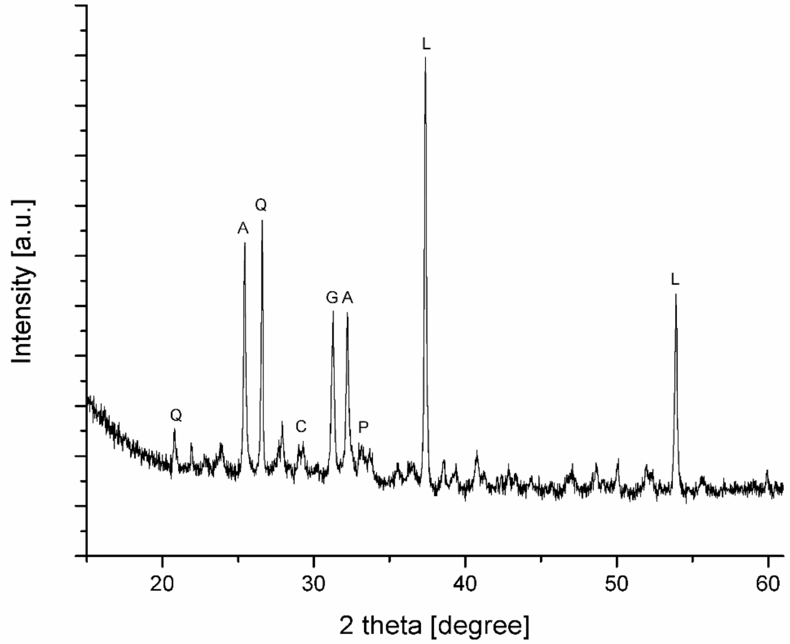

Figure 44. XRD analysis of the Ptolemais fly ash sample. Q – quartz, A – anhydrite, G – gehlenite, L – lime, M – mullite, P – portlandite.

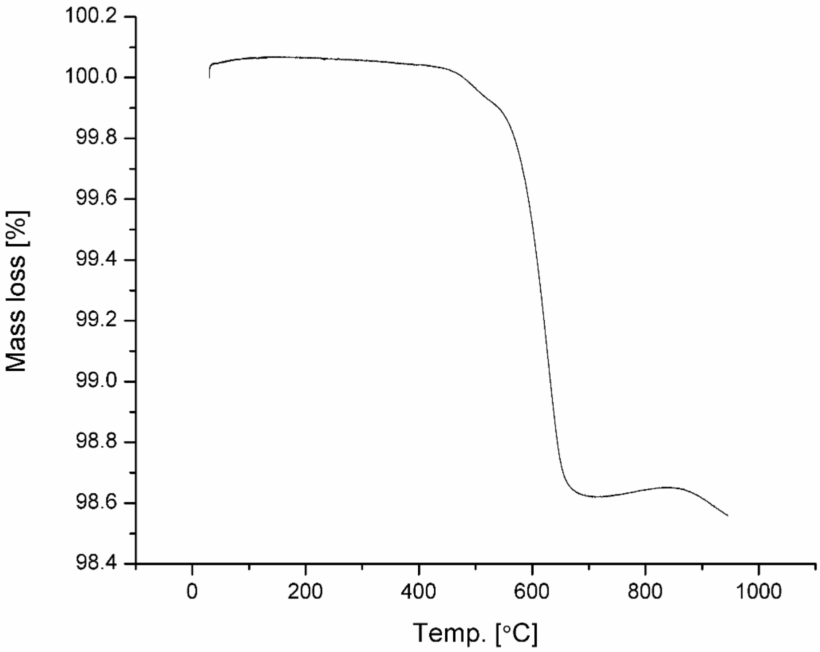

Figure 45. TGA analysis of the Ptolemais fly ash.

Considering that all of the calcium detected by the XRF analysis is accessible for carbonation, the theoretical maximum CO_2 sequestration capacity is 277.1 g CO_2/kg fly ash. The TGA analysis revealed 1.6% initial carbonation of the sample.

Figure 46 shows the major compounds of the untreated fly ash. It consists mainly of lime and round cenospheres which are made of aluminosilicates and quartz.

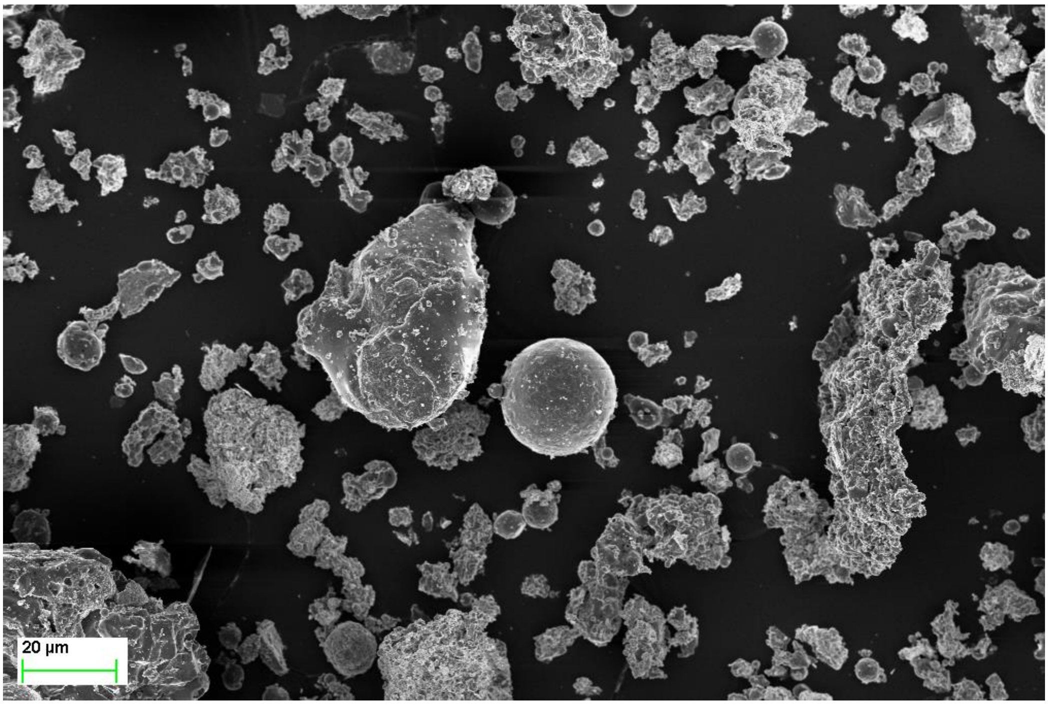

Figure 46. SEM picture of Ptolemais fly ash.

5.3.6 Megalopolis

The Megalopolis (Greece) fly ash is a residue produced from Megalopoli Power Plant in Arcadia, Greece. This power plant uses lignite and black coal and has a total power capacity of 850 MW. The sample is characterized by 13.12% CaO (Table 17).

Table 17. X-ray fluorescence analysis of Megalopolis fly ash.

Content [%]	Megalopolis
SiO_2	50.72
CaO	13.12
Al_2O_3	17.66
MgO	2.51
Na_2O	1.85

SO_3	2.61
K_2O	1.81
Fe_2O_3	8.14
TiO_2	0.88
P_2O_5	0.22
SrO	0.11

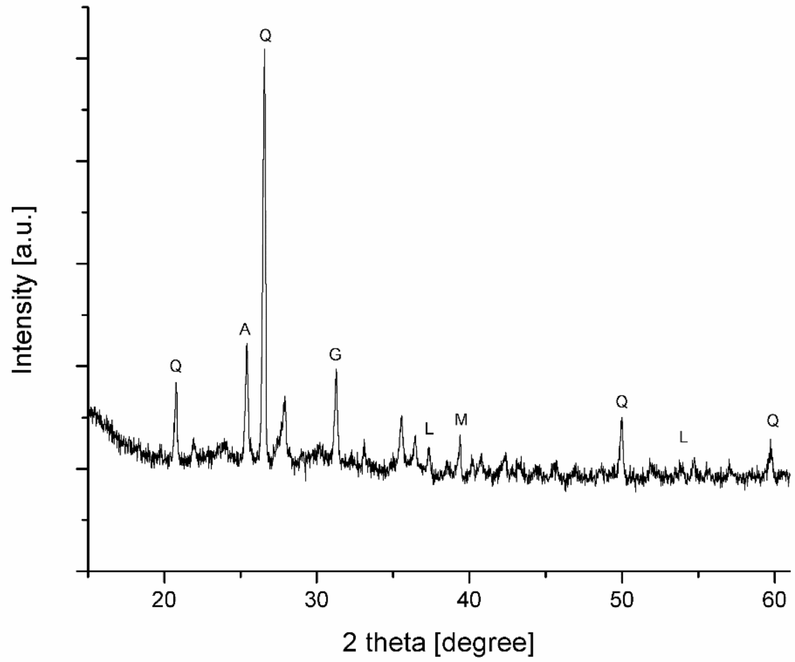

Figure 47. XRD analysis of the Megalopolis fly ash sample. Q – quartz, A – anhydrite, G – gehlenite, L – lime, M – mullite.

Megalopolis fly ash is rich in quartz (SiO_2) and mullite ($Al_6Si_2O_{13}$). Peaks of lime (CaO), anhydrite ($CaSO_4$) and gehlenite ($Ca_2Al[AlSiO_7]$) are also visible.

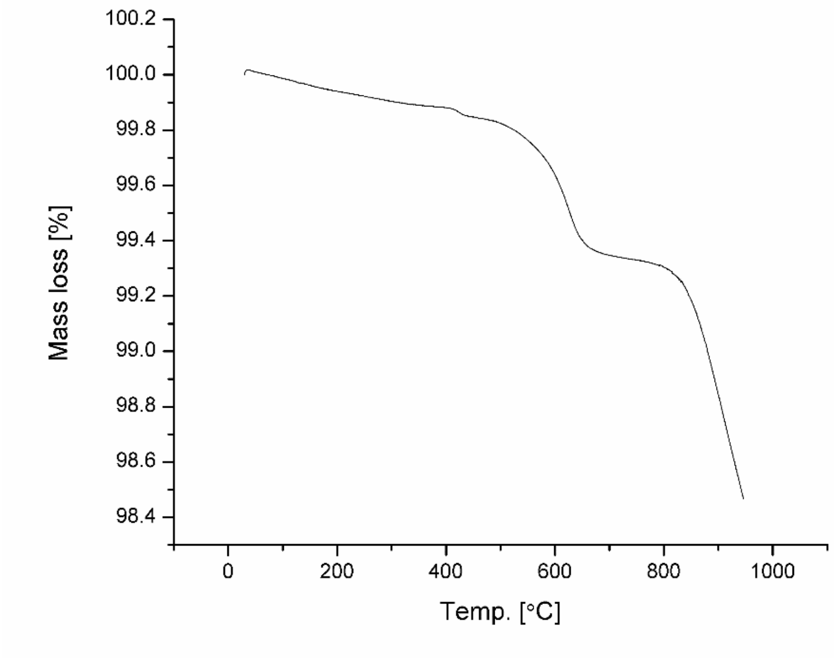

Figure 48. TGA analysis of Megalopoli fly ash.

The TGA analysis revealed a small mass loss in the region of ~400°C, corresponding to the presence of portlandite, together with two peaks in the region between 550 and 900°C, related to the calcium carbonate decomposition. Initial carbonation in this fly ash is 1.6%. The maximum theoretical CO_2 sequestration potential is 103.1 gCO_2/kg fly ash.

Figure 49 shows the microstructural analysis of the fly ash. Various shapes and sizes of particles are detected, including cenospheres.

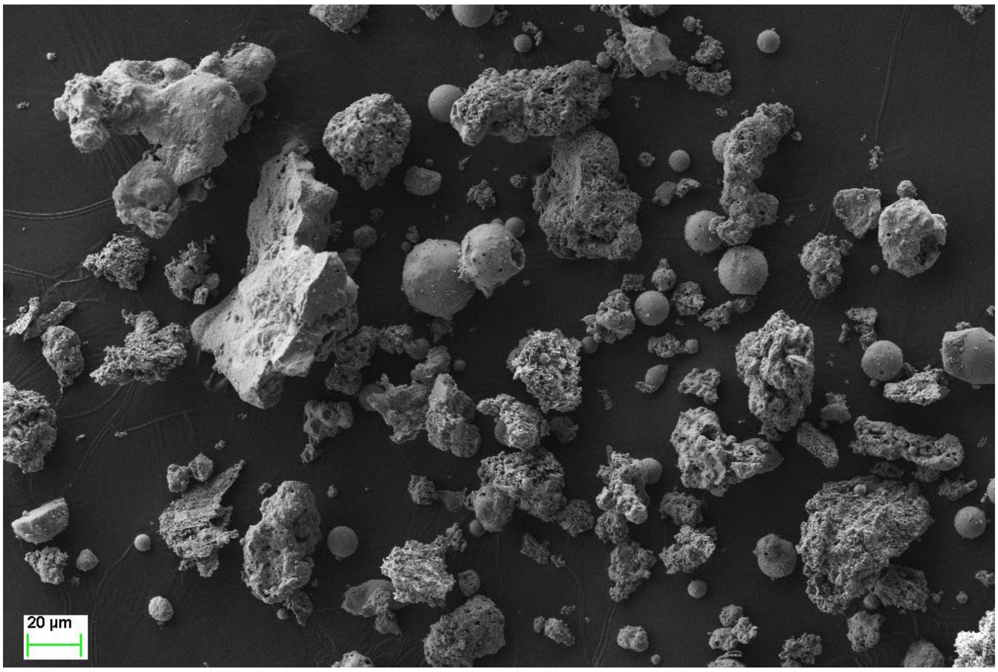

Figure 49. SEM picture of Megalopolis fly ash.

Chapter 6. Feasibility Study for Fly Ash Carbonation

This chapter presents results of the feasibility studies for the carbonation process at increased temperatures and pressures. The research was done on samples of Belchatow fly ash and biomass-derived fly ash. Experiments were performed on apparatus whose primary use is for sorption/desorption processes of gases on solids at increased pressures.

6.1 Carbonation of Belchatow Fly Ash

In this study, mineral carbonation of the high-calcium fly ash from Belchatow power plant was performed at a laboratory scale, in the temperature range from 25°C to 70°C and a CO_2 pressure range of 4-16 bar. Laboratory investigations showed that the carbon dioxide uptake increases with pressure. The results demonstrate the potential of coal fly ash as a material for CO_2 utilization.

This study has been published in [149].

6.1.1 Methodology

Fly ash from Belchatow has been described in section 5.3.1. The experiments were carried out on the original equipment used for sorption and desorption of gases at elevated pressures (Figures 50 and 51). The scheme of the system is presented in Figure 52. The principle of volumetric measurement consists in expanding a gas of known pressure and volume from a dosing ampoule into an ampoule containing a sorbent. The main part of the device is a metal container with a capacity of 1 dm^3, placed in a water thermostat. The compressed carbon dioxide is introduced into the dosing ampoule and then, by opening the valves, it is dispensed into an ampoule containing a fly ash sorbent. The thermostat provides a constant temperature with an accuracy of ±1°C. In order to obtain the correct results, it is necessary to know the dead volume of the apparatus, which was calculated by subtracting the volume of ash grains from the total volume of the apparatus. When the dead volume of the system is known, the amount of absorbed carbon dioxide can be calculated from the gas laws, taking into account gas inertia. Before each experiment, the apparatus was degassed into a vacuum.

Figure 50. Apparatus for the sorption processes (Cwik, 2017).

Figure 51. Fly ash inside the sample chamber.

The analysis of the sorption of low-pressure carbon dioxide at 0°C was also performed. The experiment was carried out using the Autosorb-1-C apparatus from Quantachrome Instruments over a wide range of relative pressures from approximately 10^{-7} to 0.99. Before the experiment, the ash sample was vacuum-cured at 105°C for 12 hours.

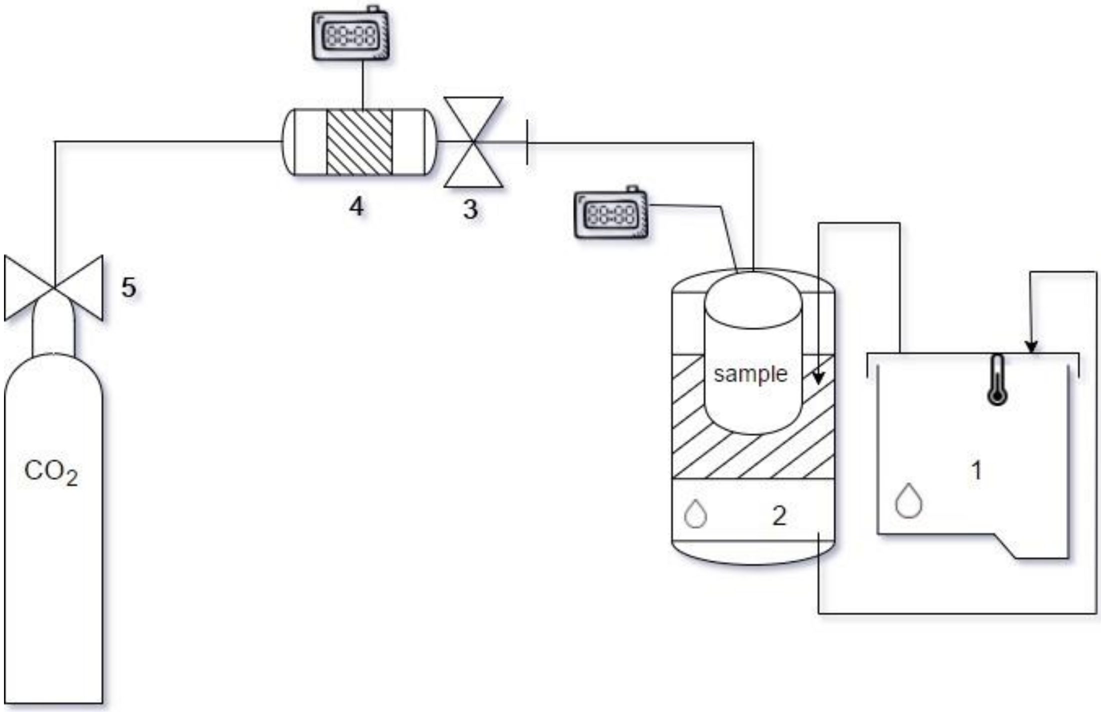

Figure 52. The scheme of the apparatus for sorption processes.

6.1.2 Procedure

Three series of experiments were carried out at three selected temperatures: 25, 50 and 70°C. In each of the experiments, three carbon dioxide pressures were used: firstly ~5 bar, secondly ~10 bar and finally ~15 bar. Subsequent gas dosing was done after achieving a pressure balance in the apparatus, i.e., no change in carbon dioxide pressure greater than 0.1 bar within 60 minutes. This resulted in a reaction time at a given temperature and pressure of between 48 and 72 hours. The mass of the samples was chosen in order to fill the measuring ampoule to the maximum extent. Table 18 presents the data regarding sample masses, temperatures and pressures.

Table 18. Experimental data.

Sample mass [g]	Temperature [^{o}C]	Pressure 1 [bar]	Pressure 2 [bar]	Pressure 3 [bar]
679.8	298	6.36	10.47	14.95
744.4	323	4.20	11.75	14.97

750.9	343	4.62	10.85	14.97

6.1.3 Results and Discussion

The results of the dependence of the amount of CO_2 absorbed as a result of carbonation on pressure and temperature, are presented in Figure 53.

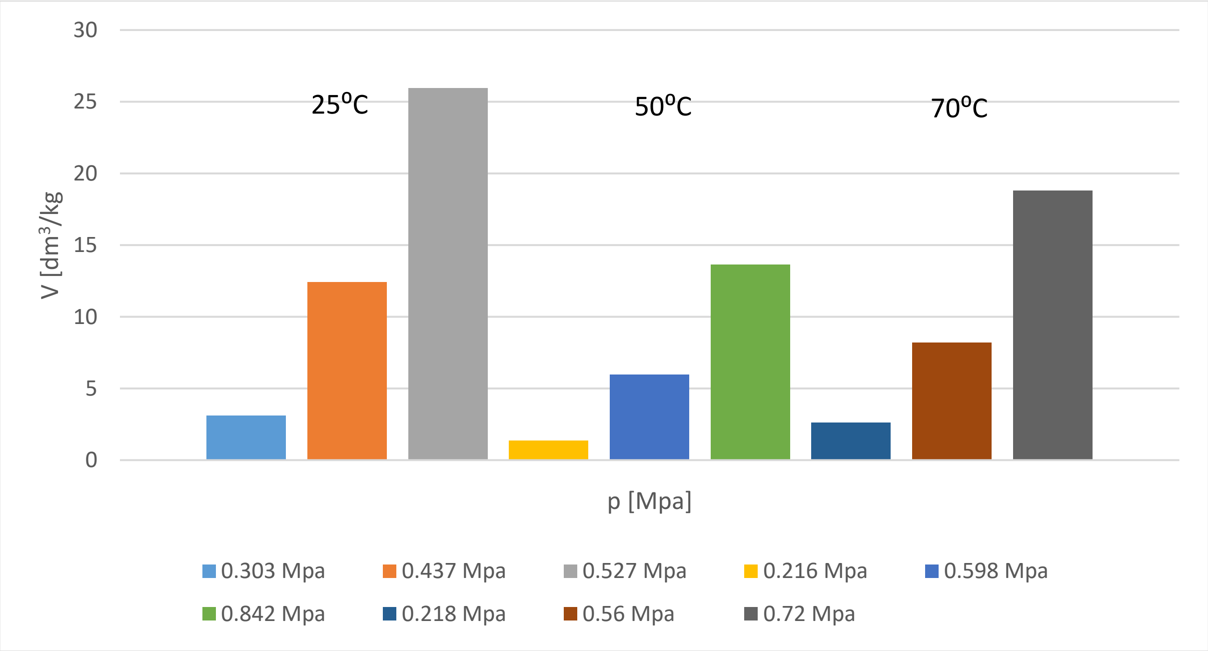

Figure 53. The amount of CO_2 absorbed, for a given pressure and temperature (Cwik, 2017).

The first observation is that there was an increase in the amount of captured carbon dioxide with increased gas pressure. The maximum value of the sorbed CO_2 volume was observed at 25°C and is at the level of almost 26 dm^3/kg of ash at a pressure of 0.527 MPa. Lackner et al. (1995) [60] showed that for a given temperature, the carbonation process depends on the pressure of carbon dioxide inside the reactor and the chemical composition of the sorbent. Comparing the results obtained at different temperatures, the highest results are achieved at a temperature of 25°C, for each of the pressure values. This may indicate the occurrence of a physical adsorption process which, taking into account the obtained high results at low temperatures, may represent in this case a CO_2 capture mechanism. The physical and chemical adsorption processes may occur simultaneously. Physical adsorption under the research conditions can occur because of the large fly ash surface area, as well as the unburned coal present [150]. Undoubtedly, physical contact at the interface allows a significant interaction between

CO_2 molecules and the ash surface, contributing to the intensification of the carbonation process. Details of the surface adsorption process for carbon dioxide were presented by Burghaus [151].
The quantitative results allow the conclusion that high-calcium fly ash from brown coal combustion is a good substrate for the storage of carbon dioxide, as it absorbs significant amounts of this gas. Both temperature and pressure have a significant impact on the amount of CO_2 captured.

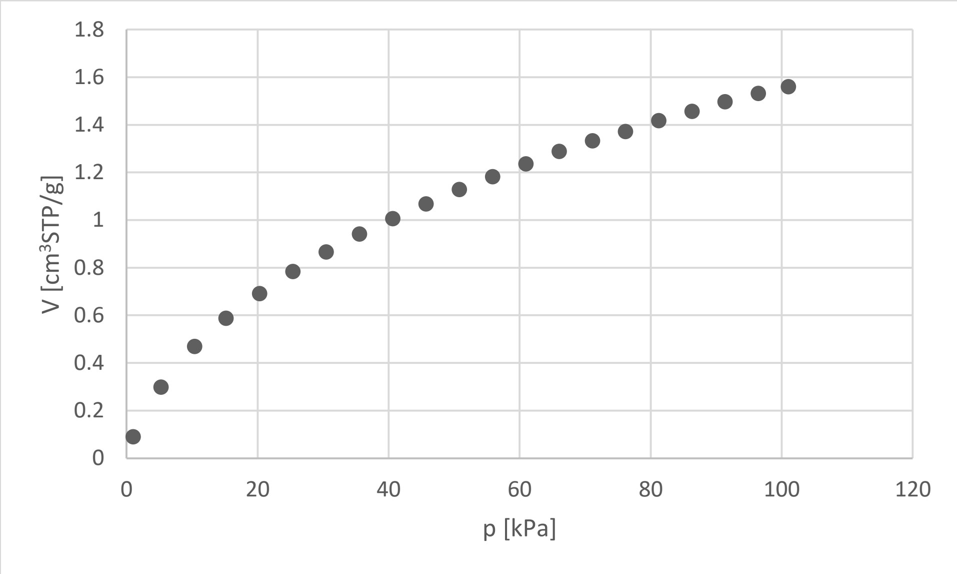

Figure 54. Isotherm of low-pressure sorption of carbon dioxide in fly ash (Cwik, 2017).

The obtained results for sorption carried out at low pressure (Figure 54) confirm the results of the main experiment. An increase in the sorbed volume of carbon dioxide was observed with an increase in pressure, and the value of sorption at a pressure of 1 bar is at a similar level as in tests at elevated pressures.

The analysis of the fly ash crystalline phase composition after reaction with CO_2 was undertaken via X-ray diffraction. Figure 55 shows the diffractograms of the untreated ash sample and the sample after the carbonation process at selected temperatures. The chemical (Table 10) and XRD analyses show the main components of high-calcium fly ash: silica, calcium oxide, aluminium oxide and iron (III) oxide. These components constitute 70% of this industrial waste. These values are consistent with the results of analyses of the composition of other fly ashes presented in the literature [152]. XRD analysis showed the presence of the following compounds: quartz (SiO_2), calcite ($CaCO_3$), anhydrite ($CaSO_4$), calcium oxide (CaO) and mullite ($Al_6Si_2O_{13}$), in both pre-and post-carbonation samples. The presence of calcite in the sample before the reaction may be related to the reaction of fresh ash with carbon dioxide in the air during the storage of this waste. The analysis did not reveal the presence of portlandite ($Ca(OH)_2$) in the sample before the reaction, which indicates a lack of natural hydration of the ash [153]. Previous studies show that the carbonation reaction between gas and solid is difficult to achieve, and water access is one of the most important parameters in the mineralization process [68].

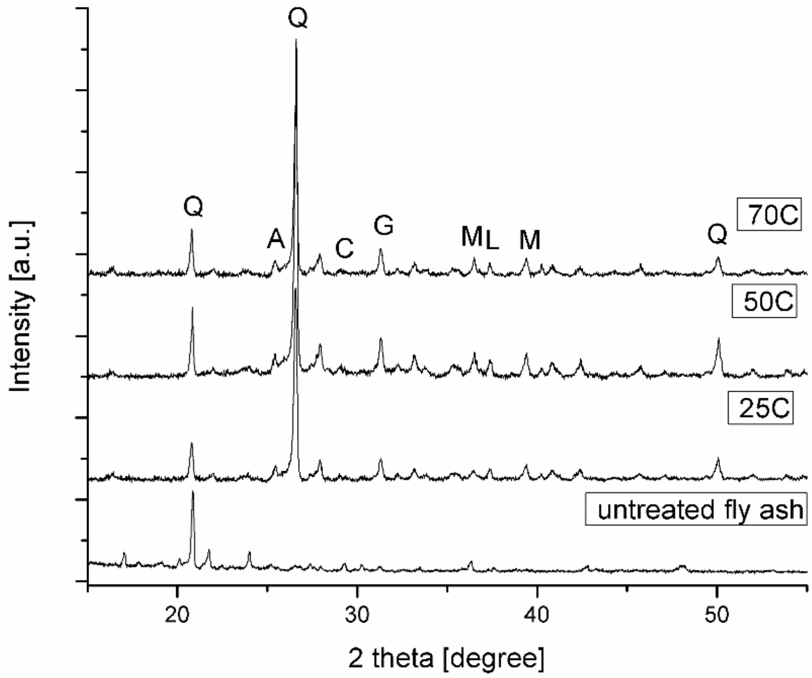

Figure 55. XRD analysis of the untreated and treated samples. Q – quartz, A – anhydrite, C – calcite, G – gehlenite, M – mullite, L – lime.

6.1.4 Conclusions

Carbonation studies are presented for high-calcium fly ash at three different temperatures, with a gradual increase of the CO_2 pressure. Laboratory tests showed that for a temperature of 25°C and a pressure spectrum of 4-15 bar, the amount of absorbed carbon dioxide was 25.937 dm^3/kg. There was an increase in CO_2 uptake with increasing pressure. However, this trend was not maintained in the event of a rise in temperature.

The research results indicate a high potential for the use of fly ash with a high calcium content for carbon dioxide capture. The XRD characteristics of the ash samples, before and after the reaction, indicate the important role of fly ash pre-hydration. Enrichment of this substrate with even a small amount of water accelerates the process and significantly increases the conversion of carbon dioxide to carbonate.

The presented test method, i.e., carbonation at low temperatures and moderate pressures, allows for a reduction of process energy costs compared to other methods presented in the literature and does not require the use of expensive materials for the construction of apparatus. In addition, it is possible to regulate the conditions of the experiment (pressure, temperature) and its duration.

6.2 Preliminary studies – Biomass Fly Ash

The aim of this section is to study gas-solid carbonation of biomass fly ash. The process is maintained at three different temperatures: 25, 50 and 70°C, in a pressure range from 4 to 16 bar. The goal of the paper is to evaluate the effect of temperature and pressure on the carbonation rate.

6.2.1 Methodology

The methodology used to perform this investigation is the same as in section 6.1.1. The test material, i.e., fly ash derived from biomass, has been described in section 5.3.2.

6.2.2 Procedure

This set of experiments was performed according to the procedure described in section 6.1.2.

6.2.3 Results and Discussion

Figure 56 shows the carbon dioxide uptake for the biomass fly ash sample, depending upon the pressure and temperature. An increase in CO_2 uptake was found with an increase in pressure. Furthermore, higher CO_2 uptake can be observed with an increase in the temperature of the process.

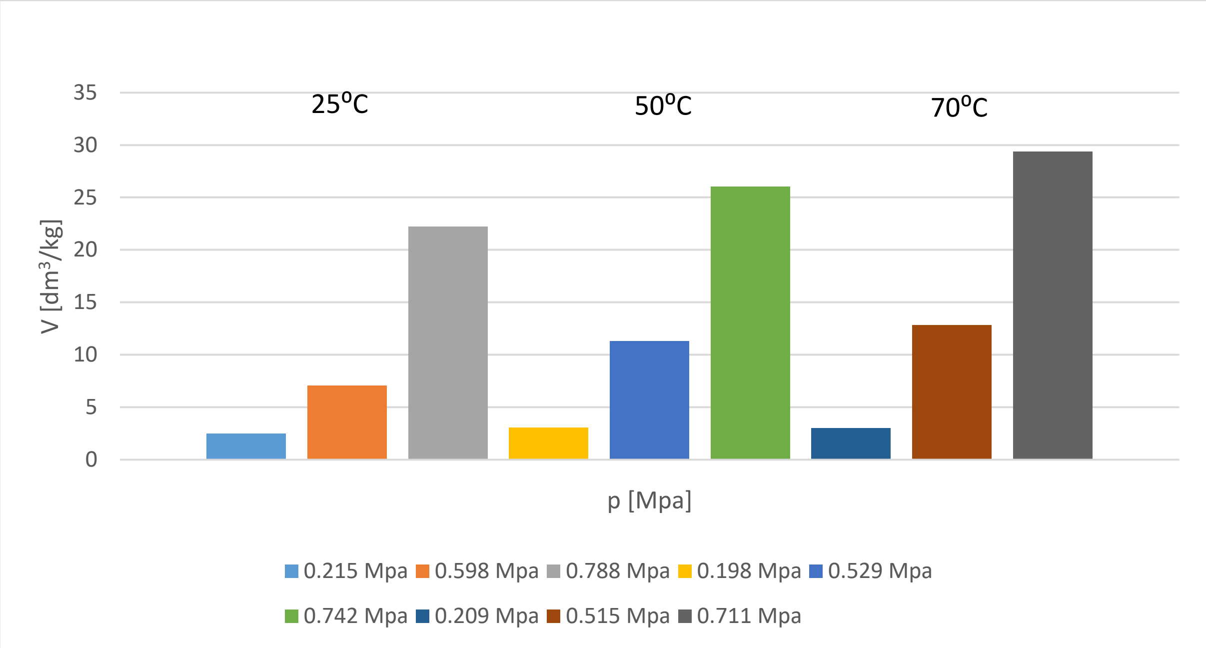

Figure 56. CO_2 uptake with increases in pressure and temperature – biomass fly ash.

The results presented in Figure 56 indicate that the carbonation of biomass fly ash is influenced by increases in pressure and temperature. The highest carbon dioxide uptake was achieved at 70°C and 0.71 MPa, equal to almost 30 dm^3/kg of fly ash. In each experiment, the CO_2 uptake increased with pressure and with temperature. Accelerating mineral carbonation via an increase in temperature is supported by other investigations [61]. Presenting a reaction mechanism to explain the increase of CO_2 uptake at higher temperatures is problematic. One can hypothesize that at low temperatures, superficial carbonation phenomena is promoted and the formation of a carbonate shell over the particle surfaces occurs. At higher temperatures, diffusion processes are more effective, and the carbonation can proceed through the bulk material. Temperature plays important role in this process since it affects diffusion, the reaction kinetics and the thermodynamic properties [83]. Compared to carbonation of Belchatow fly ash under the same conditions, the uptake of carbon dioxide by biomass fly ash is higher. This is probably caused by greater chemical absorption. Explanation of the considerable CO_2 uptake by Belchatow fly ash in 25°C could be explained by the carbon content (1.9%, Tab.11) and possibility of physical adsorption occurrence.

XRD analyses of the samples before and after carbonation are shown in Figure 57. The following compounds were detected: quartz, calcite, anhydrite, lime, portlandite, mullite and gehlenite. The presence of portlandite before reaction demonstrates ash hydration prior to the experiments, which is important for accelerating the reaction. Previous studies have shown that the carbonation reaction between gas and solid is difficult to achieve and that water access is one of the most important parameters in the mineralization process [81]. The technical analysis revealed a moisture content of

0.3% (Table 12). A higher moisture content could accelerate the process and lead to an increment in the carbon dioxide conversion to calcite [154].

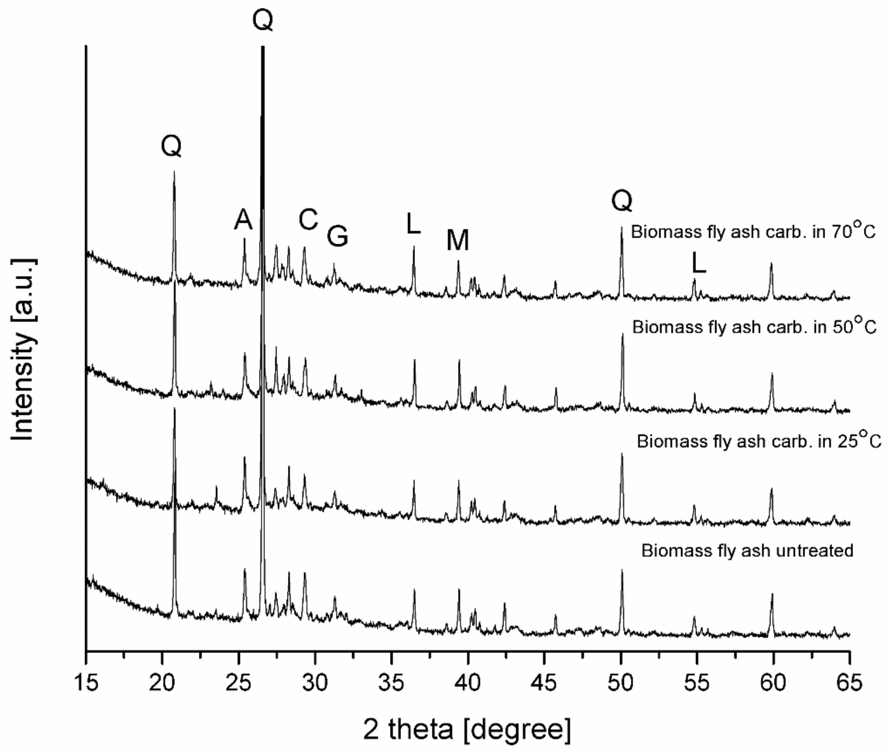

Figure 57. XRD analysis of biomass fly ash sample before and after carbonation at 25, 50 and 70°C. Q – quartz, C – calcium carbonate, P – portlandite, A – anhydrite, M – mullite, G – gehlenite, L – lime.

FTIR analysis of all samples is presented in Figure 58. A description of the FTIR technique is given in section 7.2.5. An absorption band in the region of 1,106 cm^{-1}, which represents a Si-O stretching vibration, is present in all the spectra and corresponds to the presence of quartz, the amount of which does not change throughout the experiments [100]. The dominant absorption band in the region of ~1,452 cm^{-1} and that at ~868 cm^{-1} correlate with the presence of the C-O bond [155].

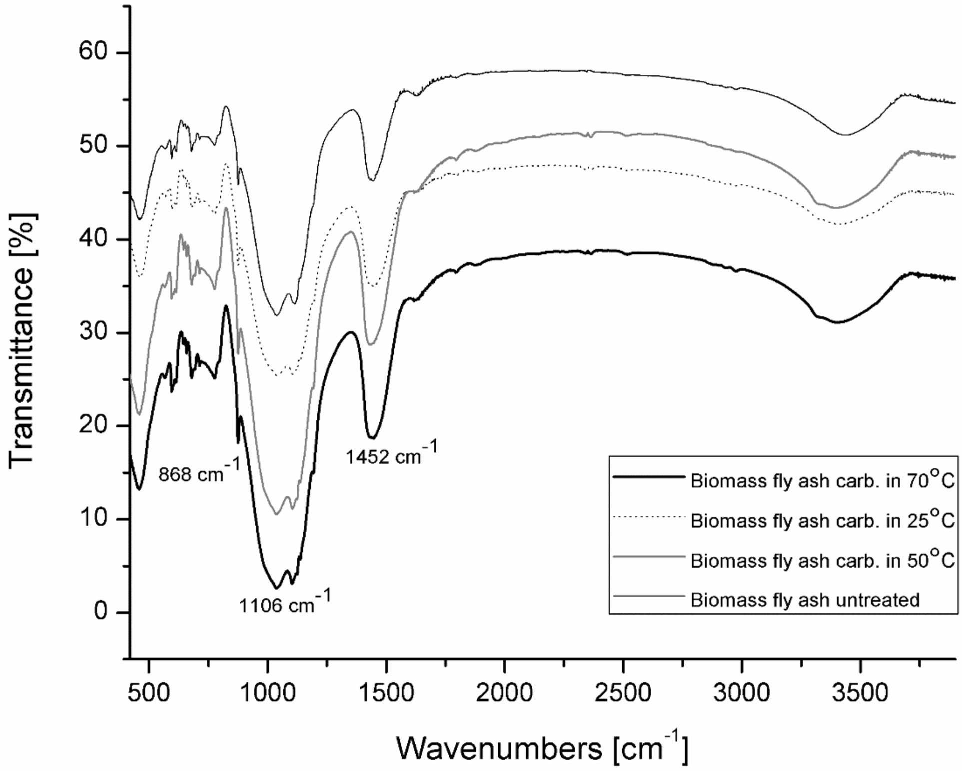

Figure 58. FTIR results for the biomass fly ash samples.

TGA analysis (a description of the technique is given in section 7.2.3) of the samples is shown in Figure 59. The mass loss in untreated fly ash corresponding to the decomposition of carbonates, is ~6%. A similar mass loss is achieved after carbonation at 25°C. Higher mass losses (~8%) are identified in the samples carbonated at higher temperatures (50°C and 70°C), proving that the carbonation process occurs [156].

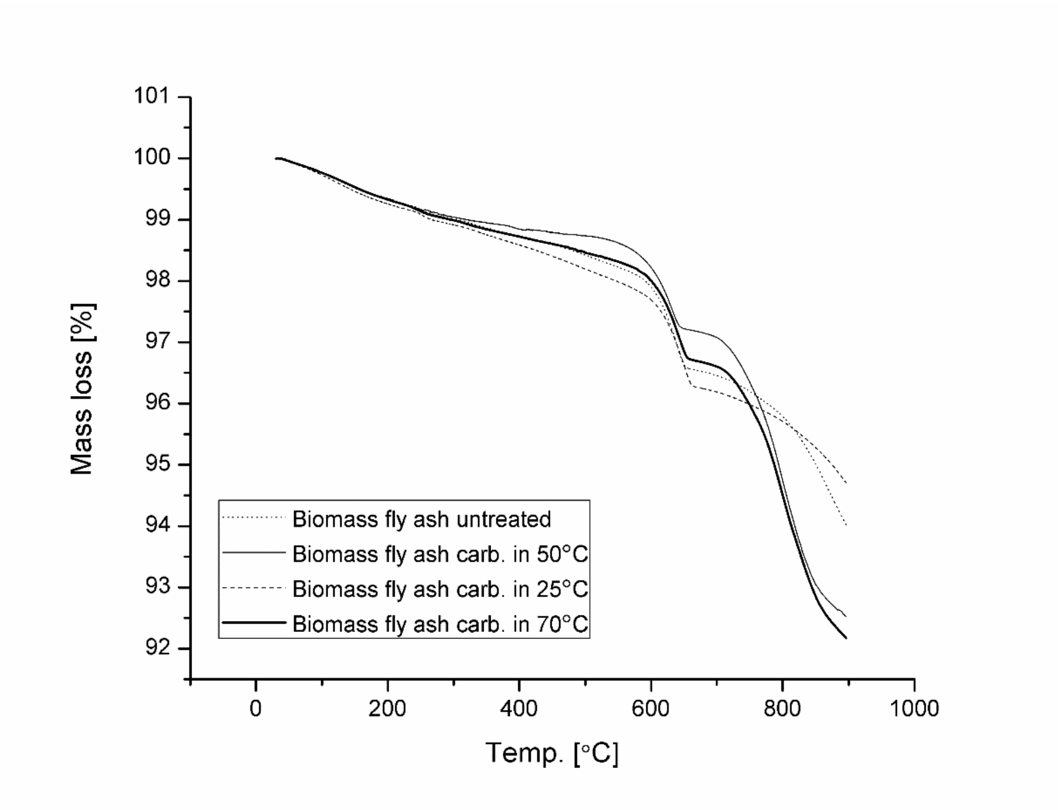

Figure 59. TGA analysis of the untreated and carbonated biomass fly ash samples.

SEM pictures of the starting material and the sample carbonated at 70°C are presented in Figure 60 (the SEM technique is described in section 7.2.4). The fly ash particles form agglomerates, as in [157]. After carbonation, particles have an irregular crystal shape. Similar shapes for the fly ash after carbonation were detected in [158].

a) 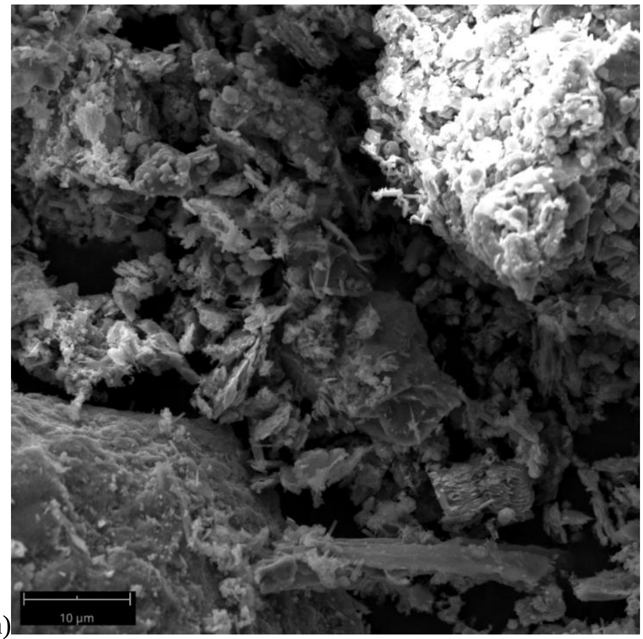

b) 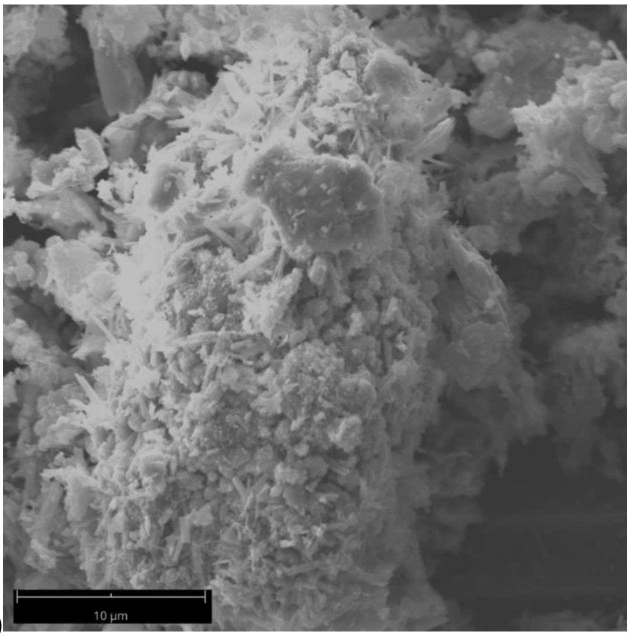

Figure 60. SEM pictures of biomass fly ash sample, untreated and carbonated at 70°C.

6.2.4 Conclusions

The study investigated the carbonation of biomass fly ash at different temperatures, with a gradual increase of pressure and temperature. Laboratory tests showed that the maximum amount of carbon dioxide absorption was 29.4 dm^3/kg at 70°C in the pressure range 4-16 bar. Increased CO_2 uptake was observed with an increase in pressure and temperature.

The results of this study indicate the high potential for development of carbonation of wastes with a high content of calcium, for example fly ashes from brown coal or biomass combustion. The XRD characteristics of the ash samples, before and after reaction, revealed the important role of the fly ash hydration process in the selection of fly ash for the mineralization process. Enriching this substrate with even a small amount of water accelerates the process and significantly increases the conversion of carbon dioxide to carbonates.

The proposed low temperature and elevated pressure mineralization method reduces the energy cost of the process at an industrial scale compared to other methods presented in the literature and does not require costly materials for the construction of the apparatus. Additionally, it is possible to adjust the experimental conditions (pressure, temperature) and the duration of the experiment.

Chapter 7. Mineral Carbonation of High-Calcium Ptolemais Fly Ash

The goal of this investigation is to study dry and moist carbonation of the high-calcium Ptolemais fly ash. The process was maintained at three different temperatures: 160, 220 and 290ºC, in a pressure range for CO_2 or CO_2 + H_2O of 1-6 bar. The aim was to evaluate the accelerating effect of temperature, pressure and water vapour on carbonation. Recently, there has been considerable interest in carbonation of both natural minerals and industrial waste, but many difficulties with this process remain unresolved [67, 159]. Most studies on carbonation of fly ash have been undertaken in aqueous conditions and only a few address direct gas-solid carbonation. This study was published in [79].

7.1 Description of Apparatus

The test material for this investigation – Ptolemais fly ash with 35% CaO, was described in section 5.3.5. Experiments were conducted using purposely designed apparatus (Figures 61 and 62). The fly ash sample is placed inside the steel reactor positioned in an oven with a maximum temperature of 300°C. The desired flow of the gases is set up with the use of flowmeters with a maximum flow of 100 ml/minute. The pressure is controlled by a back-pressure regulator with a maximum value of 6 bar, working in a pressurized continuous flow reactor. The system has an external water reservoir with a capacity of 70 ml, where the water vapour is produced for the experiments via steam. The water is heated using warming tape, to a maximum temperature of 120°C.

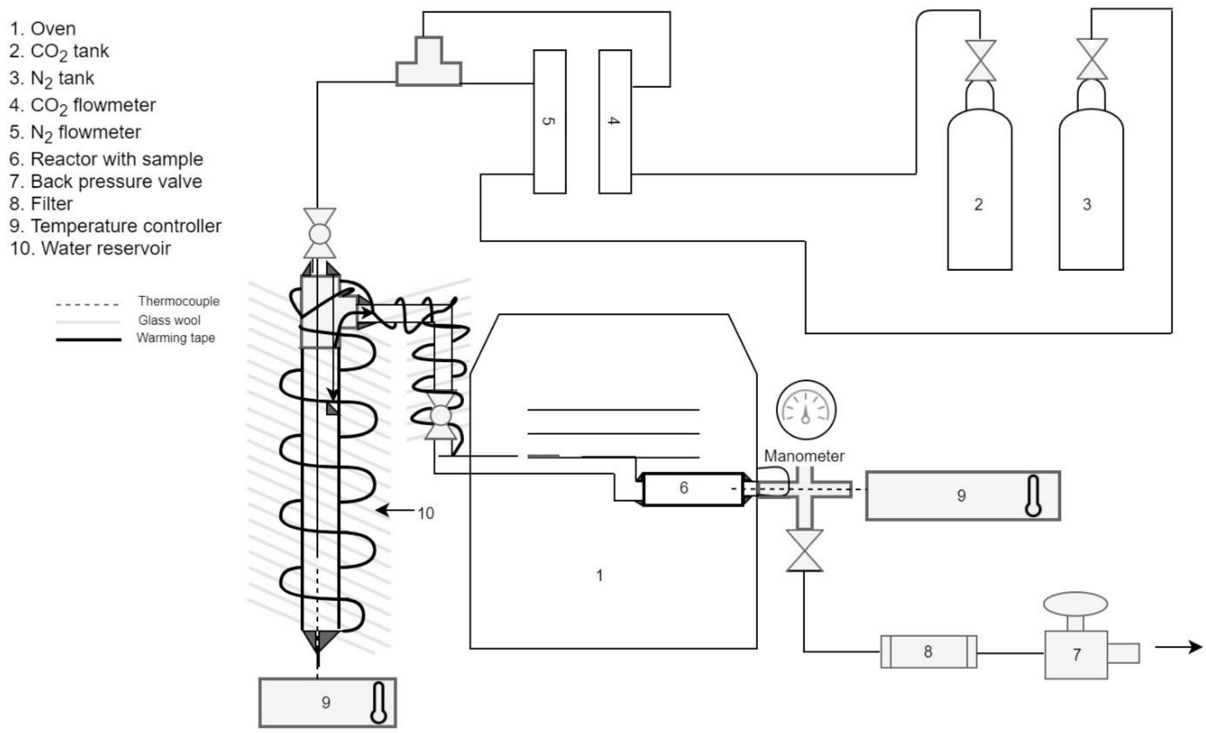

Figure 61. Experimental set-up for continuous flow low-pressure carbonation conditions (Cwik, 2018).

Figure 62. Photograph of the experimental set-up.

Experiments were carried out at three temperatures: 160, 220 and 290°C, with a heating rate of 5°C/minute and a CO_2 pressure of 1 or 6 bar. During the heating and cooling time, nitrogen was used as a carrier gas, with a flow of 30 ml/minute. After reaching the desired temperature, carbon dioxide was introduced with a flow rate of 20-40 ml/minute, depending on the target pressure. For the steam experiments, temperature in the bubbler ranged from 90 to120°C (depending on the CO_2 pressure), to achieve a constant gas mixture defined by pCO_2 = 60% and pH_2O = 40%. The carbonation reaction time in each experiment was two hours. Table 19 summarizes the conditions for the experiments.

Table 19. Experimental conditions.

No.	Sample	t [ºC]	p [bar]	Dry/moist conditions
1	Pt/1	160	1	dry
2	Pt/2	220	1	dry
3	Pt/3	290	1	dry
4	Pt/4	160	6	dry
5	Pt/5	160	1	moist, 50% water vapour
6	Pt/6	160	6	moist, 40% water vapour
7	Pt/7	290	6	moist, 40% water vapour

7.2 Characterization Techniques

7.2.1 X-ray Fluorescence Analysis

X-ray fluorescence spectroscopy was performed on a UniQuant instrument from Thermo Fisher Scientific, using the fusion bead method. Prior to the analysis, each fly ash sample was calcined for two hours at 1,000ºC.

7.2.2 X-ray Diffraction Analysis

The mineral composition of the investigated samples before and after reaction was determined by a powder diffraction (XRD) method using a Bruker D8 ADVANCE diffractometer with a theta-theta goniometer. The analysis was conducted in the range 2θ = 10 to 80° with a step size of 0.02° and a measurement time of 1 s per step.

7.2.3 Thermogravimetric Analysis

Thermogravimetric analysis was performed on a TGA G50 machine provided by TA instruments. Each sample, with a mass of about 30 mg, was heated from 30 to 950°C with a heating rate of 10°C/minute, in a nitrogen atmosphere with a flow of 60 ml/minute.

7.2.4 Scanning Electron Microscopy

Scanning electron microscopy was performed using a Zeiss NEON 40 microscope (Oxford Instruments) providing high-resolution pictures. Before the analysis, samples were coated with carbon in order to charge the grain surface.

7.2.5 Infrared Spectroscopy

For the FTIR infrared spectroscopy, a Nicolet 6700 instrument was used. The analysed spectral range was from 225 cm^{-1} to 4,000 cm^{-1}, using 64 scans and a data-spacing value of 4 cm^{-1}. The data were collected using the Ominic program. Before analysing each sample, the background spectrum was subtracted from the sample spectrum.

7.3 Dry Conditions – the Effect of Temperature on Carbonation

Figure 63 shows the X-ray diffraction results for the fresh and carbonated samples. The obtained results are grouped according to the experimental conditions. Figure 63a presents the experiments results for increasing temperature, at 1 bar of CO_2 and dry conditions. For the trials conducted at 160 and 220°C, there are no major differences from the fresh sample. In contrast, the XRD pattern of the sample carbonated at 290°C reflects the visible changes occurring during the reaction. Most of the lime peaks disappear and at the same time, calcite peaks appear. This could indicate the conversion of lime to carbonates. Another interesting point is that a portlandite ($Ca(OH)_2$) peak is visible. Liu et al. (2018) and Huntzinger et al. (2009) [80, 160] showed that formation of a stable calcium hydroxide during carbonation is possible if the temperature of the process is maintained below 300°C. Accelerating carbonation by increasing the temperature is also a well-known technique [63]. It is problematic to provide a reaction mechanism to explain the increase of CO_2 uptake at higher temperatures. One can hypothesize that at low temperatures, formation of a carbonate shell over the particle surface occurs. At higher temperatures, diffusion processes are more effective, and carbonation can proceed through the bulk material. Temperature plays an important role in this process, since it affects diffusion, the reaction kinetics and the thermodynamic properties. This investigation showed that increasing the temperature to 220°C without a further increase in CO_2 pressure was not enough to enable carbonation to occur, though a temperature of 290°C gave a positive effect.

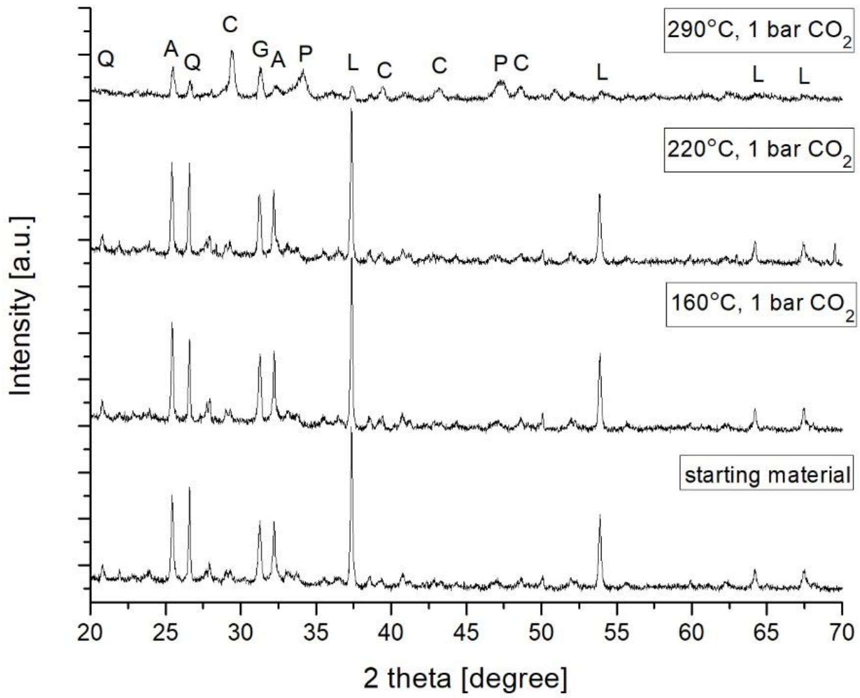

a)

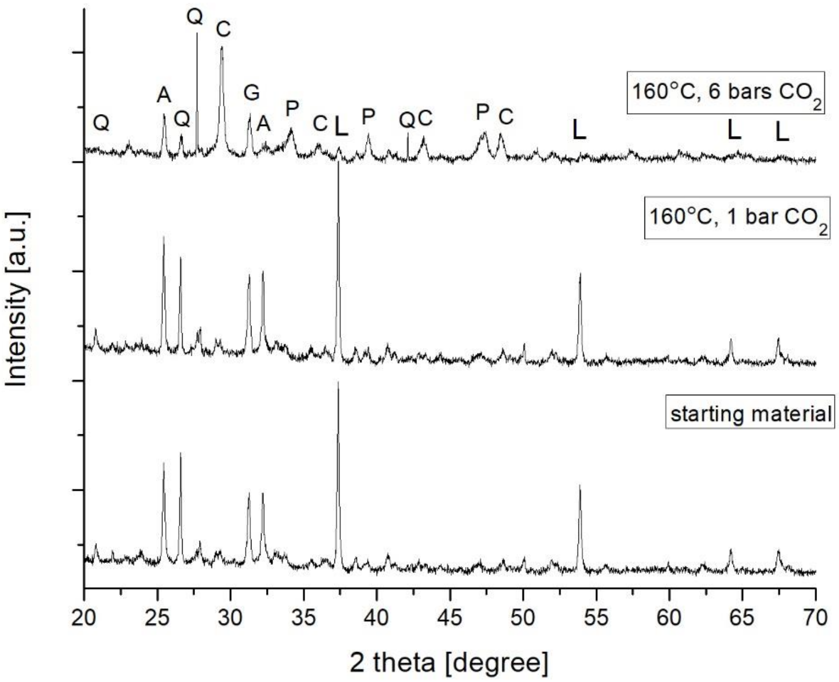

b)

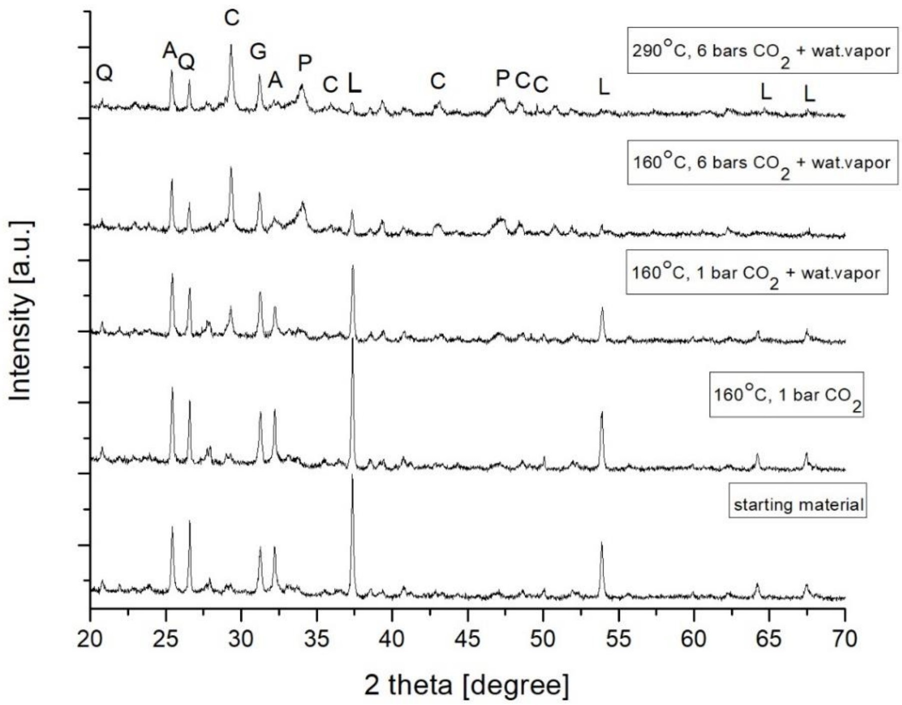

c)

Figure 63. XRD analyses of samples before and after carbonation, depending on: a) temperature, b) pressure and c) temperature, pressure and the addition of water vapour. Q – quartz, C – calcite, P – portlandite, A – anhydrite, G – gehlenite, L – lime (Cwik, 2018).

Figure 64 shows the thermogravimetric results, i.e., the mass losses and derivative weight changes as a function of temperature from 30 to 950°C. Derivative weight change graphs were produced from the TGA data, showing the sample decomposition rate. As before, the results are grouped according to the conditions of the experiments (increase of temperature, pressure and addition of water vapour). TGA analysis of the starting material shows that there is almost no mass loss in the region of 400-650°C and also that there is no peak associated with the mass loss in the derivative weight change graph. This means that in the pretreated sample, there was no $Ca(OH)_2$, and no hydration of the fly ash occurred. For all the treated samples, there are two slopes on the mass loss curve and two peaks related to the mass loss – the first positioned in the region 400-650°C corresponding to the $Ca(OH)_2$ decomposition and second in the region 650-950°C, reflecting $CaCO_3$ decomposition. It is an intriguing fact that during the experiments, not only the amount of calcite increased but also the amount of portlandite, as can clearly be seen in the XRD results (Figure 63). The possible explanation of this fly ash behaviour is that with the increase in temperature, dehydration of one of the sample compounds could occur, providing the water source for the formation of $Ca(OH)_2$. Comparing the starting material and the sample carbonated in dry conditions at 290°C and 1 bar of CO_2 (Figure 64a), it can be concluded that the amount of calcite increased, and the temperature increase enhanced the carbonation.

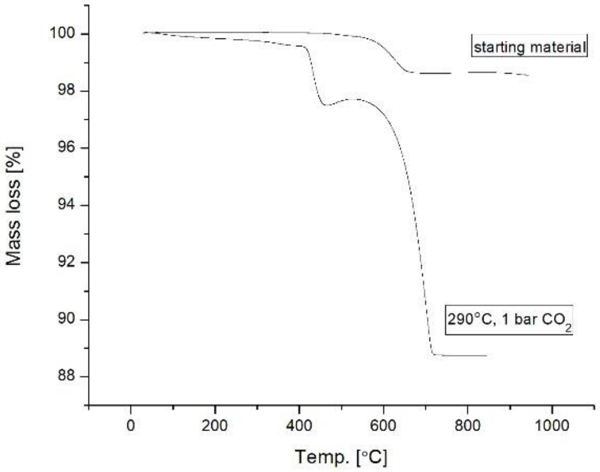
starting material
290°C, 1 bar CO2
Mass loss [%]
Temp. [°C]

a)

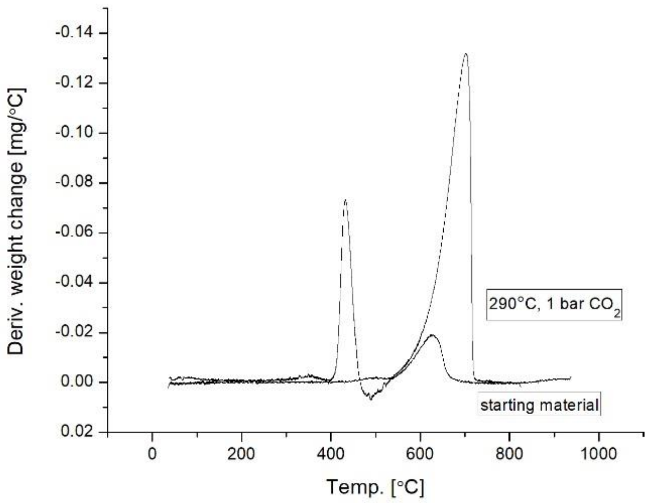
290°C, 1 bar CO2
starting material
Deriv. weight change [mg/°C]
Temp. [°C]

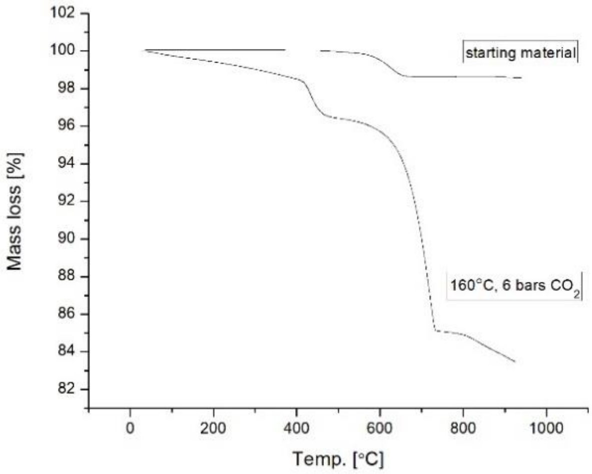

starting material
160°C, 6 bars CO_2
Mass loss [%]
Temp. [°C]

b)

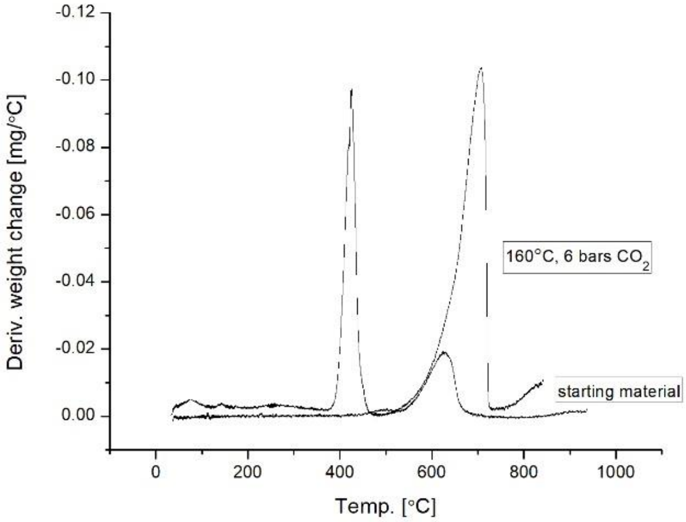

160°C, 6 bars CO_2
starting material
Deriv. weight change [mg/°C]
Temp. [°C]

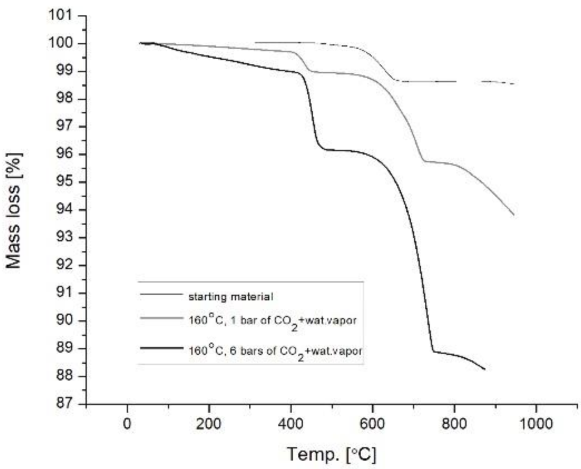

starting material
160°C, 1 bar of CO_2+wat.vapor
160°C, 6 bars of CO_2+wat.vapor
Mass loss [%]
Temp. [°C]

c)

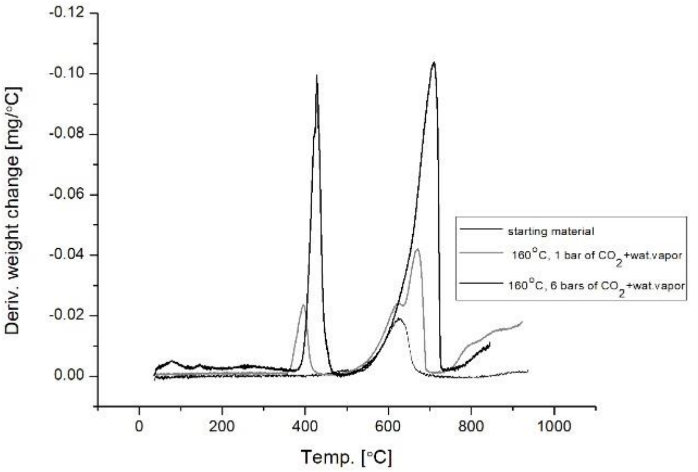

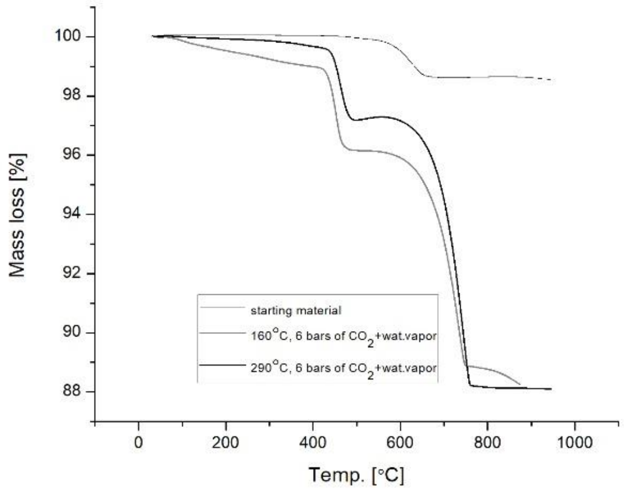

d)

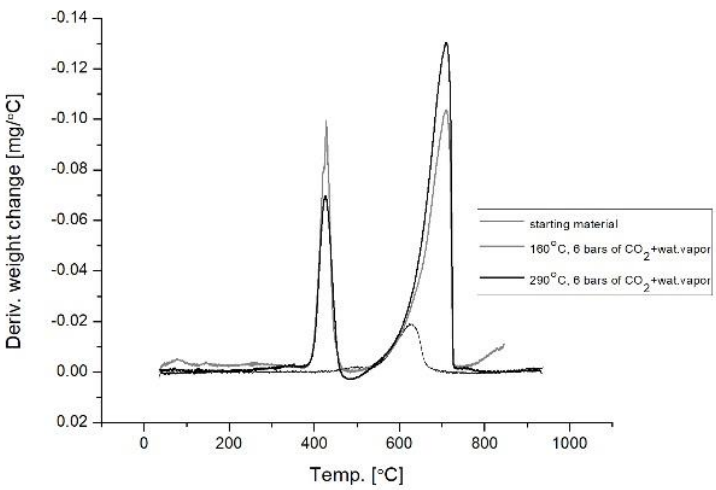

Figure 64. Results of the TGA analysis for carbonated samples – mass loss and derivative weight change: a) dependence on temperature, b) dependence on pressure, c) dependence on pressure and addition of water vapour and d) dependence on temperature and water vapour (Cwik, 2018).

7.4 Dry Conditions – Effect of Pressure on Carbonation

Figure 63b shows the XRD results for the experiments depending on the fly ash carbonation pressure, for the dry experiments performed at 160°C. Maintaining the experiment at 1 bar of CO_2 leads to no visible changes in the XRD pattern compared to the starting material, but increasing the pressure to 6 bar provides significantly different results. The lime peaks almost completely disappear and the principal calcite peak at 29.5° is evident. Similar to the results for the dependence on temperature, peaks of portlandite appear after CO_2 treatment. As mentioned in the feasibility study for carbonation in this thesis, the temperature of the carbonation process depends on the carbon dioxide pressure inside the reactor [60]. Obtaining newly formed Ca-based carbonates in dry conditions leads to the conclusion that the presence of water is not a crucial factor for fly ash carbonation to occur. Lackner et al. (1995) also showed that direct carbonation is favourable from the thermodynamic perspective. The reaction of calcium oxide with carbon dioxide is more highly exothermic than that of calcium hydroxide with CO_2.

$$CaO + CO_2 \rightarrow CaCO3 \quad \Delta H = -167\ kJ/mol \tag{41}$$

$$Ca(OH)_2 + CO_2 \rightarrow CaCO_3 + H_2O \quad \Delta H = -65\ kJ/mol \tag{42}$$

The amount of anhydrite ($CaSO_4$) seems to decrease in the samples carbonated at 290°C and 1 bar of CO_2, as well as at 160°C and 6 bar of CO_2. This may indicate that the decomposition of anhydrite is influenced by the increase in temperature/pressure, and this could be a source of calcium for calcite formation, as well as lime.

Figure 63b shows the TGA analysis for the experiment in dry conditions at 6 bar and 160°C. Compared with the other results, the TGA plot in this experiment showed the highest mass loss relating to calcite decomposition, as is reflected in the sequestration capacity calculation in the following section. This also reaffirms the XRD results. As in Figure 64a, the derivative weight change graph shows two different peaks, associated with portlandite and calcite decomposition.

7.5 Effect of Water Vapour Addition on Carbonation

In Figure 63c, all the XRD patterns of experiments performed in the presence of water vapour are shown, in the temperature range 160-290°C and the pressure range 1-6 bar of CO_2. The addition of water vapour to the experiment at 1 bar of CO_2 at 160°C generates visible changes in the XRD pattern relative to the raw material. Previous studies have shown that the carbonation reaction between gas and solid is difficult to achieve and that water access is an important parameter in the mineralization process [153]. This might be linked to the catalytic properties of H_2O through the creation of $Ca(OH)_2$, which is more reactive than CaO [154]. The XRD results for the experiment at 160°C and 1 bar of CO_2 in the presence of water vapour (Figure 63c) show that the calcite peak is more visible and emphasized, but the lime peaks are still present, which means that not all the CaO has reacted. Increasing the pressure to 6 bar and subsequently increasing the temperature to 290°C results in a significant calcite peak appearing and the lime peaks disappearing. A decrease in anhydrite ($CaSO_4$), as in dry conditions, is also visible. This could be an additional source of calcium for calcite formation.

The XRD patterns of the experiments performed at 160°C and 6 bar of CO_2 (Figure 63b) and at 290°C and 6 bar of CO_2 plus water vapour (Figure 63c) show that almost all of the lime disappears under these conditions. This may be an indicator that the chosen conditions are close to optimal for the complete carbonation of this type of fly ash.

The TGA analysis results of the moist experiments are shown in Figures 64c and 64d. Again, there are two peaks in the derivative weight change graph, associated with portlandite and calcite decomposition. Figure 63c shows the experiment performed at 160°C and 1 bar of CO_2 plus water vapour, where two different decarbonation episodes can be seen in the region 650-950°C in the derivative weight change graph. This can be explained by different amounts of calcite in the sample and also by the presence of a small amount of amorphous calcium carbonate with lower thermal stability [155]. Figure 64d shows the mass losses accompanying the temperature increase and the derivative weight change as a function of temperature for the moist experiments done at a pressure of 6 bar. It can be observed that the first peak in the derivative weight change graph for $Ca(OH)_2$ decomposition first increases (compared to the starting material and the sample carbonated at 160°C and 6 bar of CO_2 plus water vapour) and then decreases in the second experiment (290°C and 6 bar of CO_2 plus water vapour). In contrast, the second peak, relating to the calcium carbonate decomposition still increases, indicating that the carbonation rate is increasing. This could be an indicator that temperatures of around 290°C or higher are more suitable for fly ash carbonation.

7.6 Carbonation Efficiency

Calculations of the sequestration capacity and carbonation efficiency were performed based on the TGA results. Since the evaporation temperature of water and the thermal decomposition temperature of calcium hydroxide and calcium carbonates are known, it can be concluded that the weight losses observed at 30-105°C, 105-600°C and 600-950°C are caused by water vapour evaporation, calcium hydroxide decomposition and calcium carbonate decomposition respectively [145, 155]. The amount of carbon dioxide in the starting material was calculated based on its dry weight at 105°C and its mass loss between 600 and 950°C.

$$CO_{2,0}[wt\%] = \frac{\Delta m_{600-950^0C,0}[g]}{m_{105^0C,0}[g]} \; x \; 100 \tag{43}$$

where

m_{105^oC}[g] is the dry weight of the carbonated sample at 105°C and

$\Delta m_{600\text{-}950^oC}$[g] is the weight loss between 600 and 950°C for the carbonated sample.

To calculate the weight loss of CO_2 in the carbonated samples, the mass loss obtained in the clean sample was deducted from the mass loss of the carbonated sample in the temperature range 600-950°C.

$$\Delta m'_{600-950^0C}[g] = \frac{m_{105^0C}[g] - \Delta m_{600-950^0C}[g]}{m_{105^0C,0}[g] - \Delta m_{600-950^0C,0}[g]} \; x \; \Delta m_{600-950^0C,0}[g] \tag{44}$$

$$CO_2[wt\%] = \frac{\Delta m_{600-950^0C}[g] - \Delta m'_{600-950^0C}[g]}{m_{105^0C}[g]} \; x \; 100 \tag{45}$$

The total calcium content (Ca_{total} [wt%]) and the carbonation efficiency (ζCa [%]) were calculated according to equations (46) and (47) respectively [86].

$$Ca_{total}[wt\%] = \frac{\frac{(100 - CO_2[wt\%])}{100} \; x \; m_{105^0C}[g] x \frac{CaO[wt\%]}{100} x \frac{M_{Ca}[\frac{g}{mol}]}{M_{CaO}[\frac{g}{mol}]}}{m_{105^0C}[g]} \tag{46}$$

$$\zeta Ca[\%] = \frac{CO_2[wt\%] \; x \; M_{Ca}[\frac{g}{mol}]}{Ca_{total}[wt\%] \; x \; M_{CO2}[\frac{g}{mol}]} \; x \; 100 \tag{47}$$

where

CaO[wt%] is the CaO content in the fly ash obtained from the XRF results and

M_{Ca}, M_{CaO} and M_{CO2} are the molecular weights of Ca, CaO and CO_2.

Table 20 contains calculated values of the amount of CO_2 captured, sequestration capacity, total calcium content and carbonation efficiency of the samples. The initial content of CO_2 in the untreated sample is 1.4%. The highest sequestration capacity was obtained for the dry experiment at 160°C and 6 bar of CO_2, equal to 117.7 g CO_2/kg fly ash. The sequestration capacity for the experiment with the mixture of CO_2 and water vapour at 6 bar, is 65.9 g CO_2/kg fly ash (160°C) and 77.8 g CO_2/kg fly ash (290°C). In this investigation, it seems that performing the experiment in dry conditions at 6 bar of CO_2 gives better results than treating the sample with a mixture of carbon dioxide and water vapour at 6 bar (partial pressures 3.5 bar CO_2 and 2.5 bar water vapour). The values obtained are higher than those obtained by other authors [63, 77, 161]. On the other hand, the material used in this research was richer in CaO (35%) than the types of fly ash used in other investigations (4-30%). The highest value achieved (117.7 g CO_2/kg fly ash) is still much lower than the theoretical value (277.1 g CO_2/kg fly ash), which suggests the need to either extend the time of the reaction or find more suitable conditions to achieve higher sequestration capacity.

Table 20. Calculated values for the amount of CO_2 captured (CO_2 [wt%]), sequestration capacity (g CO_2/kg fly ash), total calcium content (Ca_{total} [wt%]) and carbonation efficiency (ζCa [%]) of the samples (Cwik, 2018).

Sample	290°C, 1 bar CO_2	160°C, 6 bar CO_2	160°C, 1 bar CO_2 + water vapour	160°C, 6 bar CO_2 + water vapour	290°C, 6 bar CO_2 + water vapour
CO_2 [wt%]	7.56	11.77	4.16	6.59	7.78
g CO_2/kg fly ash	75.6	117.7	41.6	65.9	77.8
Ca_{total} [wt%]	23.30	22.22	24.14	23.53	23.23
ζ_{Ca} [%]	29.51	48.14	15.65	25.44	30.44

7.7 FTIR Analysis

Figure 65 presents the infrared spectroscopy analysis results, which are divided according to the temperature, pressure and addition of water vapour influences on the carbonation process. The absorption band in the region of 1,100 cm^{-1}, which is a Si-O stretching vibration, is present in all of the spectra and corresponds to the presence of quartz, the amount of which does not change throughout the experiments [100]. Another observation is that, for each treated sample spectrum, compared to the untreated sample, a high-intensity absorption band in the region of 3,646 cm^{-1} appears, which corresponds to the presence of –OH in $Ca(OH)_2$ and confirms the results obtained from previous analyses [162]. The dominant absorption band in the region 1,418-1,423 cm^{-1} and the following band at 867-873 cm^{-1}, illustrates the presence of the C-O bond [155]. Carbonation formation is confirmed by the significant increase in intensity of peaks corresponding to calcite. For the carbonated samples in dry conditions at 290°C and 1 bar of CO_2 and at 160°C and 6 bar of CO_2, and for the all experiments in moist conditions, a new absorption band in the region 1,793-1,799 cm^{-1} is also visible, which also corresponds to calcite formation.

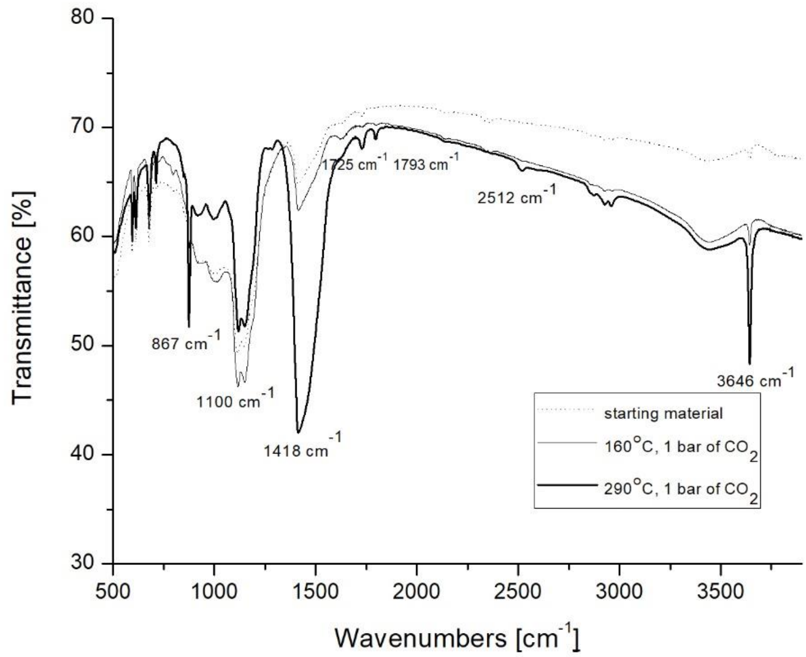
80
70
60
50
40
30
Transmittance [%]
500
1000
1500
2000
2500
3000
3500
Wavenumbers [cm-1]
1725 cm-1
1793 cm-1
2512 cm-1
867 cm-1
1100 cm-1
1418 cm-1
3646 cm-1
starting material
160°C, 1 bar of CO2
290°C, 1 bar of CO2

a)

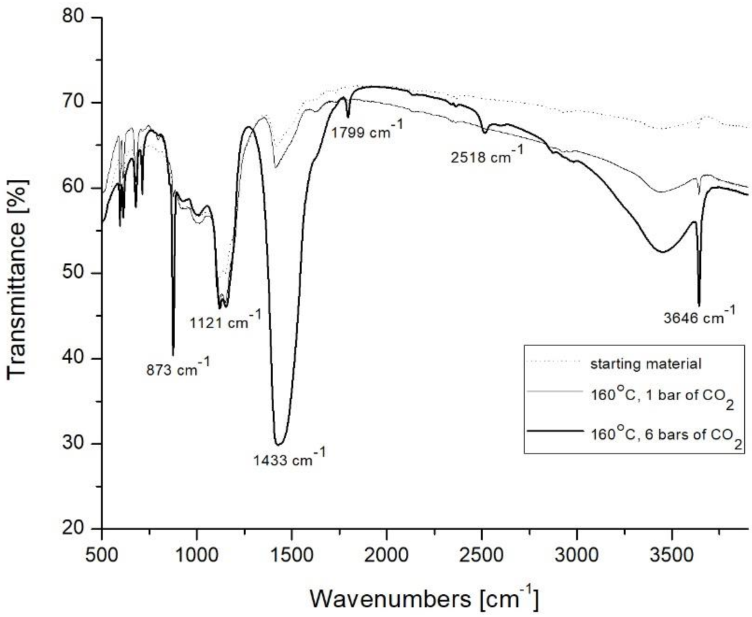
80
70
60
50
40
30
20
Transmittance [%]
500
1000
1500
2000
2500
3000
3500
Wavenumbers [cm-1]
1799 cm-1
2518 cm-1
1121 cm-1
873 cm-1
1433 cm-1
3646 cm-1
starting material
160°C, 1 bar of CO2
160°C, 6 bars of CO2

b)

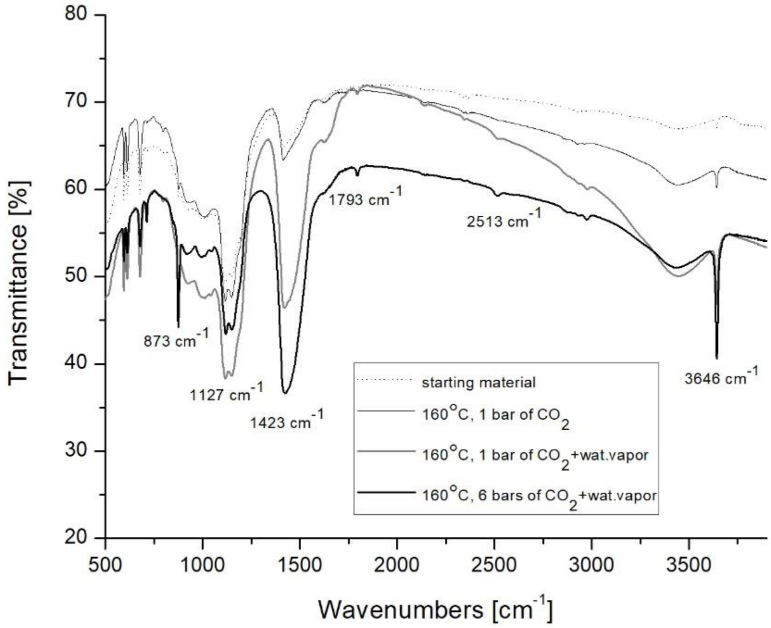

c)

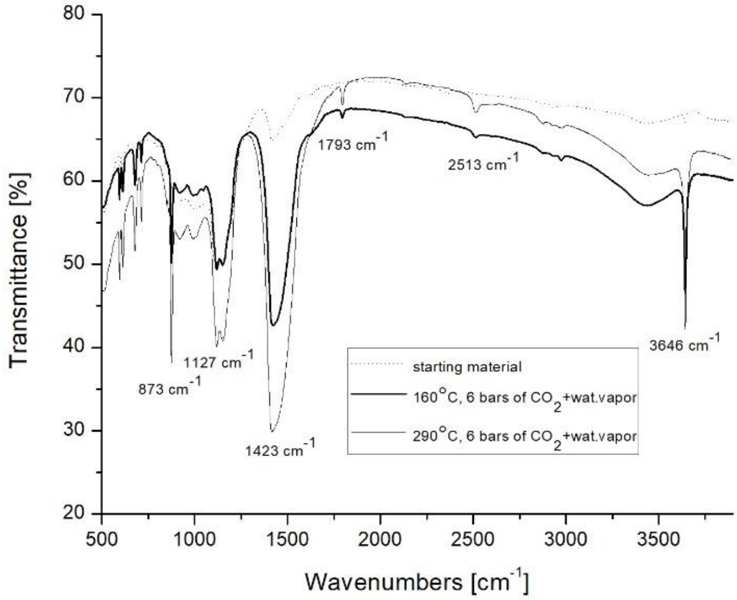

d)

Figure 65. Results of IR analysis for carbonated samples: a) dependence on temperature, b) dependence on pressure, c) dependence on pressure and addition of water vapour and d) dependence on temperature and water vapour (Cwik, 2018).

7.8 Microstructural Analysis

In Figure 66, SEM micrographs of the fresh fly ash and selected carbonated samples are shown. The morphology of the untreated fly ash particles is shown in Figure 66a. Round cenospheres form one of the main components of this fly ash. These are made of mainly aluminosilicate glass and quartz, but sometimes also contain mullite, calcite, iron oxides, calcium silicates and sulphates [129, 130]. Figure 66a shows one cenosphere with two smaller ones attached, together with a close-up of the cenosphere surface. Cenospheres appearing in this fly ash have different sizes. At a distance, the surface appears to be flat, but with higher resolution some small particles with square and triangle shapes can be seen, which are identified as ferrospheres. The mineralogical composition of these includes quartz, mullite, haematite, anhydrite and amorphous materials, mainly composed of Fe, Si, S, Al and Ca [163].

Figure 66b shows the evolution of a cenosphere and its surface after carbonation at 290°C and 1 bar of CO_2. It can be seen that the whole surface of the cenosphere is covered by new particles which, seen at a resolution of 200 nm have the shape of growing calcite. The same particles, identified as calcium carbonate, are presented in the literature [164–167]. Figure 66c shows pictures taken after the dry experiment at 160°C and 6 bar of CO_2. The cenosphere tends to be covered by bigger particles than in Figure 65b, which are detaching from it. The picture at a resolution of 100 nm shows a group of fully-grown calcite squares, as well as the newly forming carbonates. Figure 66d, which shows SEM pictures for the moist experiment at 160°C and 1 bar of CO_2 plus water vapour, also demonstrates the cenosphere evolution, where it becomes somewhat covered by newly growing formations. The second picture displays fully-grown squares of calcite attached to the cenosphere. The biggest of the calcite particles in this picture has width of 1.4 μm. The last series of pictures, in Figure 66e, shows the moist experiment (290°C and 6 bar of CO_2 plus water vapour) particles. The cenosphere is covered by the new formations, which at a resolution of 200 nm show the shapes of growing carbonates [165–167]. Similar pictures were presented in [168].

a)
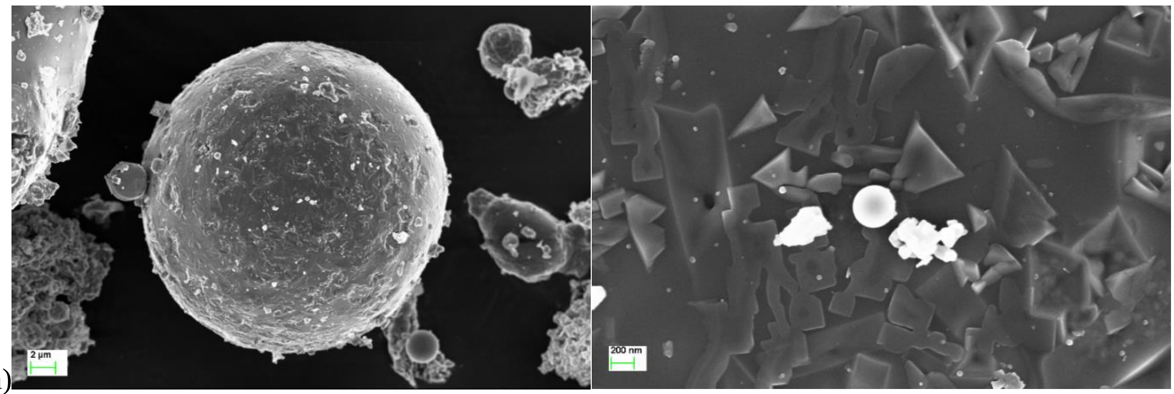

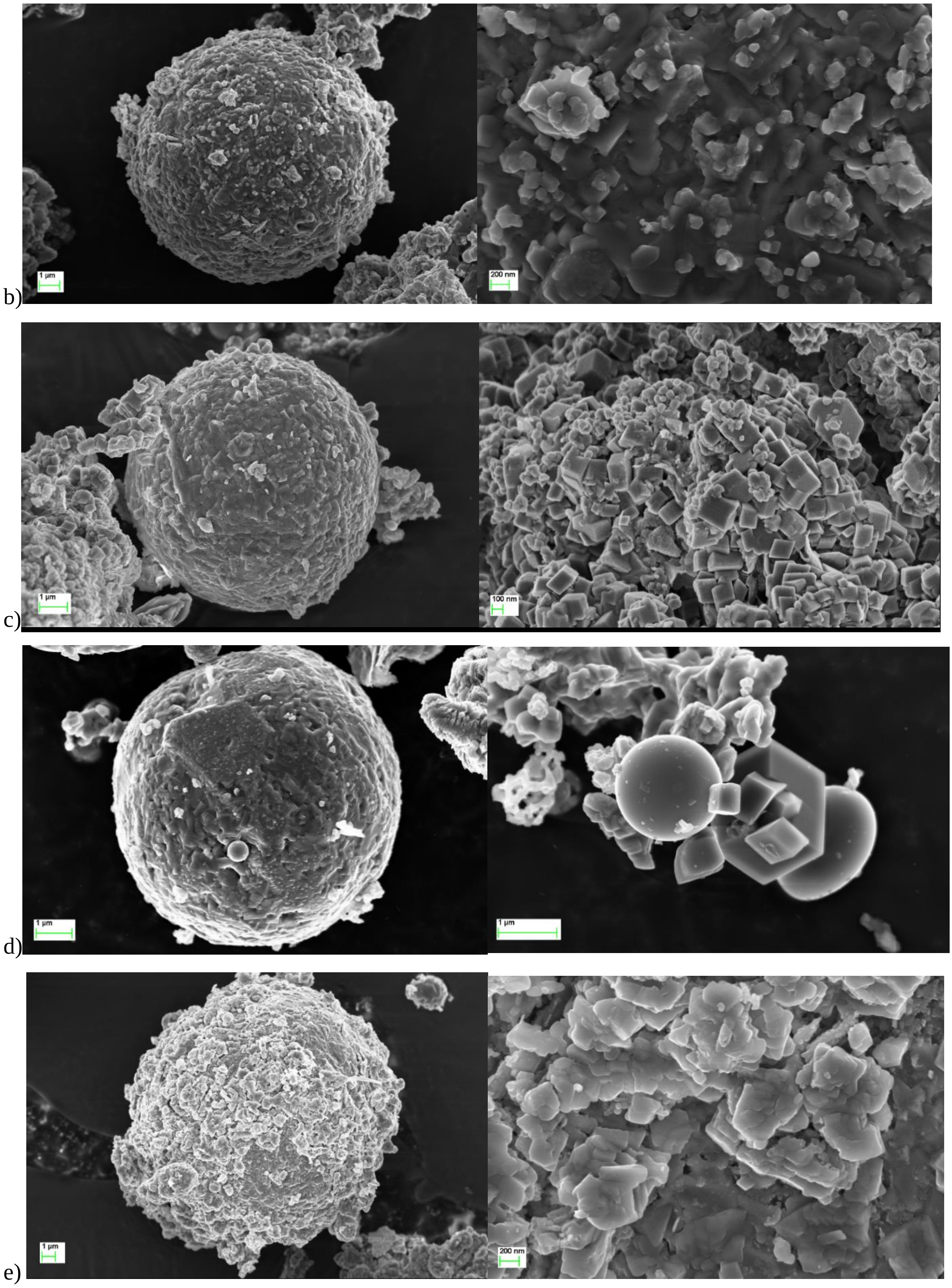

Figure 66. SEM pictures of the samples: a) starting material, b) carbonated at 290°C and 1 bar of CO_2, c) carbonated at 160°C and 6 bar of CO_2, d) carbonated at 160°C and 1 bar of CO_2 plus water vapour and e) carbonated at 290°C and 6 bar of CO_2 plus water vapour (Cwik, 2018).

7.9 Conclusions

In this study direct carbonation of high-calcium Ptolemais fly ash was performed, in the temperature range 160-290°C and under 1 or 6 bar of CO_2, in dry and moist conditions. The maximum calculated sequestration capacity obtained was 117.7 g CO_2/kg fly ash.

The influence of three different parameters on the carbonation process was studied: temperature, pressure and water vapour addition. All the performed analyses showed that an increase in temperature and pressure enhanced carbonation and that it is possible to achieve interaction between gas carbon dioxide molecules and solid particles of fly ash without the addition of water. However, comparing dry and moist experiments at 160°C and 1 bar of CO_2 (Pt/1 and Pt/5 – Figures 63c and 65c), it can be concluded that the addition of water vapour also accelerates the process of carbonation.

The SEM analysis showed the evolution of the cenosphere surface according to the experimental conditions. It seems that the surface of cenospheres is where carbonate formation occurs, due to the initial oxides present on it.

It can be concluded that direct fly ash mineral carbonation at low pressure and moderate temperatures is an attractive process for CO_2 capture. The results indicate a high potential for carbonation development for waste with a high calcium content. For the Ptolemais power plant, with an annual production of 7.6 Mt of fly ash, 2.1 Mt of carbon dioxide could be captured annually.

Chapter 8. Comparative Study of High-Calcium Fly Ash Carbonation of Samples from Poland, Spain and Greece

This chapter compares the ability of different high-calcium fly ashes produced in Europe, namely from Poland, Spain and Greece (Belchatow, La Pereda and Megalopolis samples), with similar CaO content (10-15 wt%), to react with CO_2. After achieving successful results with dry and moist carbonation of Ptolemais fly ash with high CaO content (35%) in previous research, this work is now extended to different types of fly ash. In addition, the influence of different pressure systems on carbonation is investigated. The experiments were conducted at a temperature of 160°C and an elevated pressure of 8-12 bar of pure CO_2, for dry samples and samples mixed with water vapour. Two different systems were used to create the reaction environment: a pressurized continuous flow reactor and a batch reactor. The aim of the research is to compare the potential of chosen fly ashes for the carbonation process, explore their ability to react with carbon dioxide in dry and moist conditions, compare different systems for the gas flow mechanism and determine the free lime content in the carbonated samples. This study have been published in [169].

8.1 Methods

The fly ash samples from Poland, Spain and Greece have been described in sections 5.3.1, 5.3.4 and 5.3.6. Theoretical maximum capacities for CO_2 capture for all the samples are shown in Table 21.

Table 21. Maximum theoretical CO_2 capture capacities for selected fly ash samples.

Sample	La Pereda	Megalopolis	Belchatow
gCO_2/kg fly ash	81.2	103.1	120.5

For comparison, TGA analyses of the three investigated samples are presented in Figure 67.

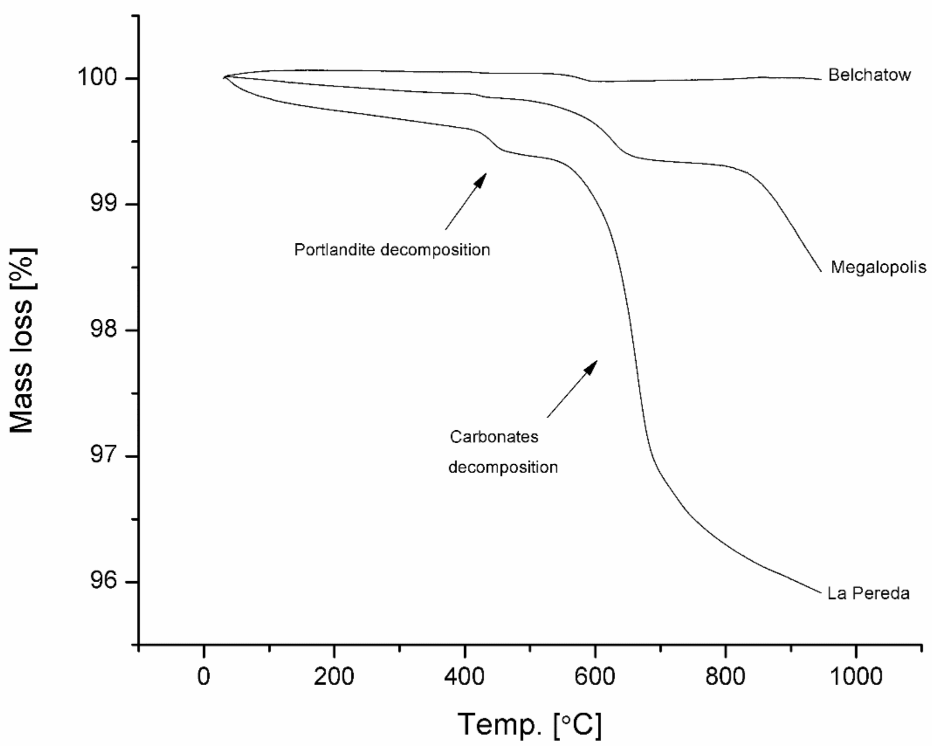

Figure 67. TGA analysis of fly ashes from Spain, Poland and Greece (Cwik, 2019).

Experiments were conducted using purposely designed apparatus, a full description of which is given in section 7.1. A new addition to the system is the possibility of using an internal water reservoir which generates steam for the experiments in the batch reactor (no continuous flow of CO_2), as shown in Figure 68.

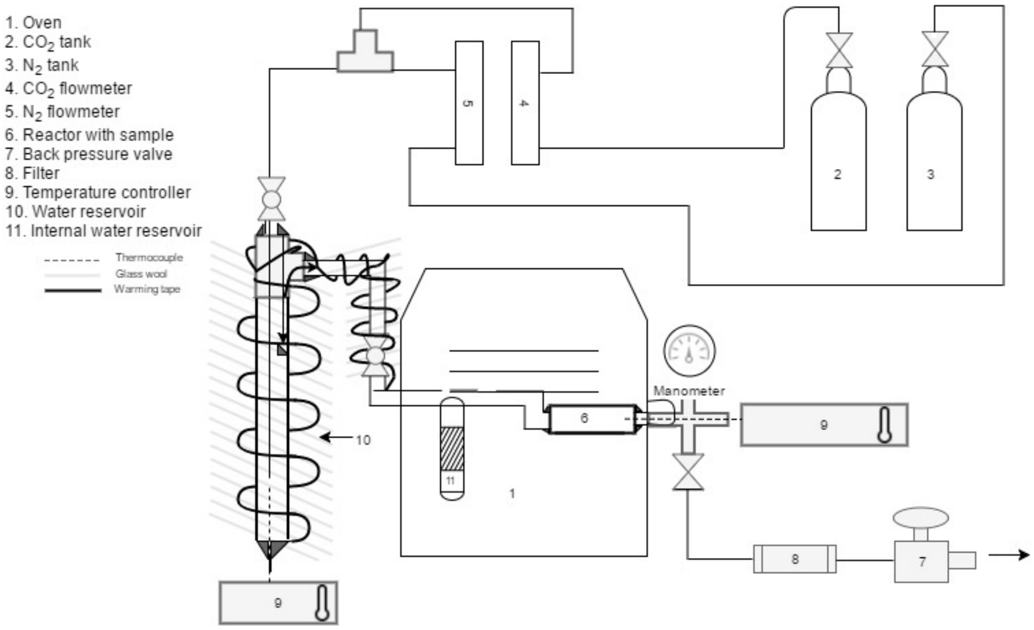

Figure 68. Experimental set-up for continuous flow and closed pressure system conditions.

All experiments were carried out at 160°C for four hours. For each sample, experiments were performed firstly under a continuous flow of 8 bar of CO_2 (open system) and secondly under 8 bar CO_2 prior to heating (closed pressure system or batch reactor mode). Both systems were used to perform carbonation in dry conditions and with the addition of steam. For the continuous flow pressure system, steam was generated with an external heated bubbler, with CO_2 forced to flow through the bubbler prior to contact with the sample. Water was added in the batch reactor by incorporating a water reservoir inside the furnace where the reactor is located (Figure 68). Steam is generated based on the water vapour pressure at the experimental conditions. In the batch reactor, heating the gas increased the pressure to values of 10 bar (dry conditions) and 12 bar (moist conditions).

8.2 Continuous Pressure Flow Conditions

Figure 69 shows the X-ray diffraction results for the fresh and carbonated samples. Figures 69a, 69b and 69c show the diffractograms for the different fly ashes and experimental conditions. For all the fly ash types, dry carbonation combined with the continuous flow pressure conditions gave negligible results. In the case of Belchatow and Megalopolis fly ashes, the calcite peak, located at 29.5° did not appear. In the case of La Pereda fly ash, a small calcite peak is visible. The results of XRD analysis are supported by the infrared spectroscopy results, which are presented in Figure 70, grouped in the same way as the XRD results.

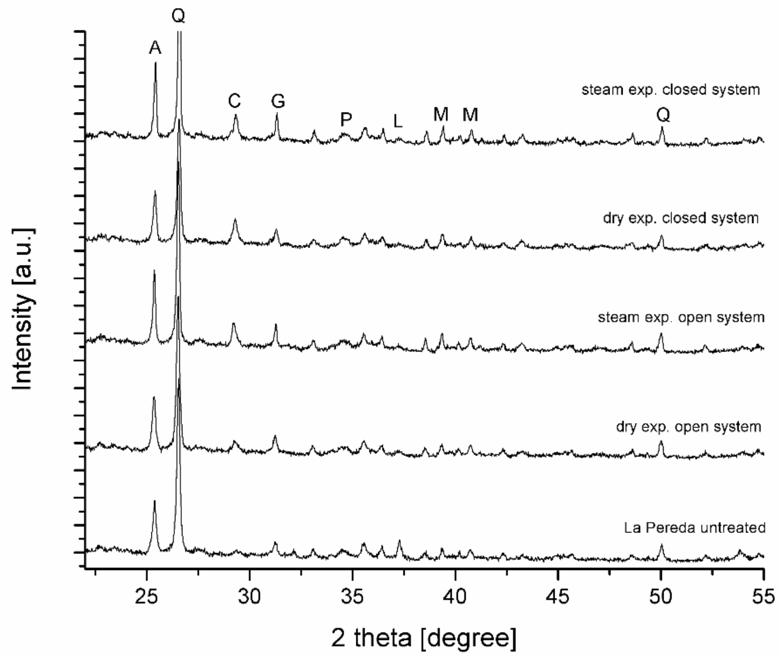

a)

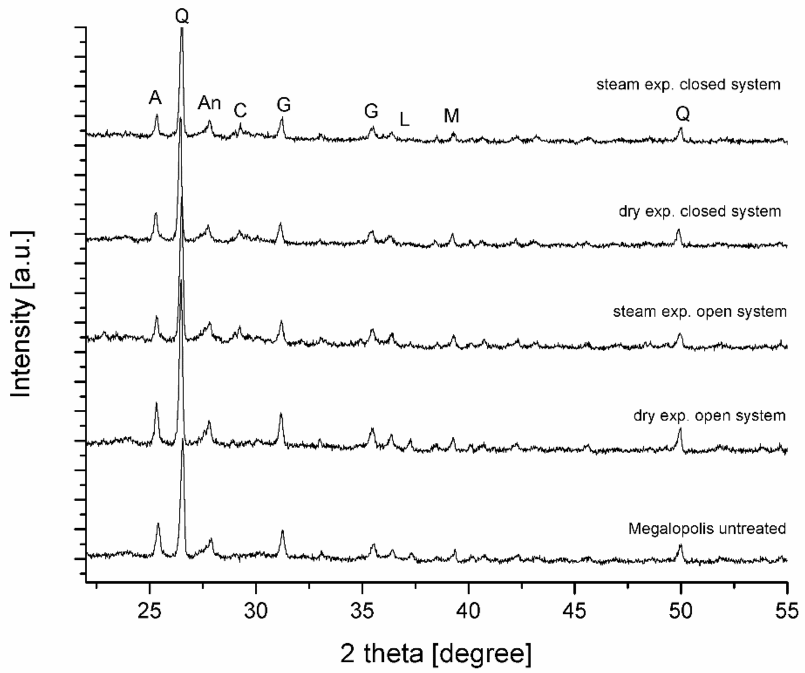

b)

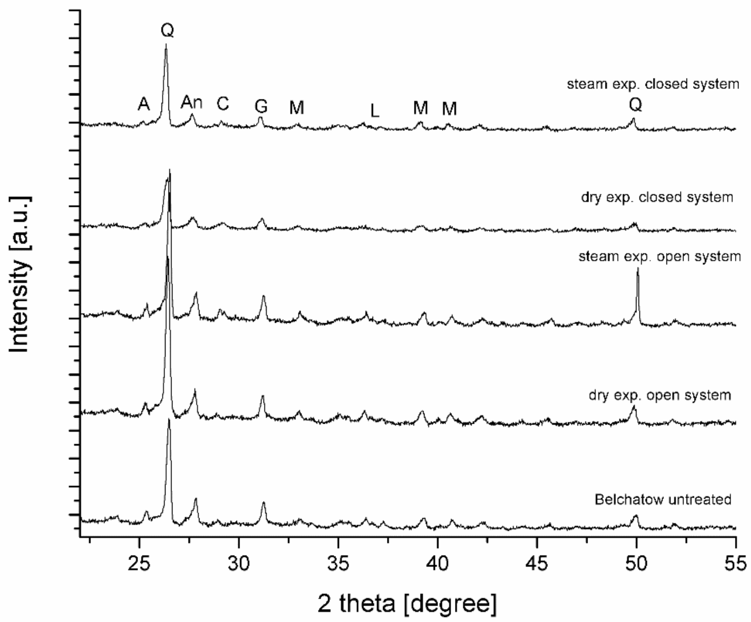

c)

Figure 69. XRD analyses of fly ashes before and after CO_2 treatment (160°C, 8 bar CO_2/CO_2+H_2O, four hours): a) La Pereda, b) Megalopolis and c) Belchatow fly ash. Q – quartz, C – calcite, P – portlandite, A – anhydrite, G – gehlenite, L – lime, M – mullite, An – anorthite (Cwik, 2019).

As previously mentioned, the characteristic absorption band for fly ash is in the region of 1,100 cm^{-1}, representing a Si-O stretching vibration. This absorption band is visible in all the spectra of the samples and corresponds to the presence of quartz [100].

The characteristic absorption band peaks for calcite are located at 1,418-1,423 cm^{-1}, 870 cm^{-1} and 1,795 cm^{-1} [155,170]. Comparing untreated samples and samples carbonated in dry conditions and an open flow system, negligible differences are observed.

In the case of the continuous flow reactor with the addition of steam, the analyses show clear evidence of carbonation occurrence. The XRD results for each fly ash type show that in contrast to the untreated material, a calcite peak is clearly visible. It is a proven fact that the addition of water vapour accelerates the carbonation process [80,81]. Furthermore, lime peaks present in the untreated samples disappear for all the fly ashes treated in these conditions. It can be concluded that conversion of lime to carbonates had taken place. As in the XRD results, FTIR analysis confirmed the presence of calcium carbonate, as there was a noticeable increase of the absorption band intensity in the region 1,418-1,423 cm^{-1} and at 867-873 cm^{-1}. Both regions correspond to the presence of calcite. For the samples from La Pereda and Belchatow in these conditions, a new absorption band in the region 1,793-1,799 cm^{-1} was present. This band also corresponds to calcite formation [170].

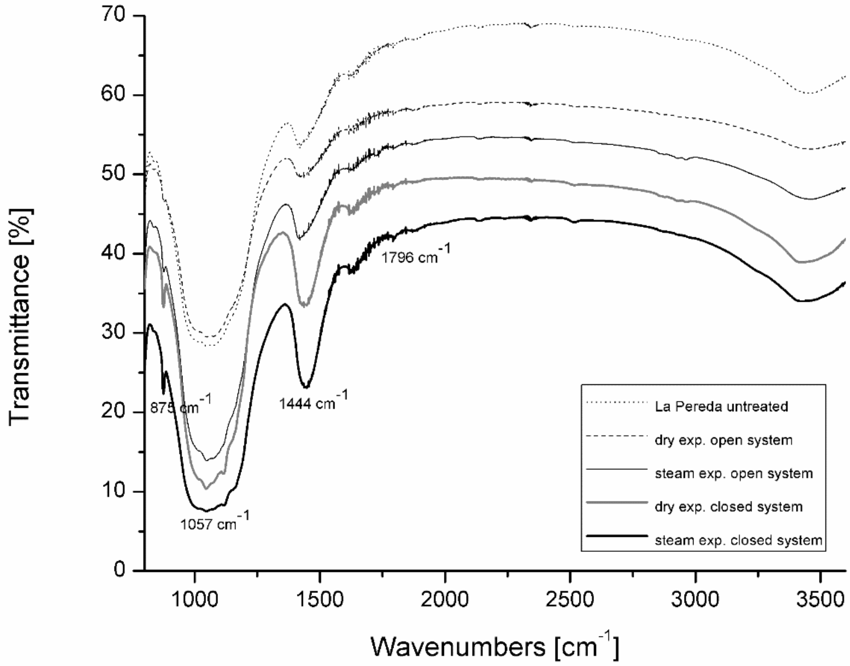

Transmittance [%]
Wavenumbers [cm-1]
875 cm-1
1057 cm-1
1444 cm-1
1796 cm-1
La Pereda untreated
dry exp. open system
steam exp. open system
dry exp. closed system
steam exp. closed system

a)

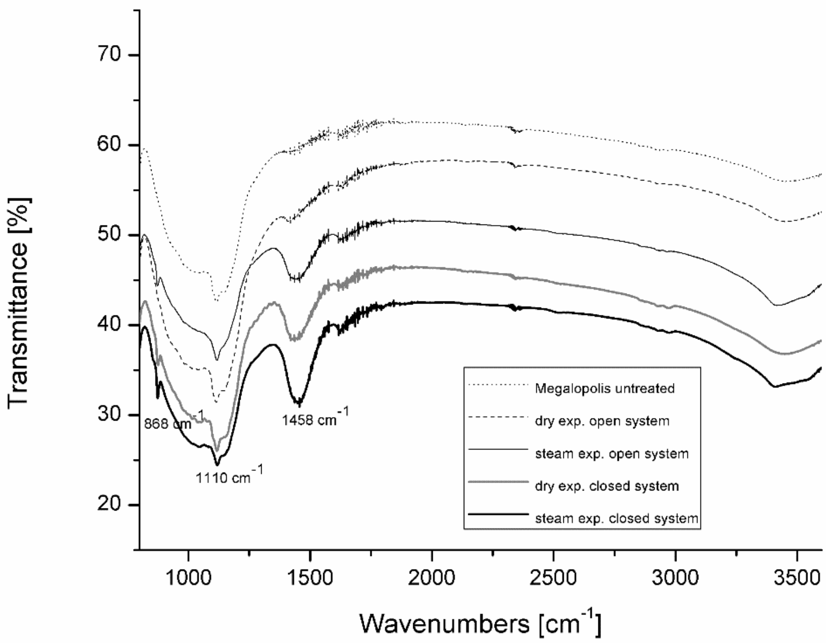

Transmittance [%]
Wavenumbers [cm-1]
868 cm-1
1110 cm-1
1458 cm-1
Megalopolis untreated
dry exp. open system
steam exp. open system
dry exp. closed system
steam exp. closed system

b)

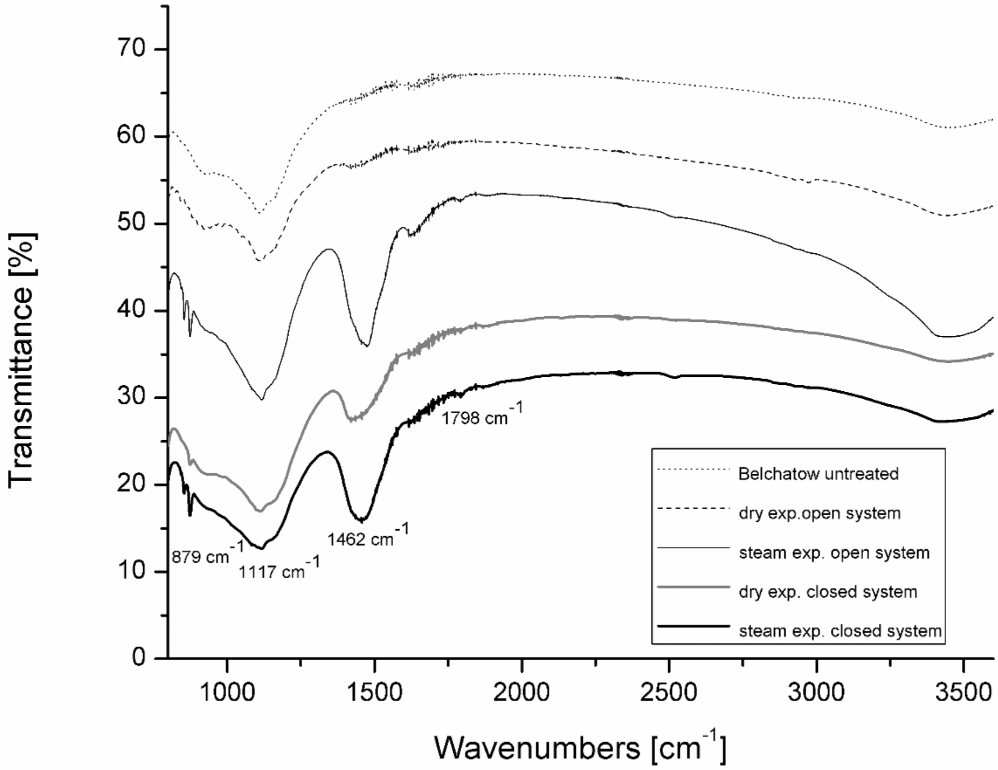

c)

Figure 70. Results of FTIR analyses for carbonated fly ash samples (160°C, 8 bar CO_2/CO_2+H_2O, four hours): a) La Pereda, b) Megalopolis and c) Belchatow (Cwik, 2019).

8.3 Batch Reactor Conditions

The second system condition is the closed pressure system. In contrast to observations of treatments using the continuous flow system, carbonates were shown to be formed after carbonation in the batch reactor under dry conditions. XRD and FTIR results (Figures 69 and 70) of the treated samples of La Pereda, Megalopolis and Belchatow fly ashes, reveal the presence of calcite peaks. As in the previous studies, newly formed calcium carbonates are observed after the reaction in dry conditions, in accordance with thermodynamic expectations [60].

Recently, there has been interest in the way different reactor types influence the carbonation reaction [99]. In a closed system, some of the CO_2 is present at the beginning of the experiment. The molecules of CO_2 have the total time of the reaction (four hours) to react with the substrate. In the case of open systems, the molecules of CO_2 are constantly pushed out by the new molecules, to maintain the same

pressure throughout the experiment, shortening the time available for them to react. Furthermore, applying 8 bar of CO_2 before the experiment and heating to 160°C led to a significant increase in pressure during the experiment (10 bar when CO_2 is admitted, 12 bar when CO_2+H_2O is admitted). This could contribute to the overall improvement in the results achieved.
Analyses of samples carbonated in the batch reactor with the addition of steam reveal that the carbonation process occurred. In the XRD results, the calcite peak is present for all the samples, and at the same time, the lime peaks disappear. Absorption bands of samples carbonated in these conditions are characterized by peaks at ~1,420 cm^{-1}, ~870 cm^{-1} and ~1,795 cm^{-1}, confirming the presence of carbonates. Maintaining the experiments in these conditions proves that water accelerates the carbonation. $Ca(OH)_2$ has better catalytic properties than CaO [171].

8.4 Thermogravimetric Analysis

Figure 71 shows the thermogravimetric analysis – mass loss as a function of temperature change, from 30 to 950°C. There are three different graphs corresponding to each of the treated fly ashes. The decomposition mechanism is very similar in all the analysed samples, until the temperature reaches 600°C. A further increase in temperature leads to a much faster and more complete decomposition in carbonated samples. In the case of La Pereda, there is a significant difference between the mass losses of untreated samples and samples treated in wet conditions (3.5% compared with 9.5-10.5%).

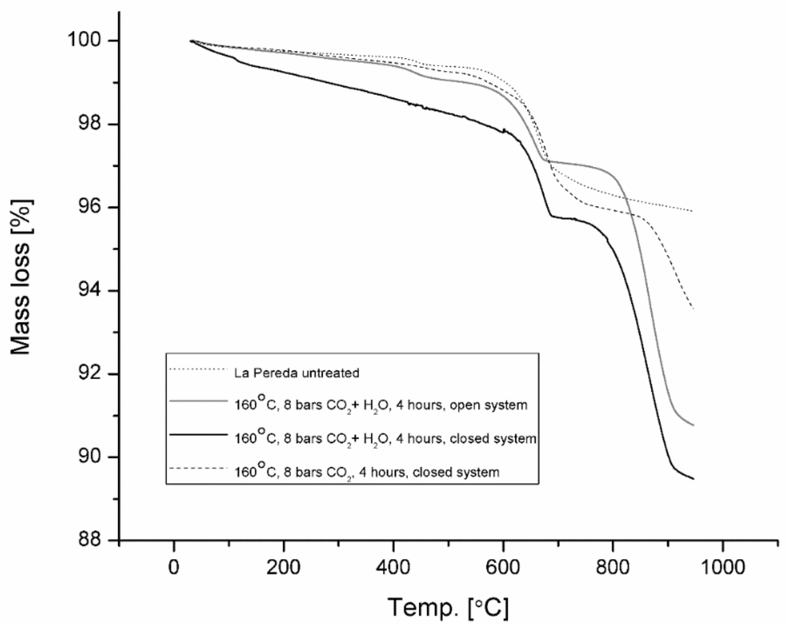

a)

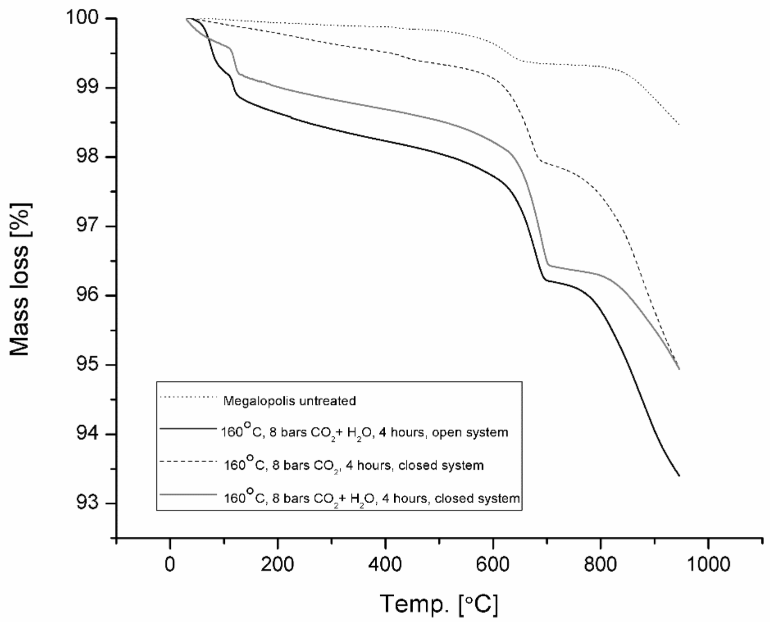

b)

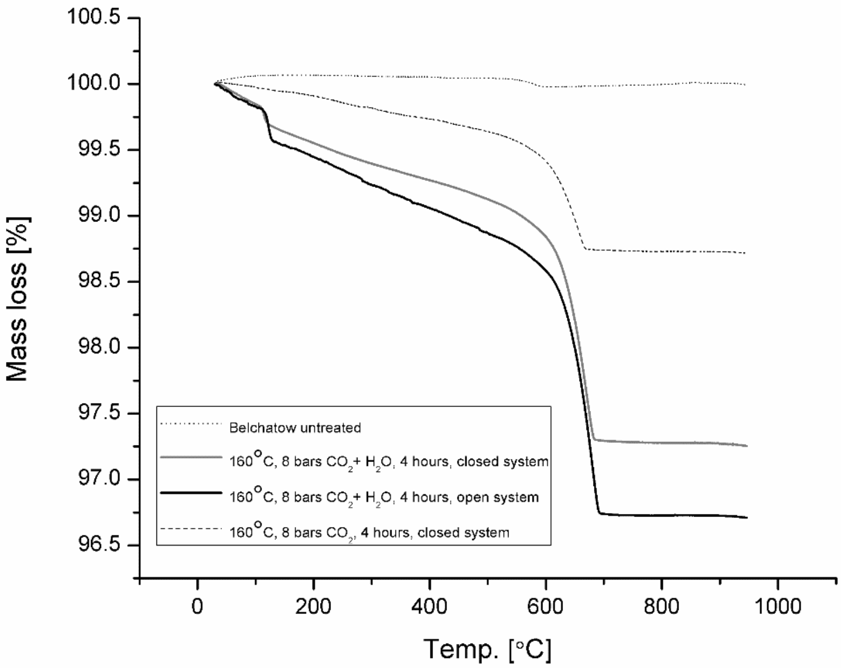

c)

Figure 71. Results of TGA analyses for the treated samples: a) La Pereda fly ash, b) Megalopolis fly ash and c) Belchatow fly ash (Cwik, 2019).

Decomposition of carbonate species in the treated samples in these conditions is characterized by two different peaks – one between 600 and 800°C, which is present in untreated and treated samples, and a second one observed between 800 and 950°C, which is not present in the untreated material. Both peaks are associated with calcium carbonate decomposition. Nevertheless, these two peaks reveal a clear difference in thermal stability, indicating possible differences between the calcium carbonate species. Previous research has stated that anhydrous calcium-based carbonates decompose at different temperatures, depending on their crystallinity and their crystal size [171]. In case of Megalopolis and Belchatow fly ashes, TGA analysis also revealed higher mass loss in the range 600-950°C for the treated samples. Additionally, for the samples treated in moist conditions, a new decomposition peak is present at 130°C, corresponding to gypsum degradation [172]. Gypsum was formed upon hydration of anhydrite during steam-enhanced carbonation.

The TGA results for the La Pereda sample treated in dry conditions are characterized by a decomposition peak similar to the peak in the untreated sample, and a second peak similar to those observed in moist conditions for this sample starting at a higher temperature. In the case of Belchatow, it is easily observed that water vapour accelerates the process, as there are larger mass losses associated with the decomposition of calcite in the experiments performed in moist conditions. Furthermore, it can be concluded that all the carbonates formed in Belchatow fly ash decomposed completely at 700°C, as no further mass loss was observed with a further increase in temperature.

8.5 Carbonation Efficiency and CO_2 Sequestration Capacity

The CO_2 sequestration capacity and the carbonation efficiency of the process were calculated using the TGA data. The calculations were performed based on those given in [145,173] and according to the following equations.

$$CO_2[wt\%] = \frac{\Delta m_{CO2}[g]}{m_{105°C}[g]}\ x\ 100 \tag{48}$$

where

CO_2 (wt%) is the CO_2 content in the original sample,

$m_{105°C}$ [g] is the dry weight of the sample at 105°C and

Δm_{CO2} [g] is the weight loss due to calcium carbonate decomposition.

The CO_2 content in the carbonated samples was calculated by subtracting the CO_2 content in the original sample. The carbonation conversion of the fly ash (ζCaO) was determined using Equation 49.

$$\zeta CaO[\%] = \frac{\frac{CO2(\%)}{100-CO2(\%)} x \frac{1}{MW_{CO2}}}{Ca_{total}/MW_{Ca}} = \frac{\frac{CO2(\%)}{100-CO2(\%)} x \frac{1}{MW_{CO2}}}{CaO_{total}/MW_{CaO}} \tag{49}$$

where

MW_{CO2} is the molecular weight of the CO_2 (g/mol),

MW_{Ca} and MW_{CaO} are the molecular weights of Ca and CaO (g/mol) and

Ca_{total} and CaO_{total} are the percentage weight fractions, determined via XRF.

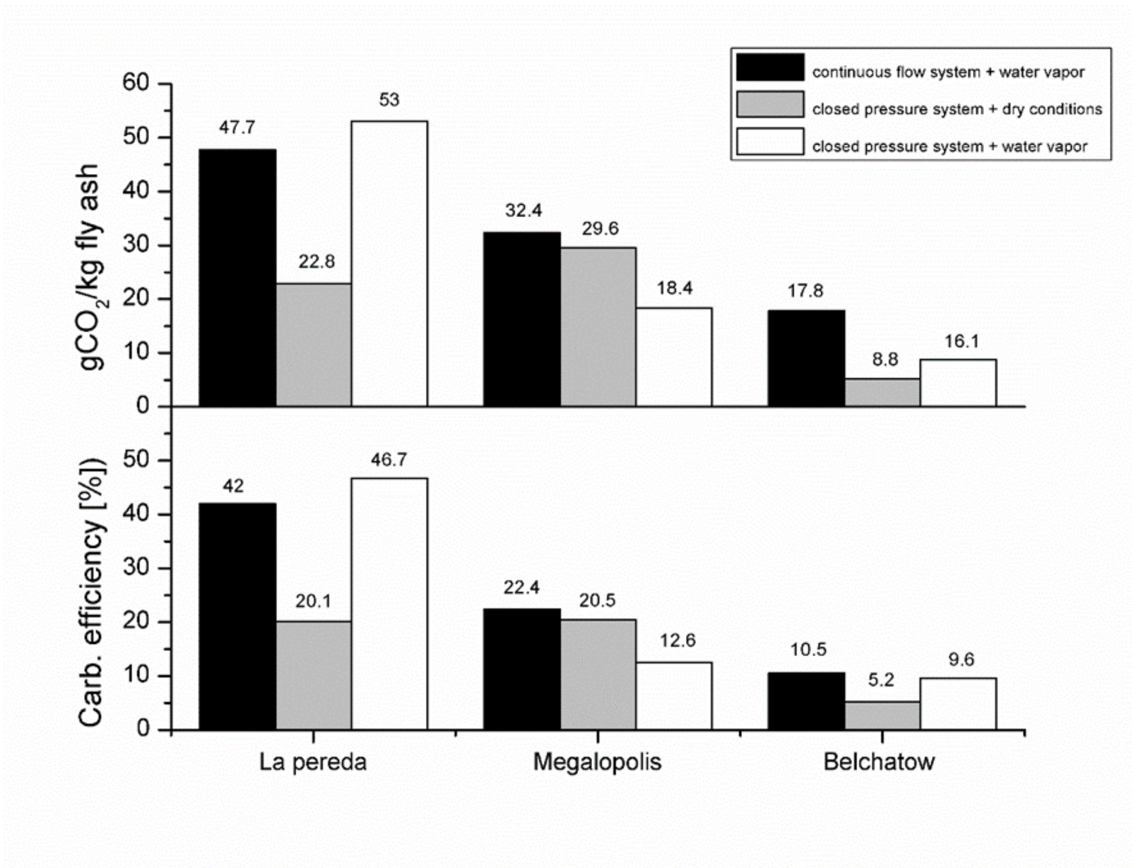

Figure 72. Calculated values of the sequestration capacities (g CO2/kg fly ash) and carbonation efficiencies (ζCa [%]) of the samples (Cwik, 2019).

Figure 72 presents the calculated values of the sequestration capacities and carbonation efficiencies of the samples. The highest sequestration capacity was achieved for La Pereda fly ash, at 46.7%, which corresponds to 53 g of CO_2 utilized per kg of fly ash. This result was achieved in the closed pressure system with steam addition. The highest carbonation efficiencies for the Megalopolis and Belchatow fly ashes were 22.4% and 10.5%, both for the open flow system with the addition of water vapour. The results for the La Pereda fly ash may be connected to the fact that this fly ash is characterized by a high value of initial carbonation (29.48%). Megalopolis and Belchatow fly ashes have lower levels of natural initial carbonation (8.92% and 0.3%) and free lime content (1.96% and 0.33%). Despite the higher total CaO content compared to La Pereda fly ash (15% and 13% compared to 10%), low amounts of free lime could be the reason for the relatively low CO_2 sequestrations capacities for Megalopolis and Belchatow fly ashes. A more detailed study of free lime content is described in chapter 10. The values obtained are higher than those reported by other authors [19,63,154]. For each fly ash, the highest achieved sequestration capacities were lower than the theoretical capacities, which suggests that the carbonation process conditions can be optimized further.

8.6 Microstructural Analysis

Figure 73 shows selected pictures of the untreated and carbonated samples. Belchatow and Megalopolis fly ashes are composed mainly of cenospheres made of aluminosilicate glass and quartz, sometimes with the addition of various oxides [174]. Cenospheres can be either closed, open, attached to each other or (for larger spheres) filled with smaller cenospheres. La Pereda fly ash is not rich in these particles.

The pictures of the carbonated samples show different formations of calcium carbonate. It has been shown that calcium carbonate forms in a large range of a different shapes, depending on the process conditions [175]. In the case of La Pereda carbonated fly ash, new particles can be seen which resemble the shape of growing calcite, as in [165,166]. Carbonation of La Pereda fly ash in a closed pressure system under moist conditions led to the formation of fully-grown calcite squares. The same conditions for the Megalopolis fly ash resulted in irregularly shaped carbonate particles and small needles which are also identified as $CaCO_3$ [176].

a)

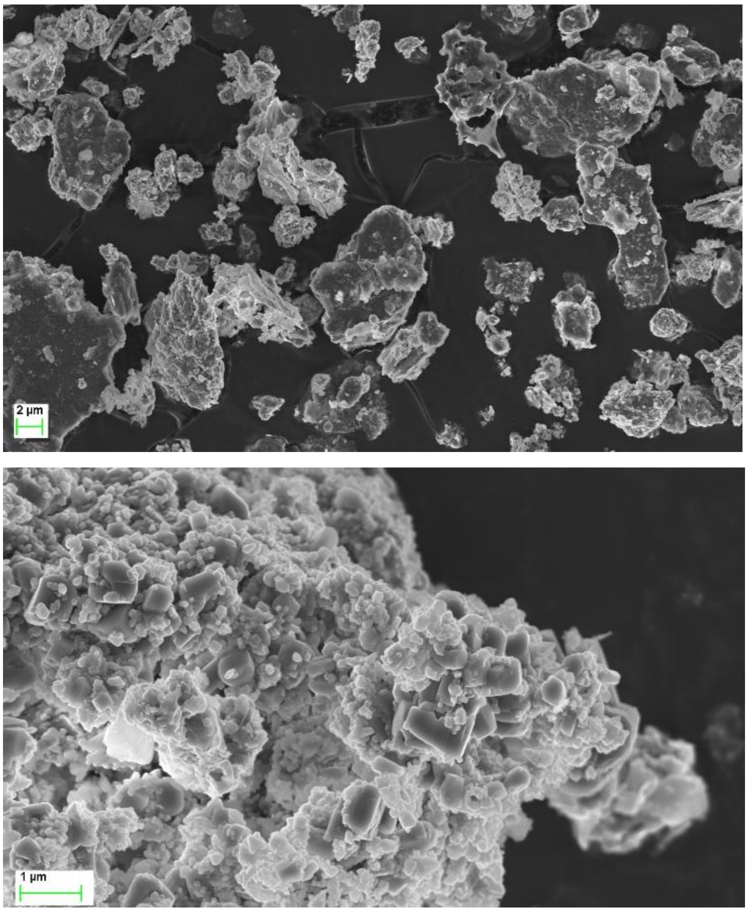

b)

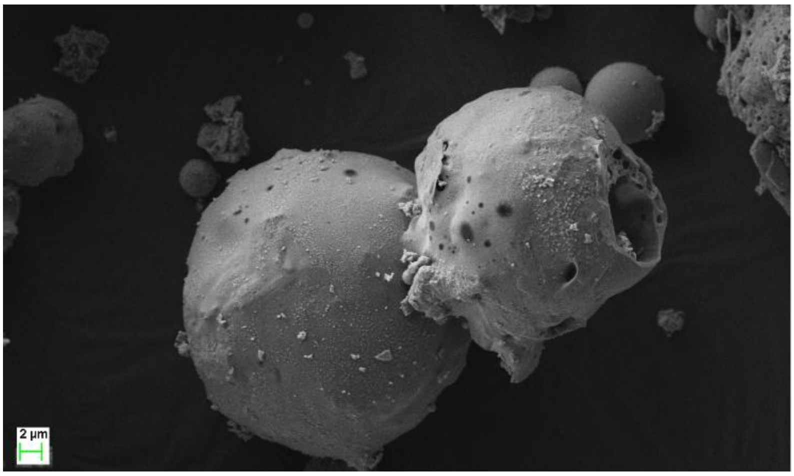

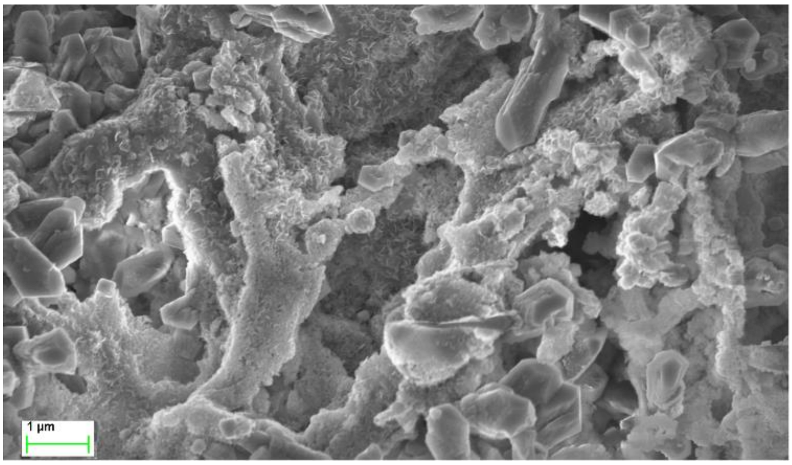

c)

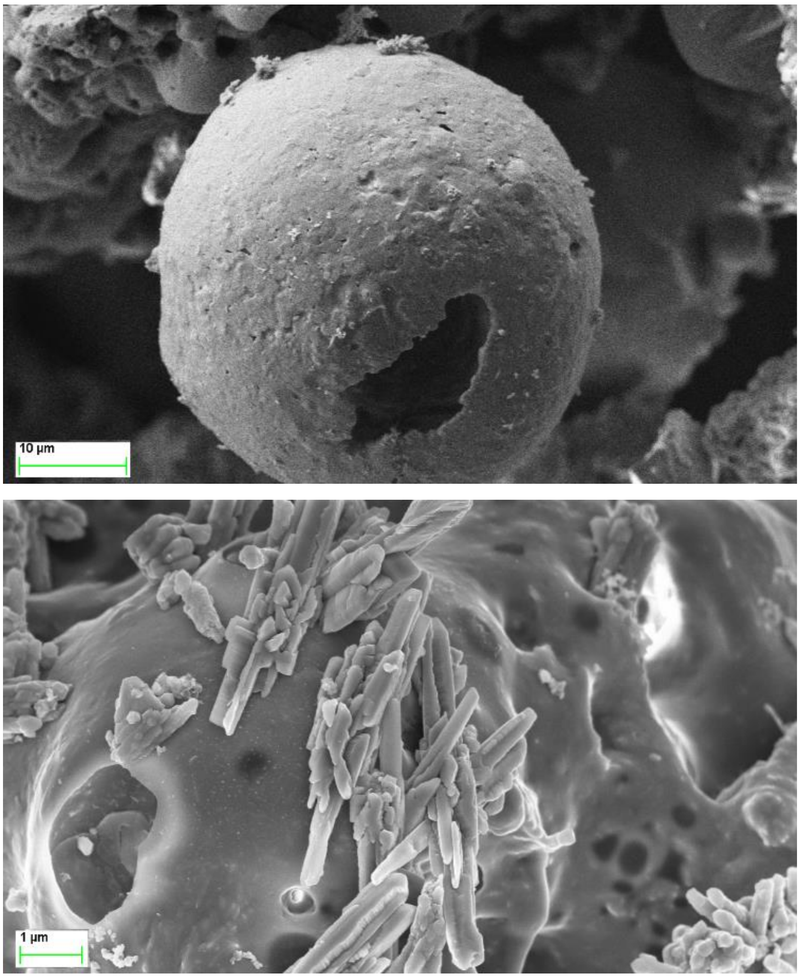

Figure 73. Representative SEM images of untreated (1) and treated (batch reactor with addition of water vapour) (2) fly ashes from: (a) La Pereda, (b) Megalopolis and (c) Belchatow (Cwik, 2019).

8.7 Conclusions

This study provides a comparison of the carbonation potential of different European fly ashes with similar CaO contents (10-15%), in order to shed light on the compositional constraints that control the reaction of CO_2 with these materials, in view of their utilization as additions to cementitious materials. La Pereda fly ash achieved the best carbonation efficiency (46.7%) among the study samples, corresponding to 53 g of CO_2/kg of fly ash. These results are similar to the values obtained in [79], where carbonation of a 35%-CaO HCFA led to 48% carbonation efficiency (117 g of CO_2/kg of fly ash sequestration capacity). The high carbonation potential of the La Pereda sample, despite its lower bulk CaO, is due to the fact that free lime is the predominant Ca-bearing mineral. Direct HCFA carbonation at low pressures and temperatures seems to be a promising technology for CO_2 sequestration, even for materials with relatively low CaO content. In order to implement this process in industry, carbonation experiments with diluted CO_2 simulating power plant flue gas should be performed to investigate its feasibility. HCFA carbonation with flue gas instead of pure CO_2 would significantly reduce the cost of the process [15].

Two different experimental systems were compared: batch and continuous flow, both with and without the addition of steam. The moist batch treatment was shown to achieve the highest carbonation efficiency.

Chapter 9. Carbonation of Fly Ash with Simulated Flue Gas

In this study, carbonation of Ptolemais fly ash with simulated flue gas (84% N_2, 15% CO_2 and 1% H_2O) at a pressure of 6 bar is performed at 160°C in an experiment of two hours' duration. As well as a general analysis of the material before and after the experiment, a free lime determination test was performed in order to reveal the decrease in calcium oxide content. This research is important from two different perspectives. Firstly, the CO_2 utilization of waste flue gas, where both reactants are produced on the same site, means that the process of carbonation could be implemented at a power plant. In addition, using flue gas for carbonation instead of a pure stream of CO_2 would save the cost of gas stream separation [177]. Secondly, the process involves the decrease of free lime in HCFA to values compatible with legislation, i.e., EU 450-1:2012. The investigation determining free lime is described in chapter 10.

9.1 Methods

This research used the Ptolemais fly ash described in section 5.3.5. Experiments were conducted using purposely designed apparatus. A full description and a graph are available in [79] and shown in Figures 61 and 62. The conditions of the procedure were as follows: 160°C and 6 bar of gas mix (84% N_2, 15% CO_2 and 1% H_2O) over two hours. The system of pressure flow used was the continuous flow reactor. To achieve the chosen mixture of gases, appropriate flow rates of CO_2 and N_2 were calculated and used throughout the experiment. Water vapour was added by introducing the water in the external bubbler to the gas pipeline. Experiments with the same conditions were performed six times, in order to ensure the experiment was repeatable. Before and after reactions, samples were analysed using XRD, TGA, FTIR and free lime determination analysis.

9.2 Analysis of Material Before and After Treatment

The X-ray diffraction results are shown in Figure 74. The graph shows a comparison between the starting material and the carbonated sample of fly ash. The major differences between the two diffractograms are disappearance of the lime peaks at 37.5° and 54° and the presence of the calcite peak at 29.5° in the carbonated sample [178]. This proves that the carbonation process occurs. An almost complete absence of the lime peaks in the carbonated sample may be a sign of full decomposition. Additionally, the anhydrite peak at position 22 [179] is not as visible in the carbonated sample as in the untreated material. $CaSO_4$ could also take part in the carbonation process.

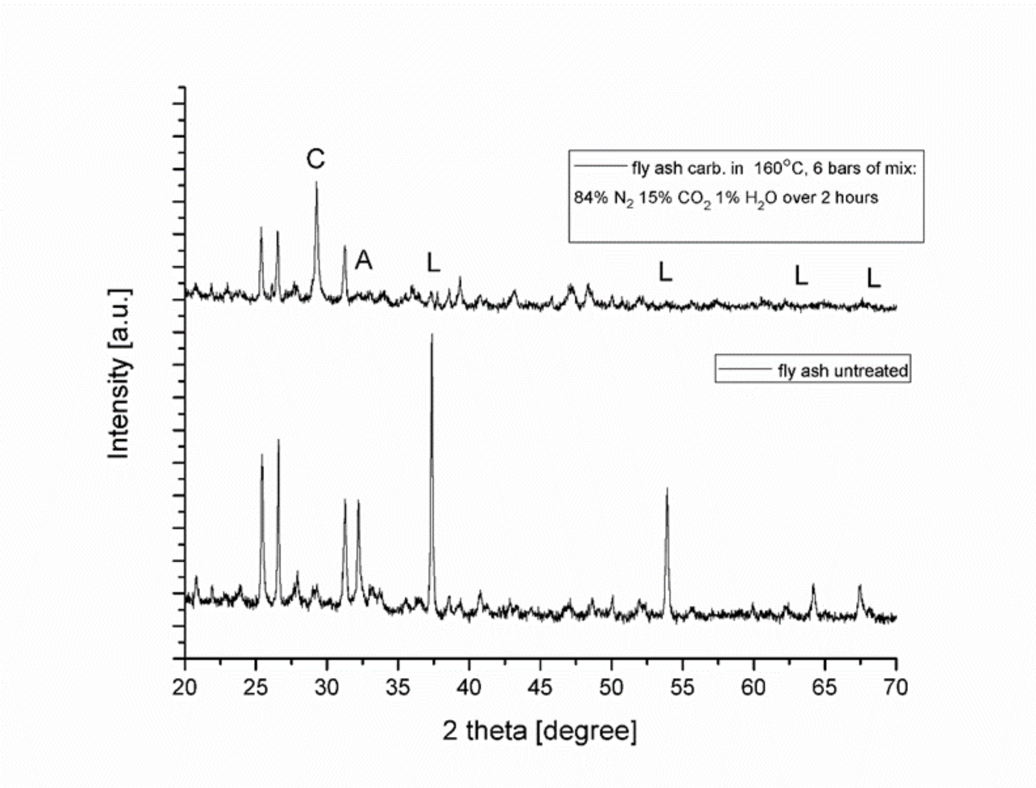

Figure 74. XRD analyses of fly ash, untreated and treated with the simulated flue gas. A – anhydrite, C – calcite, L – lime.

The results of the XRD analysis are supported by the infrared spectroscopy results. Figure 75 shows the spectra of the starting and carbonated material. One of the characteristic absorption bands for fly ash is a Si-O stretching vibration at 1,119 cm^{-1}, with a similar intensity for carbonated and uncarbonated samples [180]. The main differences between the spectra are the intensities at 872 cm^{-1}, 1,423 cm^{-1} and 1,796 cm^{-1}, which are highly increased in the carbonated sample compared to the starting material. These are the characteristic absorption bands for calcite [181].

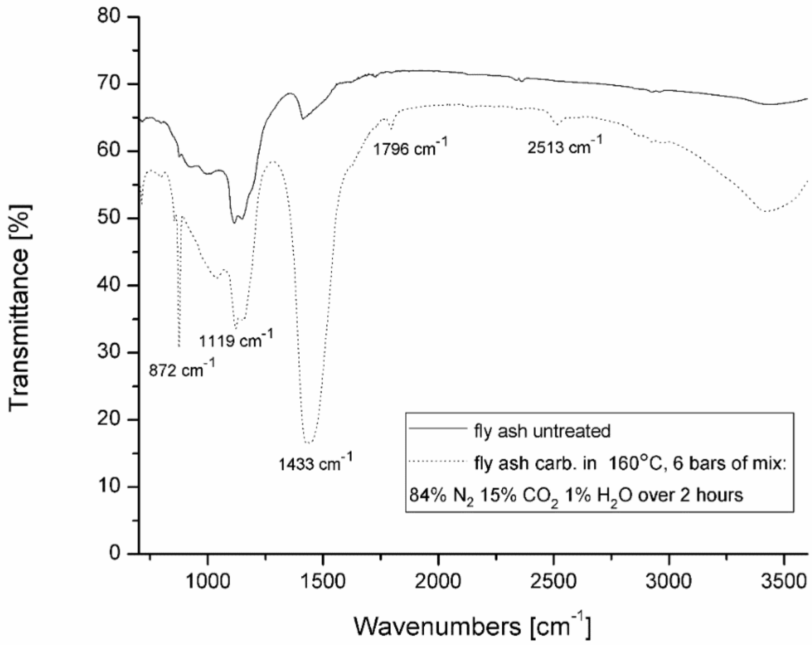

Figure 75. FTIR analyses of untreated and carbonated fly ash.

More information about the outcome of the carbonation process is obtained by performing thermogravimetric analyses. Figures 76 and 77 show the TGA results – mass loss and derivative weight change as a function of temperature in the range 30-950°C. Derivative weight changes were computed based on TGA data and show sample decomposition rates. The untreated sample of fly ash is characterized by only one region of mass loss, starting from 600°C, which reveals the natural carbonation of the sample and the initial carbonates content. In the treated sample, three different mass-loss peaks can be seen. The first, starting at 400°C, is attributed to the decomposition of portlandite, which was created during the reaction [182] as there was water present. The second peak, in a similar position to the peak in the untreated sample, is the peak starting at 600°C, related to the calcium carbonate decomposition. This leads to a much higher mass loss compared with the one in the untreated fly ash and finishes at 650°C. The next peak starts at this temperature and is also attributed to calcium carbonate decomposition, but for calcium carbonate with higher thermal stability. The decomposition is not finished at 950°C; the shape of the last peak shows that there are still more carbonates in the sample which are even more thermally stable. The different degradation temperatures of calcium carbonates present in the sample may be caused by different particle sizes or by the presence of amorphous calcium carbonate [34,168,183]. Figure 77 shows very clearly all the decomposition peaks in the carbonated sample.

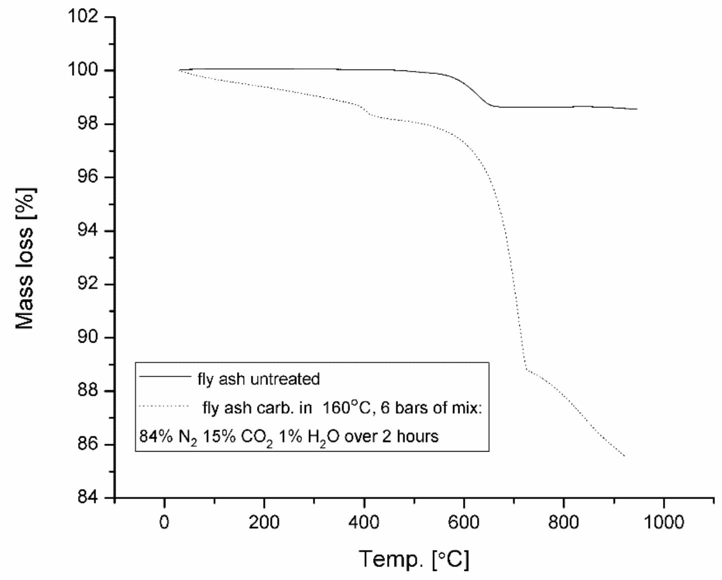

Figure 76. TGA analysis of the untreated material and fly ash carbonated with flue gas.

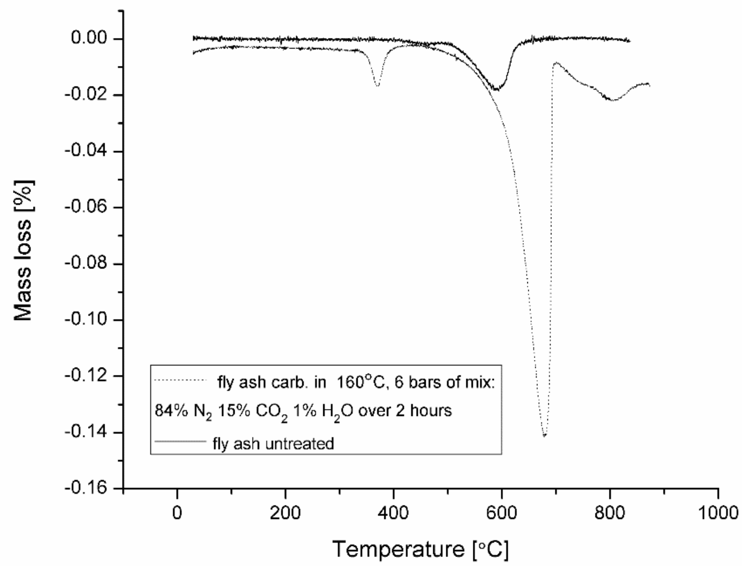

Figure 77. Derivative weight change graph computed based on the TGA analysis of the samples.

9.3 Carbonation Efficiency

Thermogravimetric data were used to calculate the CO_2 sequestration capacities and carbonation efficiencies. The methodology for these calculations is described in section 7.6.

To calculate the carbonation efficiency, the sequestration capacity calculated based on TGA was compared to the maximum theoretical value (277.1 g CO_2/kg fly ash) and shown as a percentage of this. For the purposes of comparison, the values for the experiment on the same fly ash carbonated at 160ºC and 6 bar of CO_2 over two hours, as described in [79], are also shown in Table 22.

Table 22. Calculated values of the amount of CO_2 captured (CO_2 [wt%]), sequestration capacity (g CO_2/kg fly ash) and carbonation efficiency (ζCa [%]) of the fly ash.

Sample	CO_2[wt%]	g CO_2/kg fly ash	ζ_{Ca}[%]
Ptolemais FA carbonate with flue gas	10.93	109.3	39.4
Ptolemais FA carbonated with CO_2	11.77	117.7	48.14

The carbonation efficiency achieved for the fly ash carbonated in the simulated flue gas was 39.4% and the sequestration capacity was 109.3 g CO_2/kg fly ash. These values are lower than the values for the sample carbonated in the same conditions but with a pure stream of CO_2 instead of the gas mix. When the sample is carbonated with 6 bar of flue gas, the partial pressure of the CO_2 is lower than in the pure stream of carbon dioxide at the same pressure. This is the reason why lower carbonation efficiency is achieved in flue gas carbonation than in the pure CO_2 carbonation process. Similar results are shown in [184,185], where mineral carbonation was performed with simulated flue gas with successful results. Using flue gas for carbonation avoids the cost of a CO_2 capture and separation system at power plants, and also the cost of pre-concentration.

9.4 Case Study for Ptolemais Power Plant

Using the data available in [148, 185], the experimental results of this study were used to assess the potential for reducing CO_2 emissions at the Ptolemais power plant, where the studied fly ash was produced. In 2012, the total annual fly ash production at northern Greek power plants (Ptolemais, Kardia and Amyntaio power stations) was around 7.6 Mt. The whole fly ash production in Greece is 10-11 Mt annually, and only 300 kt of that is recycled. Most of the produced fly ash is disposed of in exhausted mine workings. From 2002, Greek lignite fly ash has been eligible for use under European Standard EN 197-1. The annual CO_2 emissions from the Ptolemais power plant in 2011 were 4.33 Mt. Assuming that the total amount of 7.6 Mt of fly ash would be accessible for the carbonation process and can be characterized by a constant 35% CaO content, carbonation with 100% efficiency would result in 2.1 Mt CO_2 being utilized. This value constitutes almost half of the total annual production. With the 39.4% carbonation efficiency achieved in this study, 0.83 Mt of CO_2 could be utilized (19.2%). Values of sequestration capacity and carbonation efficiency obtained in laboratory conditions could be different on an industrial scale.

Table 23. Potential CO_2 utilization for the Ptolemais Power Plant through fly ash carbonation.

Annual fly ash production [Mt]	7.6
Annual CO_2 emissions [Mt]	4.33
Theoretical possible CO_2 utilization [Mt]	2.1 (48.5%)
CO_2 utilization with 42.4 % carbonation efficiency [Mt]	0.89 (20.6%)
CO_2 utilization with 39.4 % carbonation efficiency [Mt]	0.83 (19.2%)

9.5 Conclusions

In this work, carbonation of high-calcium fly ash at 160°C and 6 bar of gas mixture (84% N_2, 15% CO_2 and 1% H_2O) over two hours, was examined. The analysis demonstrated that carbonation occurred with 39.4% efficiency. The CO_2 sequestration capacity of fly ash in these process conditions is 109.3 g CO_2/kg fly ash. It was found that carbonation with simulated flue gas leads to lower process efficiencies compared to the process with a pure stream of CO_2, although the difference is small.

As a consequence of avoiding the cost of CO_2 separation from the flue gas at power plants and achieving similar carbonation conversion rates, implementing the carbonation technology on an industrial scale using raw exhaust gas with ~15% of CO_2 would be more economical than using a pure CO_2 stream.

Chapter 10. Free Lime Determination Studies

Restrictions introduced by governments regarding the addition of HCFA to cement, are in place because of the high content of lime present in the ash. Cement, one of the main components of concrete, consists of 60-70% lime. Adding fly ash with a high percentage of CaO to cement leads to an increase in the total lime content in cement. During the concrete curation process, when the cement is mixed with water, a higher content of lime could lead to additional activation of hardening behaviour, as the calcium compounds and alkali sulphates engage in cementitious and pozzolanic reactions. According to current regulations, if fly ash has more than 1.5% of free lime, it must be tested for conformity as well as for soundness. This topic has been previously discussed in chapter 5. Carbonation reactions involve the utilization of carbon dioxide and at the same time decrease the amount of free lime in fly ash, converting it to stable calcium carbonate. Fly ashes investigated in this thesis, were tested for their free lime content. Some of the carbonated samples were also characterized by this method in order to assess whether the final free lime content had been decreased to values compatible with current legislation in the construction industry.

10.1 Methods

Free lime determination tests were performed based on those described in [187]. For each test, 1 g of sample was mixed with 50 ml of ethylene glycol and placed in water bath at 60°C for 30 minutes. Next, the sample was filtered, and the filtrate was titrated with N/10-HCl solution with two to three drops of bromocresol green solution, to the point where the filtrate changed colour from blue to green. The CaO content was calculated as follows.

$$Free\ CaO = \frac{ml\ HCl\ x\ \ normality\ of\ HCl}{10\ x\ sample\ weight}\ x\ 28 \qquad (50)$$

10.2 Results

The free lime content in untreated fly ashes was determined for the La Pereda, Megalopolis, Belchatow, Ptolemais and biomass fly ash samples. Results are shown in Table 24.

Table 24. Free lime determination results for untreated fly ash samples.

Fly ash	Free lime content [%]
La Pereda	4.16
Megalopolis	1.96
Belchatow	0.33
Ptolemais	20.9
Biomass	0.165

The Ptolemais fly ash is characterized by the highest value of free lime at 20.9%. To determine whether this value could be reduced, the same CaO determination test was performed for the sample carbonated at 160°C and 6 bar of CO_2 over two hours, in the same conditions but using flue gas (84%N_2, 15% CO_2 and 1% H_2O). A full description of these experiments is given in chapters 7 and 9. The results of this investigation are shown in Figure 78.

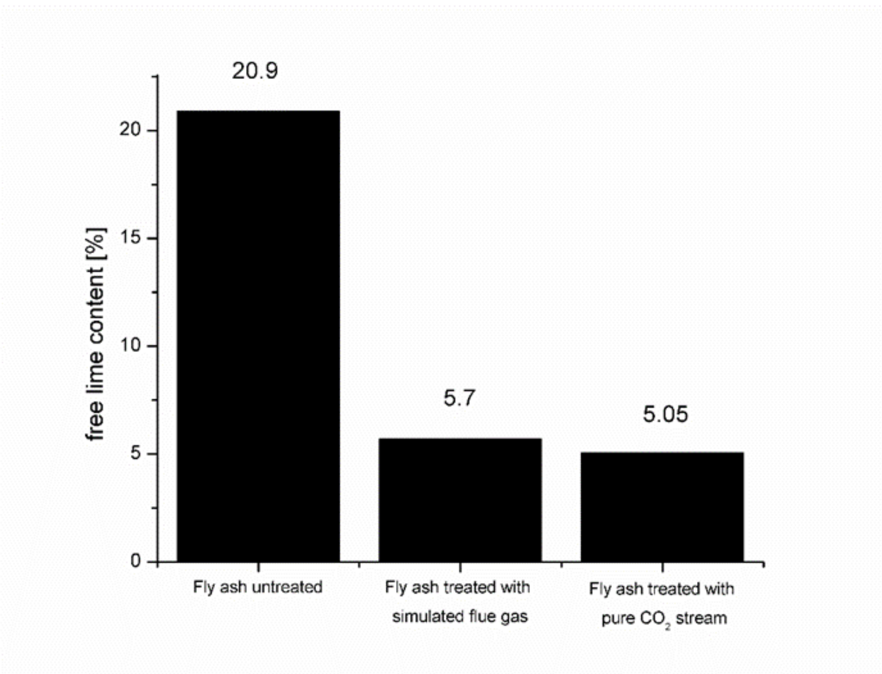

Figure 78. Free lime determination results for the untreated and carbonated samples of fly ash (160°C and 6 bar of CO_2/flue gas over two hours).

The tests show that the content of free lime decreased from 20.9% to 5.7% and 5.05% with the same carbonation conditions using flue gas or a pure CO_2 stream respectively. This value is still too high for the fly ash to be approved as a cement admixture, according to the EN 450-1:2012 regulations, but considering tests performed by other authors [146, 187, 188], a content of 5-6% free lime should not be problematic with regard to fly ash incorporation into cement. Maintaining the carbonation process over a longer time or at higher temperature or pressure, could lead to a further decrease in free lime content. Observation of a significant decrease of free lime in fly ash via carbonation is important for the application of carbonated high-calcium fly ashes in the construction industry.

The same tests were performed for the carbonated samples described in chapter 5. The free lime determination test was performed on the samples with the best CO_2 sequestration efficiency. La Pereda fly ash, with the lowest total calcium content of 10.33%, is characterized by the highest content of free lime, i.e., 4.16%.

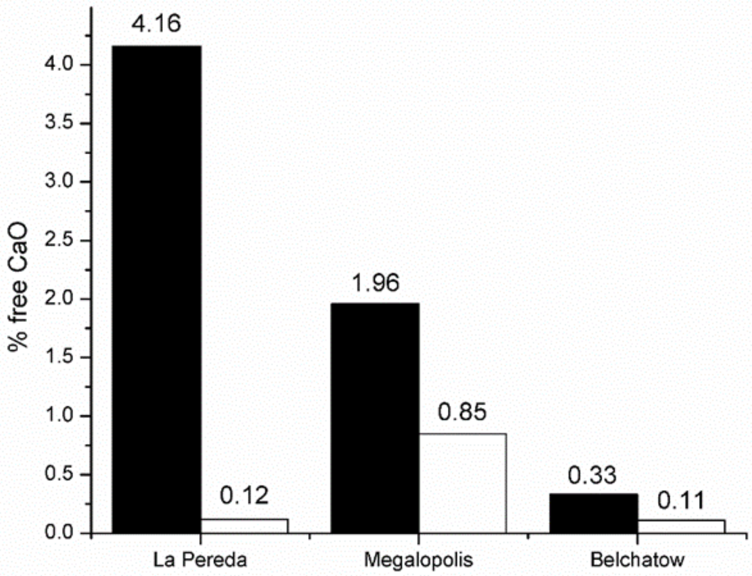

Figure 79. Results of the determination of free lime content for untreated (solid) and carbonated samples (Cwik, 2019).

The free lime content of the samples after carbonation is in every case below 1.5% (Figure 79). This means that most of the free CaO has been carbonated and transformed to calcium carbonate. This observation is very important from the point of view of the application of carbonated high-calcium fly ashes in the construction industry, as there are specific requirements regarding the free lime content in fly ashes incorporated into cement [190].

10.3 Conclusions

The free lime determination tests showed that the carbonation reaction usually leads to significant transfer of free CaO to calcium carbonate, for most of the investigated types of fly ashes. Considering the present EU regulations regarding fly ash admixtures for concretes (EN 450-1), reducing this value below 1.5% could be a starting point for implementing the carbonation process at coal-fired power plants, thus reducing their emissions and enabling the use of carbonated fly ash in the cement industry. In the case of the Ptolemais fly ash, the free lime content has been decreased from ~21% to 5%. This value is still too high for this type of fly ash to be used for cement production, but further optimization of the process conditions (longer reaction time, higher temperature or pressure) may lead to even higher efficiency and carbonated fly ash with a lower free lime content.

General Conclusions

In this work, the topic of advanced carbon capture, utilization and storage technologies is presented. There are two experimental parts of this thesis. The first involves the study of carbon dioxide and methane sorption in coal and the implications for the swelling behaviour of the material. The second involves the study of the carbonation process for high-calcium fly ashes produced in Europe.

From the perspective of possible CO_2 storage in deep underground coal seams, it is important to assess the potential gas storage volume as well as the rock's response to the sorption processes. In chapter 4, the swelling of hard coal associated with the sorption of carbon dioxide and methane in isothermal and non-isothermal conditions, was measured. These investigations are of great importance for validating the potential for CO_2 sequestration in deep unmined coalfields. Any fluctuations of the temperature in underground coal beds can change the sorption balance, resulting in volumetric strains in the coal strata, which in the end can lead to gas desorption and gas leaks at the surface. The research presented in this thesis shows that the coal strains attributed to CO_2 sorption are about twice as large as those for CH_4. Moreover, the linear strain kinetics show that the swelling of samples exposed to both gases is anisotropic and is greater in the direction perpendicular to the bedding plane than parallel to it. However, even though the sorption capacity for carbon dioxide is almost double that for methane, the dilatometric results show that the deformation of the coal sample in the presence of methane is only around half as high as the deformation in the presence of CO_2, in the same pressure range. Taking into consideration the non-isothermal process, the contraction of the sorbent proceeds more slowly than its expansion. The temperature increase gives rise to sample swelling in the presence of methane. A different pattern is observed for the CO_2 process, where the presence of the gas leads to sample contraction. This behaviour can be explained by differences in the petrographic compositions of different coals.

The experimental data obtained in section 4.2 were used to examine the ability of the kinetic equation to describe the sorption kinetics and expansion rate of the solid coal sample. It was found that sorption and swelling isotherms can be described using the stretched exponential equation. Modelling the sorption and swelling kinetics helped to determine the coal response to the gases introduced into the system and enabled the changes in the coal transport-sorption and storage properties to be predicted.

Following this study, the topic of carbonation as permanent chemical fixation of CO_2 is described. High-calcium fly ashes with significant production in Europe were chosen as substrates for the process. The experiments were performed on six different fly ashes with 5-36% of CaO, from Poland, Spain and Greece. All the fly ash samples were analysed and characterized.

Acceleration of carbonation was investigated. It was found that increasing the temperature and pressure enhanced the process of carbonation. Moreover, the addition of water vapour strongly influences the process and increases its kinetics. However, this thesis reports that performing the carbonation process without steam addition also leads to substantial carbonation efficiencies. Dry chemical fixation of gas molecules of CO_2 with the solid material of fly ash, to obtain calcium carbonate, is possible. The maximum calculated sequestration capacity achieved for Ptolemais fly ash was 117.7 g CO_2/kg fly ash, and the maximum carbonation efficiency obtained was 48%.

The microstructural analysis of fly ash samples before and after carbonation showed the evolution of the cenosphere surface, according to the experimental conditions. It was found that the surface of cenospheres is where carbonates are formed, due to the initial oxides present on the surface. In addition, different shapes and sizes of the calcium carbonate reaction product were observed.

Another aspect of carbonation described in this thesis is the comparison of the carbonation potential of fly ashes with similar CaO contents (10-15%), in order to obtain insights into the compositional constraints that control the reaction of CO_2 with these materials. The best carbonation efficiency was achieved for the La Pereda fly ash (46.7%). Direct HCFA carbonation at low pressures and temperatures is a promising technology for CO_2 sequestration, even for materials with relatively low CaO content.

The influence on carbonation of two different pressure flow experimental systems was assessed. These were batch and continuous flow systems, both with and without the addition of steam. The batch treatment with the addition of steam gave the highest carbonation efficiency.

Considering the economic aspects of applying the carbonation process at power plants, using flue gas instead of a pure stream of CO_2 would substantially lower the cost of such an installation. To determine whether flue gas would give similar carbonation efficiencies to pure CO_2, a set of experiments was performed using a simulated flue gas (84% N_2, 15% CO_2 and 1 % H_2O) in the same conditions: 160°C and 6 bar of gas over two hours of reaction time. The carbonation efficiency for the experiment with a pure stream of CO_2 was 48%, and for the reaction with simulated flue gas it was 39%. It can be concluded that switching from a 100% CO_2 stream to flue gas will only slightly affect the final carbonation rate. Considering the fact that there is no need to purify and concentrate the CO_2 present in the flue gas, so that raw exhaust gas from burning fossil fuels can be used, the cost of the whole process would be lower.

The final part of this thesis concerned determination of the change in free lime content in fly ash samples before and after carbonation. It was found that the content of free lime is the controlling factor in the carbonation process. Furthermore, carbonation reactions lead to substantial reductions in free lime content in fly ashes. For the La Pereda fly ash, the free lime content was reduced from 4.16% to 0.12%. For the Ptolemais fly ash with initial free lime content of 20.9%, carbonation led to a reduction to 5.05%. These findings are very important from the perspective of using HCFA in the building industry. Restrictions imposed by governments regarding the admixture of HCFA in cement are based

on limiting the content of free lime present in construction materials. Lack of control of the free lime content may eventually lead to durability problems, due to delayed hydration and subsequent expansion and cracking.
In the case of fly ash with an extremely high free lime content, the value was reduced from 20.9% to 5.05%. This is still too high for this type of fly ash to be used in cement, but if the carbonation efficiency is increased and the process accelerated, the free lime content could be reduced below 1.5%.

The findings in this study are very important from the perspective of the circular economy concept. CO_2 mineralization via direct carbonation is linked with valorization of HCFA, which can be used as a supplementary cementitious material. CO_2 and waste material valorization through mineral carbonation offers great potential for a sustainable carbon cycle in a circular economy [191]. In this work, both carbon dioxide and HCFA are treated as raw materials which can be reused in a sustainable way. Using carbonated fly ash materials in cement would make the construction industry more environmentally friendly. Utilizing CO_2 with solid wastes produced worldwide at power plants would result in 2% CO_2 mitigation.

Future Work

Work presented in this thesis could be extended in many different ways. There are many factors regarding the carbonation process which can be further optimized. In addition, the experimental work could be enriched by performing a techno-economic analysis of possible implementations of the process at an industrial scale.

The kinetics of the carbonation reaction could be further enhanced. The reaction times presented in this work were between two and four hours. Maintaining the reactions over longer time periods could have a beneficial impact on CO_2 sequestration.

The maximum pressures used in this research were 10-12 bar of CO_2. The literature shows that further increasing the pressure could result in achieving higher carbonation efficiencies.

The temperature range used in this work was between 25°C and 290°C. Our work confirms the findings of other researchers [75] that for carbonation reactions taking place at temperatures up to 300°C, it is mostly free lime (CaO) that is the reactive component. Increasing the temperature to values higher than 300°C could accelerate the carbonation of $Ca(OH)_2$.

It would be interesting to implement the carbonation reaction under the conditions used in this thesis on different samples of fly ashes and also different waste materials, for example, municipal waste fly ashes or mining residues.

The findings of this thesis, which were produced at laboratory scale, could be transferred to a real model of the process at an industrial scale.

Another possibility for supplementary work that could be combined with carbonation of HCFA, is testing of produced samples of carbonated fly ashes as a cement blend. Investigating the mechanical strengths of these carbonated fly ash-cement mortars would give insights into whether the properties of such materials are similar to those of pure cement.

This work could also be extended by performing an extensive techno-economic analysis, which would assess the potential impact of the implementation of HCFA carbonation reactors in power plants. Such an analysis could expose the elements of the system which could be improved, and the final cost could be optimized.

Achievements of the Author

Publications

1. **A. Ćwik**, I. Casanova, K. Rausis, N. Koukouzas, K. Zarębska, Carbonation of high-calcium fly ashes and its potential for carbon dioxide removal in coal fired power plants, *Journal of Cleaner Production* 202 (2018) 1026-1034. (IF: 5.651, MNiSW points: 40)
2. **A. Ćwik**, I. Casanova, K. Rausis, K. Zarębska, Utilization of high-calcium fly ashes through mineral carbonation: The cases for Greece, Poland and Spain, *Journal of CO_2 Utilization* 32 (2019) 155–162. (IF: 5.503, MNiSW points: 35)
3. **A. Ćwik**, K. Zarebska, P. Baran, J. Szczurowski, Mineral carbonation of high-calcium fly ash under elevated pressure and temperature, *Przemysł Chemiczny* 96 (2017). (IF: 0.367, MNiSW points: 15)
4. P. Baran, K. Czerw, N. Czuma, K. Zarębska, **A. Ćwik**, Development of temperature-induced strains in coal-CH_4 and coal-CO_2 systems, *Adsorption Science & Technology* (2018) 026361741880782. (IF: 0.609, MNiSW points: 15)
5. K. Czerw, **A. Ćwik**, P. Baran, K. Zarębska, Kinetics of methane and carbon dioxide sorption and sorption-induced expansion of coal-kinetic equations assessment, *E3S Web of Conferences* 10 (2016). (MNiSW points: 15)
6. A. Orzechowska-Zięba, K. Zarębska, P. Baran, **A. Ćwik**, Sequestration of carbon dioxide – influence of coal surface chemistry, *E3S Web of Conferences* 10 (2016). (MNiSW points: 15)

Presentations at conferences

- SEED 2017: International Conference on Sustainable Energy and Environment Development: 14th-17th November 2017, Cracow, Poland

  A. Ćwik, K. Zarębska, P. Baran, CO_2 utilization in fly ash: gas-solid carbonation in a pressure and temperature change environment.

- Conference: Energy and Fuels 2018: 19th-21st September 2018, Cracow, Poland

  K. Zarębska, **A. Ćwik**, I. Casanova, N. Czuma, P. Baran, P. Zabierowski, Application of fly ash for mineral carbonation of CO_2.

- SEED 2016: International Conference on Sustainable Energy and Environment Development: 17th-19th May 2016, Cracow, Poland.

K. Czerw, **A. Ćwik**, P. Baran, K. Zarębska, Kinetic equations assessment for methane and carbon dioxide sorption and sorption-induced expansion of coal.
A. Orzechowska-Zięba, K. Zarębska, P. Baran, **A. Ćwik**, The effect of the coal surface nature on carbon dioxide sequestration.

Posters at conferences

- Carbon Capture and Storage: Faraday Discussion: 18th-20th July 2016, Sheffield, United Kingdom
  A. Ćwik, P. Baran, K. Zarębska, I. Casanova, CO_2 storage in coal: investigation of the coal seam expansion and sorption capacity of CO_2 and CH_4 in isothermal conditions.

- Gordon Research Conference: Carbon Capture, Utilization and Storage – Tackling the Carbon Dioxide Challenge for a Sustainable Future: 5th-10th May 2019, Les Diablerets, Switzerland
  K. Rausis, I. Casanova, **A. Ćwik**, CO_2 Sequestration by accelerated carbonation of brucite in moderate pressure and temperatures.

- Gordon Research Conference: Innovative Carbon Management Pathways for a Sustainable Future: 11th-16th June 2011, New London, United States
  A. Ćwik, P. Baran, K. Zarębska, I. Casanova, CO_2 Storage in Coal: Study of coal seam expansion and sorption capacity of CO2 and CH4.

- EuroSciCon Conference on Chemistry 2018: 19th-20th February 2018, Paris, France
  P. Zabierowski, K. Zarębska**,** N. Czuma, P. Baran, **A. Ćwik**, K. Świerczek, Mineral carbonation of modified and non-modified fly ash in an elevated pressure and temperature.
  K. Czerw, P. Baran, K. Zarębska, **A. Ćwik**, N. Czuma, I. Casanova, Modelling of methane and carbon dioxide sorption and sorption-induced coal expansion.

- Conference: Energy and Fuels 2018: 19th-21st September 2018, Cracow, Poland
  P. Baran, K. Zarębska, **A. Ćwik**, K. Czerw, Development of temperature-induced strains in coal-CH4 and coal-CO2 systems.

- SEED 2017: International Conference on Sustainable Energy and Environment Development: 14th-17th November 2017, Cracow, Poland

P. Baran, K. Zarębska, **A. Ćwik**, K. Czerw, Effect of grain size on the sorption and desorption of hydrogen on crushed hard coal.

- Sorbenty Mineralne 2017: 18th-19th September 2017, Cracow, Poland
  A. Ćwik, P. Baran, K. Zarębska, I. Casanova, Składowanie CO_2 w węglu: Badanie zmian wolumetrycznych oraz chłonności sorpcyjnej CO_2 i CH_4 wytypowanego węgla kamiennego.

References

[1] W.S. Broecker, Abrupt climate change: Causal constraints provided by the paleoclimate record, Earth Sci. Rev. 51 (2000) 137–154. doi:10.1016/S0012-8252(00)00019-2.

[2] C. Varianou Mikellidou, L.M. Shakou, G. Boustras, C. Dimopoulos, Energy critical infrastructures at risk from climate change: A state of the art review, Saf. Sci. 110 (2018) 110–120. doi:10.1016/j.ssci.2017.12.022.

[3] H. Herzog, D. a N. Golomb, Carbon Capture and Storage From Fossil Fuels and Biomass, Encycl. Energy. (2004) 1–19. doi:http://dx.doi.org/10.1016/B0-12-176480-X/00422-8.

[4] U.S.E.I. Administration, Annual Energy Outlook 2018 with projections to 2050., 3 (2018) 79–83. doi:10.1002/bio.1170030209.

[5] ExxonMobil, 2017 Outlook for Energy, Http://Cdn.Exxonmobil.Com/~/Media/Global/Files/Outlook-for-Energy/2017/2017-Outlook-for-Energy.Pdf. (2017).

[6] O.E. Directorate, OECD Environmental Outlook to 2050, 39 (2011) 232–240. doi:10.19650/j.cnki.cjsi.j1702567.

[7] W.L. Theo, J.S. Lim, H. Hashim, A.A. Mustaffa, W.S. Ho, Review of pre-combustion capture and ionic liquid in carbon capture and storage, Appl. Energy. 183 (2016) 1633–1663.

[8] M.N. Anwar, A. Fayyaz, N.F. Sohail, M.F. Khokhar, M. Baqar, W.D. Khan, K. Rasool, M. Rehan, A.S. Nizami, CO2capture and storage: A way forward for sustainable environment, J. Environ. Manage. 226 (2018) 131–144. doi:10.1016/j.jenvman.2018.08.009.

[9] U.S.D. of Energy, Pre-combustion CO2 capture, Int. Energy Technol. Lab. (n.d.). https://www.netl.doe.gov/research/coal/carbon-capture/pre-combustion.

[10] D. Jansen, M. Gazzani, G. Manzolini, E. Van Dijk, M. Carbo, Pre-combustion CO2capture, Int. J. Greenh. Gas Control. 40 (2015) 167–187.

[11] G.C. Institute, High Level Pre Combustion Technology Options, (n.d.). https://hub.globalccsinstitute.com/publications/co2-capture-gas-fired-power-plants/33-high-level-pre-combustion-technology-options.

[12] C.A. Scholes, K.H. Smith, S.E. Kentish, G.W. Stevens, CO2 capture from pre-combustion processes—Strategies for membrane gas separation, Int. J. Greenh. Gas Control. 4 (2010) 739–755. doi:10.1016/J.IJGGC.2010.04.001.

[13] C. Anderson, C. Scholes, A. Lee, K. Smith, S. Kentish, G. Stevens, P.A. Webley, A. Qader, B. Hooper, Novel pre-combustion capture technologies in action–Results of the CO2CRC/HRL Mulgrave capture project, Energy Procedia. 4 (2011) 1192–1198. doi:10.1016/J.EGYPRO.2011.01.173.

[14] M. Kanniche, R. Gros-Bonnivard, P. Jaud, J. Valle-Marcos, J.-M. Amann, C. Bouallou, Pre-combustion, post-combustion and oxy-combustion in thermal power plant for CO2 capture,

Appl. Therm. Eng. 30 (2010) 53–62. doi:10.1016/J.APPLTHERMALENG.2009.05.005.

[15] E.S. Rubin, J.E. Davison, H.J. Herzog, The cost of CO2capture and storage, Int. J. Greenh. Gas Control. 40 (2015) 378–400. doi:10.1016/j.ijggc.2015.05.018.

[16] Q. Ye, H. Lu, Y. Du, S. Zhang, X. Wang, Y. Lu, Experimental Investigation of the Absorption, Phase Transition, and Desorption Behavior of Biphasic Solvent Blends for Postcombustion CO2 Capture, Energy Procedia. 114 (2017) 813–822. doi:10.1016/J.EGYPRO.2017.03.1223.

[17] D. Bonalumi, S. Lillia, G. Manzolini, C. Grande, Innovative Process Cycle with Zeolite (MS13X) for Post Combustion Adsorption, Energy Procedia. 114 (2017) 2211–2218. h (accessed November 14, 2018).

[18] S. Roussanaly, R. Anantharaman, K. Lindqvist, H. Zhai, E. Rubin, Membrane properties required for post-combustion CO2 capture at coal-fired power plants, J. Memb. Sci. 511 (2016) 250–264.

[19] H. Chen, N. Khalili, J. Li, Development of stabilized Ca-based CO2sorbents supported by fly ash, Chem. Eng. J. 345 (2018) 312–319.

[20] F. Wu, M.D. Argyle, P.A. Dellenback, M. Fan, Progress in O2separation for oxy-fuel combustion–A promising way for cost-effective CO2capture: A review, Prog. Energy Combust. Sci. 67 (2018) 188–205. doi:10.1016/j.pecs.2018.01.004.

[21] T. Lockwood, A Compararitive Review of Next-generation Carbon Capture Technologies for Coal-fired Power Plant, Energy Procedia. 114 (2017) 2658–2670. doi:10.1016/j.egypro.2017.03.1850.

[22] C.A. Scholes, M.T. Ho, D.E. Wiley, G.W. Stevens, S.E. Kentish, Cost competitive membrane—cryogenic post-combustion carbon capture, Int. J. Greenh. Gas Control. 17 (2013) 341–348.

[23] M. Wang, A. Lawal, P. Stephenson, J. Sidders, C. Ramshaw, Post-combustion CO2capture with chemical absorption: A state-of-the-art review, Chem. Eng. Res. Des. 89 (2011) 1609–1624.

[24] Y. Wang, L. Zhao, A. Otto, M. Robinius, D. Stolten, A Review of Post-combustion CO2Capture Technologies from Coal-fired Power Plants, Energy Procedia. 114 (2017) 650–665. doi:10.1016/j.egypro.2017.03.1209.

[25] A. Lawal, M. Wang, P. Stephenson, G. Koumpouras, H. Yeung, Dynamic modelling and analysis of post-combustion CO2 chemical absorption process for coal-fired power plants, Fuel. 89 (2010) 2791–2801.

[26] L. Dubois, D. Thomas, Postcombustion CO2capture by chemical absorption: Screening of aqueous amine(s)-based solvents, Energy Procedia. 37 (2013) 1648–1657.

[27] J.R. McDonough, R. Law, D.A. Reay, V. Zivkovic, Intensified carbon capture using adsorption: Heat transfer challenges and potential solutions, Therm. Sci. Eng. Prog. 8 (2018) 17–30. doi:10.1016/j.tsep.2018.07.012.

[28] J.W. Dijkstra, S. Walspurger, G.D. Elzinga, J.A.Z. Pieterse, J. Boon, W.G. Haije, Evaluation of Postcombustion CO2 Capture by a Solid Sorbent with Process Modeling Using Experimental CO2 and H2O Adsorption Characteristics, Ind. Eng. Chem. Res. 57 (2018) 1245–1261.

doi:10.1021/acs.iecr.7b03552.

[29] G. Colantuono, T. Cockerill, Selective strategy for solid sorbent replacement in CCS, Chem. Eng. Res. Des. 120 (2017) 82–91. doi:10.1016/j.cherd.2017.01.030.

[30] R. Anantharaman, D. Berstad, S. Roussanaly, Techno-economic performance of a hybrid membrane - Liquefaction process for post-combustion CO2capture, Energy Procedia. 61 (2014) 1244–1247.

[31] B. Li, Y. Duan, D. Luebke, B. Morreale, Advances in CO2capture technology: A patent review, Appl. Energy. 102 (2013) 1439–1447. doi:10.1016/j.apenergy.2012.09.009.

[32] A. Perejón, L.M. Romeo, Y. Lara, P. Lisbona, A. Martínez, J.M. Valverde, The Calcium-Looping technology for CO2capture: On the important roles of energy integration and sorbent behavior, Appl. Energy. 162 (2016) 787–807.

[33] A. Perejón, L.M. Romeo, Y. Lara, P. Lisbona, A. Martínez, J.M. Valverde, The Calcium-Looping technology for CO2 capture: On the important roles of energy integration and sorbent behavior, Appl. Energy. 162 (2016) 787–807.

[34] A. Escardino, J. García-Ten, C. Feliu, A. Saburit, V. Cantavella, Kinetic study of the thermal decomposition process of calcite particles in air and CO2atmosphere, J. Ind. Eng. Chem. 19 (2013) 886–897.

[35] B. Arias, M.E. Diego, J.C. Abanades, M. Lorenzo, L. Diaz, D. Martínez, J. Alvarez, A. Sánchez-Biezma, Demonstration of steady state CO2 capture in a 1.7 MWth calcium looping pilot, Int. J. Greenh. Gas Control. 18 (2013) 237–245.

[36] D.P. Hanak, V. Manovic, Calcium looping combustion for high-efficiency low-emission power generation, J. Clean. Prod. 161 (2017) 245–255.

[37] D.P. Hanak, V. Manovic, Economic feasibility of calcium looping under uncertainty, Appl. Energy. 208 (2017) 691–702.

[38] V. White, A. Wright, S. Tappe, J. Yan, The Air Products Vattenfall Oxyfuel CO2 Compression and Purification Pilot Plant at Schwarze Pumpe, Energy Procedia. 37 (2013) 1490–1499. doi:10.1016/J.EGYPRO.2013.06.024.

[39] R. Stanger, T. Wall, R. Spörl, M. Paneru, S. Grathwohl, M. Weidmann, G. Scheffknecht, D. McDonald, K. Myöhänen, J. Ritvanen, S. Rahiala, T. Hyppänen, J. Mletzko, A. Kather, S. Santos, Oxyfuel combustion for CO2capture in power plants, Int. J. Greenh. Gas Control. 40 (2015) 55–125.

[40] L. Chen, S.Z. Yong, A.F. Ghoniem, Oxy-fuel combustion of pulverized coal: Characterization, fundamentals, stabilization and CFD modeling, Prog. Energy Combust. Sci. 38 (2012) 156–214.

[41] A.A. Olajire, CO2 capture and separation technologies for end-of-pipe applications – A review, Energy. 35 (2010) 2610–2628.

[42] S.A. Rackley, S.A. Rackley, Introduction to geological storage, Carbon Capture and Storage. (2017) 285–304. doi:10.1016/B978-0-12-812041-5.00011-8.

[43] H.Z. Potsdam, Carbon capture-transport-storage (CCS), (n.d.). http://www.co2ketzin.de/en/co2-storage/capture-transport-storage/.

[44] G. de recherche sur les ressources énergétiques des bassins sédimentaires du Québec, CO2 Storage, (n.d.). http://grrebs.ete.inrs.ca/en/csc/csc_stockage/.

[45] M. Godec, V. Kuuskraa, T. Van Leeuwen, L.S. Melzer, N. Wildgust, CO2storage in depleted oil fields: The worldwide potential for carbon dioxide enhanced oil recovery, Energy Procedia. 4 (2011) 2162–2169. doi:10.1016/j.egypro.2011.02.102.

[46] S. Hannis, J. Lu, A. Chadwick, S. Hovorka, K. Kirk, K. Romanak, J. Pearce, CO2Storage in Depleted or Depleting Oil and Gas Fields: What can We Learn from Existing Projects?, Energy Procedia. 114 (2017) 5680–5690. doi:10.1016/j.egypro.2017.03.1707.

[47] D. Alfarge, M. Wei, B. Bai, CO 2 -EOR mechanisms in huff-n-puff operations in shale oil reservoirs based on history matching results, Fuel. 226 (2018) 112–120. doi:10.1016/j.fuel.2018.04.012.

[48] T. Holt, E. Lindeberg, D. Wessel-Berg, EOR and CO2disposal - Economic and capacity potential in the North Sea, Energy Procedia. 1 (2009) 4159–4166. doi:10.1016/j.egypro.2009.02.225.

[49] S. Bachu, Review of CO2storage efficiency in deep saline aquifers, Int. J. Greenh. Gas Control. 40 (2015) 188–202. doi:10.1016/j.ijggc.2015.01.007.

[50] Yixiang Gan, Carbon Storage, (n.d.).

[51] K. Michael, G. Allinson, A. Golab, S. Sharma, V. Shulakova, CO2 storage in saline aquifers II–Experience from existing storage operations, Energy Procedia. 1 (2009) 1973–1980. doi:10.1016/J.EGYPRO.2009.01.257.

[52] S. Bachu, D. Bonijoly, J. Bradshaw, R. Burruss, S. Holloway, N.P. Christensen, O.M. Mathiassen, CO2 storage capacity estimation: Methodology and gaps, Int. J. Greenh. Gas Control. 1 (2007) 430–443. doi:10.1016/S1750-5836(07)00086-2.

[53] P.S. Ringrose, The CCS hub in Norway: some insights from 22 years of saline aquifer storage, Energy Procedia. 146 (2018) 166–172. doi:10.1016/J.EGYPRO.2018.07.021.

[54] M.D. Corum, K.B. Jones, P.D. Warwick, CO2sequestration potential of unmineable coal-state of knowledge, Energy Procedia. 37 (2013) 5134–5140. doi:10.1016/j.egypro.2013.06.428.

[55] G. Ceglarska-Stefańska, K. Zarębska, Sorption of carbon dioxide–methane mixtures, Int. J. Coal Geol. 62 (2005) 211–222. doi:10.1016/J.COAL.2005.01.003.

[56] F. Anggara, K. Sasaki, Y. Sugai, The correlation between coal swelling and permeability during CO2 sequestration: A case study using Kushiro low rank coals, Int. J. Coal Geol. 166 (2016) 62–70. doi:10.1016/J.COAL.2016.08.020.

[57] M. Mukherjee, S. Misra, A review of experimental research on Enhanced Coal Bed Methane (ECBM) recovery via CO2sequestration, Earth-Science Rev. 179 (2018) 392–410. doi:10.1016/j.earscirev.2018.02.018.

[58] W.F.C. van Wageningen, H.M. Wentinck, C. Otto, Report and modeling of the MOVECBM

field tests in Poland and Slovenia, Energy Procedia. 1 (2009) 2071–2078. doi:10.1016/J.EGYPRO.2009.01.270.
[59] F. van Bergen, H.J.M. Pagnier, L.G.H. van der Meer, F.J.G. van den Belt, P.L.A. Winthaegen, R.S. Westerhoff, Development of a Field Experiment of CO2 Storage in Coal Seams in the Upper Silesian Basin of Poland (Recopol), Greenh. Gas Control Technol. - 6th Int. Conf. (2003) 569–574. doi:10.1016/B978-008044276-1/50091-X.
[60] K.S. Lackner, C.H. Wendt, D.P. Butt, E.L. Joyce, D.H. Sharp, Carbon dioxide disposal in carbonate minerals, Energy. 20 (1995) 1153–1170.
[61] M. Mazzotti, J. Carlos, R. Allam, K.S. Lackner, F. Meunier, E.M. Rubin, J.C. Sanchez, K. Yogo, R. Zevenhoven, Mineral carbonation and industrial uses of carbon dioxide, IPCC Spec. Rep. Carbon Dioxide Capture Storage. (2005) 319–338.
[62] A.A. Olajire, A review of mineral carbonation technology in sequestration of CO2, J. Pet. Sci. Eng. 109 (2013) 364–392. http://dx.doi.org/10.1016/j.petrol.2013.03.013.
[63] A. Mazzella, M. Errico, D. Spiga, CO2 uptake capacity of coal fly ash: Influence of pressure and temperature on direct gas-solid carbonation, J. Environ. Chem. Eng. 4 (2016) 4120–4128.
[64] G.C. Institute, Appendix F: CO2 as feedstock for carbonate mineralisation, (n.d.). https://hub.globalccsinstitute.com/publications/accelerating-uptake-ccs-industrial-use-captured-carbon-dioxide/appendix-f-co2-feedstock.
[65] O.R. Energy, Carbon Sequestration Project Uses Water to Turn CO2 into Rocks, (n.d.). https://www.greenoptimistic.com/carbon-sequestration-carbfix/amp/.
[66] R.Zevenhoven, AN EXERGY ANALYSIS FOR MINERAL CARBONATION, Environ. Technol. Resour. 21 (2003) 49–53.
[67] F. Klein, C.J. Garrido, Thermodynamic constraints on mineral carbonation of serpentinized peridotite, Lithos. 126 (2011) 147–160.
[68] W.J.J. Huijgen, Carbon dioxide sequestration by mineral carbonation, Phd Thesis. (2003).
[69] T. Su, H. Yang, Y. Shau, E. Takazawa, Y. Lee, ScienceDirect CO 2 sequestration utilizing basic-oxygen furnace slag : Controlling factors , reaction mechanisms and V – Cr concerns, Jes. 41 (2015) 99–111.
[70] E.R. Bobicki, Q. Liu, Z. Xu, H. Zeng, Carbon capture and storage using alkaline industrial wastes, Prog. Energy Combust. Sci. 38 (2012) 302–320.
[71] O. Rahmani, CO2sequestration by indirect mineral carbonation of industrial waste red gypsum, J. CO2 Util. 27 (2018) 374–380.
[72] J.C. Picot, D. Cassard, F. Maldan, C. Greffié, F. Bodénan, Worldwide potential for ex-situ mineral carbonation, Energy Procedia. 4 (2011) 2971–2977. doi:10.1016/J.EGYPRO.2011.02.206.
[73] H. Schaef, Q. Miller, C. Thompson, J. Loring, M. Bowden, B. Arey, B. McGrail, K. Rosso, Silicate Carbonation in Supercritical CO2 Containing Dissolved H2O: An in situ High Pressure

X-Ray Diffraction and Infrared Spectroscopy Study, Energy Procedia. 37 (2013) 5892–5896. doi:10.1016/J.EGYPRO.2013.06.514.

[74] Ex-Situ and In-Situ Mineral Carbonation as a Means to Sequester Carbon Dioxide S.J. Gerdemann, D.C. Dahlin, W.K. O'Connor, L.R. Penner, and G.E. Rush, (n.d.).

[75] G. Montes-Hernandez, R. Chiriac, F. Toche, F. Renard, Gas-solid carbonation of Ca(OH)2and CaO particles under non-isothermal and isothermal conditions by using a thermogravimetric analyzer: Implications for CO2capture, Int. J. Greenh. Gas Control. 11 (2012) 172–180.

[76] S.P. Veetil, G. Mercier, J.F. Blais, E. Cecchi, S. Kentish, CO2 Sequestration by Direct Dry Gas-Solid Contact of Serpentinite Mining Residues: A Solution for Industrial CO2 Emission, Int. J. Environ. Pollut. Remediat. (2014).

[77] R.R. Tamilselvi Dananjayan, P. Kandasamy, R. Andimuthu, Direct mineral carbonation of coal fly ash for CO2 sequestration, J. Clean. Prod. 112 (2016) 4173–4182.

[78] V. Prigiobbe, A. Polettini, R. Baciocchi, Gas–solid carbonation kinetics of Air Pollution Control residues for CO2 storage, Chem. Eng. J. 148 (2009) 270–278. doi:10.1016/J.CEJ.2008.08.031.

[79] A. Ćwik, I. Casanova, K. Rausis, N. Koukouzas, K. Zarębska, Carbonation of high-calcium fly ashes and its potential for carbon dioxide removal in coal fired power plants, J. Clean. Prod. 202 (2018) 1026–1034.

[80] W. Liu, S. Su, K. Xu, Q. Chen, J. Xu, Z. Sun, Y. Wang, S. Hu, X. Wang, Y. Xue, J. Xiang, CO 2 sequestration by direct gas–solid carbonation of fly ash with steam addition, J. Clean. Prod. 178 (2018) 98–107.

[81] R. Zevenhoven, M. Slotte, J. Åbacka, J. Highfield, A comparison of CO2 mineral sequestration processes involving a dry or wet carbonation step, Energy. 117 (2016) 604–611. https://www.sciencedirect.com/science/article/abs/pii/S0360544216306831 (accessed December 5, 2018).

[82] J.M. Matter, P.B. Kelemen, Permanent storage of carbon dioxide in geological reservoirs by mineral carbonation, Nat. Geosci. 2 (2009) 837–841.

[83] R. Zevenhoven, S. Teir, S. Eloneva, Heat optimisation of a staged gas-solid mineral carbonation process for long-term CO2storage, Energy. 33 (2008) 362–370. doi:10.1016/j.energy.2007.11.005.

[84] S. Santos, IEA GHG Introduction • IEA Greenhouse Gas R & D Programme, (2012).

[85] S. Teir, R. Kuusik, C.-J. Fogelholm, R. Zevenhoven, Production of magnesium carbonates from serpentinite for long-term storage of CO2, Int. J. Miner. Process. 85 (2007) 1–15. doi:10.1016/J.MINPRO.2007.08.007.

[86] W.J.J. Huijgen, G.-J. Witkamp, R.N.J. Comans, Mechanisms of aqueous wollastonite carbonation as a possible CO2 sequestration process, Chem. Eng. Sci. 61 (2006) 4242–4251.

[87] M. Kakizawa, A. Yamasaki, Y. Yanagisawa, A new CO2 disposal process via artificial weathering of calcium silicate accelerated by acetic acid, Energy. 26 (2001) 341–354.

doi:10.1016/S0360-5442(01)00005-6.

[88] X. Wang, M.M. Maroto-Valer, Dissolution of serpentine using recyclable ammonium salts for CO2 mineral carbonation, Fuel. 90 (2011) 1229–1237. doi:10.1016/J.FUEL.2010.10.040.

[89] A.H.A. Park, L.S. Fan, CO2 mineral sequestration: Physically activated dissolution of serpentine and pH swing process, Chem. Eng. Sci. 59 (2004) 5241–5247. doi:10.1016/j.ces.2004.09.008.

[90] M.M. Maroto-Valer, D.J. Fauth, M.E. Kuchta, Y. Zhang, J.M. Andrésen, Activation of magnesium rich minerals as carbonation feedstock materials for CO2 sequestration, Fuel Process. Technol. 86 (2005) 1627–1645. doi:10.1016/J.FUPROC.2005.01.017.

[91] S. Zhang, D.J. DePaolo, T. Xu, L. Zheng, Mineralization of carbon dioxide sequestered in volcanogenic sandstone reservoir rocks, Int. J. Greenh. Gas Control. 18 (2013) 315–328. doi:10.1016/J.IJGGC.2013.08.001.

[92] J.M. Matter, T. Takahashi, D. Goldberg, Experimental evaluation of in situ CO2-water-rock reactions during CO2 injection in basaltic rocks: Implications for geological CO2 sequestration, Geochemistry, Geophys. Geosystems. 8 (2007). doi:10.1029/2006GC001427.

[93] L. Marini, Developments in Geochemistry, Dev. Geochemistry. 11 (2007) ii. doi:10.1016/S0921-3198(13)60001-0.

[94] S.R. Gíslason, H. Sigurdardóttir, E.S. Aradóttir, E.H. Oelkers, A brief history of CarbFix: Challenges and victories of the project’s pilot phase, Energy Procedia. 146 (2018) 103–114. doi:10.1016/j.egypro.2018.07.014.

[95] G. Beaudoin, A. Nowamooz, G.P. Assima, K. Lechat, A. Gras, A. Entezari, E.H.B. Kandji, A.-S. Awoh, M. Horswill, S. Turcotte, F. Larachi, C. Dupuis, J. Molson, J.-M. Lemieux, X. Maldague, B. Plante, B. Bussière, M. Constantin, J. Duchesne, R. Therrien, R. Fortier, Passive Mineral Carbonation of Mg-rich Mine Wastes by Atmospheric CO2, Energy Procedia. 114 (2017) 6083–6086.

[96] M. Ahmaruzzaman, A review on the utilization of fly ash, Prog. Energy Combust. Sci. 36 (2010) 327–363. 0360128509000604.

[97] M. Mun, H. Cho, Mineral carbonation for carbon sequestration with industrial waste, Energy Procedia. 37 (2013) 6999–7005. doi:10.1016/j.egypro.2013.06.633.

[98] M. Thesis, Master Thesis Assessing the Mineral Carbonation Science and Technology MSc program in Chemical and Bioengineering, Bioengineering. (n.d.).

[99] F. Brück, K. Schnabel, T. Mansfeldt, H. Weigand, Accelerated carbonation of waste incinerator bottom ash in a rotating drum batch reactor, J. Environ. Chem. Eng. 6 (2018) 5259–5268.

[100] M. Criado, A. Palomo, A. Fernández-Jiménez, Alkali activation of fly ashes. Part 1: Effect of curing conditions on the carbonation of the reaction products, Fuel. 84 (2005) 2048–2054.

[101] J.A. Schramke, Neutralization of alkaline coal ash by CO2, 7 (1992) 481–492.

[102] M.S. Masoudian, Journal of Rock Mechanics and Geotechnical Engineering Multiphysics of carbon dioxide sequestration in coalbeds : A review with a focus on geomechanical

characteristics of coal, J. Rock Mech. Geotech. Eng. 8 (2016) 93–112. doi:10.1016/j.jrmge.2015.08.002.

[103] X. Jian, Carbon dioxide sorption and diffusion in coals : Experimental investigation and modeling Carbon dioxide sorption and diffusion in coals : Experimental investigation and modeling, (2014). doi:10.1007/s11430-011-4272-4.

[104] G. Ceglarska-Stefańska, A. Czapliński, Correlation between sorption and dilatometric processes in hard coals, Fuel. 72 (1993) 413–417. doi:10.1016/0016-2361(93)90064-9.

[105] A. Czapliński, S. Hołda, Changes in mechanical properties of coal due to sorption of carbon dioxide vapour, Fuel. 61 (1982) 1281–1282. doi:10.1016/0016-2361(82)90035-7.

[106] C.Ö. Karacan, Swelling-induced volumetric strains internal to a stressed coal associated with CO2 sorption, Int. J. Coal Geol. 72 (2007) 209–220. doi:10.1016/J.COAL.2007.01.003.

[107] D.R. Viete, P.G. Ranjith, The mechanical behaviour of coal with respect to CO2 sequestration in deep coal seams, Fuel. 86 (2007) 2667–2671. doi:10.1016/J.FUEL.2007.03.020.

[108] P. Baran, K. Czerw, N. Czuma, K. Zarębska, A. Ćwik, Development of temperature-induced strains in coal–CH 4 and coal–CO 2 systems, Adsorpt. Sci. Technol. (2018) 026361741880782. doi:10.1177/0263617418807829.

[109] P. Baran, K. Zarębska, M. Bukowska, Expansion of hard coal accompanying the sorption of methane and carbon dioxide in isothermal and non-isothermal processes, Energy and Fuels. 29 (2015) 1899–1904. doi:10.1021/ef502312p.

[110] H.-H. Lee, H.-J. Kim, Y. Shi, D. Keffer, C.-H. Lee, Competitive adsorption of CO2/CH4 mixture on dry and wet coal from subcritical to supercritical conditions, Chem. Eng. J. 230 (2013) 93–101. doi:10.1016/J.CEJ.2013.06.036.

[111] S. Hol, Y. Gensterblum, P. Massarotto, Sorption and changes in bulk modulus of coal — experimental evidence and governing mechanisms for CBM and ECBM applications, Int. J. Coal Geol. 128–129 (2014) 119–133. doi:10.1016/J.COAL.2014.04.010.

[112] Y. Gensterblum, A. Ghanizadeh, B.M. Krooss, Gas permeability measurements on Australian subbituminous coals: Fluid dynamic and poroelastic aspects, J. Nat. Gas Sci. Eng. 19 (2014) 202–214. doi:10.1016/J.JNGSE.2014.04.016.

[113] J. Milewska-Duda, The coal-sorbate system in the light of the theory of polymer solutions, Fuel. 72 (1993) 419–425. doi:10.1016/0016-2361(93)90065-A.

[114] J.W. Larsen, The effects of dissolved CO2 on coal structure and properties, Int. J. Coal Geol. 57 (2004) 63–70. doi:10.1016/J.COAL.2003.08.001.

[115] K. Czerw, Methane and carbon dioxide sorption/desorption on bituminous coal—Experiments on cubicoid sample cut from the primal coal lump, Int. J. Coal Geol. 85 (2011) 72–77. doi:10.1016/J.COAL.2010.10.002.

[116] Z. Majewska, S. Majewski, J. Ziętek, Swelling of coal induced by cyclic sorption/desorption of gas: Experimental observations indicating changes in coal structure due to sorption of CO2 and

CH4, Int. J. Coal Geol. 83 (2010) 475–483. doi:10.1016/J.COAL.2010.07.001.

[117] B.B. Saha, S. Jribi, S. Koyama, I.I. El-Sharkawy, Carbon dioxide adsorption isotherms on activated carbons, J. Chem. Eng. Data. 56 (2011) 1974–1981. doi:10.1021/je100973t.

[118] M.. Iglesias, A. Jiménez, J.. del Río, I. Suárez-Ruiz, Molecular characterisation of vitrinite in relation to natural hydrogen enrichment and depositional environment, Org. Geochem. 31 (2000) 1285–1299. doi:10.1016/S0146-6380(00)00086-3.

[119] C.Ö. Karacan, G.D. Mitchell, Behavior and effect of different coal microlithotypes during gas transport for carbon dioxide sequestration into coal seams, Int. J. Coal Geol. 53 (2003) 201–217. doi:10.1016/S0166-5162(03)00030-2.

[120] K. Czerw, A. Äwik, P. Baran, K. Zarębska, Kinetics of methane and carbon dioxide sorption and sorption-induced expansion of coal-kinetic equations assessment, E3S Web Conf. 10 (2016). doi:10.1051/e3sconf/20161000012.

[121] K. Czerw, P. Baran, K. Zarębska, Application of the stretched exponential equation to sorption of mine gases and sorption induced swelling of bituminous coal, Int. J. Coal Geol. 173 (2017) 76–83. doi:10.1016/j.coal.2017.02.010.

[122] A. Busch, Y. Gensterblum, CBM and CO2-ECBM related sorption processes in coal: A review, Int. J. Coal Geol. 87 (2011) 49–71. doi:10.1016/J.COAL.2011.04.011.

[123] F. Brouers, O. Sotolongo-Costa, Generalized fractal kinetics in complex systems (application to biophysics and biotechnology), Phys. A Stat. Mech. Its Appl. 368 (2006) 165–175. doi:10.1016/J.PHYSA.2005.12.062.

[124] G. Staib, R. Sakurovs, E.M.A. Gray, Dispersive diffusion of gases in coals. Part I: Model development, Fuel. 143 (2015) 612–619. doi:10.1016/J.FUEL.2014.11.086.

[125] C. Heidrich, H. Feuerborn, A. Weir, Coal Combustion Products : a Global Perspective, World Coal Ash Conf. 22-25th April. Lexington, USA. (2013).

[126] S. V. Vassilev, R. Menendez, Phase-mineral and chemical composition of coal fly ashes as a basis for their multicomponent utilization. 4. Characterization of heavy concentrates and improved fly ash residues, Fuel. 84 (2005) 973–991. doi:10.1016/J.FUEL.2004.11.021.

[127] ASTM C618-05, Standard specification for coal fly ash and raw or calcined natural pozzolan for use in concrete, (2005).

[128] T. Hemalatha, A. Ramaswamy, A review on fly ash characteristics – Towards promoting high volume utilization in developing sustainable concrete, J. Clean. Prod. 147 (2017) 546–559.

[129] S. V Vassilev, R. Menendez, D. Alvarez, M. Diaz-Somoano, M.R. Martinez-Tarazona, Phase-mineral and chemical composition of coal fly ashes as a basis for their multicomponent utilization. 1. Characterization of feed coals and fly ashes, Fuel. 82 (2003) 1793–1811.

[130] M. Żyrkowski, R.C. Neto, L.F. Santos, K. Witkowski, Characterization of fly-ash cenospheres from coal-fired power plant unit, Fuel. 174 (2016) 49–53.

[131] H. Feuerborn, Coal Combustion Products in Europe - an update on Production and Utilisation ,

Standardisation and Regulation -, World Coal Ash Conf. 10-12th May, Color. (2011).

[132] Euracoal, European Association for Coal and Lignite, (2013).

[133] I. Papayianni, S. Tsimas, A. Moutsatsou, Standardization aspects concerning high calcium fly ashes, 3rd World Coal Ash, WOCA Conf. , 4-7th May, Lexington, USA. Proc. (2009).

[134] EN, 450-1:2013, UNE-EN 450-1:2013. Fly ash for concrete - Part 1: Definition, specifications and conformity criteria, (2012).

[135] EN 197-1:2011, Cement. Part 1: Composition, specifications and conformity criteria for common cement., (2011).

[136] I. Papayianni, E. Anastasiou, Utilisation of Calcareous Fly Ash in Construction, (2014).

[137] UNE83420:1991, Additions for concrete. Fly ash. Specifications for fly ashes with a content more than 10% in CaO., (1991).

[138] J. Papayianni, Use of a high-calcium fly ash in blended type cement production, Cem. Concr. Compos. 15 (1993) 231–235.

[139] A. Dindi, D.V. Quang, L.F. Vega, E. Nashef, M.R.M. Abu-Zahra, Applications of fly ash for CO2 capture, utilization, and storage, J. CO2 Util. 29 (2019) 82–102. doi:10.1016/j.jcou.2018.11.011.

[140] B. Reynolds, K. Reddy, M. Argyle, Field Application of Accelerated Mineral Carbonation, Minerals. 4 (2014) 191–207.

[141] J.-H. Wee, A review on carbon dioxide capture and storage technology using coal fly ash, Appl. Energy. 106 (2013) 143–151.

[142] A. Ebrahimi, M. Saffari, D. Milani, A. Montoya, M. Valix, A. Abbas, Sustainable transformation of fly ash industrial waste into a construction cement blend via CO2 carbonation, J. Clean. Prod. 156 (2017) 660–669.

[143] S.L. Pei, S.Y. Pan, X. Gao, Y.K. Fang, P.C. Chiang, Efficacy of carbonated petroleum coke fly ash as supplementary cementitious materials in cement mortars, J. Clean. Prod. 180 (2018) 689–697.

[144] L. Ji, H. Yu, X. Wang, M. Grigore, D. French, Y.M. Gözükara, J. Yu, M. Zeng, CO2sequestration by direct mineralisation using fly ash from Chinese Shenfu coal, Fuel Process. Technol. 156 (2017) 429–437.

[145] M.G. Nyambura, G.W. Mugera, P.L. Felicia, N.P. Gathura, Carbonation of brine impacted fractionated coal fly ash: Implications for CO2 sequestration, J. Environ. Manage. 92 (2011) 655–664.

[146] Z. Wei, B. Wang, G. Falzone, E.C. La Plante, M.U. Okoronkwo, Z. She, T. Oey, M. Balonis, N. Neithalath, L. Pilon, G. Sant, Clinkering-free cementation by fly ash carbonation, J. CO2 Util. 23 (2018) 117–127.

[147] B. Arias, M.E. Diego, A. Méndez, J.C. Abanades, L. Díaz, M. Lorenzo, A. Sanchez-Biezma, Operating Experience in la Pereda 1.7 MWth Calcium Looping Pilot, Energy Procedia. 114

(2017) 149–157.

[148] S. Mills, Prospects for coal and clean coal technologies in Greece, IEA Clean Coal Cent. (2015) 2–122.

[149] A. Cwik, K. Zarebska, P. Baran, J. Szczurowski, Mineral carbonation of high-calcium fly ash under elevated pressure and temperature, Przem. Chem. 96 (2017).

[150] A. Orzechowska-Zięba, K. Zarębska, P. Baran, A. Äwik, Sequestration of carbon dioxide-influence of coal surface chemistry, E3S Web Conf. 10 (2016). doi:10.15420/aer.2015.4.3.163.

[151] U. Burghaus, Surface chemistry of CO2 – Adsorption of carbon dioxide on clean surfaces at ultrahigh vacuum, Prog. Surf. Sci. 89 (2014) 161–217. doi:10.1016/J.PROGSURF.2014.03.002.

[152] A. Uliasz-Bocheńczyk, M. Mazurkiewicz, E. Mokrzycki, Popioly z energetyki - odpad, produkt uboczny, surowiec, Gospod. Surowcami Miner. / Miner. Resour. Manag. 31 (2015) 139–150.

[153] M. Żygadło, M. Woźniak, Obserwacje zmian właściwości popiołów powęglowych w procesach wietrzeniowych, Energetyka. nr 11 (2009) 771–775.

[154] R.R. Tamilselvi Dananjayan, P. Kandasamy, R. Andimuthu, Direct mineral carbonation of coal fly ash for CO2 sequestration, J. Clean. Prod. 112 (2016) 4173–4182.

[155] Y. Soong, D.L. Fauth, B.H. Howard, J.R. Jones, D.K. Harrison, A.L. Goodman, M.L. Gray, E.A. Frommell, CO2sequestration with brine solution and fly ashes, Energy Convers. Manag. 47 (2006) 1676–1685.

[156] T. Kim, J. Olek, Effects of Sample Preparation and Interpretation of Thermogravimetric Curves on Calcium Hydroxide in Hydrated Pastes and Mortars, Transp. Res. Rec. J. Transp. Res. Board. 2290 (2012) 10–18.

[157] U. Kleinhans, C. Wieland, F.J. Frandsen, H. Spliethoff, Ash formation and deposition in coal and biomass fired combustion systems: Progress and challenges in the field of ash particle sticking and rebound behavior, Prog. Energy Combust. Sci. 68 (2018) 65–168. doi:10.1016/j.pecs.2018.02.001.

[158] M.A. Nahil, X. Wang, C. Wu, H. Yang, H. Chen, P.T. Williams, Novel bi-functional Ni-Mg-Al-CaO catalyst for catalytic gasification of biomass for hydrogen production with in situ CO2 adsorption, RSC Adv. 3 (2013) 5583–5590. doi:10.1039/c3ra40576a.

[159] A. Uliasz-Bochenczyk, Waste used for CO2 bonding via mineral carbonation, Gospod. Surowcami Miner. Resour. Manag. 23 (2007) 121–128.

[160] D.N. Huntzinger, J.S. Gierke, L.L. Sutter, S.K. Kawatra, T.C. Eisele, Mineral carbonation for carbon sequestration in cement kiln dust from waste piles, J. Hazard. Mater. 168 (2009) 31–37.

[161] S.Y. Lee, S.J. Park, A review on solid adsorbents for carbon dioxide capture, J. Ind. Eng. Chem. 23 (2015) 1–11. doi:10.1016/j.jiec.2014.09.001.

[162] P. Duan, C. Yan, W. Zhou, Effects of calcined layered double hydroxides on carbonation of concrete containing fly ash, Constr. Build. Mater. 160 (2018) 725–732.

[163] Q. Xue, S. Lu, Microstructure of ferrospheres in fly ashes: SEM, EDX and ESEM analysis, J.

Zhejiang Univ. A. 9 (2008) 1595–1600.

[164] Ö. Cizer, C. Rodriguez-Navarro, E. Ruiz-Agudo, J. Elsen, D. Van Gemert, K. Van Balen, Phase and morphology evolution of calcium carbonate precipitated by carbonation of hydrated lime, J. Mater. Sci. 47 (2012) 6151–6165.

[165] I. Galan, F.P. Glasser, D. Baza, C. Andrade, Assessment of the protective effect of carbonation on portlandite crystals, Cem. Concr. Res. 74 (2015) 68–77.

[166] B. Kremer, J. Kazmierczak, L.J. Stal, Calcium carbonate precipitation in cyanobacterial mats from sandy tidal flats of the North Sea, Geobiology. 6 (2008) 46–56.

[167] O. Regnault, V. Lagneau, H. Schneider, Experimental measurement of portlandite carbonation kinetics with supercritical CO2, Chem. Geol. 265 (2009) 113–121.

[168] G. Montes-Hernandez, D. Daval, R. Chiriac, F. Renard, Growth of nanosized calcite through gas-solid carbonation of nanosized portlandite under anisobaric conditions, Cryst. Growth Des. 10 (2010) 4823–4830.

[169] A. Ćwik, I. Casanova, K. Rausis, K. Zarębska, Utilization of high-calcium fly ashes through mineral carbonation: The cases for Greece, Poland and Spain, J. CO2 Util. 32 (2019) 155–162. doi:10.1016/j.jcou.2019.03.020.

[170] L. Regev, K.M. Poduska, L. Addadi, S. Weiner, E. Boaretto, Distinguishing between calcites formed by different mechanisms using infrared spectrometry: Archaeological applications, J. Archaeol. Sci. 37 (2010) 3022–3029. doi:1.

[171] G. Montes-Hernandez, F. Renard, R. Chiriac, N. Findling, J. Ghanbaja, F. Toche, Sequential precipitation of a new goethite-calcite nanocomposite and its possible application in the removal of toxic ions from polluted water, Chem. Eng. J. 214 (2013) 139–148.

[172] F. Paulik, J. Paulik, M. Arnold, Thermal decomposition of gypsum, Thermochim. Acta. 200 (1992) 195–204.

[173] S.Y. Pan, E.E. Chang, H. Kim, Y.H. Chen, P.C. Chiang, Validating carbonation parameters of alkaline solid wastes via integrated thermal analyses: Principles and applications, J. Hazard. Mater. 307 (2016) 253–262. doi:10.1016/j.jhazmat.2015.12.065.

[174] N. Ranjbar, C. Kuenzel, Cenospheres: A review, Fuel. 207 (2017) 1–12.

[175] H. Wang, V. Alfredsson, J. Tropsch, R. Ettl, T. Nylander, Formation of CaCO3 deposits on hard surfaces - Effect of bulk solution conditions and surface properties, ACS Appl. Mater. Interfaces. 5 (2013) 4035–4045.

[176] M.M. Tlili, M. Ben Amor, C. Gabrielli, S. Joiret, G. Maurin, On the initial stages of calcium carbonate precipitation., Eur. J. Water Qual. 37 (2006) 89–108.

[177] Y. Zhang, Y. Xie, Y. Zhu, X. Lu, X. Ji, Energy consumption analysis for CO2separation from gas mixtures with liquid absorbents, Energy Procedia. 61 (2014) 2695–2698.

[178] C.G. Kontoyannis, N. V. Vagenas, Calcium carbonate phase analysis using XRD and FT-Raman spectroscopy, Analyst. 125 (2000) 251–255.

[179] S. Seufert, C. Hesse, F. Goetz-Neunhoeffer, J. Neubauer, Quantitative determination of anhydrite III from dehydrated gypsum by XRD, Cem. Concr. Res. 39 (2009) 936–941.

[180] W. Mozgawa, M. Król, J. Dyczek, J. Deja, Investigation of the coal fly ashes using IR spectroscopy, Spectrochim. Acta - Part A Mol. Biomol. Spectrosc. 132 (2014) 889–894.

[181] M. Farhadi Khouzani, D.M. Chevrier, P. Güttlein, K. Hauser, P. Zhang, N. Hedin, D. Gebauer, Disordered amorphous calcium carbonate from direct precipitation, CrystEngComm. 17 (2015) 4842–4849.

[182] E. Tajuelo Rodriguez, K. Garbev, D. Merz, L. Black, I.G. Richardson, Thermal stability of C-S-H phases and applicability of Richardson and Groves' and Richardson C-(A)-S-H(I) models to synthetic C-S-H, Cem. Concr. Res. 93 (2017) 45–56.

[183] G. Montes-hernandez, R. Chiriac, F. Toche, F. Renard, International Journal of Greenhouse Gas Control Gas – solid carbonation of Ca (OH) 2 and CaO particles under non-isothermal and isothermal conditions by using a thermogravimetric analyzer : Implications for CO 2 capture, Int. J. Greenh. Gas Control. 11 (2012) 172–180.

[184] S.P. Veetil, L.C. Pasquier, J.F. Blais, E. Cecchi, S. Kentish, G. Mercier, Direct gas–solid carbonation of serpentinite residues in the absence and presence of water vapor: a feasibility study for carbon dioxide sequestration, Environ. Sci. Pollut. Res. 22 (2015) 13486–13495.

[185] Y.İ. Tosun, Benefaction from Carbonation of Flue Gas CO2 as Coal Mining Filling, (2014) 64–72.

[186] N. Koukouzas, I. Papayianni, E. Tsikardani, D. Papanikolaou, C. Ketikidis, Greek fly ash as a cement replacement in the production of paving blocks, (2007).

[187] H.S. Lee, H.S. Lim, M.A. Ismail, Quantitative evaluation of free CaO in electric furnace slag using the ethylene glycol method, Constr. Build. Mater. 131 (2017) 676–681.

[188] K. Kaewmanee, P. Krammart, T. Sumranwanich, P. Choktaweekarn, S. Tangtermsirikul, Effect of free lime content on properties of cement-fly ash mixtures, Constr. Build. Mater. 38 (2013) 829–836.

[189] A. Nawaz, P. Julnipitawong, P. Krammart, S. Tangtermsirikul, Effect and limitation of free lime content in cement-fly ash mixtures, Constr. Build. Mater. 102 (2016) 515–530.

[190] I. Papayianni, S. Tsimas, A. Moutsatsou, Standardization aspects concerning high calcium fly ashes, 3rd World Coal Ash, WOCA Conf. 4-7th May, Lexington,USa.-Proceedings. (2009).

[191] S.Y. Pan, P.C. Chiang, W. Pan, H. Kim, Advances in state-of-art valorization technologies for captured CO2 toward sustainable carbon cycle, Crit. Rev. Environ. Sci. Technol. 48 (2018) 471–534. doi:10.1080/10643389.2018.1469943.

Summary

In this work two research topics are presented: investigation of carbonation reactions of high – calcium waste materials and CO_2 storage in coal.

Firstly, sorption capacity of CO_2 and CH_4 of hard coal and associated sorption-induced expansion of the material was measured. This investigation was maintained in isothermal and non-isothermal conditions. Experiments were done on purpose-design apparatus allowing simultaneous measurement of sorption kinetics and sorption-induced swelling/contraction of coal. Chosen coal sample had higher sorption capacity for CO_2 when compare to capacity for CH_4. Additionally, coal strains attributed to the CO_2 sorption are twice the size as of CH_4. The linear strain kinetics show that the expansion of coal sample, induced by both gases is anisotropic, and greater in the perpendicular direction to the bedding plane than parallel. Dilatometric analysis refers that the deformation of the material in the presence of CH_4 is nearly twice as low as the deformation in the CO_2 presence, in the same pressure range. Maintaining the sorption experiments in rising temperature results in additional expansion of coal when exposed to CH_4. CO_2 sorption on coal in iso-thermal conditions leads to the sample contraction. This could be associated with petrographic composition of the coal.

The sorption and expansion kinetics of solid coal sample data were fit into kinetic equation. The model used was Stretched Exponential Equation. Modelling sorption and expansion kinetics is important in order to determine coal response to potential gas storage and allows to predict the changes in the coal transport-sorption.

Next to CO_2 storage, the topic of CO_2 utilization has been investigated. Carbonation of European high-calcium fly ashes is assessed. The experiments have been done on different fly ashes with content of 5-36% CaO. Complementary, characterization and analysis of fly ash samples has been performed.

Acceleration of carbonation has been explored. Experiments has been done in temperature range between 25 and 290ºC, 1-12 bar of CO_2, CO_2 + H_2O and simulated flue gas over reaction times between 2 and 72 hours. Major conclusions of this work is that increasing the temperature and pressure strongly enhances the process of carbonation. Also, addition of water vapor substantially accelerates the process and increase its kinetics.

This thesis reports that maintaining the carbonation process without steam addition leads to effective carbonation conversion. Chemical fixation of CO_2 molecules with solid material of fly ash with high content of CaO to produce calcium carbonate is possible. The highest sequestration capacity achieved is 117.7 g CO_2/kg fly ash and highest carbonation efficiency obtained is 48%.

The microstructural analysis of fly ash samples showed the evolution of the cenosphere surface according to the carbonation experiments conditions. Different shapes and sizes of calcium carbonate has been detected after carbonation experiments.

The compositional constraints of fly ashes that control reaction with CO_2 has been described. It was found that not the bulk content of CaO is the factor controlling the carbonation reaction, but the content of free lime.

Impact on carbonation of two pressure flow systems was assessed: batch and continuous flow, with and without addition of steam. Using he batch treatment with addition of steam gave the highest carbonation efficiency.

Another set of carbonation experiments which has been done was with using simulated flue gas (84% N_2, 15% CO_2, 1 % H_2O) instead of pure CO_2 stream, in conditions: 160ºC, 6 bar of gas and 2 hours of reaction time. It was concluded that using flue gas instead of pure stream of carbon dioxide lowers the carbonation rate of about 9%.

Final part of this research was to determine the change of free lime content in fly ash samples before and after carbonation. Carbonation reactions lead to substantial decrease of free lime contents in fly ashes. In most cases, the amount of free lime in fly ash after carbonation was compatible with the current EU legislations regarding fly ash incorporation to cement as admixture.

Streszczenie

W niniejszej przedstawiono dwa tematy badawcze: badanie reakcji karbonatyzacji odpadów wysoko wapniowych i składowania CO_2 w węglu.

W pierwszej części badawczej dokonano analizy pojemności sorpcyjnej CO_2 i CH_4 węgla kamiennego oraz zmiany wolumetryczne węgla spowodowane procesem sorpcji. Eksperymenty prowadzono w warunkach izotermicznych i nieizotermicznych. Do pomiarów użyto specjalistycznego aparatu do jednoczesnego pomiaru sorpcji oraz ekspansji próbek wywołanej sorpcją. Wybrana próbka węgla charakteryzowała się większą pojemnością sorpcyjną dla CO_2 niż dla CH_4. Odkształcenia próbki węgla spowodowane sorpcją CO_2 były dwa razy większe niż odkształcenia próbki wzbudzone sorpcją metanu. Ekspansja próbki jest anizotropowa w wyniku sorpcji obu gazów i większa w kierunku prostopadłym niż równoległym. Analiza dylatometryczna wskazuje, że ekspansja węgla w obecności CH_4 jest prawie dwukrotnie mniejsza niż ekspasnsja węgla podczas sorpcji CO_2, w tym samym zakresie ciśnień. Prowadzenie eksperymentów sorpcji w warunkach nieizotermicznych powoduje dodatkową ekspansję węgla podczaj reakcji z CH_4. Sorpcja CO_2 na węglu w tych warunkach prowadzi do kontrakcji próbki. Przedstawione różnice wolumetryczne mogą być związane ze składem petrograficznym węgla. Dane kinetyk sorpcji i rozszerzalności próbki węgla kamiennego zostały dopasowane do równania kinetycznego. Zastosowanym modelem było równanie 'Stretched Exponential Equation'. Modelowanie kinetyki sorpcji i rozszerzalności węgla jest ważne w celu określenia potencjalu zmagazynowania CO_2 w węglu oraz pozwala przewidzieć zmiany wolumetryczne pokładów węglowych.

W drugiej części niniejszej pracy zbadano temat utylizacji ditlenku węgla. Przedstawiono oraz zbadano temat karbonatyzacji europejskich popiołów lotnych o wysokiej zawartościści tlenku wapnia. Doświadczenia przeprowadzono na różnych popiołach lotnych o całkowitej zawartości CaO w przedziale 5-36%. Dokonano również charakteryzacji oraz analizy wybranych próbek popiołów lotnych.

Przeprowadzono próby akceleracji kinetyki procesu karbonatyzacji. Eksperymenty wykonano w zakresie temperatur od 25 do 290°C, ciśnienia 1-12 barów CO_2, CO_2 + H_2O lub mieszaniny gazów. Czas reakcji eskerymentów mieścił się w przedziale 2 a 72 godzin. Podwyższenie temperatury oraz ciśnienia CO_2 zwiększa konwersję gazu i CaO do węglanu wapnia. Ponadto, dodanie pary wodnej do strumienia CO_2 przyśpiesza proces karbonatyzacji.

Uzyskane wyniki eskerymentów pozwalają wnioskować, że karbonatyzacja w warunkach gaz – ciało stałe, bez dostępu wody jest możliwa do przeprowadzenia. Opisane warunki doświadczeń pozwoliły na interakcję cząsteczek CO_2 z tlenkiem wapnia zawartym w popiele lotnym i wytworzenie kalcytu. Najwyższa uzyskana pojemność sekwestracyjna CO_2 wyniosła 117,7 g CO_2/kg popiołu lotnego, a najwyższa uzyskana wydajność karbonatyzacji wyniosła 48%.

Analiza mikrostrukturalna próbek popiołów lotnych ukazała ewolucję powierzchni cenosfer podczas zmieniających się warunków eskerymentalnych procesu karbonatyzacji. Podczas analizy próbek popiołu po karbonatyzacji wykryto w materiale różne kształty i rozmiary węglanu wapnia.

Zdeterminowano wpływ składu chemicznego popiołów lotnych na reakcję z ditlenkiem węgla. Stwierdzono, że zawartość wolnego wapna jest czynnikiem kontrolującym reakcję, a nie całkowita zawartość CaO.

Oceniono wpływ na reakcję karbonatyzacji dwóch układów przepływu ciśnieniowego: reaktor zamknięty oraz reaktor z ciągłym przepływem gazu, z dodatkiem pary wodnej lub bez. Zastosowanie reaktora zamkniętego z dodatkiem pary dało najwyższą wydajność karbonatyzacji.

W finalnej partii eskerymentów karbonatyzacji użyto symulowanego gazu spalinowego (84% N_2, 15% CO_2, 1% H_2O) zamiast czystego strumienia CO_2, w warunkach: 160°C, 6 barów ciśnienia i 2 godzin czasu reakcji. Stwierdzono, że stosowanie gazu spalinowego zamiast czystego strumienia dwutlenku węgla obniża wydajność karbonatyzacji o około 9%.

Końcową częścią badań procesu karbonatyzacji było określenie zmiany zawartości wolnego wapna w próbkach popiołu lotnego przed i po nasyceniu ditlenkiem węgla. Reakcje karbonatyzacji prowadzą do znacznego zmniejszenia zawartości wolnego wapna w popiele lotnym. W większości przypadków ilość wolnego wapna w popiele lotnym po nasycaniu ditlenkiem węgla była zgodna z obowiązującymi przepisami UE dotyczącymi utylizacji popiołów lotnych w cemencie, jako domieszki.

Resumen

En este trabajo se presentan dos temas de investigación: almacenamiento de CO_2 en carbón y carbonatación de residuos industriales con un alto contenido en calcio.

En primer lugar, se midió la capacidad de sorción de CO_2 y CH_4 de la hulla y su asociada expansión. Esta investigación se mantuvo en condiciones isotérmicas y no isotérmicas. Los experimentos se realizaron en un aparato diseñado específicamente, el cual permite la medición simultánea de la cinética de sorción y su asociada expansión y contracción. La muestra de carbón elegido tenía una mayor capacidad de absorción de CO_2 comparado a CH_4. Además, la absorción de CO_2 indujo una expansión de volumen en el carbón, duplicando la obtenida tras la absorción de CH_4. La cinética de deformación lineal muestra que la expansión del carbón inducida por ambos gases es anisotrópica, y es mayor en la dirección perpendicular al plano de estratificación que en paralelo a este. El análisis dilatométrico hace referencia a la deformación del material en presencia de CH_4 es casi dos veces más baja que la obtenida en presencia de CO_2, en el mismo rango de presión. El aumento de temperatura da como resultado una expansión adicional del carbón cuando se expone a CH_4. La absorción de CO_2 en el carbón en condiciones iso-térmicas conduce a la contracción de la muestra. Esto podría estar asociado con la composición petrográfica del carbón.

Los datos obtenidos de la cinética de absorción y expansión de carbón se ajustaron en una ecuación cinética. El modelo utilizado fue: 'Ecuación Exponencial Estirada'. El modelado de la cinética de absorción y expansión es importante para determinar la respuesta del carbón como posible almacenamiento de gas y permite predecir los cambios en la absorción-transporte de carbón.

Junto al almacenamiento de CO_2, la utilización de este también ha sido investigado. Se evalúa la carbonatación de las cenizas volante de origen europeo con alto contenido en calcio. Los experimentos se han realizado en diferentes cenizas volantes con un contenido entre 5-36% de CaO. Un estudio detallado de la carbonatación acelerada de las cenizas volantes has sido llevado a cabo

Los experimentos se han realizado en un rango de temperatura entre 25 y 290°C, 1 - 12 bares de CO_2, CO_2 + H_2O y gases de combustión simulados durante tiempos de reacción entre 2 y 72 horas. La principal conclusión de este trabajo es: el aumento de temperatura, presión y la adición de vapor de agua acelera considerablemente el proceso de carbonatación en estos materiales.

Evidencias experimentales sugieren que una carbonatación efectiva se puede obtener sin la adición de vapor de agua. La mayor capacidad de CO_2 secuestrado es de 117.7 g CO_2/kg de cenizas volantes y la mayor eficiencia de carbonatación obtenida equivale a 48%.

El análisis microestructural de las cenizas volantes mostró una evolución de la superficie de la cenosferas según las condiciones de los experimentos de carbonatación. Se han detectado diferentes formas y tamaños de carbonato de calcio después de los experimentos de carbonatación.

Se han descrito las restricciones referidas a la composición de las cenizas volantes que controlan su reacción con CO_2. Se encontró que el factor dominante que controla la reacción de carbonatación es el contenido mineralógico de cal libre, en lugar del contenido total de CaO.

Se evaluó el impacto en la carbonatación de dos sistemas presurizados: batch y flujo continuo, con y sin adición de vapor. Las reacciones llevadas a cabo en sistemas tipo batch con la adición de vapor produjeron la mayor eficiencia de carbonatación.

Otra serie de experimentos de carbonatación realizados consistieron en el uso de gas de combustión simulado (84% N_2, 15% CO_2, 1% H_2O) en lugar de CO_2 puro. Las condiciones experimentales fueron: 160°C, 6 bares de presión total y 2 horas de tiempo de reacción. Se concluyó que el uso de gas de combustión en lugar de dióxido de carbono puro reduce la tasa de carbonatación de aproximadamente el 9%.

Finalizando, el contenido de cal libre ha sido determinado para cada muestra antes y después de las reacciones de carbonatación en una variedad de cenizas volantes. Las reacciones de carbonatación produjeron una disminución sustancial del contenido de cal libre en las cenizas volantes. En la mayoría de los casos, el contenido de cal libre después de la carbonatación fue compatible con las legislaciones actuales de la UE con respecto a la incorporación de cenizas volantes al cemento como aditivo.

List of Figures

List of Tables